January 2011

Comparison of Cam and Servomotor Solutions to a Motion Problem

Matthew B. Rhodes
Worcester Polytechnic Institute

Patrick D. Hunter
Worcester Polytechnic Institute

Raymond Ranellone
Worcester Polytechnic Institute

Toby Michael Callahan
Worcester Polytechnic Institute

Comparison of Cam and Servomotor Solutions to a Motion Problem

A Major Qualifying Project Report:

Submitted to the Faculty

of the

WORCESTER POLYTECHNIC INSTITUTE

In partial fulfillment of the requirements for the

Degree of Bachelor of Science

By

Toby Callahan **Patrick Hunter** **Raymond Ranellone** **Matthew Rhodes**

Date:

Approved:

Professor Eben C. Cobb **Professor Robert L. Norton**

1) Cam
2) Servo

This report represents the work of one or more WPI undergraduate students submitted to the faculty as evidence of completion of a degree requirement.WPI routinely publishes these reports on its web site without editorial or peer review.

1 Abstract

The manufacturing lines of the sponsoring company utilize cam-follower systems where complex motion is required, as they are the traditional means of obtaining such motion. Some equipment utilizing servomechanism actuation has been introduced by the sponsoring company as a potential avenue for the improvement of manufacturing systems. Further insight into the suitability of such mechanisms as replacements for cam-follower systems was desired. To that end, design and manufacture of a Cam-Servo Test Machine actuated by either cam-follower or servomechanism was undertaken by the project's participants. The resulting Cam-Servo Test Machine was intended to output 200 cycles per minute of a complex reciprocating motion in either mode of actuation. The machine design employed a timing belt speed reduction in its drive train, which had an unintended deleterious impact on system stiffness. A revised design employing a larger servomotor without a speed reduction was developed and analyzed in its stead. The project team concluded that a larger servomotor, directly mounted, can be a suitable replacement for a cam-follower system at a cost that is several orders of magnitude greater.

Table of Contents

2 Introduction

Machines incorporating specifically designed mechanisms to perform simple or complex movements are often utilized to achieve desired production tasks. An example of this type of mechanism would best be explained by the mechanism inserting a detail into a component as the assembly progresses through a production line. This type of mechanical process is typically performed by a function generator. The definition of a function generator "is the correlation of an output motion with an input motion in a mechanism"[1]. The data contained within this report explored the feasibility of replacing a cam-driven crank-slider mechanism, which has been a common function generation method in a wide range of applications, with a servomotor-driven crank-slider mechanism.

The sponsor of this study currently utilizes constant-speed motor driven cam-based mechanisms almost exclusively on their production assembly lines; however, the sponsor has experimented with a limited number of servomotor driven mechanisms as an alternative. Servomotors have become popular with machine designers "in part because they have become less costly than in the past. Servomotors also offer many advantages over conventional motors because they provide constant speed against dynamic variations in load torque due to their closed-loop operation"[2].

The purpose of this project was to explore the advantages and disadvantages of such a replacement. A Cam-Servo Test Machine (CSTM) was designed utilizing a single crank-slider mechanism that allowed interchangeability between cam- and servomotor-driven motion function output.

The output motion characteristics were pre-defined. The crank-slider mechanism was specified to operate at 200 cycles per minute with an output slider displacement of 1.5 inches. Output tolerances were supplied by the client, which permits a position error no greater than ±0.005 inches.

3 Background

The Cam-Servo Test Machine (CSTM) was designed to determine the feasibility of replacing a cam with a servomotor for a general motion output. A working knowledge of the individual components was required in order to apply both drive types to the same task. A dynamic analysis and comparison between the two drive types was conducted. A variety of computer software programs were utilized in this project.

3.1 Core Components

The CSTM utilizes the same crank-slider mechanism configuration (discussed in Appendix D: Linkages) for both cam and servomotor application. By doing this the mechanism's core components are shared, minimizing the potential for manufacturing or assembly variation between the two modes of operation.

3.1.1 Cam Driven Linkages

A cam-driven linkage is one way of generating a variable output motion from a constant input shaft velocity. Figure 1 shows an example of a cam-driven crank-slider linkage. Cam-follower systems are widely used in modern machinery especially in automotive applications; almost all conventional internal combustion engines utilize cams to control intake and exhaust valve timing.

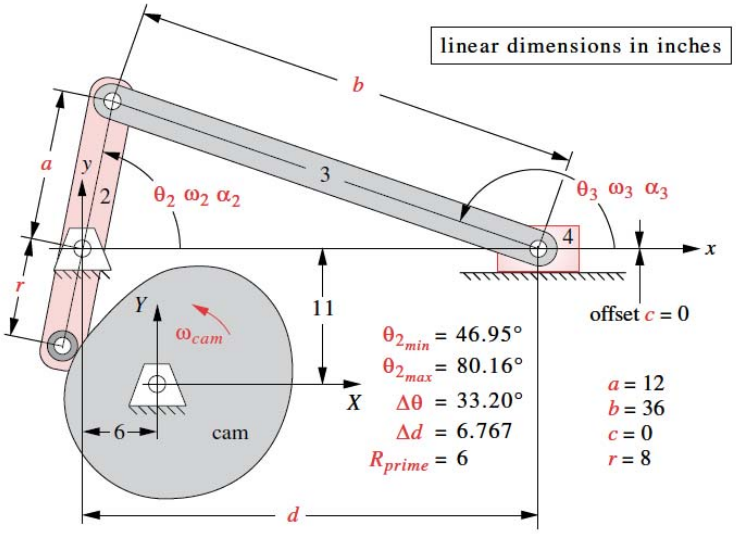

Figure 1: Cam-driven slider-crank linkage[3]

A cam-follower system has considerable advantages over other methods of motion function generation. These advantages include motion function flexibility, relatively compact size, straightforward design principles, and a large mechanical advantage.

3.1.2 Servomotor Driven Linkages

Figure 2 below shows a crank-slider linkage controlled by a servomotor. The servomotor drives the crank (2) in pure rotation about its ground link. The crank is attached to a coupler(3) in complex motion which drives a slider (4) in pure translation.

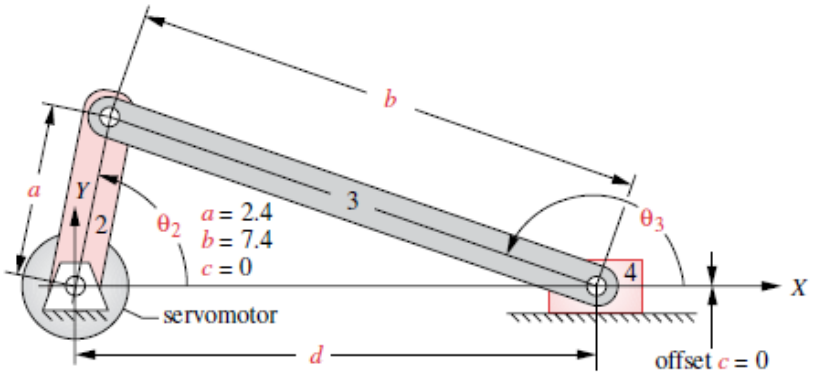

Figure 2: Servo-driven slider-crank linkage[4]

In a closed loop servomotor system angular position is the controlled variable. The position variable is defined by the constant feedback from the encoder or resolver. A Programmable Logic Controller (PLC) is a compact standalone industrial computing device that allows the execution of complex motion output functions in a servomotor system. In some instances, a Human-Machine Interface (HMI) is utilized to allow a human operator to control the PLC through a touch screen or other device.

Servomotor-driven linkages have advantages over other motion output methods. The programmability of the servomotor controller presents the flexibility to adjust the output motion profile with minimal effort. This controller coupled with the use of the encoder or resolver allows the servomotor to maintain any velocity subject to the design tolerance regardless of variations in the load torque.

3.1.3 Cam-Driven Versus Servomotor-Driven Mechanisms

The project objective was to design a mechanism to be driven by a cam or a servomotor interchangeably in order to assess the advantages and disadvantages of replacing a cam with a servomotor in a linkage-based mechanism. The comparison between the cam and servomotor was based on cost, reliability, load capacity, complexity, flexibility, robustness, and packaging.

Both cams and servomotors are relatively reliable. If properly sized and designed, each will have a long operational life. Cams running in an ideal environment, lubricated with filtered oil, can last over a billion camshaft cycles; an example of this is in a high mileage automobile. The project sponsor operates their cam-driven mechanism in a dry state. Although the non-lubricated environment is not ideal, cam performance may last several years on a machine that could accumulate up to 100-million cycles per year[5]. Servomotors possess the potential for

their more complicated electronic components and bearings to fail; a cam surface will wear and need replacing if run without proper lubrication. The adverse effects of dry-running a cam system is the typically high concentrated point- or line-contact force (shown in Figure 3) between the cam surface and follower.

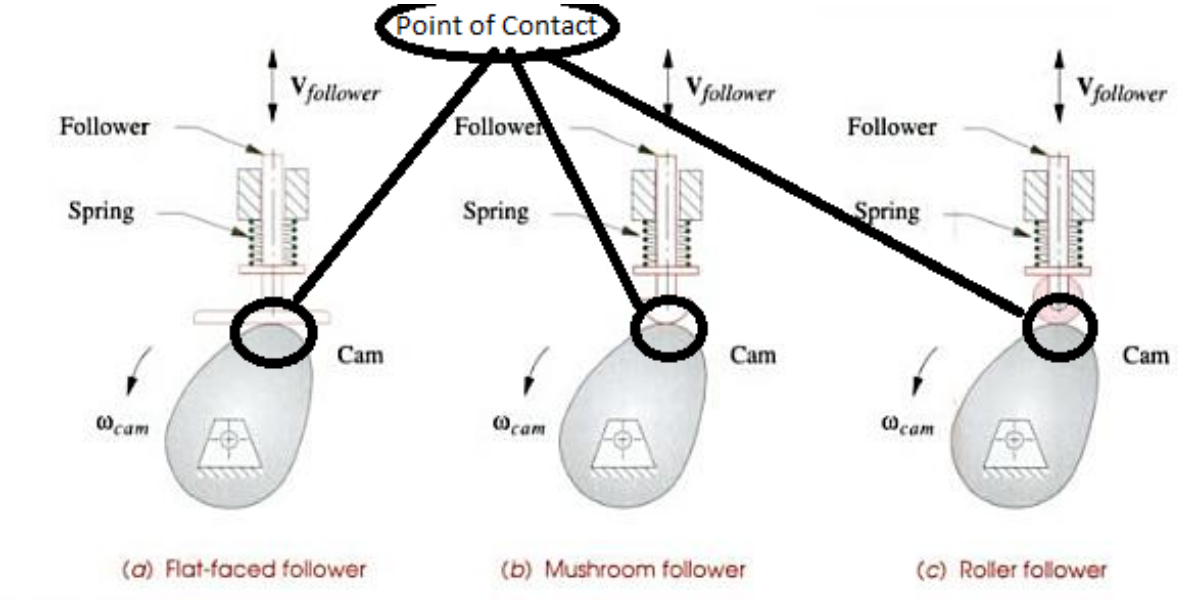

Figure 3: Point of Contact[6]

This concentrated force can lead to premature wear and/or excessive vibration if the cam is not properly sized. Additionally, the follower must maintain contact with the cam surface to function properly. This often involves the use of a follower return spring. In some cases the force required to keep the roller-follower in contact with the cam surface exceeds the range of a return spring's capabilities. For these situations a form-closed cam can be used. Form-closed cams (shown in Figure 4) enclose the roller follower between two surfaces and are capable of closely specifying the return profile of the follower.

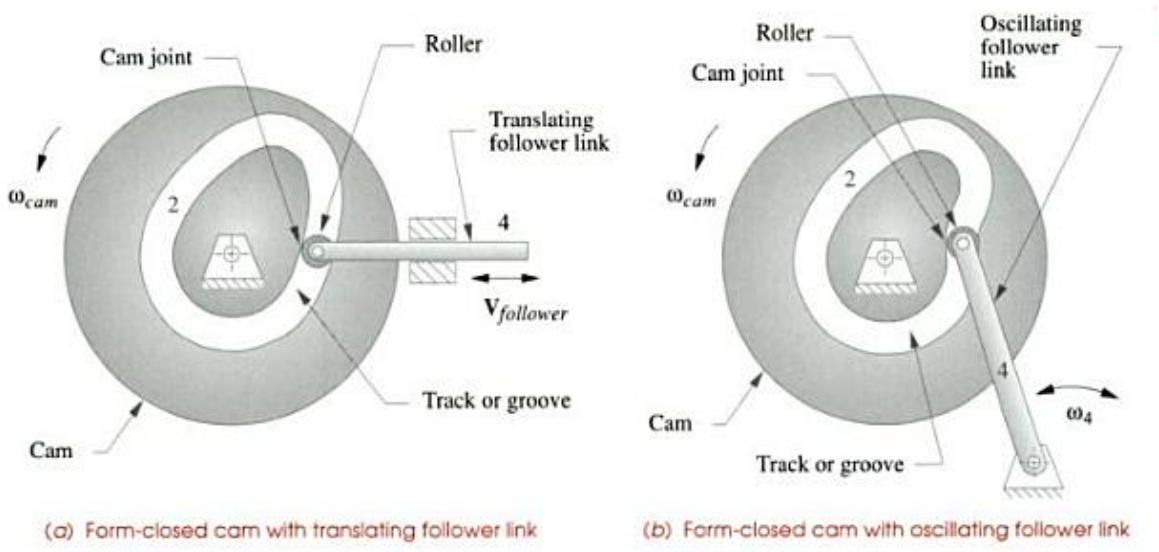

Figure 4: Form-closed cams[7]

In applications with large inertia loads or where high force or torque is required, a design incorporating a non-geared servomotor provides only a mechanical advantage of one over the end effector. A servomotor in conjunction with a gearbox provides a constant mechanical advantage capable of producing a large force; however, a cam offers potentially infinite mechanical advantage, providing a superior force output per force input over the servomotor.

Unique design complexities are inherent to both cam and servomotor applications. To obtain accurate servomotor motion output, highly trained personnel must tune the servo controller to achieve the desired dynamic conditions for each application. In addition, servomotor manufacturers recommend the ratio of load inertia to servomotor-shaft (internal) inertia be no greater than 10:1 and optimally 1:1; cams do not possess this requirement. If the application requires a change in dynamics, the servomotor controller has the ability to be reprogrammed. In some instances, controllers have the ability to store programs that an operator can select from a menu and load. A cam's dynamics are engineered and machined into

the cam profile with no ability to adjust the rise, fall or dwell at a constant velocity without machining a new cam profile. Once designed properly, a cam requires no further tuning and only minimal servicing. If machine design performance is revised, a new cam can be manufactured rapidly by a technician to obtain a change in dynamics.

Cam-driven mechanisms are robust because they maintain synchrony and phasing between mechanisms mechanically. In the event of a power failure, the machine stops without phase change[5]. A servomotor-driven mechanism however must be reset to home if a power failure occurs. The system does not maintain phase and relative position if power is lost. Servomotor controllers have been known to lose phase and relative position which may cause damage to the manufacturing system[8]. Servomotors are designed to make a rapid emergency stop using dynamic braking. "High speed manufacturing machines are often required to come to a stop from full speed within one product cycle, which may be a tenth of a second or less"[9]. Servomotor driven systems may also incorporate an electromagnetic brake on the drive shaft, which engages automatically if electric power is cut to the motor or if a stop condition is triggered.

Some applications have design constraints for space, for instance if a cam-driven mechanism may be too large a compact servomotor-driven mechanism may be used an alternative. In addition, 360 degrees of input rotation to the mechanism is not always required. A servomotor-driven mechanism is able to achieve a desired motion without traveling a full revolution whereas a cam-driven mechanism typically must.

3.2 Software Tools

Several computer software programs were utilized in this project to assist in the process of defining a solution space and ultimately obtaining a working model. Each software package is specialized to ascertain a specific solution for this project.

3.2.1 Pro/ENGINEER

Pro/ENGINEER, sold by the Parameteric Technology Company (PTC), is a three dimensional Computer Aided Design software that can be utilized to build and assemble a mechanism (modeled parametrically) with the virtual interface shown in Figure 5.

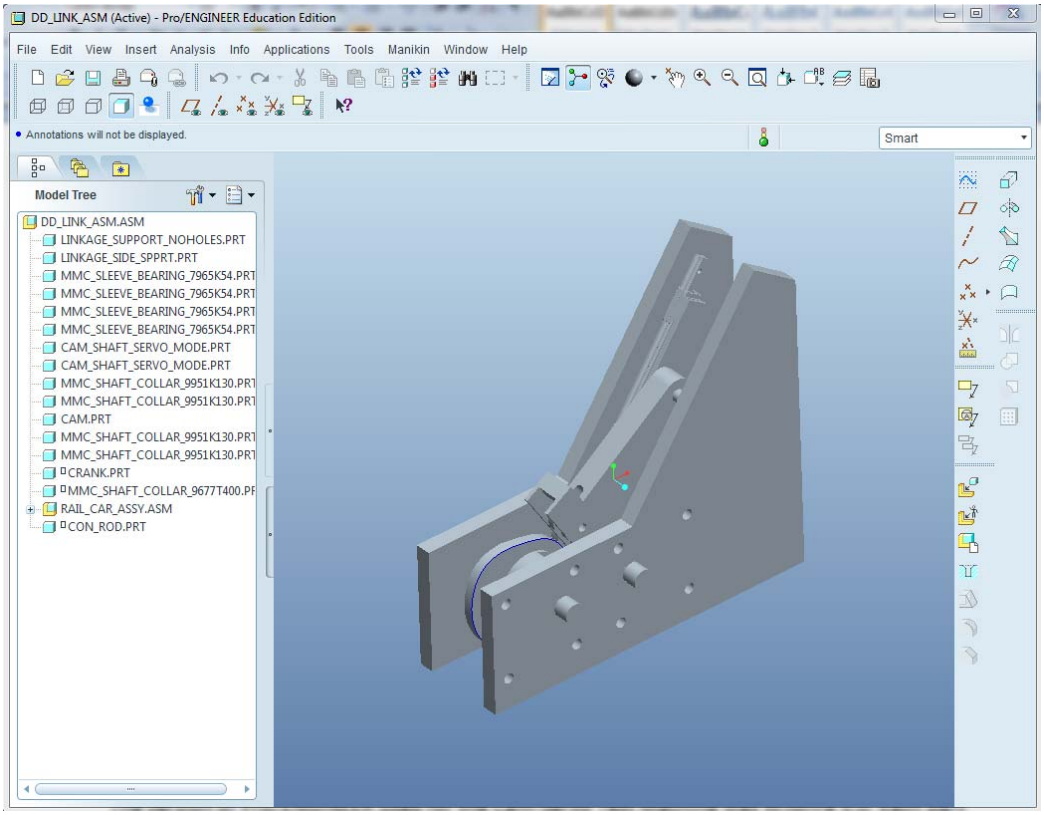

Figure 5: Pro/ENGINEER

The version of Pro/ENGINEER used for the Cam-Servo Test Machine was Wildfire 5.0. Each part of the Cam-Servo Test Machine was created individually so that they could be

assembled into a virtual machine. Pro/ENGINEER allowed dynamic analysis of mechanisms through specification of their connections and mass properties.

By building a virtual mechanism, the team was able to iterate through many potential designs without the expense of physically building prototypes. This capability allowed the team to visually assess how each of the mechanisms fit together, check for problems in the overall assembly and be able to make on-the-fly changes to the design. In addition, this software package was pivotal in making measurements of parts, or between parts, in the overall assembly. For manufacturing Pro/ENGINEER allows creation of conventional ANSI standard drawings, which can be supplied to a machine shop. The models themselves could also be loaded into a Computer Aided Manufacturing program and tool paths for Computer Numeric Control machinery could be generated to manufacture the parts.

3.2.2 Mathcad

Mathcad, also a PTC product, is an engineering calculation software package that allows the team to conduct analysis of the engineering elements of the Cam-Servo Test Machine with an interface (shown in Figure 6) that incorporates features of word processing software.

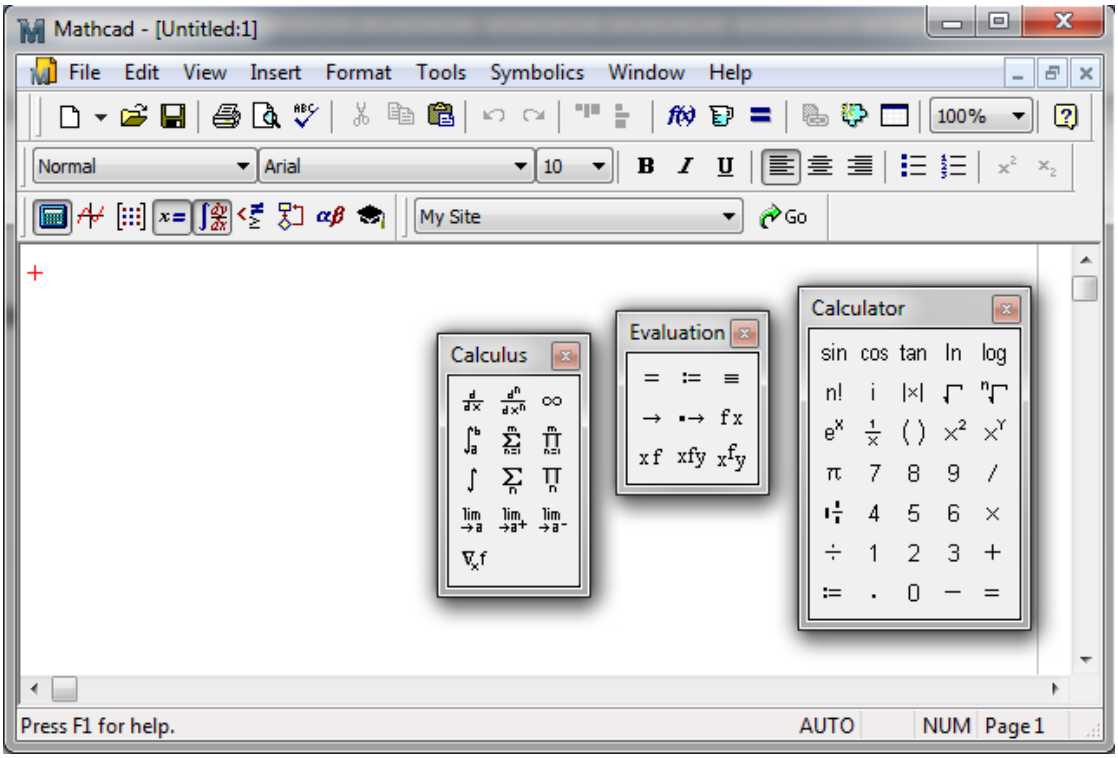

Figure 6: Mathcad

These analyses include vibrations, stress, and kinematics. The version of Mathcad used for the CSTM was Mathcad 15. Each engineering analysis for the CSTM was created in its own separate Mathcad file. Mathcad has the ability to input variables and equations with units and yields symbolic or numerical solutions with the units intact. Mathcad's ability to be able to change the value of a variable and have the entire worksheet update all calculations instantaneously makes re-doing complex calculations repeatedly unnecessary. The understanding gleaned through these analyses was critical to the design process, as the team was able to assess the impact of changes to aspects of the design with regard to its governing equations quickly.

3.2.3 DYNACAM\LINKAGES

DYNACAM and LINKAGES by Norton Associates Engineering are powerful programs that allowed the team to design and analyze cam and linkage systems. Through the use of these tools the team was able to rapidly adjust the design parameters and see the effect these variables would have on the behavior of the machine.

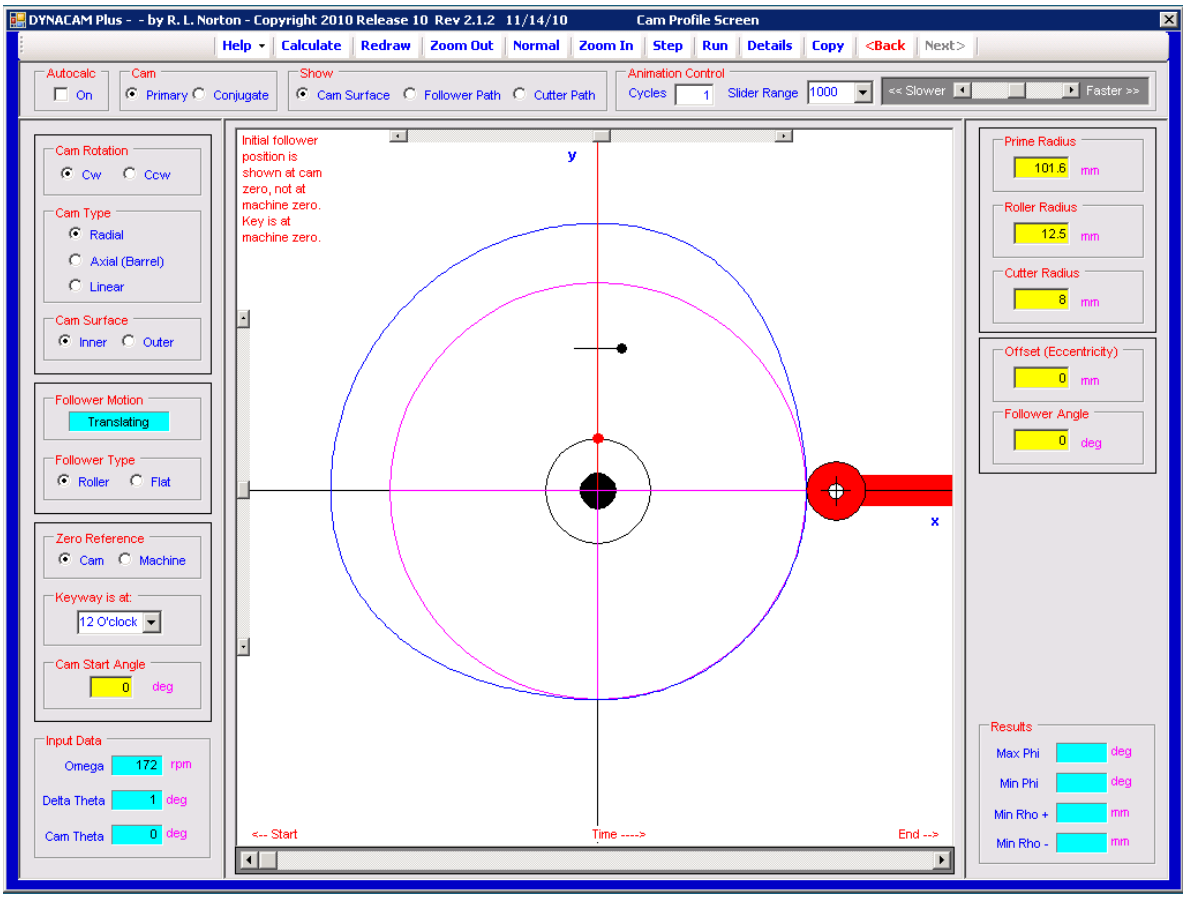

Figure 7: DYNACAM Plus

DYNACAM offers a graphical interface (shown in Figure 7) to software solving of the governing equations of different cam-and-follower systems. The team specified parameters such as roller dimension, eccentricity, start angles, and angular speed to fully define the system, and ran it virtually with analysis of the system's dynamic characteristics. DYNACAM also allowed the team to see the position, velocity, acceleration, and jerk functions associated with

the cam profile essential to designing a suitable cam. Cam profile information from DYNACAM could then be used in conjunction with Pro/ENGINEER and a CAM package to manufacture the cam.

LINKAGES is similar to DYNACAM except it is for linkage design, with an interface similar to that of DYNACAM. Once the defining characteristics of the linkage are entered and intermediate properties are calculated LINKAGES outputs information such as the position, velocity, and acceleration of the slider, as well as the angular position, angular velocity and angular acceleration on the system's dynamic behavior.

4 Goal Statement

The goal of this project is to design and package a mechanism that will create oscillating linear motion with a displacement of 1.5 inches articulated by either a cam-follower or servomotor system, approximating the behavior of insertion machinery used by our sponsor. Comparison will be made between output behavior of the two drive systems to develop an understanding of the advantages and disadvantages of the two in a manufacturing environment. The mechanism will be used in future laboratory experiments for machine design courses at Worcester Polytechnic Institute.

5 Task Specifications

1. Device must be actuated by either a cam-follower system or a servomotor at different times; swapping between configurations may require hand tools and up to 15 minutes to complete.
2. Device must have a substantially identical output motion profile for both driving methods and will ideally share instrumentation for both configurations
3. Subcomponents of device must not introduce unnecessary vibration
4. Device must be approximately table-top in scale
5. Output motion must be repeatable to +/-0.005 inches
6. Device must cycle 200 times per minute
7. Device must compress a spring representing the insertion load
8. Device need not be designed for infinite life
9. Device must be movable by two people
10. Device must be safe to operate and adherent to ergonomic standards
11. Device must run on household voltage

6 Design

While funding was available to purchase new components (as well as the raw materials for any machined piece or any needed fittings), the team began with the devices available if a solution to the problem using them could be devised. The most crucial of these available devices were two motors: a 0.75hp B-102-A-14 AC servomotor from Kollmorgen (paired with a servo driver) and a 1hp C4D17FKSJ permanent magnet DC motor from Leeson. Various gearboxes and mounting hardware were also available. With information on the two motors, individual team members were given the task specifications and came up with a number of creative solutions to the problem. These solutions were discussed and the optimal design was selected for further development.

6.1 Linkage Solution

It is often required in machinery to have a straight line motion as an output function of a simple input. This is especially needed in applications using conveyor systems where a machine must "chase" a product on an assembly line. To accomplish this straight line motion, past inventors have created complicated linkages with a coupler point path that approximates straight line motion. Among such linkages are James Watt's eight bar linkage (which was used in his early steam engines) and Richard Robert's fourbar linkage, along with many others[10]. Most of these inventions produce pseudo-linear output motion over only some of the coupler point path, as in Robert's fourbar linkage, which outputs approximately straight line motion over a certain portion of input rotation.

Another possibility was the use of exact straight line linkages including more than four links, such as those developed by Peaucellier and Hart[10]. The added complication of designing

and analyzing a six or eight bar linkage are impediments to their selection, despite the increase in output linearity.

In these earlier inventions, machining was not as advanced as it is today: devices of the past were restricted to use only revolute joints. With the current state of machining and the ability through it to form precise sliding joints, it is possible to get almost perfect straight line motion with a basic fourbar linkage. One such linkage is shown in Figure 8: a slider-crank fourbar linkage which will create straight line motion at the output from an angular motion of the driving link. Given that the fourbar crank-slider is the simplest solution considered, it was selected for further development.

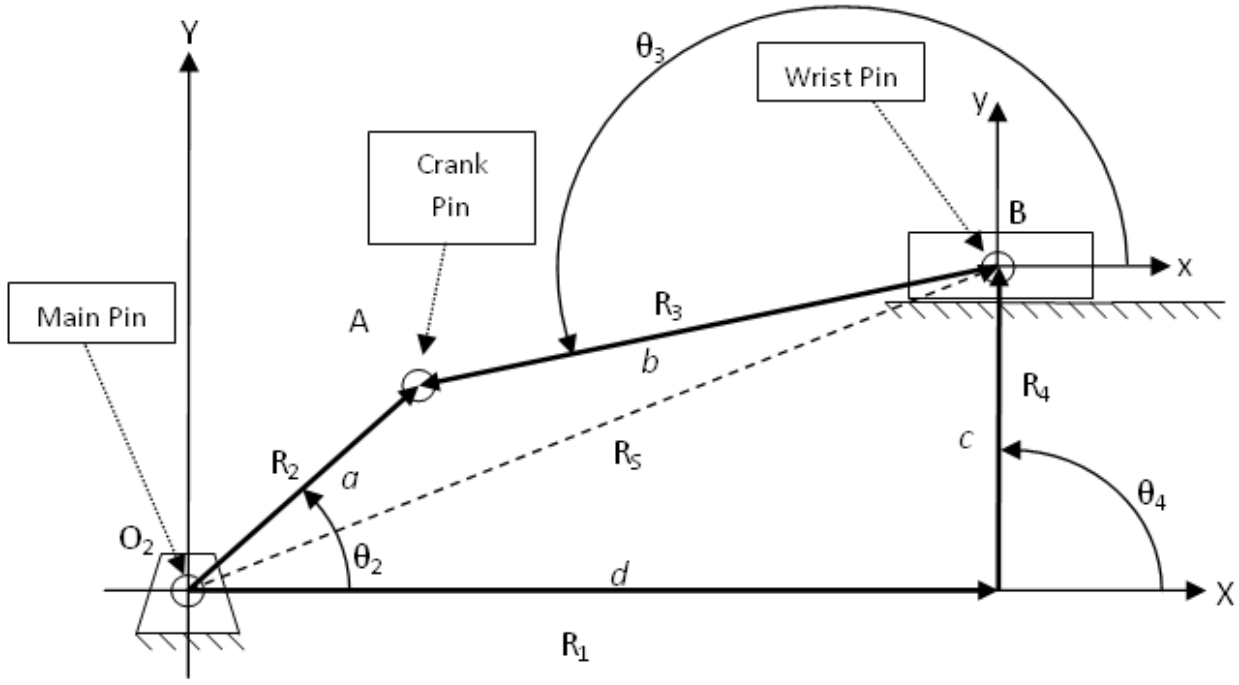

Figure 8: Position Vector Loop for a Slider-Crank Fourbar Linkage

For the fourbar slider crank linkage shown in Figure 5, the link R_2 (of length a) is the driving link of the mechanism. It is desired in linkage synthesis and analysis to show the output

of the linkage as a function of the input. To accomplish this, a position vector loop analysis is done. For this slider-crank linkage the vector loop is:

$$R_2 - R_3 - R_4 - R_1 = 0$$

With R_1 and R_4 being the components of R_S along the X and Y axis respectively. This is done to simplify analysis because as the input link R2 rotates about O_2 the magnitude and angle of R_2 will vary. By using the components of R_S link R_1 will vary in length but not angle, and R_4 will maintain both magnitude of length and angle θ_4 with respect to the X axis.

Taking the vector loop equation from above and substituting link length and position in for each link vector, as well as separating the X components and Y components of the equation, the two following equations will represent the vector loop:

X Component:

$$a\cos\theta_2 - b\cos\theta_3 - c\cos\theta_4 - d = 0$$

Y Component:

$$a\sin\theta_2 - b\sin\theta_3 - c\sin\theta_4 = 0$$

Solving these two equations simultaneously for angle θ_3 and d:

$$\theta_3 = \arcsin\left(\frac{a\sin\theta_2 - c}{b}\right)$$

$$d = a\cos\theta_2 - b\cos\theta_3$$

Therefore, at any instant in time, the position of the slider, B, is a function of the input linkage, its angle θ_2 from the x axis, and the lengths of the remaining links.

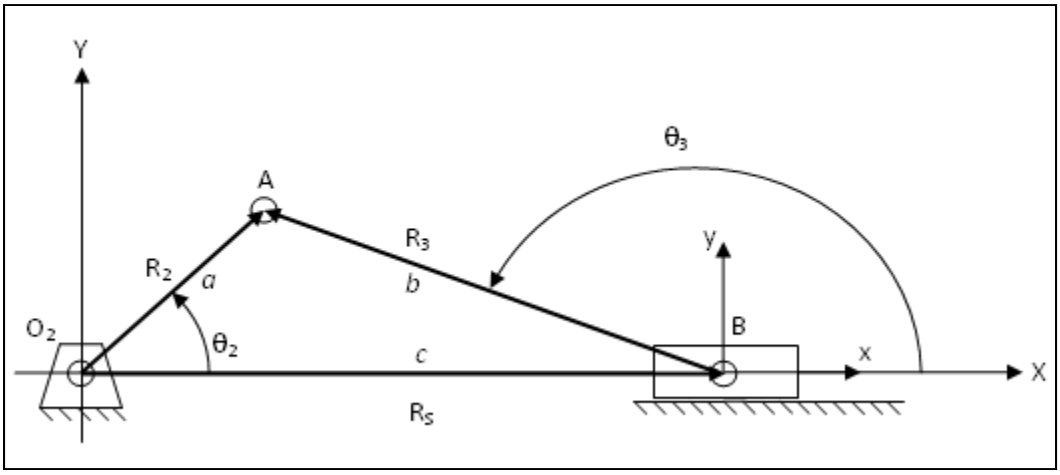

Figure 9: Position Vector Loop Analysis for Crank-Slider with Zero Offset

Taking this generalized case and applying it to the special case of a zero offset slider crank, as shown in Figure 9, results in the following position equations for the slider B:

$$c = a\cos\theta_2 - b\cos\theta_3$$

$$\theta_3 = \sin^{-1}\left(\frac{a\sin\theta_2}{b}\right)$$

Therefore, *c,* or the distance along the X axis of the slider is a function of the link lengths *a* and *b* and angles $\theta_2$and θ_3, all of which are known, and $\theta_3$is a function of link lengths *a* and *b* and angles θ_2. (The derivation of this position, as well as the following velocity and acceleration analysis can be found in Appendix A: Vector Loop Analysis for Fourbar Linkage with zero offset).

From here it is desired to find the velocity of the slider B. Figure 10 shows the velocity vector loop diagram resulting from giving link *a* an angular velocity. This is accomplished by differentiating the position of the slider with respect to time as well as using vector diagrams to find direction of velocities.

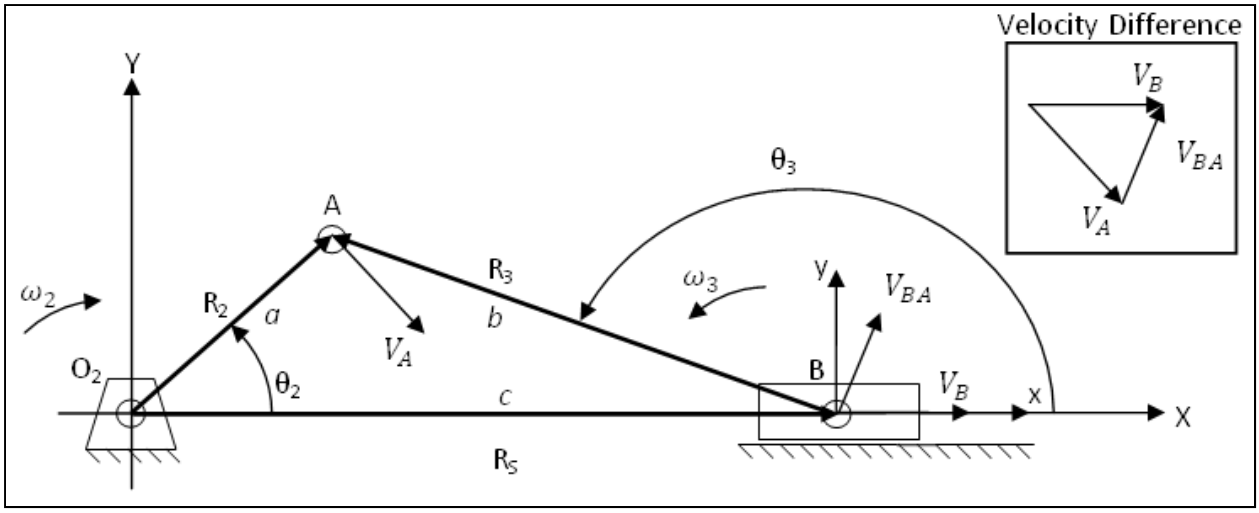

Figure 10: Velocity Vector Loop Analysis for Crank-Slider with Zero Offset with Angular Velocity

Following the same process as described in the position analysis, the linear velocity of the slider as well as the angular velocity of Link 3 are calculated as follows:

$$\dot{c} = -a\omega_2 \sin\theta_2 + b\omega_3 \sin\theta_3$$

$$\omega_3 = \frac{a\cos\theta_2}{b\cos\theta_3}\omega_2$$

Therefore $\dot{c}$, or the velocity of the slider along the X axis is a function of the link lengths a and b and angles θ_2, θ_3, and the angular velocities ω_2, ω_3; all of which are known.

$$\dot{c} = f(a, b, \theta_2, \theta_3, \omega_2, \omega_3)$$

ω_3 is a function of link lengths a and b, angles θ_2, $\theta_3$and angular velocities ω_2.

$$\omega_3 = f(a, b, \theta_2, \theta_3, \omega_2)$$

Now that the position and velocity of the slier is known, the final step is to derive the acceleration function. Figure 11 shows the acceleration vector loop diagram resulting from giving link *a* an angular velocity and acceleration. This acceleration derivation is accomplished by differentiating the velocity functions with respect to time as well as using vector diagrams to find the direction of the acceleration components.

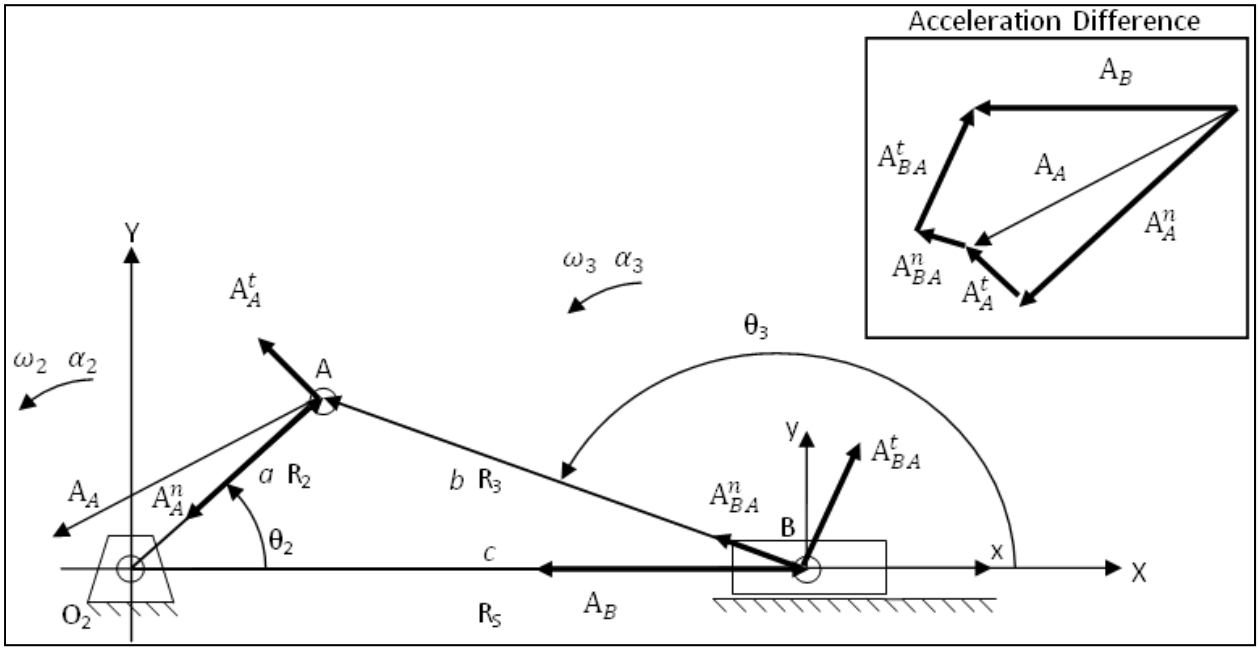

Figure 11: Acceleration Vector Loop Analysis for Crank-Slider with Zero Offset with Angular Acceleration

Again, following the same process as described in the position analysis the linear acceleration of the slider as well as the angular acceleration are calculated as follows:

$$\ddot{c} = -a\alpha_2 \sin\theta_2 - a\omega_2^2 \cos\theta_2 + b\alpha_3 \sin\theta_3 + b\omega_3^2 \cos\theta_3$$

$$\alpha_3 = \frac{a\alpha_2 \cos\theta_2 - a\omega_2^2 \sin\theta_2 + b\omega_3^2 \sin\theta_3}{b\alpha_3 \cos\theta_3}$$

Therefore $\ddot{c}$, or the acceleration of the slider along the X axis is a function of the link lengths *a* and *b*, angles θ_2, θ_3, the angular velocities ω_2, ω_3, and angular acceleration α_2, and α_3; all of which are known.

$$\ddot{c} = f(a, b, \theta_2, \theta_3, \omega_2, \omega_3, \alpha_2, \alpha_3)$$

$\alpha_3$is a function of link lengths *a* and *b*, angles θ_2, θ_3 angular velocities ω_2, ω_3, and angular acceleration α_2.

$$\alpha_3 = f(a, b, \theta_2, \theta_3, \omega_2, \omega_3, \alpha_2)$$

6.2 Application of Slider Linkage to Design Problem

A major element of the design challenge at hand was determining how best to swap between two different modes of actuation and retain the same motion profile. Furthermore, it was highly desired to maximize the number of parts of the machine shared by the two configurations. This commonality would potentially allow the same instrumentation to be used in both modes, minimizing set-up time and the potential for error.

With several preliminary designs (discussed in Appendix B: Preliminary Designs) dismissed, a more traditional solution remained to be considered: a four-bar slider crank linkage driven by either a cam in contact with a roller follower located at the crank pin driven by a programmable servomotor at the main pin of the linkage (see Figure 12).

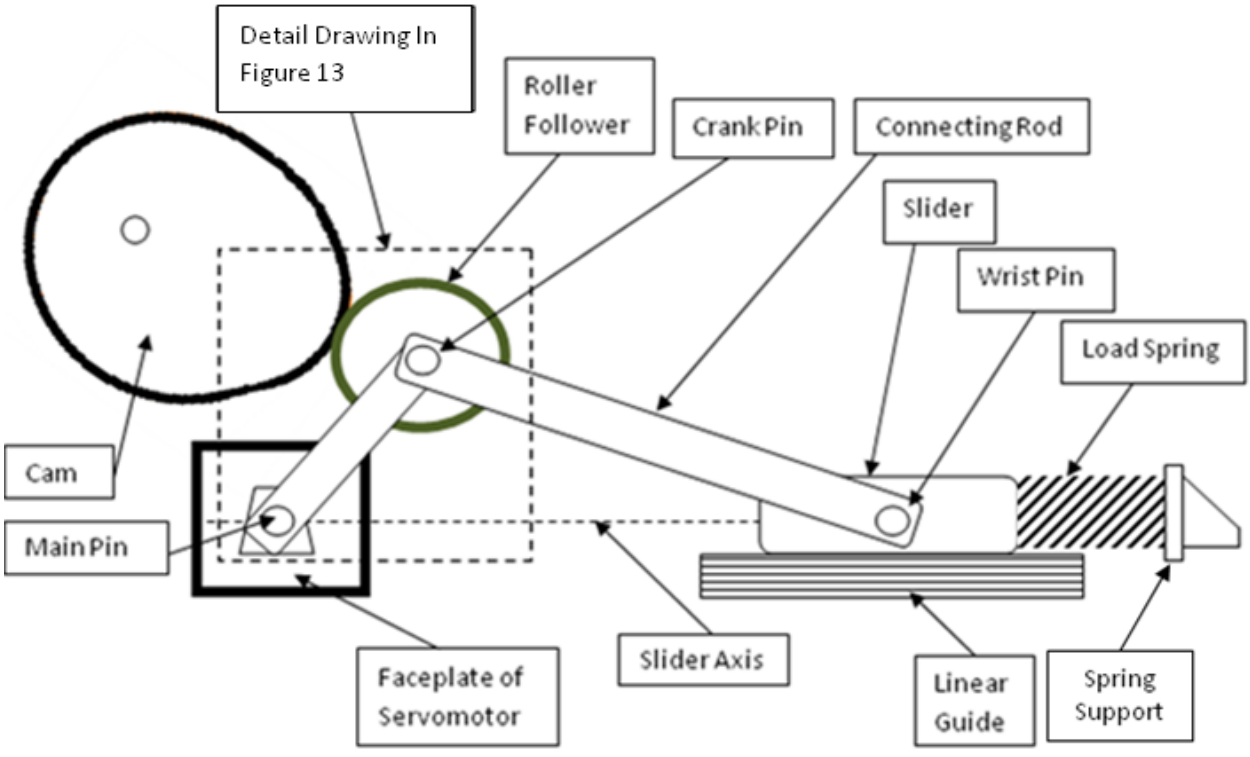

Figure 12: Linkage Solution System Diagram

Keeping the geometry of the four-bar slider, the crank pin joint will be used as the attachment point for the follower mechanism of the cam. The load spring, supported by a

gusseted block, will provide the force needed to keep the follower pressed against the cam. The cam is driven by the servo through a separate drive train. A means of disconnecting the servomotor from the crank pin to allow the cam to drive the mechanism is included in the design.

The servomotor, located in the bottom left corner of Figure 12, is attached to the crank shaft of the four-bar crank-slider mechanism. The servomotor will oscillate the crank effecting oscillating linear motion at the slider on the linear guides. When the system is driven by the servo, the cam will be rotated out of contact with the follower, and the follower removed to clear the crank. This is necessary because vibration in the system would otherwise cause the follower to impact the cam each cycle, damaging it.

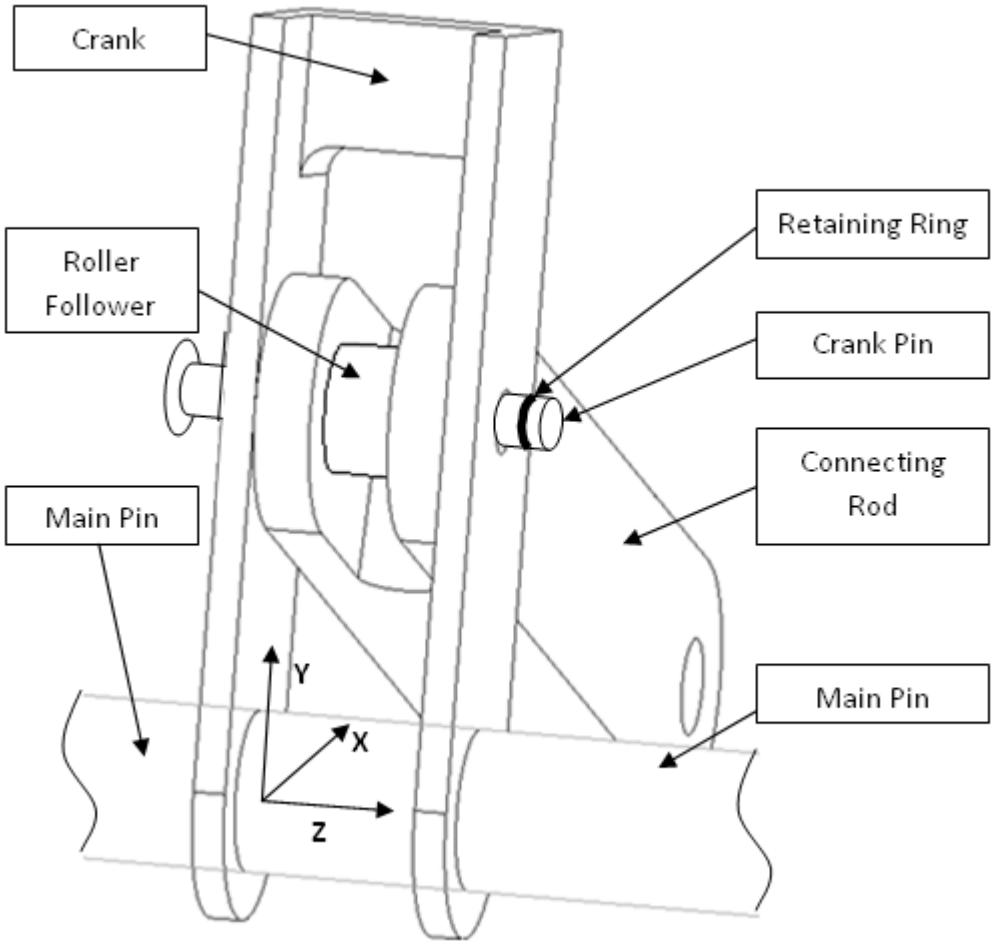

Figure 13: Yoke-Style Crank Pin Joint

All links in the linkage will be made in such a way that the forces created at the pins will all be in the same plane. This will eliminate any out of plane moments and torques at the pins. This may be achieved at the main pin of the linkage as illustrated in Figure 13. This Figure shows the roller follower in the center of the crankpin. To facilitate removing the follower during switchover, the crank pin is removable by removing the retaining ring on the right side of the pin and sliding the pin out. This connection is of a yoke configuration; the joint will be symmetrical about the X-Y plane, eliminating moments about the X-axis.

Because of the limited life required of the Cam-Servo Test Machine mechanism, a lubrication system is not needed. As the roller follower and cam are exposed, it is not possible to create an oil bath system, nor is it practical to create an oil pump system. Therefore, topical oil applied to the revolute joints will be the sole lubrication method. This system will rely upon a fully hardened cam profile and a hard follower to hold up to the limited duty cycle.

6.3 Cam Geometry

A radial-type cam profile with a double-dwell was designed in program DYNACAM. This design uses a 3-4-5 polynomial for rise and fall. This function was chosen over a higher-order polynomial because continuity in the jerk function of the follower motion was not an initial design requirement. The 3-4-5 proved to be capable of satisfying the motion requirements of the CSTM; this was beneficial for both cam and servomotor operation, as constraining the jerk function with a higher-order function typically increases the peak follower acceleration. An increase in follower acceleration would require a stiffer return spring, increasing the force of the follower on the cam and thus increasing wear during operation (possibly to the point where cam lubrication would be a necessity). In servo mode, higher follower acceleration would require more power from the servomotor both to accelerate the system mass and to work against the stiffer return spring. Considering the significant disadvantages and the lack of direct advantages in this application for using a higher-order motion function, the 3-4-5 poly was used as the baseline; had later analysis shown it insufficient for the CSTM a higher order polynomial would have been used.

As shown in Figure 14, the 3-4-5 polynomial function produces continuous and smooth displacement, velocity, and acceleration curves, which are satisfactory. The jerk function has several discontinuities but this does not violate the fundamental rules of cam design which only require that the jerk function be finite. On that basis, this cam function was judged acceptable[11].

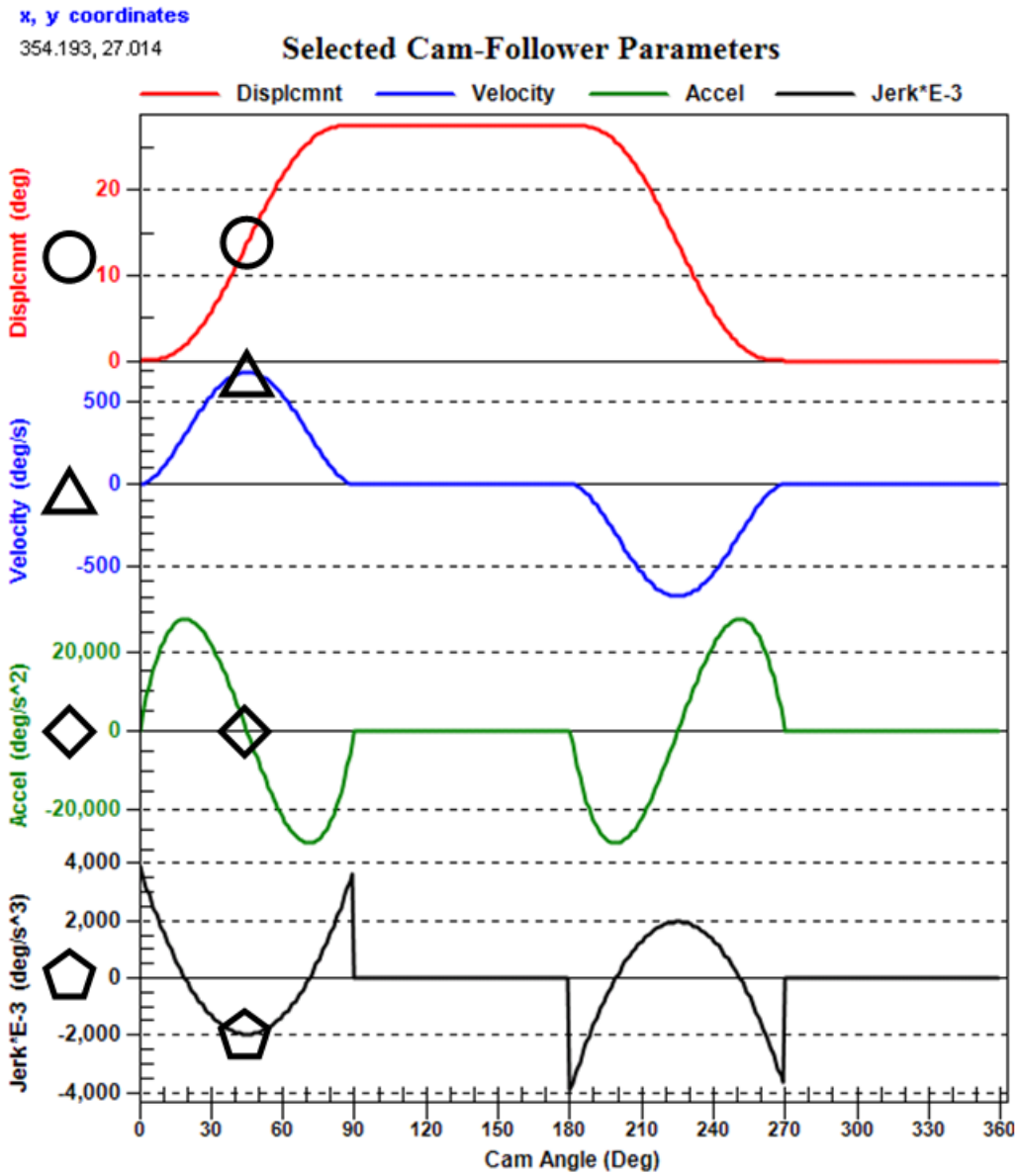

Figure 14: Cam S-V-A-J Diagram (Oscillating Follower)

6.4 Linkage Geometry

The linkage was designed based on the requirements of the cam. The servomotor was not considered as a primary design effector for this because of its flexibility; a servomotor with enough power could drive any linkage via the crankshaft without consideration to its starting

position or range of travel. Cam system design, however, has more specific requirements that limit the total possible range of plausible configurations.

To determine the ideal linkage geometry and motion configuration, the linkage and cam were constrained via geometric parameters that ensured ideal operation. Figures 15 and 16 show the variables in the system.

Linkage geometry was reliant on five variables: crank length (r_{crank}), coupler length, neutral angle (β), crank angular displacement (γ), and slider displacement (D_{slider}). Slider displacement was given to be 1.5 inches and the coupler length was determined from an acceptable crank to coupler ratio of 1:3[12]. Iterative testing using DYNACAM led to an optimum crank length of 3 inches and a neutral angle of approximately 71 degrees; the plots of the effects of varying the crank or neutral angle are found in Appendix C: Linkages. Having determined these parameters, γ was calculated using the equation below which was derived from the kinematic position analysis equations in Section 6.1.

$$D_{slider} = \left(r_{crank} \cos\left(\beta - \frac{\gamma}{2}\right) - 3r_{crank} \cos\left(\sin^{-1}\left(-r_{crank} \frac{\sin\left(\beta - \frac{\gamma}{2}\right)}{3r_{crank}} \right) + \pi \right) \right)$$

$$- \left(r_{crank} \cos\left(\beta + \frac{\gamma}{2}\right) - 3r_{crank} \cos\left(\sin^{-1}\left(-r_{crank} \frac{\sin\left(\beta + \frac{\gamma}{2}\right)}{3r_{crank}} \right) + \pi \right) \right)$$

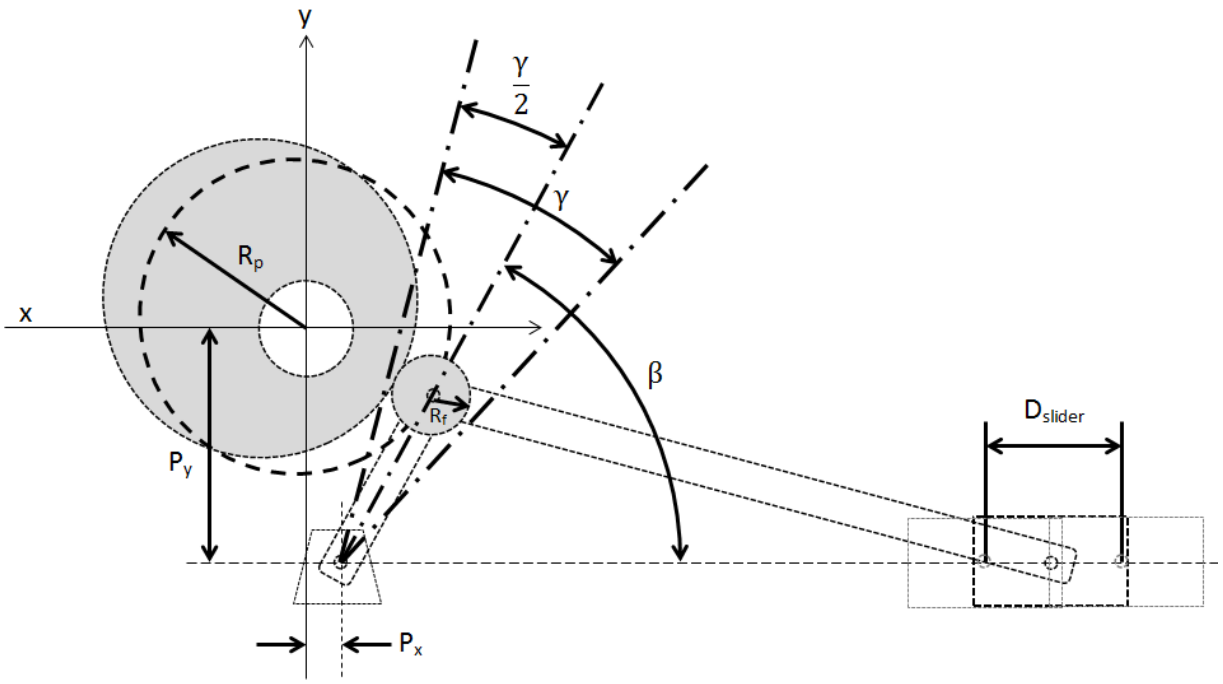

Figure 15: Linkage Geometric Variables

To position the cam relative to the fully-defined linkage, more parameters were developed to constrain the geometry. The primary geometric constraint of the cam position was that the camshaft axis was to lie on a line normal to the crank when the crank was positioned at the neutral angle. This constraint regulated the transmission angle (the complement of the pressure angle) from cam to follower-roller to be as close to 90 degrees (as it ideally should be, as a 90-degree transmission angle would result in a 0-degree pressure angle) as possible over a complete cycle.

This constraint required certain geometric quantities to be calculated: the distance between camshaft and crankshaft axes (C) and the prime radius (R_p). Prime radius is the radius of the roller-follower plus the smallest diameter of the cam surface; this quantity is often set by design because it affects pressure angle magnitude. Common practice is to make the prime

radius as large as is physically allowable on the cam (holding the roller-follower radius constant).

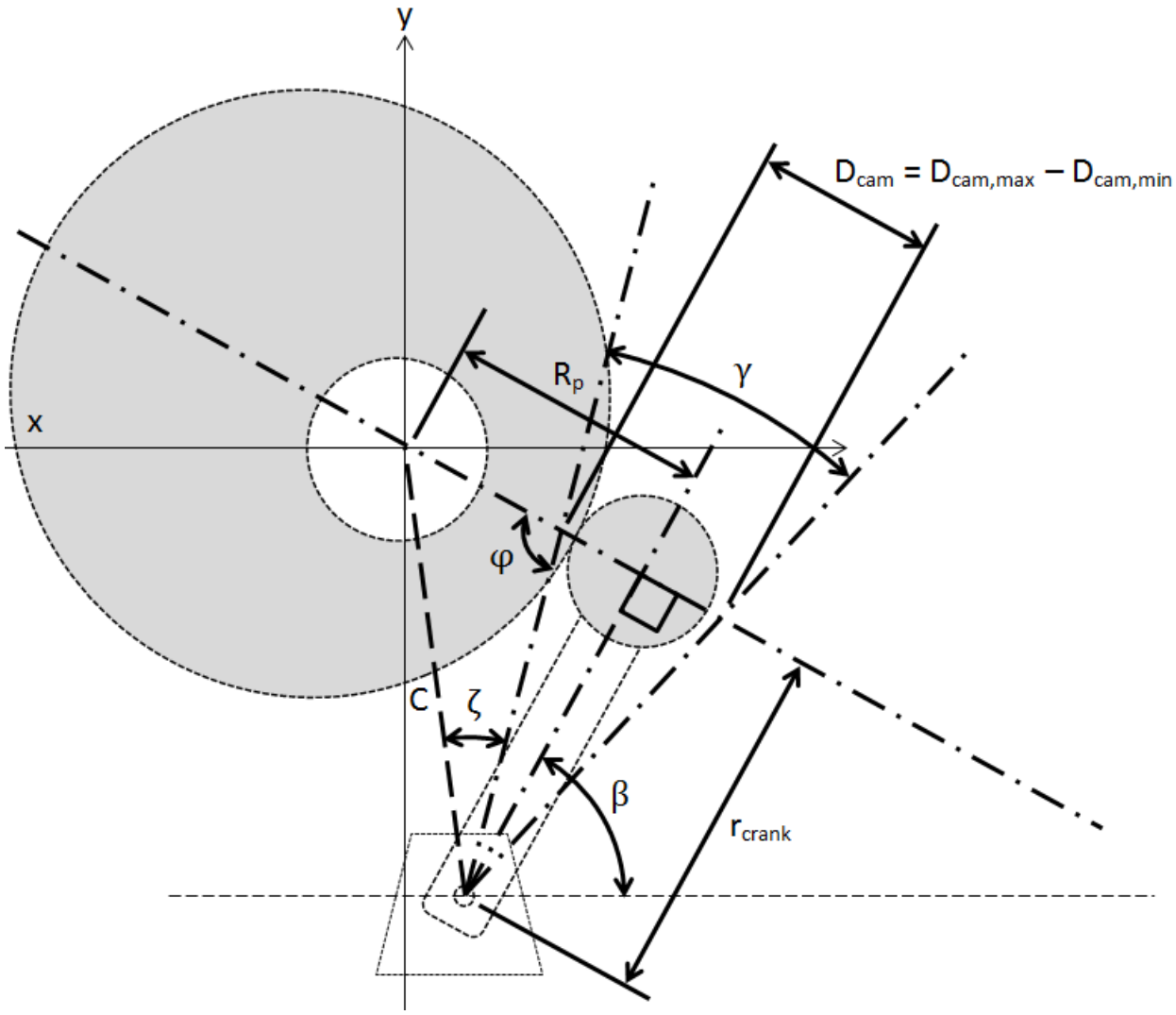

Figure 16: Cam Geometry Variables

The design team had at their disposal pre-hardened cam blanks (cam parts with everything but the motion profile cut) from the client in order to expedite the cam manufacturing process. A constraint was developed to make the prime radius as large as possible on the given cam blank, which had an outer radius of 4.125 inches (detail drawing

found in Appendix D: Linkages). This would make the cam profile's maximum radius 4.125 inches, with a minimum radius specified by the total required travel of the roller-follower.

$$D_{cam} = 2r_{crank} \sin\frac{\gamma}{2}$$

The total required travel of the roller-follower (D_{cam}) was calculated as the chord length of the motion arc of the roller-follower, i.e. its total displacement. This gave a total cam profile displacement of 1.428 inches.

$$R_p = 4.125 + R_f - D_{cam}$$

The roller-follower radius was chosen to be 0.5 inches. This is a standard roller-follower radius and was appropriate given the size of the cam and the low magnitude of the pressure angles (approximately 24 degrees maximum).

These components composed a prime radius of 3.197 inches. The distance between shaft axes (C) was then calculated to be 4.877 inches via the equations shown below.

$$\phi = 90 + \frac{\gamma}{2}$$

$$C = \sqrt{R_p^2 + r_{crank}^2 - 2R_p r_{crank} \cos\phi}$$

This distance was then projected onto the x- and y-axes (2.749 inches,-4.028 inches) in order to comply with DYNACAM's input requirements. These parameters fully defined the cam and linkage geometry.

$$\zeta = sin^{-1}\left(R_p \frac{\sin\phi}{C}\right)$$

$$P_x = C\cos\left(180 - \beta - \zeta - \frac{\gamma}{2}\right)$$

$$P_y = -C\sin\left(180 - \beta - \zeta - \frac{\gamma}{2}\right)$$

6.5 Drive-Train Selection

Link	Length (with linkage in neutral position)
Crank	3 inches
Connecting Rod	9 inches
Ground	9.57 inches

Table 1: Table of Link Lengths

With a linkage geometry (shown in Table 1) selected, determining how to drive the mechanism effectively became the next task. This task began with investigation of the equipment on hand to see if it was sufficient. It was calculated that 90 lb-in of torque would be required at the main pin to create a 30 lb force at the crank pin, presumed to be enough to actuate the mechanism. This figure would of course be adjusted later as a more accurate understanding of the mechanism was developed.

6.5.1 On-Hand Motors and Speed Reduction

The first priority while investigating the motors on hand was to determine their speed and torque characteristics so suitable speed reductions could be specified. It was known that the cam motor would need to spin at exactly 200 RPM to provide the required 200 cycles per minute, while the servomotor would have to oscillate through approximately 30 degrees at the same rate. A maximum instantaneous shaft velocity for the servomotor of 200 RPM was chosen as a benchmark, as it was judged unlikely that the servomotor driven crank would move faster than the cam, depending on the exact motion profile determined later.

The motors available were a Leeson C4D17FKSJ Permanent Magnet DC motor and a Kollmorgen B-102-A-14 brushless AC servomotor. As shown in Table 2, the Leeson motor had an unloaded speed of 1920 RPM, while the servomotor was capable of providing 0-7500 RPM.

Motor	Size (Length*Width*Height)	Mass	Max Speed	Rated Power
Kollmorgen B-102-A-14 brushless AC servomotor (www.kollmorgen.com)	14.82in*6.5in*6.67in	5.5lb	1920 RPM	1hp
Leeson C4D17FKSJ Permanent Magnet DC motor (www.leeson.com)	8.115in*2.82in*2.82in	47lb	7500 RPM	0.75hp

Table 2: Motor Capabilities

With a shaft speed range of 0-200 RPM desired from the Kollmorgen and continuous 200 RPM operation desired of the Leeson, it is clear that a discrepancy existed that necessitated some form of speed reduction for each.

6.5.2 Permanent Magnet DC Motor

In the case of the Leeson permanent magnet DC motor, specification sheets and mechanical drawings were freely available on the manufacturer's website (address listed in Table 2). While no torque curve was given, the specification sheet listed three points on that curve (displayed in Table 2 and used to compute the linear regression in Figure 17) and stated the design had "linear speed/torque characteristics over the entire speed range." The speed range provided in the data is from 1607 to 1920 RPM, with the upper value representing an unloaded maximum velocity at 90 VDC and the speeds in between corresponding to the amount of DC voltage provided to the motor and its loading. While perhaps the Leeson motor

could be run at 200 RPM, achieving that fine an adjustment with a DC motor controller might be problematic. Even if the torque curve maintained its linearity near zero RPM (certainly not the case), the achievable torque would be much less than if some kind of speed reduction was used. Furthermore, the efficiency would likely be terrible as the motor was designed to operate at speeds within its nameplate speed range. Without a speed reduction, it was clear that the desired 90 in*lb was unattainable.

Power	RPM	Amperage	Torque	Eff.
0HP	1920RPM	0.6A	0lb-in	0
1HP	1764RPM	10A	36lb-in	0.84
2HP	1607RPM	19.3A	72lb-in	0.79

Table 3: Nameplate Torque Curve for Leeson Motor

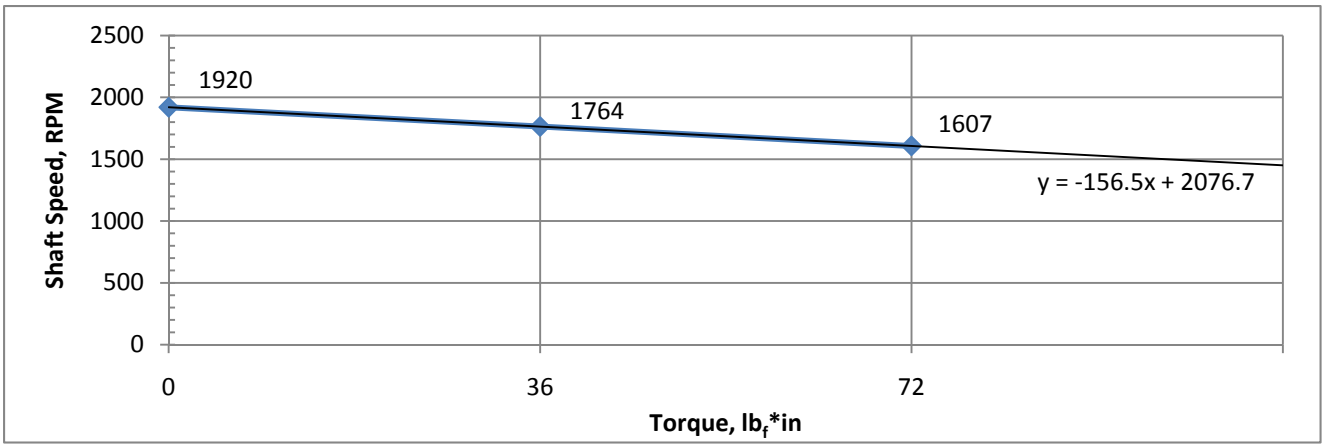

Figure 17: Constructed Torque Curve for Leeson Motor

If the motor was mounted some distance away from the camshaft, a belt or chain drive speed reduction might be feasible. In the McMaster catalog[13], the smallest driving V-Belt pulleys are approximately 2 inches in diameter. The design would require a 16 inch driven pulley to obtain 200 RPM at the minimum speed where the torque information is listed in the

specifications for the Leeson motor. A 16 inch pulley is not available, indicating that a single stage reduction would not reduce the speed enough to provide the required torque of 90 lb-in.

The task of finding a suitable gearbox to mate to the Leeson motor was simplified by the fact that the National Electrical Manufacturer's Association has established standard forms for the faceplate of motors, standardizing the attachment of gearboxes. Review of the McMaster-Carr company catalog revealed a wide variety of gearboxes that bolt directly onto the NEMA 56C faceplate of the Leeson motor[14], providing either a parallel or 90-degree offset shaft output. Some high-accuracy gearboxes with negligible backlash can cost thousands of dollars, but more reasonable models start at around $200. One promising high-efficiency spur gear reduction, part number 6481K76, had hardened steel spur gear construction yielding a 7.6:1 speed reduction and 285 lb-in of torque at the output shaft. At 1725RPM input speed, the output shaft would rotate at 226RPM, adjustable to 200RPM easily. Considering that the motor shaft might be subjected to side loads from the follower, the information that the gearbox could withstand a continuous 237lbf overhung load was noted. Since the cam torque function crosses zero, the more expensive anti-backlash gearbox might be needed for precise operation.

6.5.4 Kollmorgen AC Servomotor

The Kollmorgen B-102-A-14 brushless AC servomotor has a much higher maximum speed than the Leeson DC motor considered earlier. With the power output being comparable, it follows that the torque provided (shown in Figure 18) is much smaller.

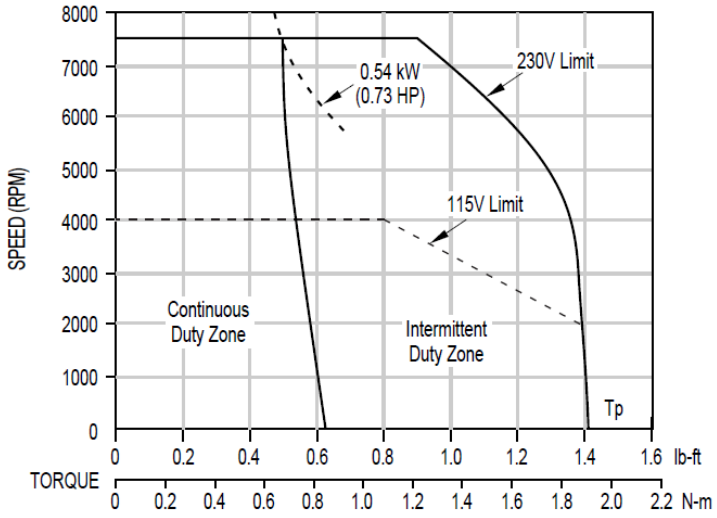

Figure 18: Kollmorgen B-102-A-14 Brushless AC Servomotor Torque Curve

There are two factors determining available torque: the motor speed and the reduction provided. At 1000 RPM, for example, the servomotor is shown to develop around 7.4 lb-in of torque without a speed reduction. With a reduction of 5:1 (by any means, be it a gearbox or otherwise) to 200 RPM, the resultant torque should be approximately 37 lb-in, which is unimpressive. At 7500 RPM, however, with a suitable reduction to bring the 7500 RPM input to 200 RPM, the output torque is close to 224 lb-in, which is much more than the acceptable 90 lb-in.

The first step in calculating available torque accurately was recording data from the Servomotor Torque Curve shown in Figure 18 above and re-creating the torque curve accurately. Each intersection of the torque curve with one of the major gridlines was added as a

point in a Pro/ENGINEER copy of the diagram. The use of Pro/ENGINEER allowed more precise measurement of the distances between these points than simply reading the graph without the assistance of a computer. With the precise distances between the major gridlines also measured, the curve was re-created in Microsoft Excel.

After recreating the torque curve from the data given by the manufacturer, the reductions in speed necessary to bring the output speeds to 200 RPM was calculated by dividing the output speed through to obtain the ratio. That ratio was then applied to the original torque curve repeatedly, reduction by reduction, to see the effect of each reduction on torque over the speed range. With an ideal reduction in speed, the inverse of the ratio's impact on speed is applied to the output torque relative to the input. The product is a set of torque curves incorporating the possible speed reductions.

Regardless of which reduction is chosen, the motor will have to cover much of the possible output speed range (0-200 RPM, represented by the bold lines on each curve in Figure 19 below) through each cycle of the machine, as the servomotor must repeatedly reverse directions. The dotted lines are for reference only, as they represent speeds the servomotor is not expected to operate at.

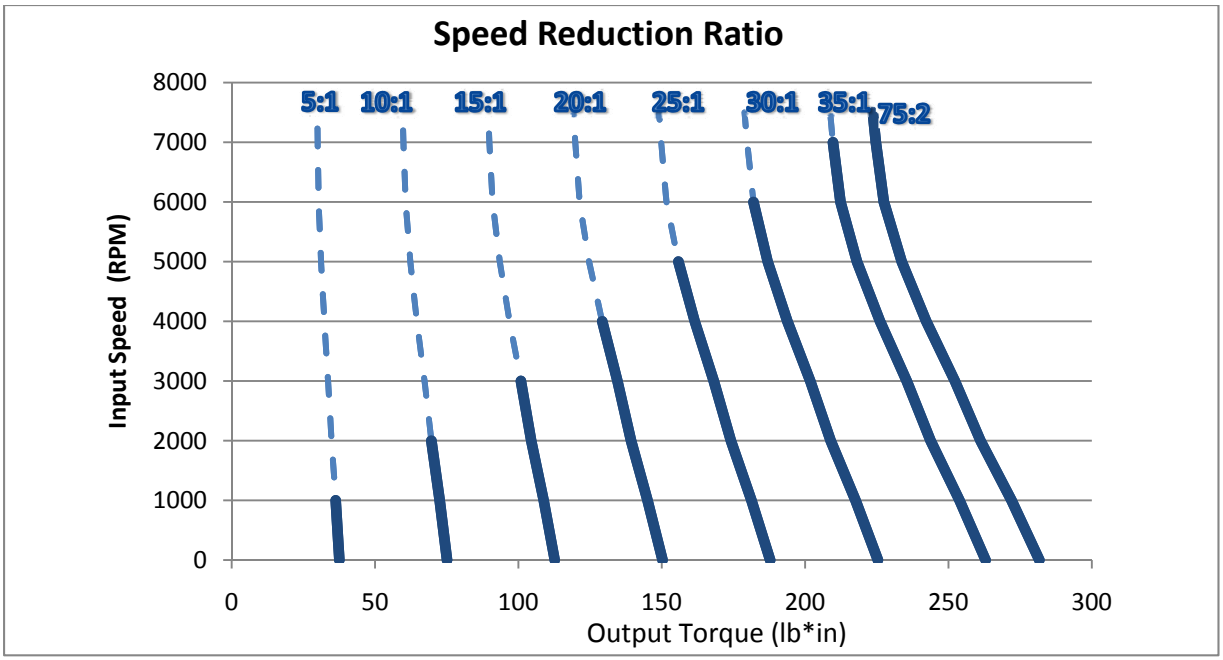

Figure 19: Torque Curve with Various Reductions Applied, Kollmorgen B-102-A-14 Brushless AC Servomotor

Physical packaging for the Kollmorgen servomotor was more problematic than that for the Leeson motor. Instead of NEMA, the relevant trade association is the International Electrotechnical Commission, a global consortium using the Metric system instead and promulgating a similar but distinct standard set of form factors for motors. It was eventually determined that the faceplate was an IEC B5 flange. Since backlash in a servomotor setup would be unacceptable, either a low-backlash gearbox or a belt drive would be required. While there were anti-backlash gearboxes available from Worcester Polytechnic and the project's sponsor, they fit the NEMA form factor instead, and a conversion plate would be needed to use them. Obtaining such a plate would be problematic, as the B5 flange is much smaller than the NEMA 56C flanges the boxes were intended for and such a conversion plate would need to be designed and machined, rather than purchased. It was decided that a toothed belt system might be simpler to execute.

6.5.5 Timing Belts

In Design of Machinery[15], caution is given against using v-belts for any application where correct phase angle is critical. The application at hand requires a high degree of phase angle maintenance. Thus, a timing belt was chosen as an alternative. Several tooth profiles are in common use, with trapezoidal teeth being some of the most time-tested, having a long history in automotive use. Trapezoidal pitch belts are series X, L, H, and XH in the U.S. system and series T in Metric. AT-series Metric belts provide a longer trapezoidal tooth for higher torque applications.

A timing belt moving at constant speed around a pair of pulleys will cause vibration: there is no acceleration as the timing belt travels in a straight line at constant speed, unsupported between the pulleys, but there exists a transition to finite acceleration as the belt begins to wind around the second pulley. This jump between zero acceleration and finite acceleration means a discontinuity in the jerk function (the time-derivative of acceleration), and thus vibration, whether or not this problem is ameliorated with curvilinear profiles that ease the transition.

In Figure 20, a selection guide[16] for timing belts is shown with a dotted line at the horsepower of Kollmorgen AC servomotor (0.75hp) and a diagonal-line textured box around the expected shaft speed. The XL series is designed for transmission of more power than expected, and the H series would clearly be insufficient at the upper end of the expected speed range, which could reach 7500 RPM. From the chart it is seen that the L series would be acceptable. From the speed reduction ratios considered in Kollmorgen AC Servo section above, a two-stage 36:1 reduction with L series timing belt pulleys is the optimal choice.

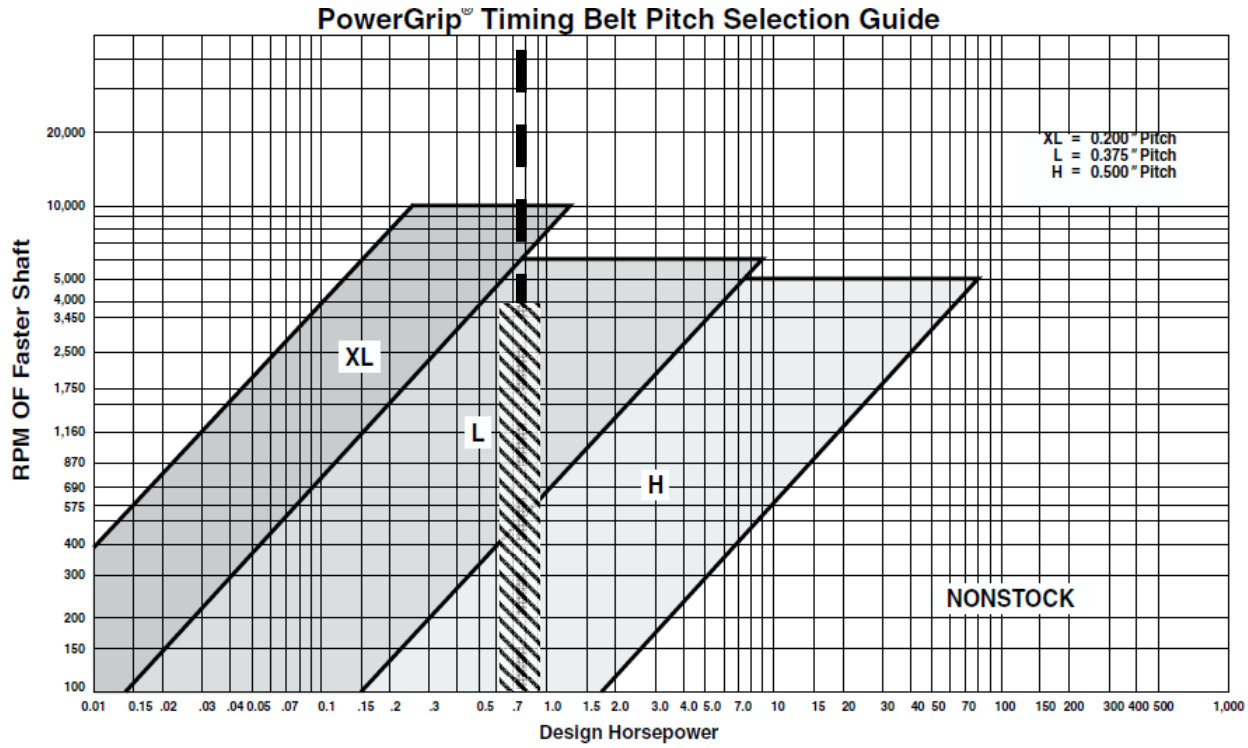

Figure 20: Timing Belt Selector[16]

6.5.6 Potential Single-Motor Drive Trains

It was observed that a functional design could be realized with the use of only one motor to power either the camshaft or the crankshaft at different times, i.e. actuating either the cam or the crank. From the analysis considered above, the Kollmorgen brushless AC servomotor can deliver the required torque through a two-stage timing belt reduction. The next design problem was the question of how to switch between the two configurations and leave the un-driven side fully supported. Several solutions were considered.

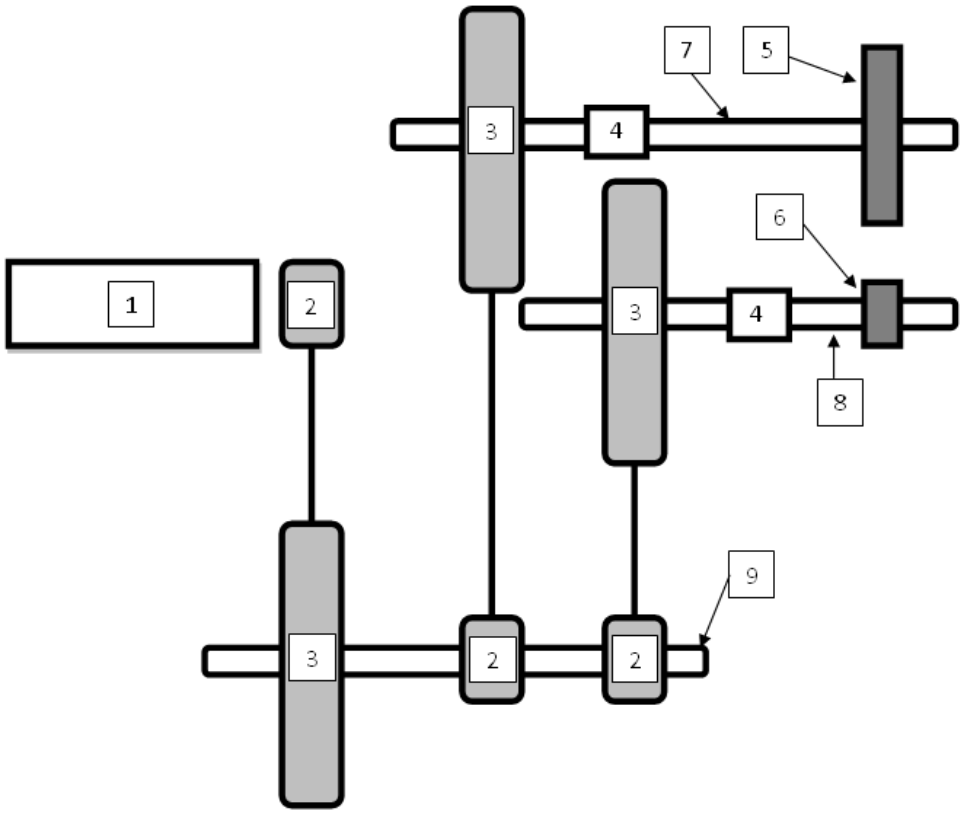

Figure 21: Single-Motor Coupling Version System Diagram

Number	Description	Quantity
1	Brushless AC Servo Motor	1
2	1.194 Pitch Diameter Timing Belt Pulley	3
3	7.162 Pitch Diameter Timing Belt Pulley	2
4	Two-Piece Shaft Coupling	2
5	Double-Dwell Cam	1
6	Crank	1
7	Cam Shaft	1
8	Crank Shaft (also referred to as a main pin when discussing planar linkage analysis)	1
9	Transmission Shaft	1

Table 4: Bill of Materials for Single-Motor Coupling Version System Diagram (Fig. 21)

The first solution, diagrammed in Figure 21, was to use a single coupling to connect either one of two driven shafts, fully supported by pillow block bearing assemblies. Both of the second stages of the timing belt speed reductions would remain installed and tensioned, obviating the need for re-tensioning.

This design compromise carries with it the problem of maintaining phase angle during switching of drive modes: the couplings could be attached to position the main pin at any phase relative to the servomotor. A readily apparent solution is to have a fixture that attaches to the spring support and the slider very precisely, as shown in Figure 22. Since the spring constant would only be 15lb/in, it is possible to depress the crank by hand by pressing on the crank pin, line up precisely drilled holes on the slider and spring support with the tooling pins on the fixture, and slide the fixture into position. Once engaged, the coupling could be attached and the cam removed, the angle being chosen to give clearance to install the cam with the phase angle between the main pin and mechanism fully preserved .

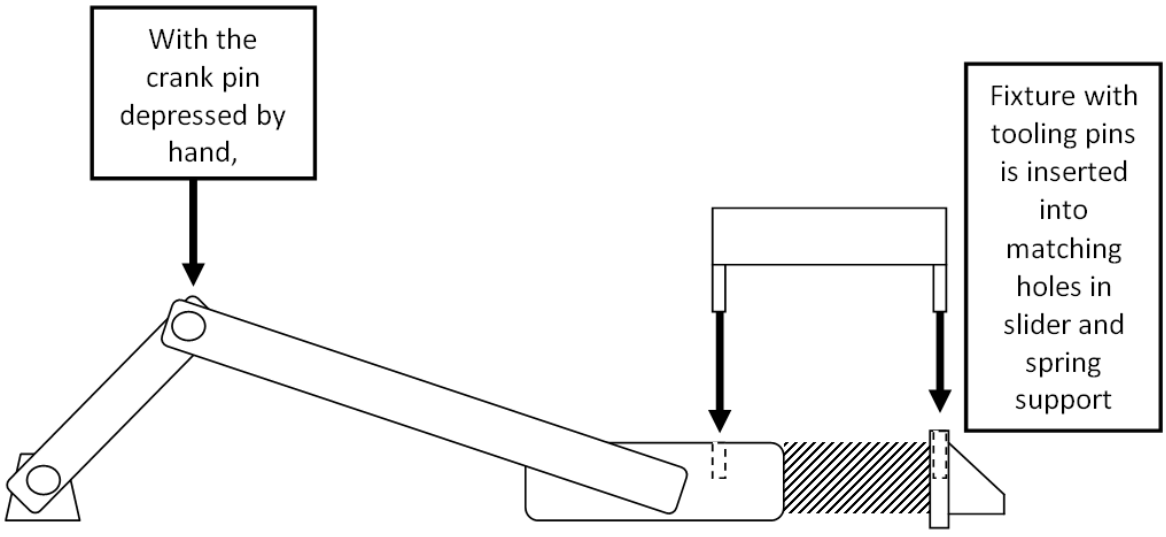

Figure 22: Phase-Lock Fixture Diagram

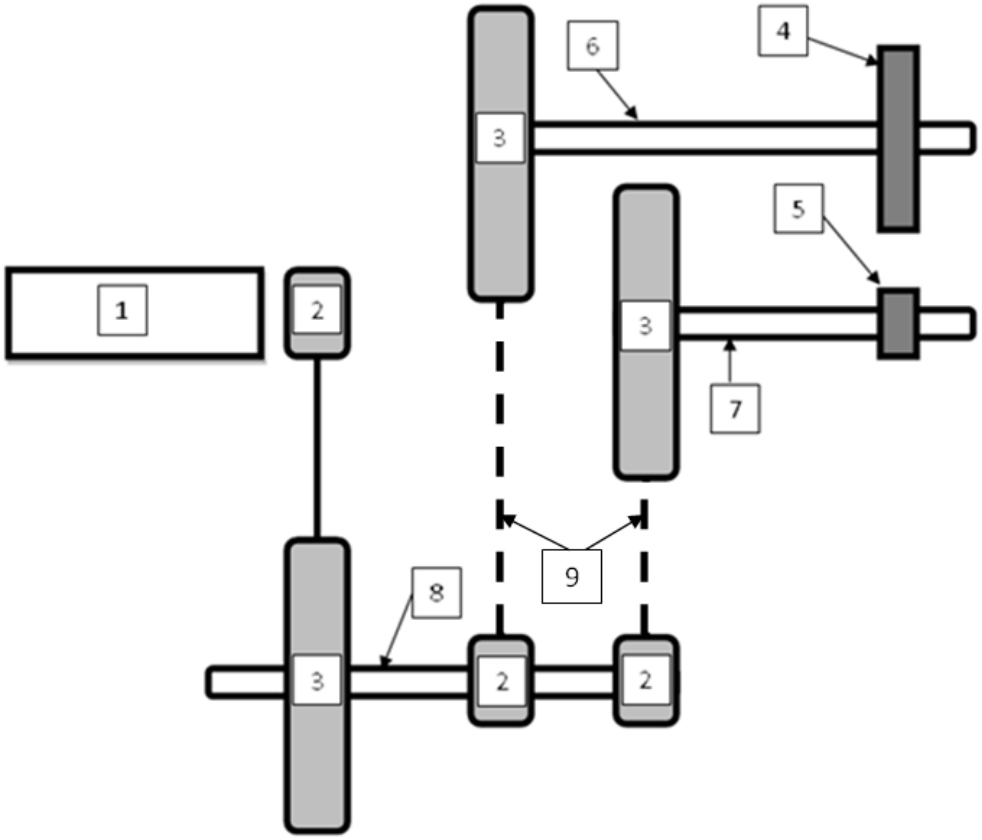

Figure 23: Single-Motor Belt Version System Block Diagram

Number	Description	Quantity
1	Brushless AC Servo Motor	1
2	1.194 Pitch Diameter Timing Belt Pulley	3
3	7.162 Pitch Diameter Timing Belt Pulley	2
4	Cam	1
5	Crank	1
6	Cam Shaft	1
7	Crank Shaft (also referred to as a main pin when discussing linkage analysis)	1
8	Transmission Shaft	1
9	Possible Timing Belt Positions	2

Table 5: Bill of Materials for Single-Motor Belt Version System Block Diagram (Fig. 23)

An alternative to the moving a coupling from one position to another to switch mode is to use pulleys in a cantilevered position (diagrammed in Figure 23) so that a belt can be installed on either of two different pulleys, switching between the two configurations. In this case, the transmission shaft is positioned so that the same length belt could be used for both pulleys.

This configuration does not avoid the phase angle problem, however. It also adds the issue of how to remove and add tension to the belts without too much effort on the part of the person switching back and forth. Spring tensioners were found[17] that would push an idler pulley against the flat side of the timing belts from the ground plane, but this solution was discarded in the end as the belts would be in reciprocating motion, and would need equal tensioning on both sides.

Fixed center distances between shaft axes have been used successfully in timing belt applications, but the difficulty of installing or removing the timing belt and the advised difficulty of correctly implementing this option instead suggested some means of moving the assemblies relative to each other, which must take into account the fixed relation between the cam and crank shafts as part of the required linkage geometry.

6.5.7 Potential Two Motor Drive Train

An alternative to a one-motor solution to the motion problem is to use separate motors to drive the cam and crank. A 20:1 gear box mounted to the faceplate of the DC motor would be used to provide sufficient torque. Power transmission to the cam shaft would be achieved with a V-belt. This V-belt could be left attached even when the mechanism is in servo mode if the cam-driving motor is stopped and locked in the correct position, as the need for clearance from the crank arm is met by removing the follower instead. When the mechanism is in cam mode, the follower will be reinstalled and the servo side's timing belt will be removed. This allows the crank shaft to oscillate back and forth freely. While this design requires another motor controller, it is a much cheaper DC motor speed control, not a servo driver. The gearbox and V-belt pulleys required are also inexpensive, and the system is easy to design. While the added weight of another motor is significant, it is small in comparison to the mass of the system and would not make the Cam Servo Test Machine much more difficult to move. The use of a second motor would be thus be an acceptable design compromise with regard to the overall system.

6.6 Drive Train Decision

After modeling these configurations, a drive system was selected. It was readily observed that the coupling design added far too much rotating mass. The couplings themselves contributed, but the more important contributor was the near half of the coupling camshaft which would have to be spun while the servomotor configuration was being used. Furthermore, with the added complexity of machining and the introduced additional possibility of non-co linearity of shafts near the couplings (which would result in the entire mechanism seizing up),

the belt choice was clearly the better of the two single-motor solutions. While a two-motor solution would be acceptable, it lacks the elegance of a one-motor solution to the problem, which has the added cachet of using only the minimum equipment possible.

6.7 Servomotor Analysis

In order to determine the feasibility of a servomotor driven system, extensive modeling of the system was performed. In the case of the cam design, the process was simplified by the program DYNACAM which allowed the motion profile to be designed almost automatically given a set of constraining parameters. With the complete operation of the cam-mode linkage motion already determined, the servomotor was designed to replicate the cam driven output motion.

The challenge of this motion replication was not kinematic; a fully-featured servomotor is capable of outputting virtually any motion profile it can be programmed to do. The dynamics of the system required design decisions such as the two-stage speed reduction from the servomotor to the crank shaft discussed in Section 6.5. Given the Kollmorgen servomotor's limited power capabilities, ensuring its ability to run the single-motor CSTM was a design imperative.

The calculations required to answer this question began with a complete derivation of the cam's 3-4-5 polynomial motion function with respect to the crank angle (reference Appendix D: Linkages for full calculations). Such polynomial equations are derived by setting boundaries on (in the cam's case) follower's position, velocity, and acceleration relative to the cam's rotational progress. The design required that the servomotor match the cam's follower

motion profile; this necessitated describing the motion of the follower with an input at the crank shaft rather than at the roller follower surface.

To do this a 3-4-5 polynomial function was constrained for position using crank angles to describe the rise, fall, and two dwells. The velocity and acceleration were constrained to be zero at the end of each motion segment, which were the same constraints used to develop the cam profile. The results of the derived position, velocity, and acceleration were then checked against DYNACAM's calculated follower motion profile for accuracy.

Once the motion of the crank was defined, a complete kinematic analysis of the linkage was performed using techniques described in Section 6.1. This was a straightforward process; all linkage motion could be described in terms of the crank angle.

For the dynamic analysis, the most important factor for design feasibility was the required input torque because of the low power of the servo motor and the high quantity of rotating mass in the system. Having done the kinematic analysis, the linkage was then dynamically modeled using estimates of component dimensions for mass and mass-moment-inertia inputs. The preliminary calculations utilized a variant of the Lagrange energy equivalence method for calculating the dynamics of a mechanism.

A lumped mass model was constructed (see Figure 24). The crank, in pure rotation, was modeled as a rotating disc by transferring the mass moment about its center of gravity ($I_{CG,crank}$) to the input link via the parallel axis theorem. The coupler was more complicated, as it was in complex motion. A slider crank however has motion that allows this complexity to be relatively easily broken down into a very close approximation by modeling the coupler as a rotating disc (by transferring the mass-moment-inertia about its center of gravity to the wrist pin) that is also

in linear translation at the slider pin. The aforementioned kinematic analysis facilitated this method; such a dynamic model requires the angular velocity of the coupler and the linear velocity of the slider block to be known. Combining all the parts of this dynamic model resulted in a highly accurate mass model that was a function of the estimated mass properties and time-changing velocities and angular positions of all the components.

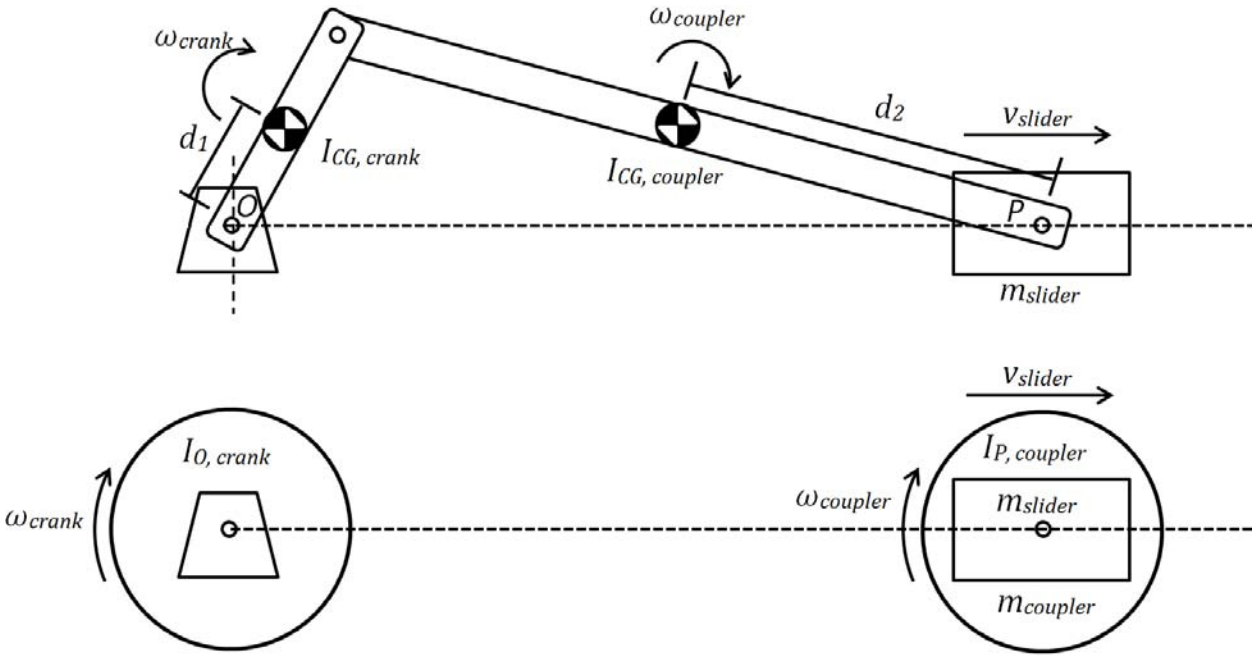

Figure 24: Linkage Lumped Mass Model

The final component of the dynamic model was the torque requirement created by the return spring. The spring constant and preload had been calculated for the cam system. The torque calculation was done kinetostatically i.e. independent of the mass or motion properties of the system. This process is described for gas force in a slider-crank in Design of Machinery[18] and was in the case of this design a function of the time-varying slider displacement and coupler angle.

$$I_{eq,crank} = \frac{I_{O,crank}\omega_{crank}^2 + I_{P,coupler}\omega_{coupler}^2 + \left(m_{slider} + m_{coupler}\right)v_{slider}^2}{\omega_{crank}^2}$$

The equivalently modeled mass-moment-inertia (shown above) of the system about the crank shaft was then multiplied by the required angular acceleration of the crankshaft as defined by the polynomial function. The kinetostatic spring torque was added to that figure in order to get a final torque requirement.

$$T_{required,crank} = I_{eq,crank}\alpha_{crank} + T_{spring}$$

The maximum required torque at the crank shaft was found to be initially approximately 112lb-in. with a maximum velocity of approximately 130 RPM. These requirements indicated that a speed reduction of significant magnitude would be necessary to bring the torque requirements into the servomotor's capability. With the selection of the speed reduction method discussed in Section 6.5, it remained to implement the methods. The first reduction design was a two-stage belt-based system with a total reduction of 36:1. Such a speed reduction would theoretically magnify the available torque at the crank by 36 minus the inertial torque requirement of the additional rotating mass of the reduction apparatus. In order to get such a large reduction, the initial design contained two large cast-iron pulleys with pitch diameters of 7.162 inches and two small steel pulleys with pitch diameters of 1.192 inches.

To add the speed reduction apparatus to the model and calculate a required torque for the servo motor, the crank angular velocity (ω_{crank}) was multiplied by the appropriate pulley pitch diameters in the energy equation (shown below). This is because the pulleys reduce the servo speed to the crank; thus, the transmission shaft spun at roughly 6 times and the servo spun roughly 36 times the crankshaft. For the servomotor and transmission shafts, the mass-moment values (I_{servo} and $I_{transmission}$) were taken directly from the material-accurate Pro/E CAD models as they were in pure rotation and required no further modification.

$$I_{eq,servo}$$

$$= \frac{I_{servo}\left(\left(\frac{7.162}{1.192}\right)^2 \omega_{crank}\right)^2 + I_{transmission}\left(\frac{7.162}{1.192}\omega_{crank}\right)^2 + \left(I_{eq,crank} + \frac{T_{spring}}{\alpha_{crank}}\right)\omega_{crank}^2}{\left(\left(\frac{7.162}{1.192}\right)^2 \omega_{crank}\right)^2}$$

$$T_{required,servo} = I_{eq,servo}\left(\left(\frac{7.162}{1.192}\right)^2 \alpha_{crank}\right)$$

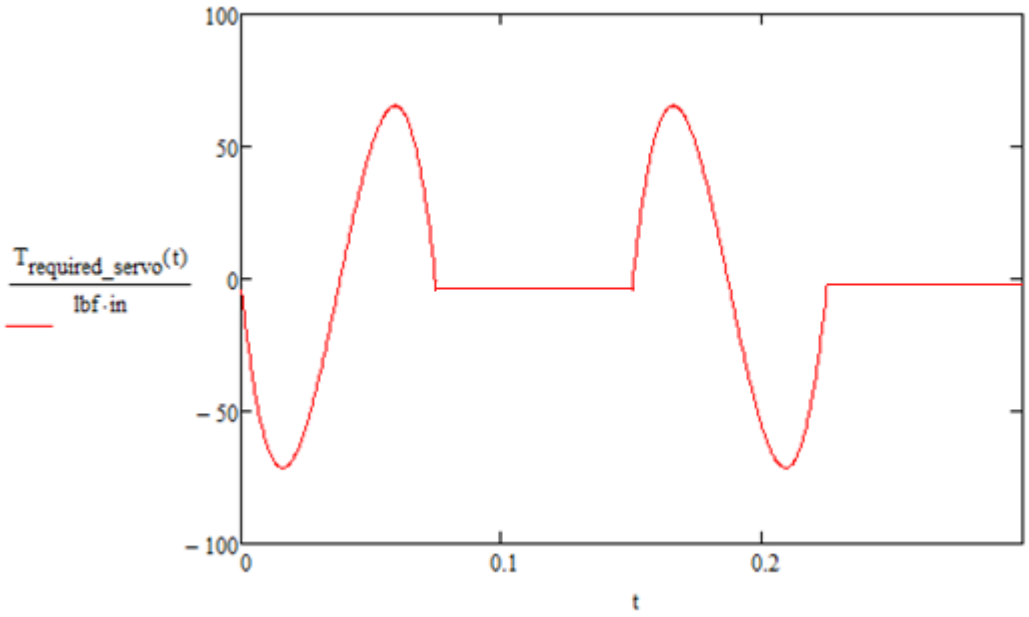

Figure 25: Required Servo Torque Curve

Including the mass-moments of these components in the dynamic model to reflect the rotating inertial load back to the servo shaft while accounting for the speed reduction at each stage resulted in a peak torque requirement of approximately 73 lb-in at the servo shaft, as shown in Figure 25. The RMS torque of the Kollmorgen servomotor was approximately 7 lb-in across a wide range of speeds with a peak of 21 lb-in, well below the requirement. This constituted a redesign of the timing belt train in an attempt to significantly reduce the amount of rotating mass in the system while still reducing the servo speed enough to run the linkage.

6.7.1 Inertial Mass Reduction

As dynamics calculations on the drive train progressed (see Appendix E), it became clear that the torque requirements did not significantly depend on the load at the output end of the drive train. The primary inertial load turned out to be the mass moments of inertia of the pulleys, and to a lesser extent, those of the shafts. A small rotational mass added at the input end of the system produced much more of a load on the servomotor. Calculated peak torque required was close to 60in-lb, when only 7in-lb could be sustained continuously by the selected servomotor. Rapid redesign of the system was needed.

The first step was to replace the steel 1.194 Pitch Diameter pulley mounted directly to the servomotor (Part #17 in Drawing 1-2, Section 6.8, below) with a lighter-weight one. A pulley was found from Nordex, Inc. that had an aluminum boss in the center surrounded by hollow glass-filled nylon. Revolved-solid models reconstructed from the section views in catalog drawings (shown in Appendix G) indicated that the mass moment of inertia of the pulley relative to the steel pulleys originally used could be reduced by 84 percent, from .046 lb-in^2 to .0074lb-in^2, as the mass of the composite pulley is concentrated close to the axis of rotation.

The large cast iron pulleys present on the original design added a mass moment of inertia of 48.5in-lb^2 each. It was possible, however, to machine out much of each pulley and reduce its mass moment of inertia to only 12.6in-lb^2, a reduction of 74 percent. A pulley modified in this way is shown in Drawing 1-1 in Section 6.8, below. This was not enough reduction in rotational inertia for the servomotor end of the drive train, however, and an easy replacement of the pulley speed reduction was not possible. The largest nylon replacement available had a pitch diameter of 3.820 inches. The ratio of a speed reduction using nylon 1.194

and 3.820 pitch diameter pulleys and a reduced mass iron 7.162 pulley was calculated as follows:

$$\left(\frac{3.820}{1.194}\right)\cdot\left(\frac{7.162}{1.194}\right) = 19.191$$

The 20:1 torque curve shown in Figure 19 in Section 6.5.4 above approximates the torque available at the main pin. The achievable 140-150 lb-in with this ratio was more than the desired 90 lb-in discussed in Section 6.5, it was decided that a ratio of 19:1 would be acceptable

Replacing the 7.162 inch pitch diameter cast iron pulley with the smaller 3.820 inch pitch diameter nylon pulley (Part #19 in Drawing 1-2, Section 6.8, below) reduced rotational inertia from 12.6in-lb^2 to 0.40in-lb^2 at the drive train. As shown in Figure 26, the RMS torque was reduced to just over 6 in-lbs, just within the servomotor's capability to deliver.

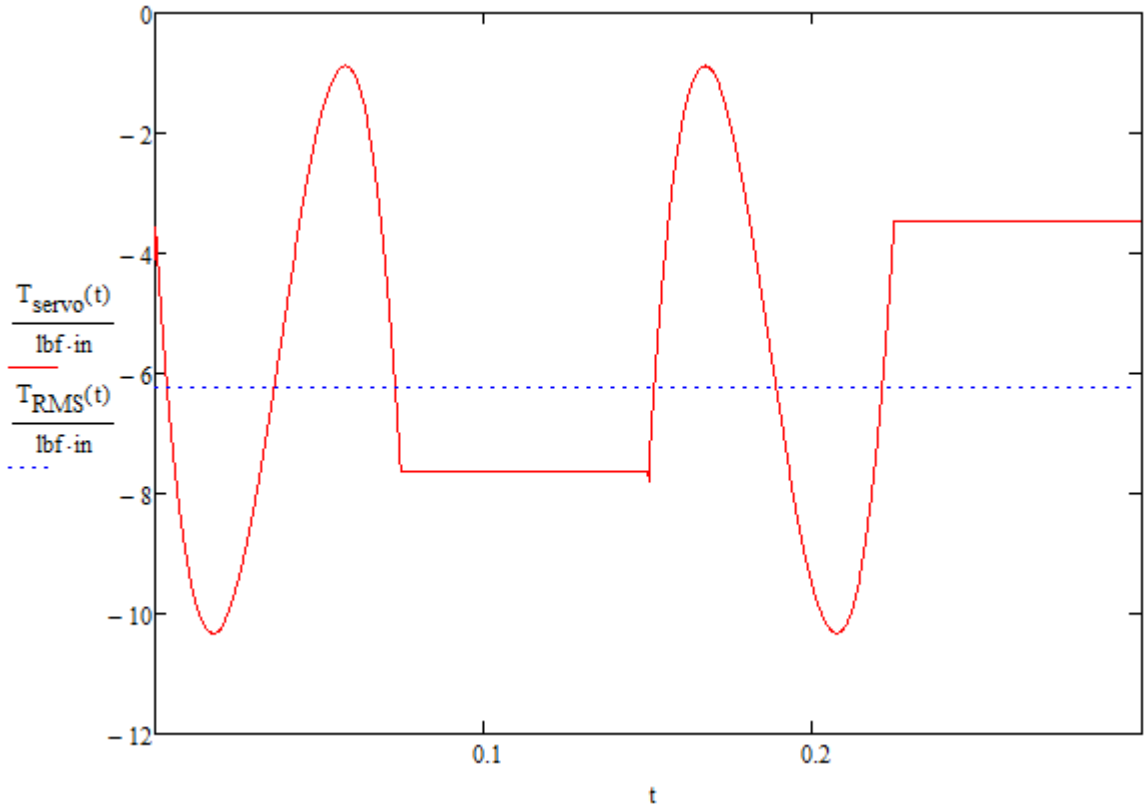

Figure 26: Torque Required from Servomotor

6.7.2 Transmission Shaft Mass Reduction

Once the mass reduction of the speed reduction train had been completed and preliminary feasibility calculations had indicated that the servomotor would be able to drive the system, the mechanism was packaged in Pro/ENGINEER. The packaging process further reduced some of the rotating mass by shortening shafts where allowable. The finalization of the geometry and materials selection for the mechanism prompted a more accurate determination of the required torque.

The initial energy model was verified through Newtonian force equations described in Section 3 of Machine Design[19]. The dynamic analysis showed the maximum required torque at the main pin had been reduced to approximately 93lb-in. and the required torque at the servo peaked at 10.33lb-in. with a peak RMS of 6.22lb-in. and a maximum speed of approximately 2470 RPM, well within the servomotor's capabilities.

6.7.3 Theoretical Servomotor Accuracy

Feedback methods for motor control fall mainly into two categories: resolvers and encoders. Encoders are further divided into absolute and relative, each with different possibilities for electronic configuration. An encoder is an assembly centered on a disc with markings read by photoelectric sensors. Encoders incorporate at least two detectors, allowing seeing which direction a motor is moving by monitoring transitions between marked portions of the encoder disk as read by the two sensors. This also allows "quadrature multiplication," effectively multiplying the line count by four. An absolute encoder has a third sensor track on the disk to provide a zero reference point allowing at any given time at what angular position the shaft is, a relative encoder can only compare two readings and describe the displacement.

An important distinction is that when an absolute encoder is turned on, absolute position is not known until the first zero reference mark is crossed.

The servomotor available has a resolver. A resolver takes the form of two static windings interacting magnetically with the shaft. The resolver is energized by the servo drive, and the phase separation of the two generated signals is compared to provide position at all times. A resolver is also mechanically much simpler, and thus is suitable for harsh environments. The resolver signal is analog, so the resolution provided by this arrangement is determined by the resolution of the servo driver's analog-to-digital conversion capabilities. The present servo driver has a 12-bit capacity, meaning that it registers 0.08 degrees of rotation.

This does not mean that the resolver is accurate to that resolution. That is only the theoretical maximum accuracy of resolver feedback for this case. In motor application guides, typical resolver error is listed as 14 arc-minutes, or 0.233 degrees. The guide consulted[20] goes on to state that "resolver error is also cyclic, meaning the positioning error will vary by the full range +14 to -14 arc-min for this example for one complete revolution of the shaft." This was helpful for the application at hand, absolute position is critical, an accumulation of error (as is inevitable with an encoder) requires some kind of homing procedure.

In a system with speed reduction, the accuracy required of the resolver is reduced. Since the error introduced by the resolver applies to the shaft angle, a speed reduction (which increases the amount of angular travel necessary to effect a similar change in the crank angle) increases the effective precision of the position of the crank. The minimum change in crank angle registered by the resolver is referred to here as the "crank resolution," and is much smaller than the resolution of the resolver.

Speed Reduction Ratio	Resolver Resolution (degrees)	Crank Resolution (degrees)	Magnitude of Resulting Displacement at Follower (Inches)	Magnitude of Resulting Displacement at Slider (Inches)
0	0.233	0.233	1.22E-02	1.28E-02
1/5	0.233	0.047	2.44E-03	2.57E-03
1/10	0.233	0.023	1.22E-03	1.28E-03
1/15	0.233	0.016	8.13E-04	8.56E-04
1/19	**0.233**	**0.012**	**6.42E-04**	**6.76E-04**
1/20	0.233	0.012	6.10E-04	6.42E-04
1/25	0.233	0.009	4.88E-04	5.14E-04
1/30	0.233	0.008	4.07E-04	4.28E-04
1/35	0.233	0.007	3.49E-04	3.67E-04
2/75	0.233	0.006	3.25E-04	3.42E-04

Table 6: Effect of Resolver Error Across Various Speed Reductions on Mechanism Precision

With position analysis performed previously, calculating the effects of uncertainly of input shaft position due to the resolver was simply a matter of applying the equations derived and the laws of cosines. The results, shown in Table 6 above, show that while the input shaft may be off by 0.233 degrees, the crank will be out of angular position by some much smaller amount. At the chosen 19:1 reduction, the worst-case crank resolution will be 0.012°, less than 1 arc-minute. The displacement of the roller follower that would be unnoticed by the resolver would be 0.000642 inches, with a corresponding positioning error at the slider of 0.000674 inches, an order of magnitude less than the specified precision of the mechanism, which is 0.005 inches.

6.8 Packaging

With the drive train selected, it remained to package the mechanism in a sensible way. Key criteria for a successful packaging were the following:

1. Able to be assembled repeatedly
2. Sturdy enough to withstand operation
3. Facilitates changing of mode (belt tensioning included)
4. Minimum number of parts

Based on the first three design criteria, it was decided to design two subassemblies: a cam and linkage enclosure, the "driven mechanism subassembly," and a servomotor enclosure, the "driving mechanism subassembly". Both subassemblies were mounted to a large aluminum base plate. This configuration is shown in Drawing 1-1 (Cam-Servo Test Machine, Full Assembly, Cam Drive Configuration).

Each subassembly has two sets of opposing plates, boxing each in and improving rigidity. By machining the opposing plates together, the geometric relationship between the various features could be maintained across each plate, and dimensions to the edge of each piece for critical features (such as holes for sleeve bearings) could be ensured to be equal. This is in contrast to earlier attempts, which would have had the mechanism consist of shafts mounted on pillow blocks and bolted down, with associated problems with repeatable assembly, as each pillow block had to be located precisely. With tooling pins to take the shear and moment loads, all screws in the assemblies were intended to be subjected only to tension.

6.8.1 Driving Subassembly

The Driving Subassembly of the Cam-Servo Test Machine is based on the simple box configuration discussed in Section 6.8, with one modification: one corner of the box has been "scooped" out to accommodate the tapered bearing of the timing belt pulley while the mechanism is being driven by the servomotor. The servo was mounted to a pocket in the "servomotor plate," with the plate opposing it designated as the "servomotor opposing plate."

The L Timing Belt inside of the subassembly needed to be tensioned properly. This was initially accomplished by making the clearance holes for the bolts used to affix the servo into slots. The servo would then have to be held away from the matching pulley and four nuts tightened in such a position. A more elegant solution (shown in Detail A of Drawing 2-2) was suggested by Professor Norton: allow one bolt to act as a pivot so that only the opposing bolt would need to be tightened to fix the motor. The central hole is large enough to clear the pulley when assembled to the motor shaft (space and mass moment of inertia on that shaft being at a premium, introducing a coupling would undesirable). In this manner, the belt can be conveniently tensioned before completed assembly of servomotor plate with the rest of the subassembly.

6.8.1.1 Transmission Shaft

The transmission shaft is machined to several diameters along its length to accommodate the two nylon timing belt pulleys, which are fixed with a key to keyways on the shaft and a setscrew to press the key into place. The boss of the 3.820 pitch diameter pulley sits directly against a step up in shaft diameter (as shown in Drawing 2-4A), with the other end against a oil-impregnated bronze thrust bearing and the servomotor plate. The other end of the

transmission shaft inside of the enclosure is fixed translationally with a shaft collar and thrust bearing against the servomotor opposing plate. Both shaft ends pass through bronze sleeve bearings press fitted into the support plates. The only sliding surfaces of the subassembly are made of oil-lubricated bronze, which will provide smooth and quiet operation, without the noise that might be introduced by rolling element bearings. Driven Subassembly

The linkage geometry having been determined, packaging of the linkage, as shown in Drawing 3-1, consisted only of modification of simple members and packaging them within an enclosure, as discussed in Section 6.8.

6.8.1.2 Linkage Members

The linkage members are key components in the Driven Subassembly of the C.S.T.M. To clear the cam with the main pin position used to calculate cam geometry, the crank (Figure 27) needed a somewhat unusual shape: a three sided box section with a cross-member offset from the center plane.

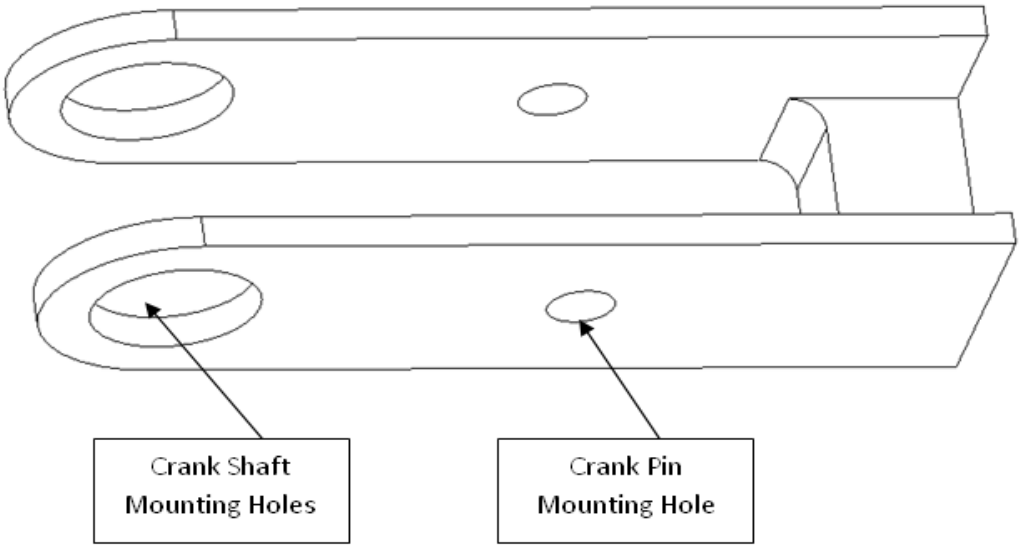

Figure 27: Crank Geometry for Cam Servo Test Machine

The connecting rod took the shape of a simple rounded member, the only complication being the yoked configuration of the crank pin joint shown in Figure 27. The slider subassembly (discussed and shown later) is attached to the connecting rod with a simple journal bearing joint.

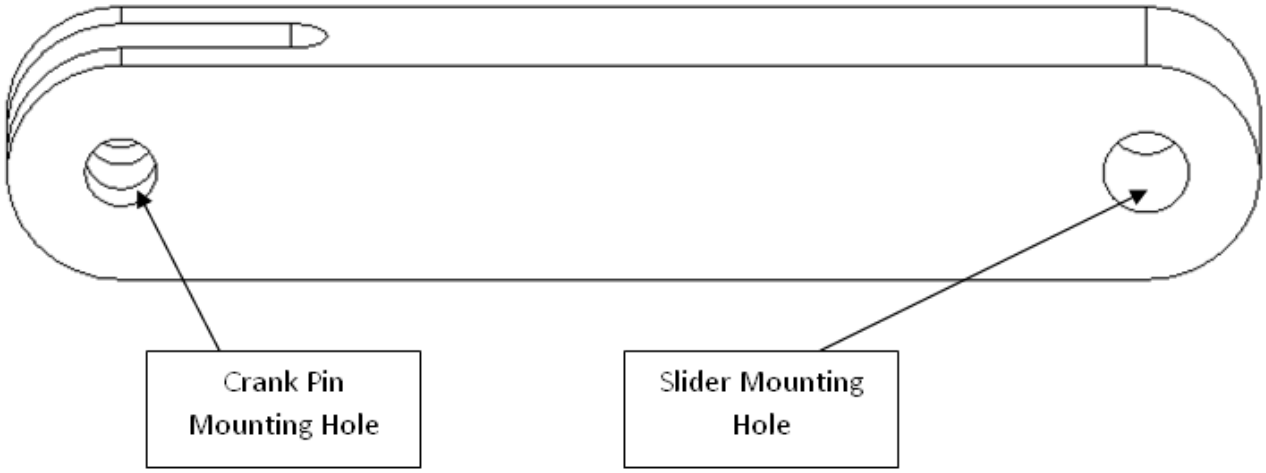

Figure 28: Connecting Rod Geometry for Cam-Servo Test Machine

6.8.1.3 Cam and Crank Shafts

The cam and crank shafts, within the Driven Subassembly, are mounted similarly to the transmission shaft, with each shaft passing through sleeve bearings in the supporting plates of the enclosure. The shafts are located translationally by shaft collars which are spaced from the plates with thrust bearings. In Drawings 3-2A and 3-2B, it is shown how each shaft is located translationally by a pair of shaft collars, spaced from the nearest enclosure wall by oil-impregnated bronze thrust bearings.

The crank was attached to the crank shaft with “crank mount shaft collars,” one on each side, that have threaded holes. The use of this pair of attachment points means that the shaft itself is responsible for much of the torsional rigidity of the crank.

A deficiency of the design as shown is that no method for attaching the cam to the cam shaft was envisioned. This stemmed from the fact that later developments in the design process halted progress on the design, before a final cam blank was selected. For the same reason, the packaging shown does not include fasteners. It is possible that the cam shaft would be redesigned at a greater thickness so that the two-piece cam blank on hand would bolt directly to the shaft, or a step in shaft diameter would be incorporated to accomplish the same result with the rest of the packaging being identical.

6.8.1.4 Slider

The slider, shown in Drawing 4-1, consists of an aluminum slider block fastened atop two linear motion blocks mated to a length of linear motion rail. The blocks used are full-ball bearing type, with the contact angle between ball and rail set to 45 degrees, making the rated load equal in all directions. The blocks are therefore capable of operating in any orientation. This feature is fully utilized in the packaging, as putting the slider assembly on its side allows a simple wrist joint: a post machined or pressed into the slider block and a journal bearing on the connection rod is all that is necessary.

The length of assembly afforded by this design in comparison to a mounting to a single guide was chosen to provide an ample bearing ratio for smooth motion. The critical aspect of a sliding mechanism is the bearing ratio, the ratio of the length of the sliding component along the axis of motion to the width of the component. A slider consisting of single linear motion block, 34 millimeters wide and 56.6 millimeters long, would have a bearing ratio of only 1.66.

While a bearing ratio of 1.5 is the bare minimum to avoid having the mechanism operate poorly[21], more is recognized as better. With that in mind, a longer slider incorporating

two linear motion blocks was designed. The overall length of the slider is 272 millimeters, making the bearing ratio 8.00, more than enough to ensure smooth operation.

6.9 Method of Changing Drive Mode

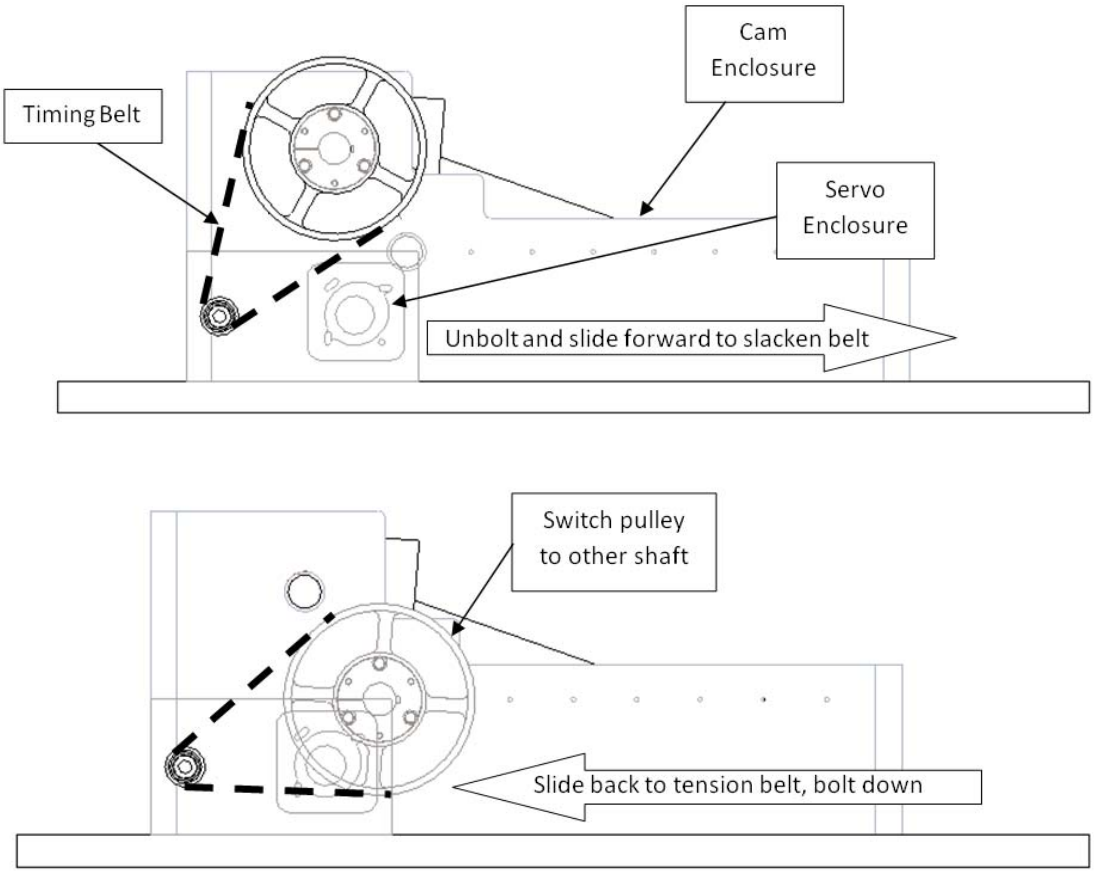

Figure 29: Changing Drive Mode and Re-Tensioning Belt

Tensioning of the belt between the two assemblies was implemented by allowing the bottom of the servo-side enclosure, keyed to a groove in the base plate, to slide back and forth (Figure 29) when unbolted. With the servomotor's output pulley being the pinnacle of a roughly isosceles triangle relative to the crank and cam axes, tensioning of either configuration could be accomplished with a jack screw (not shown) and the servo-side enclosure plate could be bolted down for operation.

7 Stress Analysis

In the single motor drive train solution the servomotor will be used to drive the two different configurations of the mechanism. In the first configuration the servomotor is directly drives the crank. In this mode the servomotor will reverse direction 200 times per minute, as dictated by the period of 0.3 seconds. In the second configuration the servomotor will drive the cam directly. In this mode the servomotor will rotate in only one direction at a constant speed.

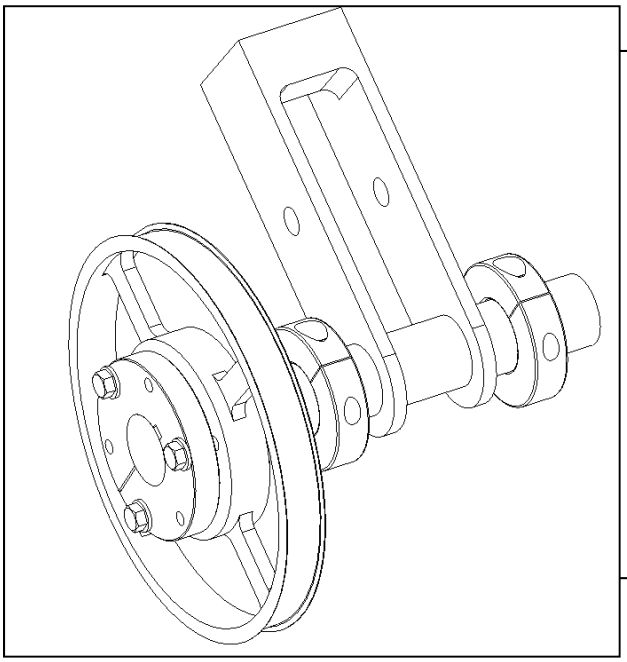

Figure 29: Crank Shaft Subassembly (See Drawing 3-5)

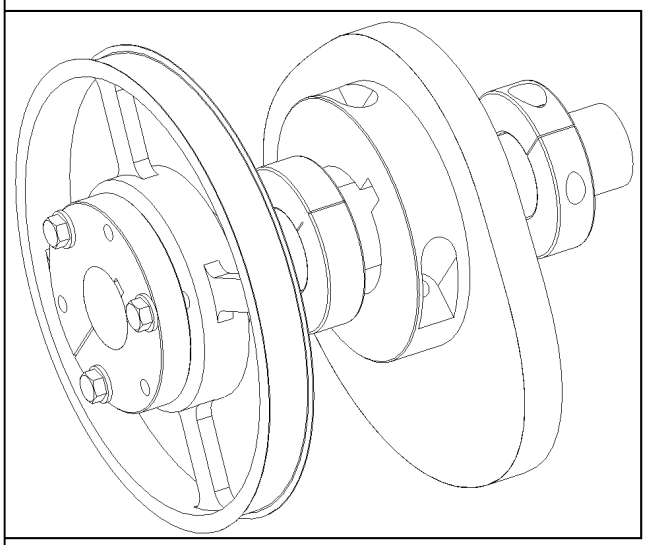

Figure 30: Cam Shaft Subassembly (See Drawing 3-3)

Figure 30 and Figure 31 show the cam and crank shaft sub assemblies, respectively the cam shaft sub assembly will be considered first.

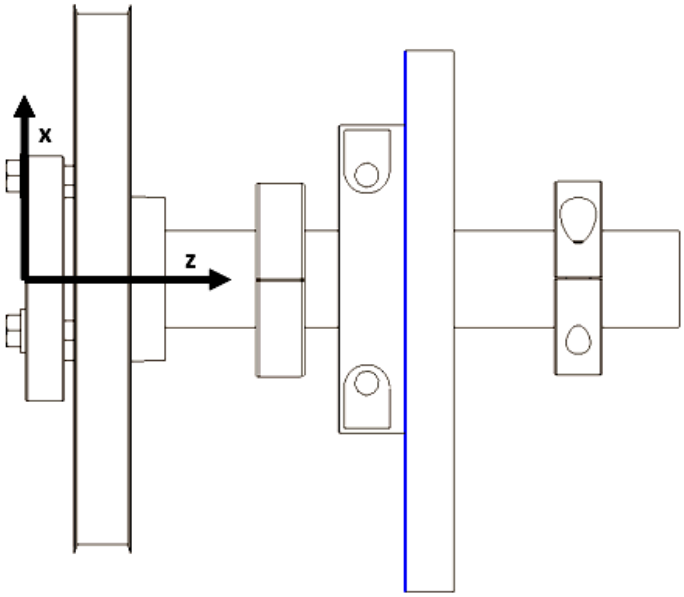

Figure 32: Cam Shaft Detail

(See Drawing 3-3)

Figure 32 shows the cam shaft from Figure 31 in the x-z plane with the z axis following the centerline of the shaft. This shaft will be used for explanation of analysis done for both shafts as the process of analysis is identical, but with different results. The two shafts are similar in geometry and arrangement.

As seen in the picture (Figure 32) of the shaft, the geometric configuration is quite simple. In this configuration there is a non-keyed shaft with two bearing, a pulley, and cam. All attachments to the shaft are done without keying or shoulders, which eliminates stress concentrations due to the presence of keyways or changes in shaft geometry. Due to the belts attached to the pulley and the forces exerted by the follower on the cam, there are forces directed in more than one plane, and since the loading analysis is for a two dimensional plane,

the loading must be done in two planes. All applied loads can be simplified to point concentrated forces. In reality, locations such as where the shaft supported by a bearing, there will be a distributed load, but for worst case scenarios, for which this analysis is done, the simplification of reaction forces as point forces is valid. It should also be noted that in the derivation of stresses and any other calculations done for the stress analysis are depicted as worst case scenarios. It is understood that the force exerted on the cam by the follower will fluctuate with respect to time, as well as the input torque from the motor, and therefore the tensions in the belt. For all these varying magnitude forces and torques, the maximum value is used. Also it is understood that all these maximum values will not be occurring at the same instant of time, but for the purpose of determining if the shaft will survive the absolute worst case scenarios there are assumed to be simultaneous. If the safety factor is determined to be greater than one at the end of analysis, the shaft won't fail, as actual operating conditions will never approach this worst case scenario. (For this section, detailed MathCAD derivations and computations can be found in Appendix E).

7.1 Tension of Belt on Camshaft Pulley:

To understand where the two tensions come from, the tensions on the pulley must be examined. The pulley is wrapped by the timing belt which drives it. The belt will have two different magnitudes of tension depending on which side is the driving side, and which is the slack side. The driving side of the belt will have a greater tension value than the slack side as the driving side is where the transmission of power occurs. The general rule for belt tension is that the slack side will have about half of the tension of the driving side, although using to input torque of the system, along with manufacturer's tensioning recommendations [16] the exact

tensions were derived. (This is further explained in Appendix E). The corresponding tensions will be at an angle, θ, off of the horizontal as dictated by the packaging of the system. Figure 35 shows the x-y plane of the pulley system with tensions shown. (All tension forces act in this plane, with no tension translating to the z direction).

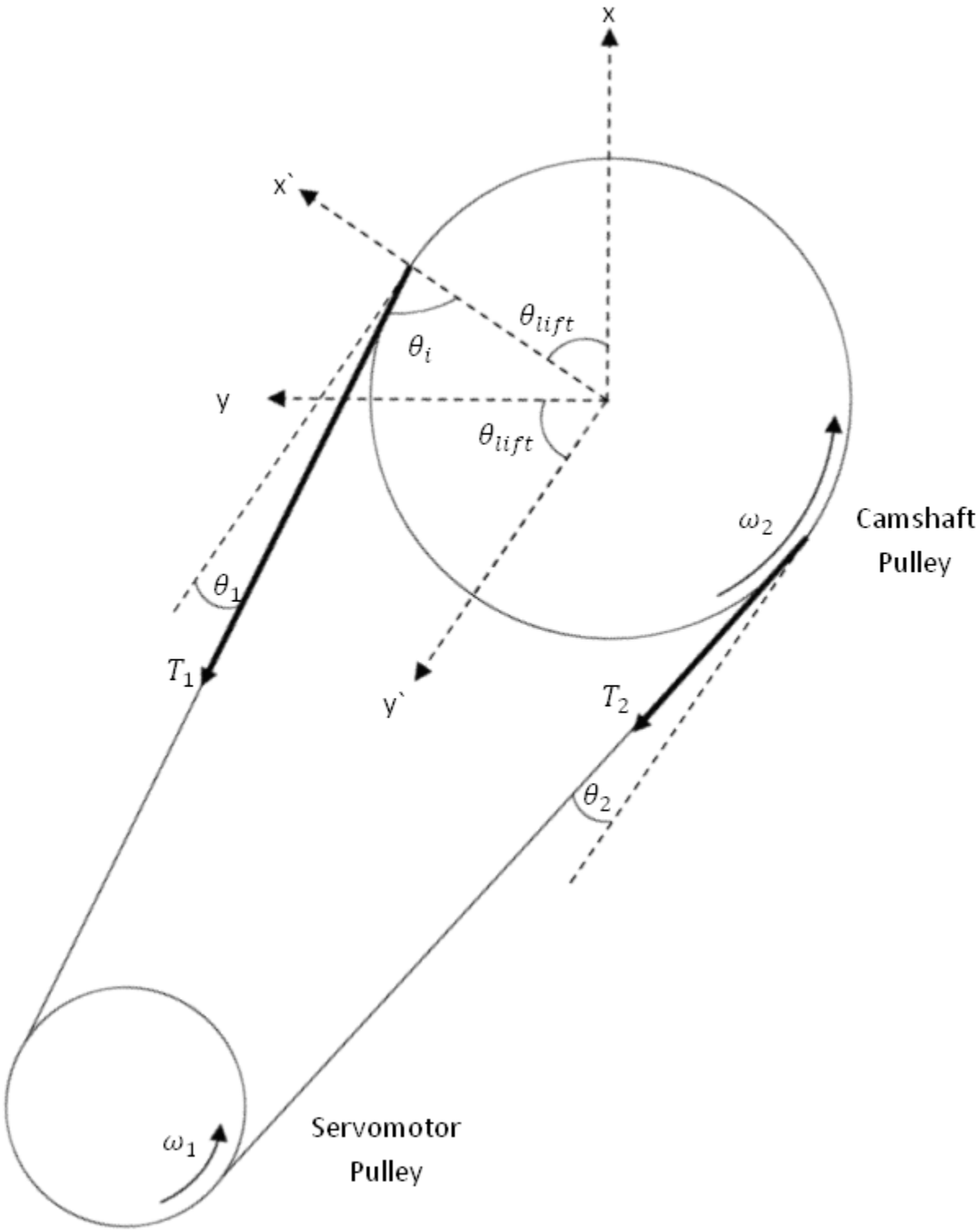

Figure 35: Pulley Forces

Basic trigonometric functions were used to separate the tensions into forces following the x and y components in their respective planes to be applied to the corresponding two axis analysis, as shown in Figure 36.

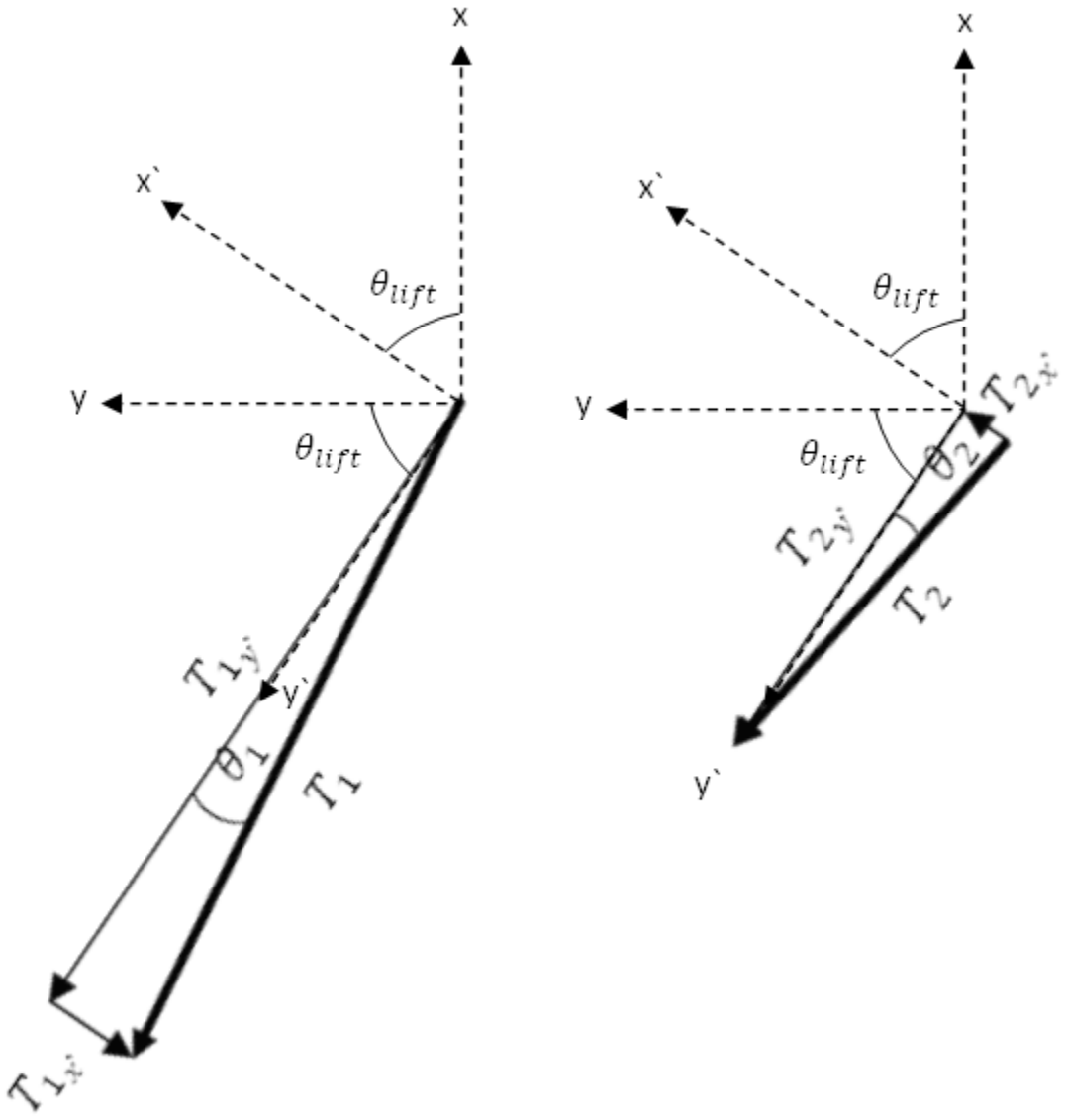

Figure 36: Separating Tensions into x and y components

7.2 Shaft Loading and Stress and Moment Analysis

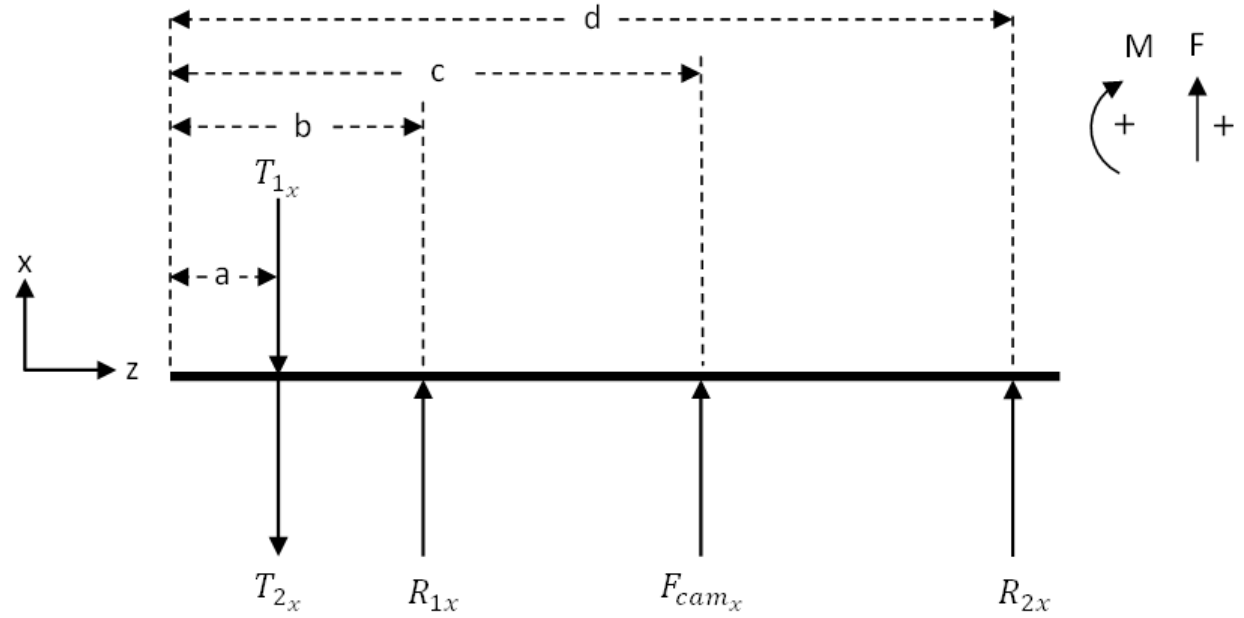

Figure 33: Free Body Diagram of Cam Shaft (x-z plane)

The first plane analyzed is showed in the above free body diagram of the camshaft (Figure 33), which shows the X-Y plane, with z running along the axis of the shaft, and x being perpendicular to the shaft. Looking at the x-z plane of the above shaft the following equations represent the initial loading conditions, shear, and moment equations using singularity functions:

$$q_x(x) := -\text{Tension}_{1x}\cdot S(x,a)\cdot(x-a)^{-1} - \text{Tension}_{2x}\cdot S(x,a)\cdot(x-a)^{-1} \ldots + R_{1x}\cdot S(x,b)\cdot(x-b)^{-1} + F_{camx}\cdot S(x,c)\,(x-c)^{-1} \ldots + R_{2x}\cdot S(x,d)\,(x-d)^{-1}$$

$$V_x(x) := -\text{Tension}_{1x}\cdot S(x,a)\cdot(x-a)^{0} - \text{Tension}_{2x}\cdot S(x,a)\cdot(x-a)^{0} \ldots + R_{1x}\cdot S(x,b)\cdot(x-b)^{0} + F_{camx}\cdot S(x,c)\,(x-c)^{0} \ldots + R_{2x}\cdot S(x,d)\,(x-d)^{0}$$

$$M_x(x) := -\text{Tension}_{1x}\cdot S(x,a)\cdot(x-a)^{1} - \text{Tension}_{2x}\cdot S(x,a)\cdot(x-a)^{1} \ldots + R_{1x}\cdot S(x,b)\cdot(x-b)^{1} + F_{camx}\cdot S(x,c)\,(x-c)^{1} \ldots + R_{2x}\cdot S(x,d)\,(x-d)^{1}$$

Where:

$Tension_{1_x}$ Tension from the top of pulley

$Tension_{2_x}$ Tension from the bottom of pulley

R_{1x} Reaction force from first bearing

R_{2x} Reaction force from second bearing

F_{cam_x}Force of the follower on the cam in the y direction

a Distance to pulley ($Tension_{1_x}$ and $Tension_{2_x}$)

b Distance to first bearing (R_{1x})

c Distance to Cam (F_{cam_x})

d Distance to second bearing (R_{2x})

The next plane analyzed is the y-z plane. This is looking down on the shaft, at a 90 degree rotation about the z axis of the shaft from the x-z plane. Figure 34 shows this free body diagram.

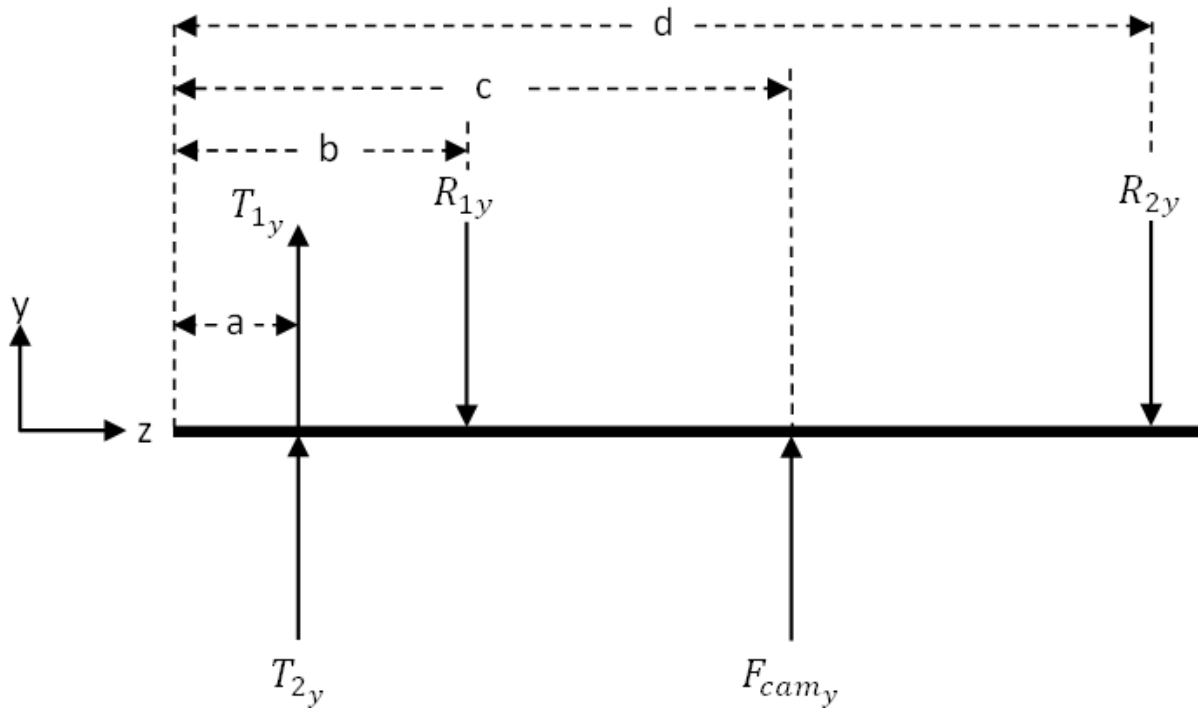

Figure 34: Free Body Diagram of Cam Shaft (y-z plane)

From this free body diagram, the following loading, shear and moment equations are formulated:

$$q_y(x) := \text{Tension}_{1y}\cdot S(x,a)\cdot(x-a)^{-1} + \text{Tension}_{2y}\cdot S(x,a)\cdot(x-a)^{-1} \ldots + -R_{1y}\cdot S(x,b)\cdot(x-b)^{-1} + F_{camy}\cdot S(x,c)\,(x-c)^{-1} \ldots + -R_{2y}\cdot S(x,d)\,(x-d)^{-1}$$

$$V_y(x) := \text{Tension}_{1y}\cdot S(x,a)\cdot(x-a)^{0} + \text{Tension}_{2y}\cdot S(x,a)\cdot(x-a)^{0} \ldots + -R_{1y}\cdot S(x,b)\cdot(x-b)^{0} + F_{camy}\cdot S(x,c)\,(x-c)^{0} \ldots + -R_{2y}\cdot S(x,d)\,(x-d)^{0}$$

$$M_y(x) := \text{Tension}_{1y}\cdot S(x,a)\cdot(x-a)^{1} + \text{Tension}_{2y}\cdot S(x,a)\cdot(x-a)^{1} \ldots + -R_{1y}\cdot S(x,b)\cdot(x-b)^{1} + F_{camy}\cdot S(x,c)\,(x-c)^{1} \ldots + -R_{2y}\cdot S(x,d)\,(x-d)^{1}$$

To further define the variables used in the loading, shear and moment equations the overall system must be examined.

7.3 Reaction Forces Exerted by Bearing onto Camshaft

R_1 and R_2, the reaction forces, are the forces exerted on the shaft from the bearings. These forces are assumed to be purely in the vertical direction and located in the center of the bearing slot. Letters a-d are the distances from the pulley end of the shaft to each of the points of interest. Using calculated values of each parameter, MathCAD is used to carry out all complex calculations. (Full derivation of these equations and results can be found in the appendices of the report.) The following graphs are the resulting shear and moment diagrams from combining the two planes.

7.3.1 Shear and Moment Diagrams:

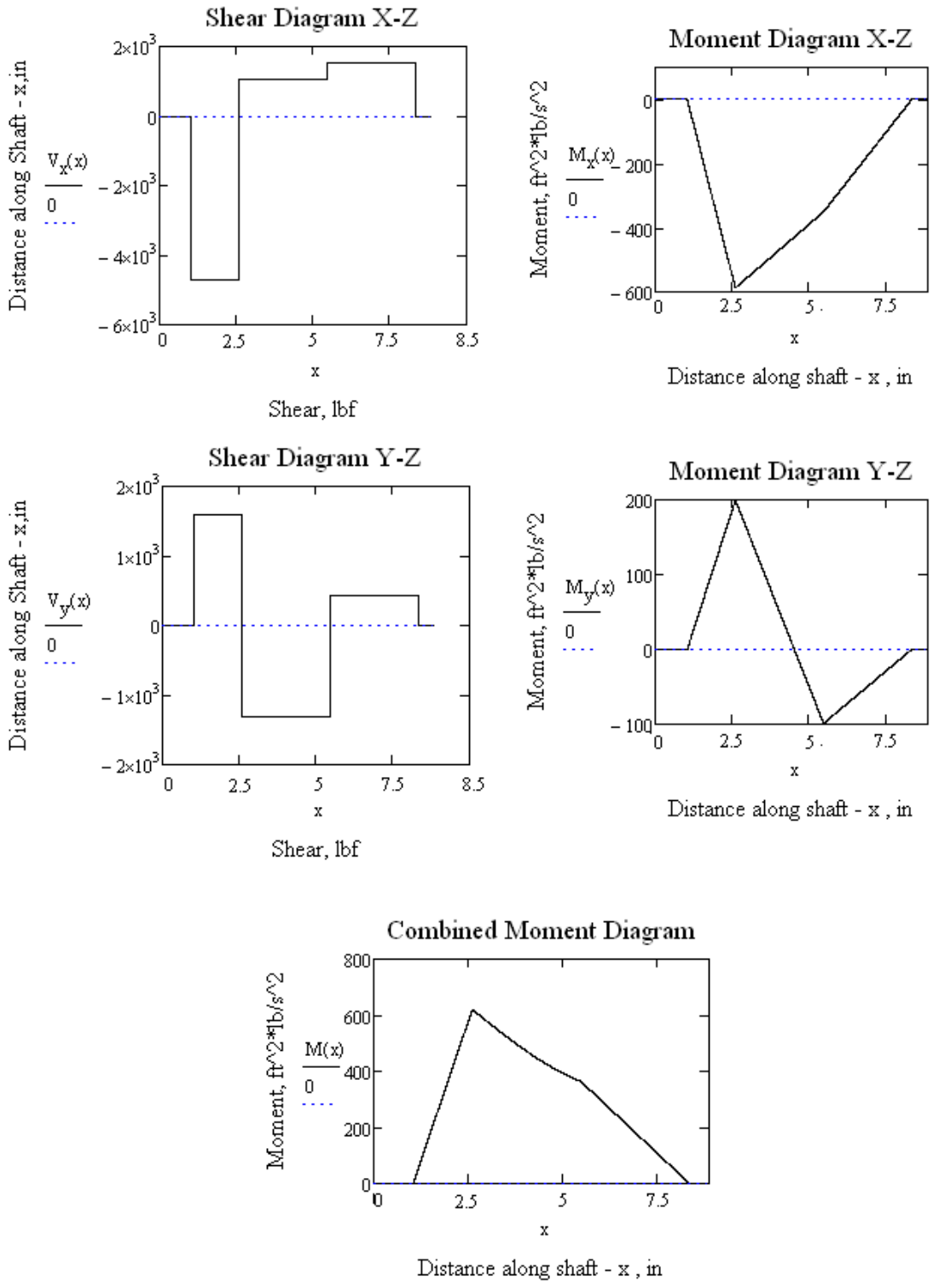

Figure 36– Resulting Shear and Moment Diagrams from Loading Conditions on the Camshaft

Both shafts undergo fully reversed bending with steady torsions as the forces will cause bending and deflections. Using the loading diagrams created the points of interest of located along the shaft. As seen in both the shear and moment diagrams, the largest magnitude of both shear and bending is experienced at point x=2.5 in, which is the location of the first bearing, therefore the location of the reaction force R_1.

7.3.2 Points of Interest and Stress Cubes:

With the area of interest being located at point b deferential areas must be examined along the outer fibers of the shaft. Figure 38 shows a cross sectional "slice" of the shaft locating the internal points of interest.

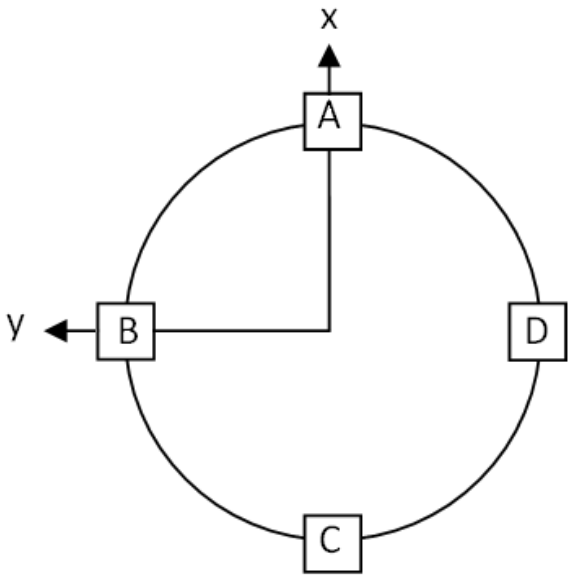

Figure 38: Points of interest at x=2.5 in

Within the points of interest A, B, C, and D stress cubes are drawn to understand the loading on the surface of the shaft on a differential level. A stress cube shows the normal and shear stresses of the differential element. Figure 39 shows a generalized stress cube and the resulting three normal stresses, and six shear stresses.

Alternating Stresses:

Point A:

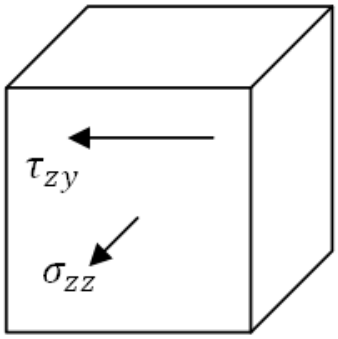

Point B:

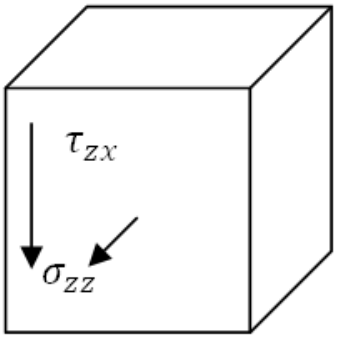

Point C:

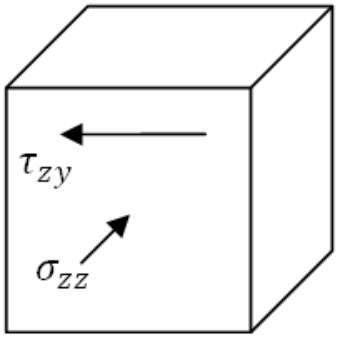

Point D:

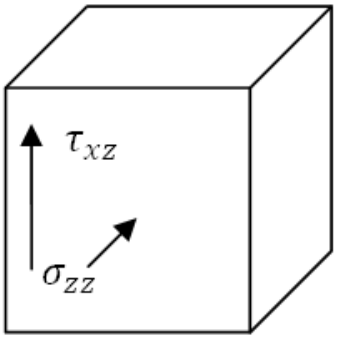

Mean Stresses:

Point A:

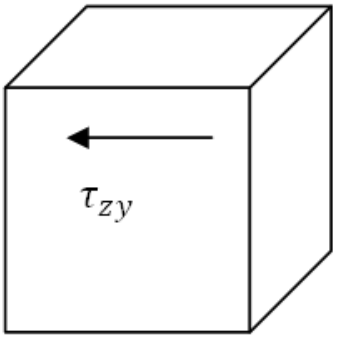

Point B:

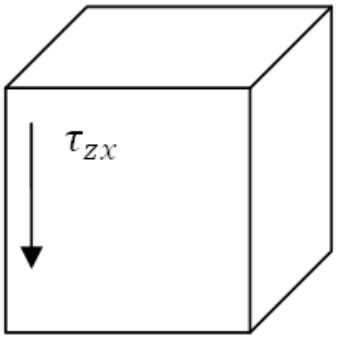

Point C:

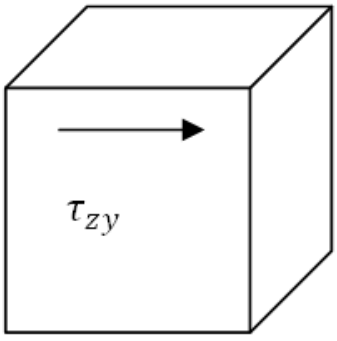

Point D:

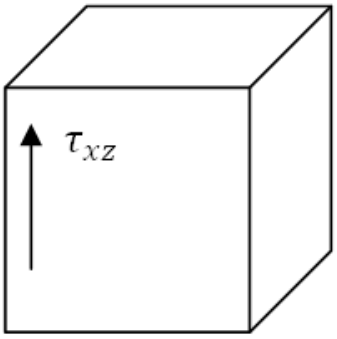

Figure 39: Stress Cubes

The areas of pure compression and pure shear are focused on as they will be the most severe loading conditions which could cause failure. Locations B and D will experience torsion from the applied torque as dictated by the following equation:

$$\tau_{max} = \frac{3V}{2A}$$

Where τ is the maximum torsional stress, V is the shear stress, and A is the cross sectional area of the shaft. The maximum torsional stress will be at the outer fibers of the shaft, with no torsional stress along the neutral axis of the shaft. Locations A and C will experience the following compressive and tensile stresses:

$$\sigma_x = \frac{M(x)c}{I}$$

Where σ is the normal stress, *M(x)* is the moment, *c* is the distance from the center of the shaft to the outer fibers, and *I* is the second moment of inertia.

After determining the stress at these locations, the Von Mises stress is found and applied to the distortional energy method for determining failure. The following formula is the equation for the Von Mises effective stress:

$$\sigma' := \sqrt{\sigma_1^{\,2} + \sigma_2^{\,2} + \sigma_3^{\,2} - \sigma_1 \cdot \sigma_2 - \sigma_2 \cdot \sigma_3 - \sigma_1 \cdot \sigma_3}$$

From here the Von Mises stress are used in determining safety factors for the shaft. Any SF numbers less than 1 show that the shaft is bound to fail under normal operating conditions. A safety factor of above 5 is optimal to account for all simplified assumptions of loading and any defects present due to the craftsmanship of the parts.

Using these adjustment factors, the corrected endurance limit of the shaft is found. The adjusted endurance limit leads to the formation of the S-N diagram, and the Goodman Diagram.

$$S_e := C_{load} \cdot C_{surf} \cdot C_{temp} \cdot C_{size} \cdot C_{reliab} \cdot S_{e'}$$

The adjustment factors take into consideration the type of load applied which in this case is bending. The surface finish also plays a factor in the corrected limit as any impurities may cause an increase of preexisting fractures. If the temperature that the machine is operated in is a moderately high temperature, the corrective temperature factor would decrease the endurance limit of the shafts.

The S-N diagram in Figure 40 shows the applied stress versus the number of cycles of life expected. At $1x10^6$ cycles is the knee of diagram. What this point indicates is that as long as the repeated stress on the shaft stays below $1.45x10^8$ the shaft will continue to operate without failure for eternity. This is considered designing for infinite life. From here, and values of stress above this limit will cause a limited life span for the shaft.

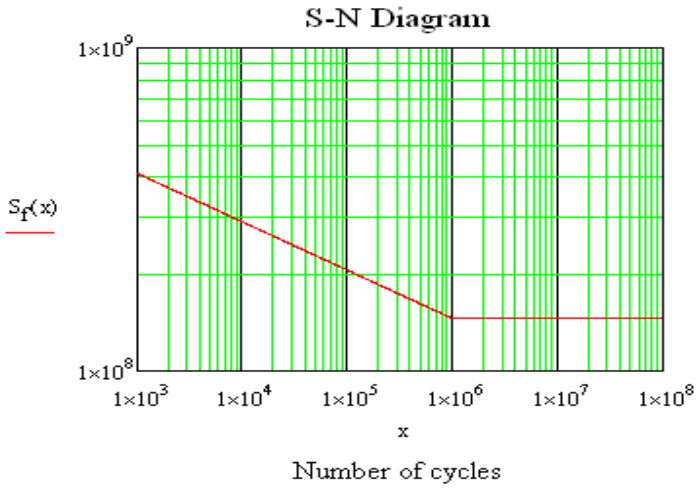

Figure 40: S-N Diagram for Cam Shaft

7.4 Shaft Failure Modes and Safety Factors:

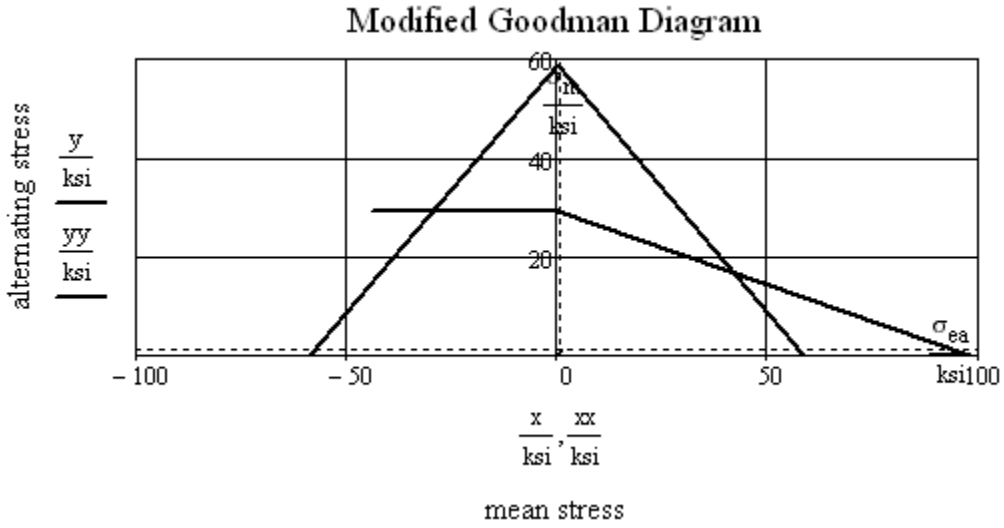

Figure 41: Modified Goodman Diagram

Figure 41 shows the relationship between the alternating stresses versus the mean stresses experienced by the shaft. The lines represent failure lines at which any point above the lines will produce a failure.

8 Vibration Analysis (Single-Motor CSTM)

The next analysis performed on the Single-Motor CSTM was a vibration analysis. Such an analysis was crucial because of the accuracy required of the CSTM; if the slider could not maintain an allowed maximum position error of ±0.005 inches, the machine would be effectively useless. In order to calculate the position error of the slider due to vibration, a complete spring-mass-damper (SMD) vibration model was created.

8.1 Vibration Model

The software used for this analysis was DYNACAM, which contains an appropriate cam-follower vibration model as a preset. Figure 42 shows the elements of the model used. The cam shape at the bottom represents the input position function (s). The first spring and damper (k_1 and ζ_1) represent the spring constant and damping ratio of the mechanism. The mass (m) represents the equivalent mass of the system and the final spring and damper (k_2 and ζ_2) represent the spring constant and damping ratio of the return spring. Position error in this model is calculated as **s** minus **x**, the difference between the input position function (s) and the mass's actual position (x). With zero vibration in the system, **x** would be equal to **s**.

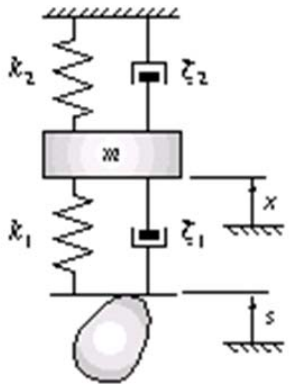

Figure 42: DYNACAM Vibration Model of the Cam Servo Test Machine

8.2 Mass Model

The effective mass of the system was lumped at the slider in linear translation using a Lagrangian energy method (shown in Equation 1). This equation is very similar to the equation used in Section 6.7 to determine the required torque of the system. For this model the equivalent mass ($m_{eq,slider}$) was focused in linear translation at the slider, the pulley pitch diameters had been revised based on the mass-reduction efforts discussed in Section 6.7.2, and the return-spring torque was removed from the mass model because the vibration model accounts for the return spring separately.

Equation 1: Lagrange System Energy Equivalence

$$m_{eq,slider} = \frac{I_{servo}\left(\frac{7.162 \times 3.820}{1.192^2}\omega_{crank}\right)^2 + I_{transmission}\left(\frac{7.162}{1.192}\omega_{crank}\right)^2 + I_{eq,crank}\omega_{crank}^2}{v_{slider}^2}$$

The angular velocity of the crankshaft (ω_{crank}), the linear velocity of the slider (v_{slider}), and the effective mass-moment inertia at the crankshaft ($I_{eq,crank}$) were calculated from the kinematic and dynamic analyses discussed previously in Section 6.7. The angular velocity of the transmission shaft and servomotor shaft were calculated by multiplying ω_{crank} by the proper pitch diameter ratios of the pulley system. The mass-moment inertias of the transmission ($I_{transmission}$) and servo (I_{servo}) shafts were calculated in the Pro/ENGINEER CAD package with accurate material properties for all parts.

Table 7: Angular Velocities and Mass-Moment Inertias of CSTM Components

Part/Assembly	ω_{max} (rpm)	I (lbm-in^2)
Linkage (Effective @ Crankshaft)	114.6	70.0
Transmission shaft	687.4	0.37
Servomotor shaft	2062	8.46×10^{-3}

Solving Equation 1 for the effective mass at the slider gave an equivalent mass ($m_{eq,slider}$) value of 0.028blobs or 4.9kg. The values for each variable used are given in Table 7. All moving components were considered in the mass model except the timing belts which were assumed to be negligible due to their relatively low density and small size.

8.3 Spring Model

Modeling the many components of the linkage as a single spring was a more intensive operation. The spring constants of many system components were readily calculated using deflection equations re-arranged to solve for the ratio of applied force and deflection. There were three shafts in essentially pure torsion; all of these shafts were modeled initially as torsion springs based on Equation 2. Torsion spring constants are factors of shear modulus (G) of the shaft material, the shaft diameter (d), and the shaft length (L). The unit of the torsion spring constant is torque per degree or radian; a torsion spring constant can be converted to a linear spring constant at some distance (r) from the shaft axis by dividing the torsion constant by the distance squared (this assumes small angular deflection, which is a safe assumption for this model). The distances for each shaft were defined by the pulley pitch radii such that the equivalent linear spring of the shaft could be placed directly in series with the equivalent spring of the timing belts (visualization shown in Figure 43).

Equation 2: Shaft Torsional Spring Constant

$$(Torsion)\ Spring\ Constant\ of\ a\ Solid\ Shaft = \frac{\pi G d^4}{32L}$$

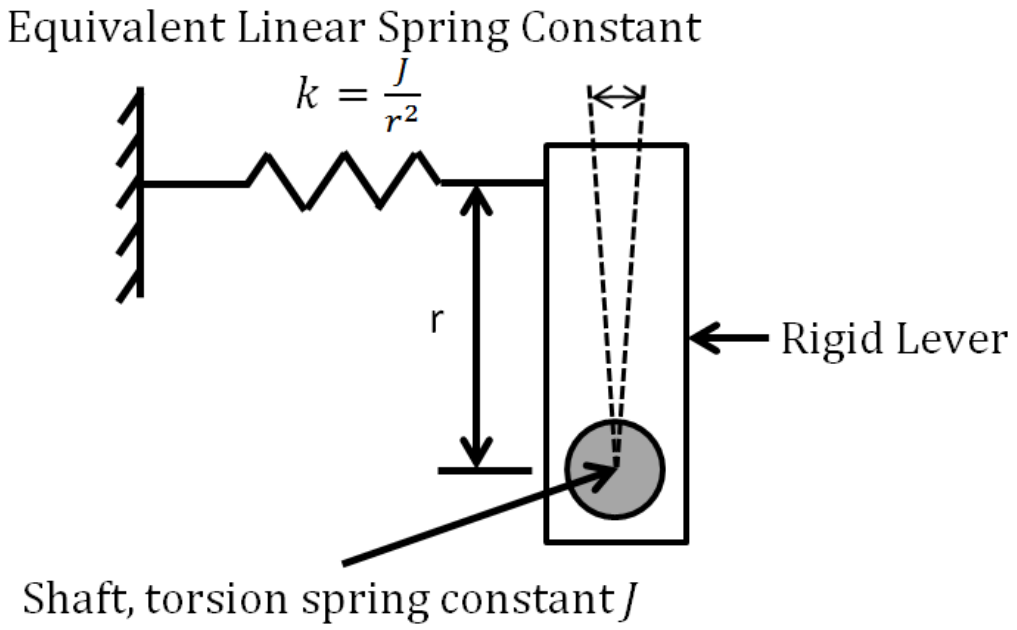

Figure 43: Torsion to Linear Spring Conversion

It is important to note that there were more components contributing to the torsional stiffness of the shafts in this assembly, such as shaft collars and pulley bushings placed in some cases very close together. These elements were assumed to be rigidly attached to the shaft; as such the placement, thickness, and diameter of the shaft collars were measured and each individual shaft was modeled as a series of short shafts with varying diameters (the shaft collars and the shafts were all steel alloys). Items 7, 9, and 10 (Figure 47) are examples of these kinds of components.

The pulleys were assumed rigid because of their relative robustness and because modeling their spring constant with any degree of accuracy would have required FEA due the complex geometry of the parts. Thus only the length of shaft between the pulley geometry itself and the crank link was modeled.

The spring rates of timing belts are difficult to find from manufacturers or resellers. The belts used in this design were 1/2-inch wide glass-fiber-cord polyurethane timing belts. A

specific spring rate for timing belts in tension was found in a study (Dalgarno, Day, Childs, & Moore) testing the effects of fatigue on belt efficiency. The study determined the specific stiffness (spring rate per unit length) of one glass-fiber belt cord to be approximately 5688lb/in per inch. The study used 0.75 inch wide belts which contained 12 cords; the single-motor CSTM used 0.5inch belts and so the cord count was reduced proportionally to 9. Factoring the length of the belts in the design from tangency on the output pulley to tangency on the input pulley (the straight-line length of one side of the belt, pulley-to-pulley) calculated linear tension spring constants for each belt instance.

$$k_{servo\ belt} = 5688\,{\frac{lb}{in}}\Big/_{in} \times 9 \times 5.083in = 1.007 \times 10^4\,\frac{lb}{in}$$

$$k_{transmission\ belt} = 5688\,{\frac{lb}{in}}\Big/_{in} \times 9 \times 7.288in = 2.107 \times 10^4\,\frac{lb}{in}$$

The crank-slider linkage was modeled as a cantilever beam with an end load (crank) in series with two linear tension/compression springs (coupler and slider). This model sufficed for a preliminary analysis. The equations used to convert link geometry into springs are given in Equation and are factors of elastic modulus (E), mass-moment-inertia (I), length (L), and cross-sectional area (A).

Equation 3: Spring Equations for Linkage Components

$$k_{eq}(Cantilever\ Beam) = \frac{3EI}{L^3} \qquad\qquad k_{eq}(Rod\ in\ tension/compression) = \frac{EA}{L}.$$

Figure 44 offers a view of how complex link geometry was modeled; all links were broken down in this manner to calculate approximations with greater accuracy.

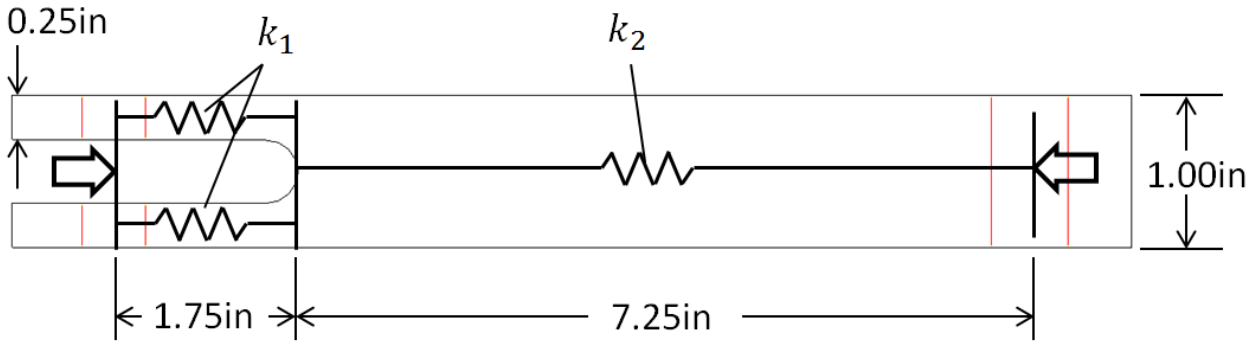

Figure 44: Top view of Coupler Link with Axial Spring Visualization

$$k_1 = \frac{E_{Al} \times (1in \times 0.25in)}{1.75in} = 1.429 \times 10^6 \frac{lb}{in}$$

$$k_2 = \frac{E_{Al} \times (1in)^2}{7.25in} = 1.379 \times 10^6 \frac{lb}{in}$$

$$k_{eq,coupler} = \frac{2k_1 k_2}{2k_1 + k_2} = 9.302 \times 10^5 \frac{lb}{in}$$

The equivalent springs for the linkage components were then arranged such that they were in series along the coupler axis. Note that for this approximate analysis, only axial stiffness components were accounted for; any other force vector components created by the angular differences between the linkages were ignored. The linkage spring rate approximation including the crank shaft torsional stiffness (which was reflected as linear to the crank pin via the method discussed previously) is shown in Figure 45.

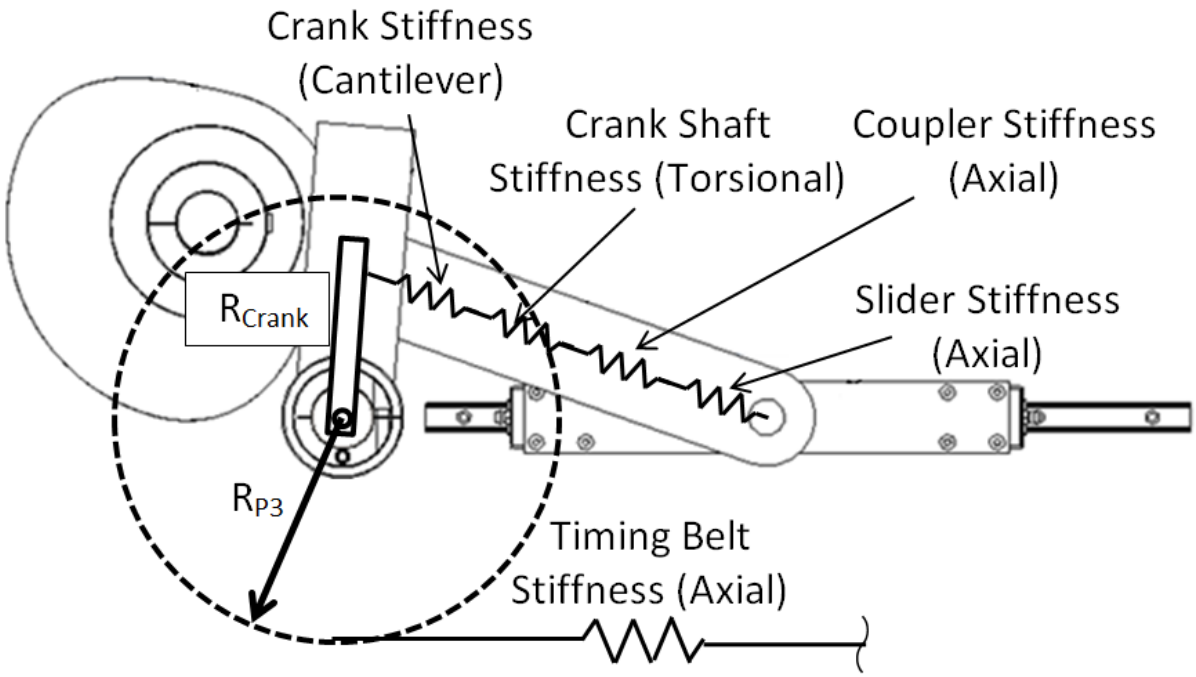

Figure 45: Linkage Spring Approximation

Figures 46-47 display isometric and top views of the CSTM with all supports hidden and spring-modeled components shaded gray. Calculated component spring constants are presented in Table 8 (full calculations in Appendix E); the full spring arrangement visualization is found in Figure 48.

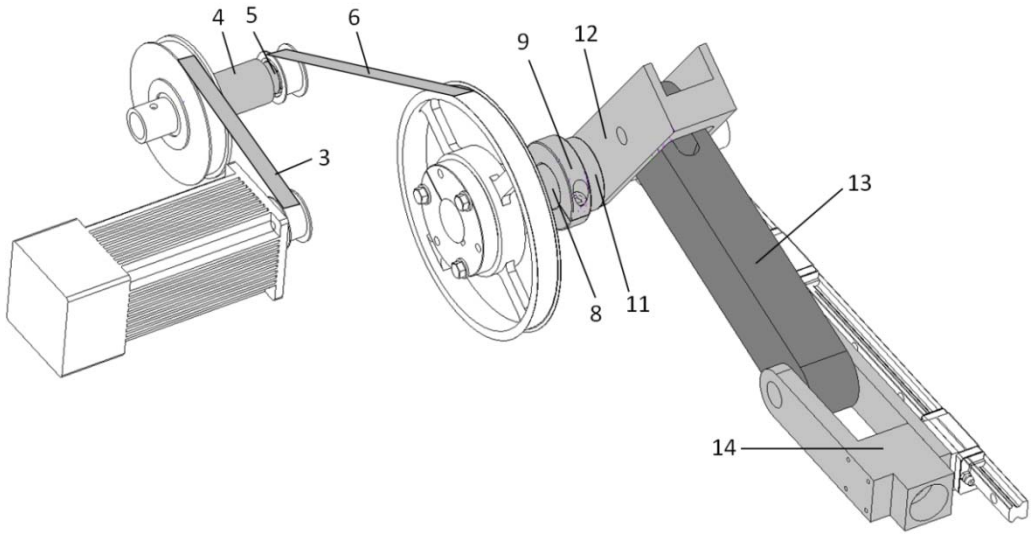

Figure 46: Isometric View of Single-Motor CSTM, all supports hidden. Spring components are shaded grey.

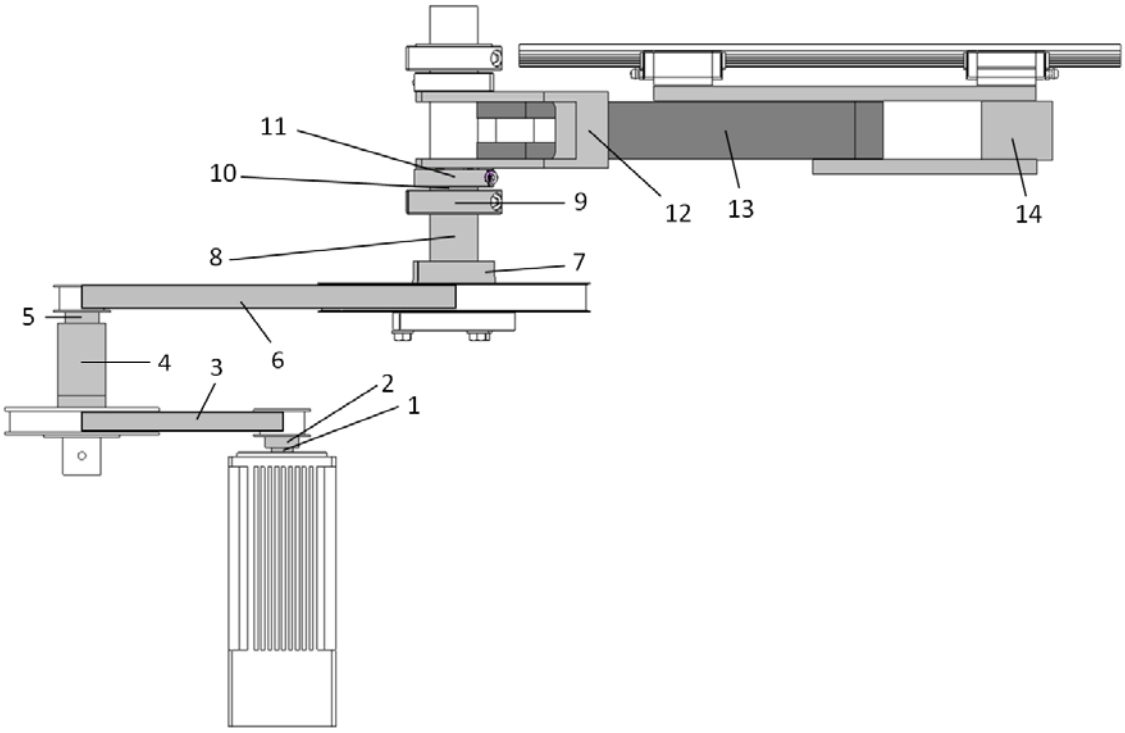

Figure 47: Top View of Single-Motor CSTM, all supports hidden. Spring Components shaded gray.

Table 8: Spring Component Spring Rate Values

Drawing Ref. #	Spring Components	Spring Rate	Lumped Linear Spring Rate (lb/in)	Lumped Spring Name
1	Servo Shaft	6.154 x 10^4 lb-in/rad	1.727 x 10^5	Servo shaft
2	Small-pulley bushing			
3	Timing belt	3.021 x 10^4 lb/in	3.021 x 10^4	Servo belt
4	Transmission shaft	2.494 x 10^6 lb-in/rad	6.046 x 10^5	Transmission shaft
5	Small-pulley bushing	3.603 x 10^5 lb-in/rad		
6	Timing belt	2.107 x 10^4 lb/in	2.107 x 10^4	Transmission belt
7	Large pulley bushing	5.284 x 10^7 lb-in/rad	2.088 x 10^5	Crank Shaft
8	Crank shaft segment	2.341 x 10^6 lb-in/rad		
9	Large shaft collar	7.492 x 10^7 lb-in/rad		
10	Crank shaft segment	2.046 x 10^7 lb-in/rad		
11	Small shaft collar	4.206 x 10^7 lb-in/rad		
12	Crank	3.704 x 10^5 lb/in	2.472 x 10^5	Linkage
13	Coupler	9.302 x 10^5 lb/in		
14	Slider	3.707 x 10^6 lb/in		

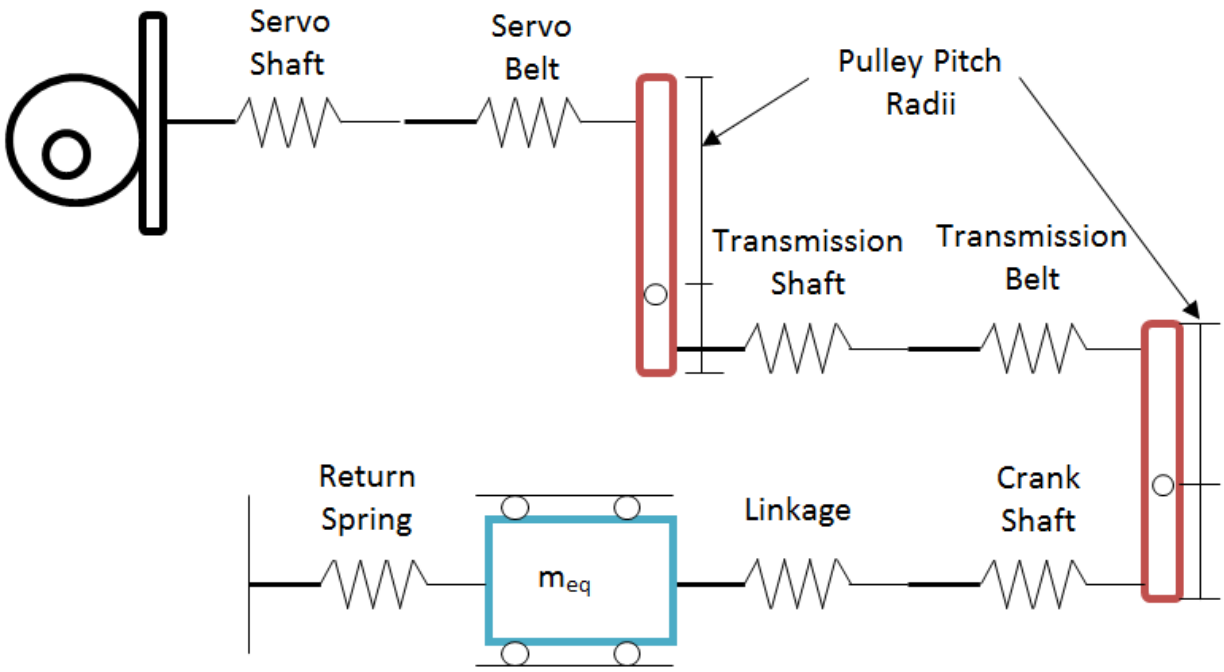

Figure 48: Spring Arrangement Layout

The final pieces to tie the spring components together were the pulleys. While the pulleys themselves were not modeled as springs, the pitch diameters/radii were critical to the model as they magnified force transfer significantly. In order to reflect the spring models of the linkage and transmission back to the function generator as a single spring, the pitch diameter (or in this case, radius) ratios were included as part of a spring potential-energy equality. The pitch radii are shown in Figure 44 and follow the arrangement of the pulleys in the speed reduction apparatus; the servo pulley (not modeled as the servo motion profile is transferred directly through it) connected to the mid-sized pulley (R_{P1}) which had a pitch radius of 1.91 inches and shared a connecting (transmission) shaft with a small pulley (R_{P2}) which had a pitch radius of 0.597 inches. The small pulley connected to the large-diameter pulley (R_{P3}) located on the crank shaft along with the crank (R_{Crank}), which had a pin-to-pin length of 3 inches.

In this model the crank length is accounted as a lever ratio because it is modeled as a cantilever beam “grounded” at the crank shaft with an end load at the crank pin. This model forces the linear spring model location to be at the crank pin, which aligned it with the coupler “spring” but required that the length of the crank be held as a rigid lever.

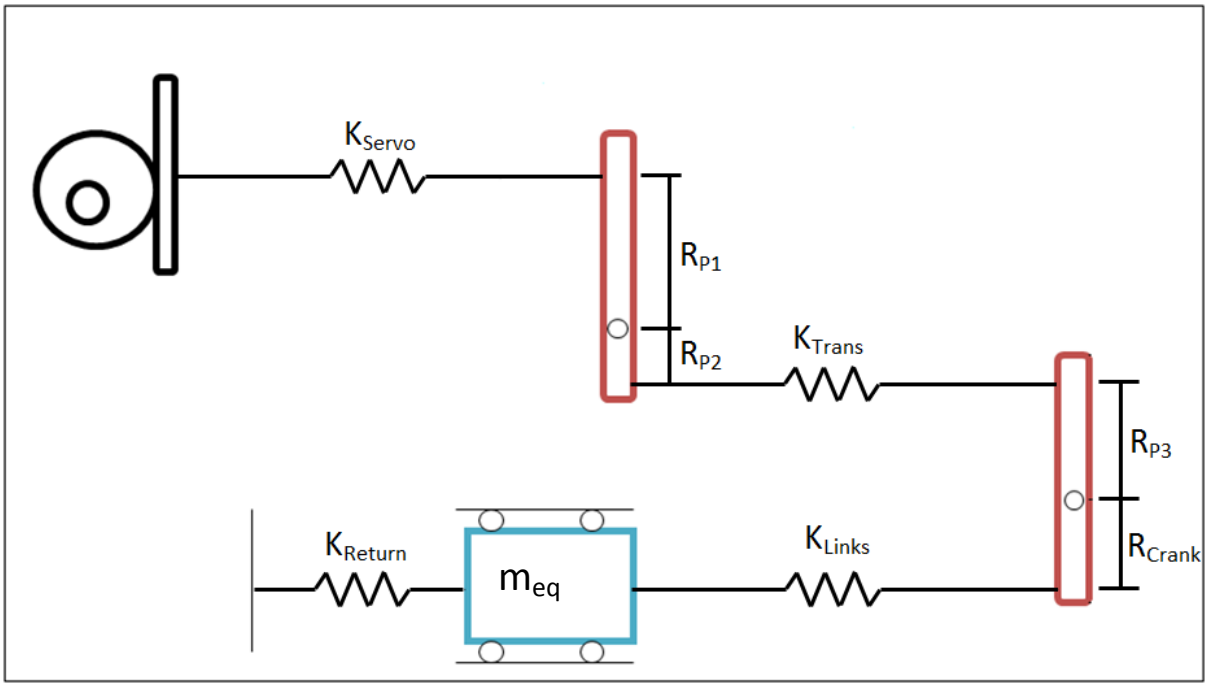

Figure 49: Simplified System Spring Layout

To input the system spring model into DYNACAM the system springs and pulleys shown in Figures 48-49 had to be reduced to a single spring equivalent. Spring-series and potential energy equations were used to do this (example of the latter shown below) where translation on the slider side of the lever (x_{Links}) is related to translation on the transmission side of the lever/pulley (x_{Trans}) to effectively move the linkage equivalent spring (k_{Links}) to an effective spring ($k_{eff,Links}$) on the transmission side of the lever. The result of this arrangement is shown in Figure 50.

$$x_{Trans} = \frac{R_{P3}}{R_{Crank}} x_{Links}$$

$$\frac{1}{2}k_{eff,Links}x_{Trans}^2 = \frac{1}{2}k_{Links}\left(\frac{R_{Crank}}{R_{P3}}x_{Trans}\right)^2$$

$$k_{eff,links} = \left(\frac{R_{crank}}{R_{P3}}\right)^2 k_{Links}$$

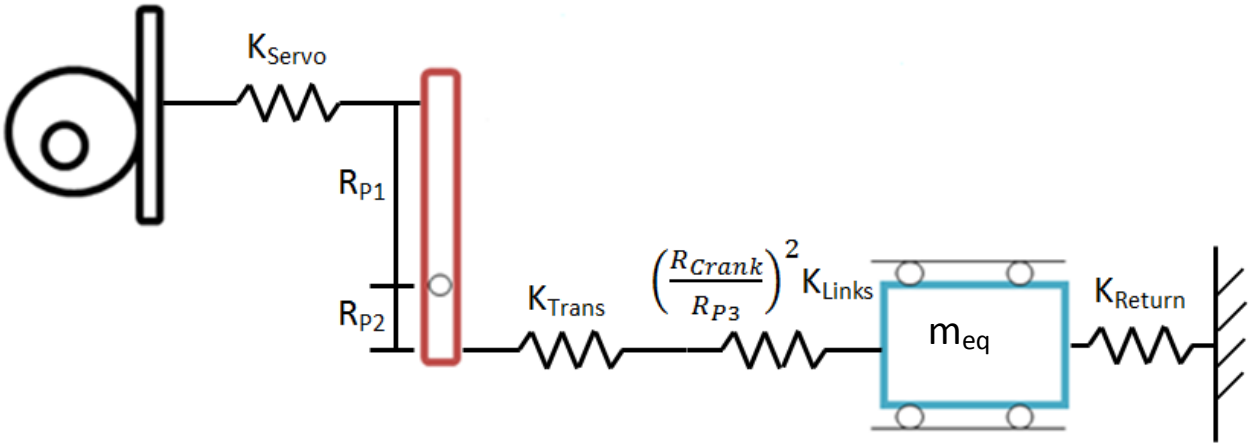

Figure 50: Single-Lever Simplified Spring Model

This process was repeated to reduce the system spring model to three effective springs in series as shown in Figure 51.

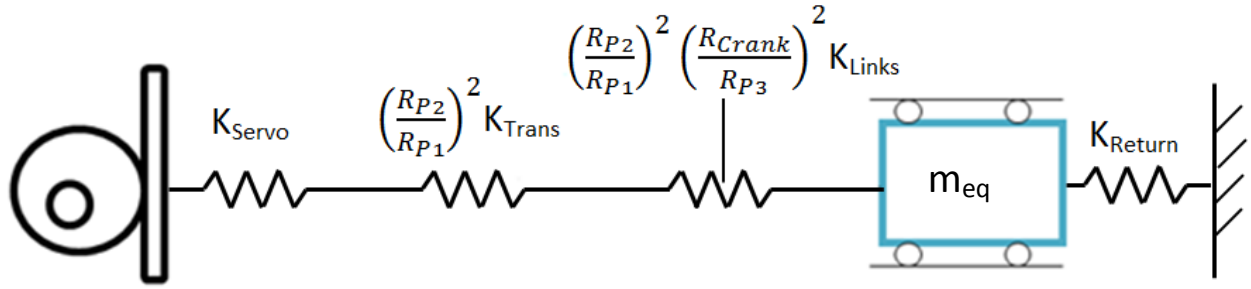

Figure 51: Zero-Lever Simplified Spring Model

These three springs were then combined into one system equivalent via the spring series calculation shown below:

Equation 4: Total System Stiffness, Servo Mode

$$k_{eq,system} = \left(\frac{1}{k_{Servo}} + \frac{1}{\left(\frac{R_{P2}}{R_{P1}}\right)^2 k_{Trans}} + \frac{1}{\left(\frac{R_{P2}}{R_{P1}}\right)^2 \left(\frac{R_{Crank}}{R_{P3}}\right)^2 k_{Links}}\right)^{-1}$$

$$k_{eq,system} = 579.66 \frac{lb}{in}$$

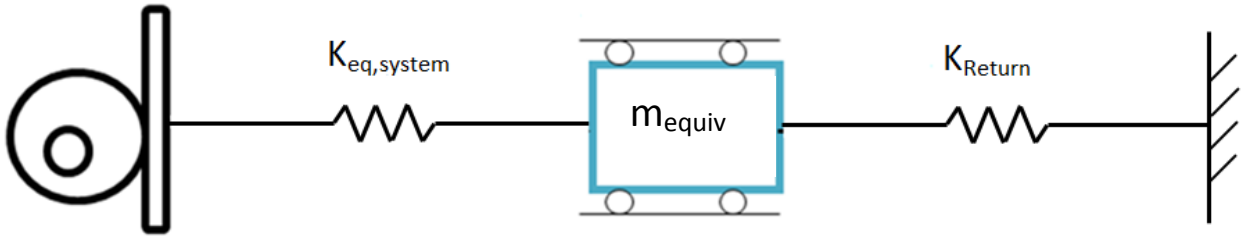

Figure 52: Final CSTM Spring Model Simplification

8.4 Damper Model

Damping in this system was taken to be minimal. The design team used low-friction journal bearings (typical damping coefficient of 0.01) and the THK slider rail is known to exhibit comparably low friction as well. The only damping in the system other than friction is the internal damping of the components themselves; this is also very low for solid metal components. A generally-accepted cam-follower system damping coefficient of 0.05 was used in the differential equation solver; this was DYNACAM's default value. The design team did not see significant reason to either raise or lower this value given the aforementioned absence of significant dampers in the system. The model results also demonstrated low sensitivity to changing this value by approximately ±0.03.

8.5 Cam Mode

The model as discussed relates only to the Servo Mode of the CSTM. This is because the cam mode model is much simpler and can be discussed here very briefly, having previously covered many assumptions and modeling techniques used for the servomotor mode model. In cam mode the spring model is reduced to the links only (Figure 45, with modification). In the cam driven mode, the links are modeled as three tension/compression springs in series. In the servomotor driven mode the crank link was modeled as a cantilever beam with an end load.

The reason for changing the crank model was the difference in force input to the crank between cam and servomotor drive modes. In servomotor drive mode the force is transferred normal to the length of the crank. This can be closely approximated by treating the link as a cantilevered beam with an end load.

In cam drive mode, however, the follower force almost completely bypasses the crank and goes straight to the coupler because the roller follower is mounted to the crank pin.

Thus the design team modeled the crank as another tension/compression spring in series with the other components. This model more accurately reflects the small impact of the crank stiffness on cam mode operation without eliminating it entirely. Also, such a model helped offset some of the inaccuracy of modeling the coupler in tension/compression only.

In cam drive mode, the number of components is reduced significantly because none of the speed reduction components are part of the analysis. This removed the belts, pulleys, and shafts from the spring model and dramatically increased the stiffness of the cam mode model versus the servomotor mode. The design team considered that these components were not significant contributors of position error in cam mode given that it had constant-velocity operation with no stops or direction changes. Any backlash caused by a change in sign of the torque function on the cam was assumed to be mostly offset by the “flywheel effect” of the cam itself and 7-inch-diameter cast-iron pulley, both of which would significantly reduce the magnitude of any such fluctuations.

The mass of the cam drive model was largely unchanged even though the pulleys and shafts were eliminated. This is because, as seen in Table 8, the inertial contributions of these

parts are very low. Eliminating these components reduced the system mass concentrated at the slider by approximately 0.005 blobs (approximately 0.9kg) to 0.0235 blobs.

The calculated spring constant of the cam mode system was approximately 5.142×10^5 lb/in. This spring rate proved to be very high, and due to the assumption made above was most certainly an overestimate. Complete calculations can be found in Appendix 17.3.

8.6 Results

Having discussed the creation and parameters of the model, the data was entered into DYNACAM for a solution. Parameters for the return spring specified a 20lb/in spring with a 20lb preload; these parameters were determined to be acceptable from a kinetostatic force analysis of the system.

The results of the cam mode model simulation in cam mode using DYNACAM's equation solver resulted in a maximum estimated position error of approximately ±0.0004 inches and was thus well within the 5 thousandths of an inch allowable maximum deviation. The result of this calculation can be found in Figure 53. It should be noted that DYNACAM's equation solver could not resolve the solution with a spring rate of 5.142×10^5 lb/in; in order for the Runge-Kutta solver to converge, a spring rate of 1.00×10^5 lb/in was used. While the magnitude of the reduction is significant, the simulated position error was still very low.

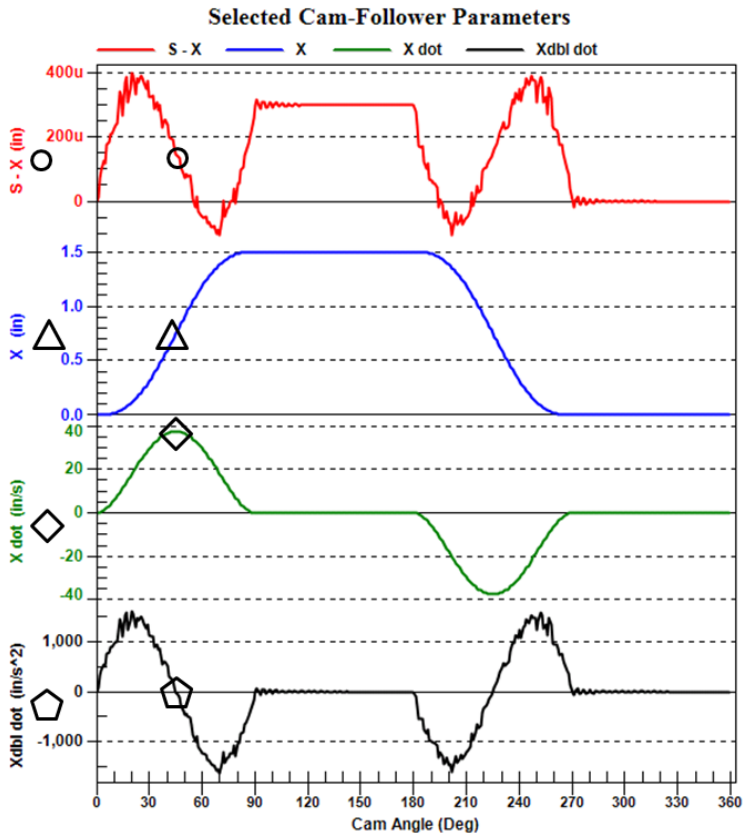

Figure 53: Cam Mode Slider Position Error, Position, Velocity, and Acceleration

This calculation showed that the CSTM single-servomotor design would be capable of the required accuracy in cam mode. The servomotor mode calculations showed that the single-servomotor CSTM design had serious design flaws that were capable of at worst causing catastrophic failure. Calculating the position error in DYNACAM with the specified parameters resulted in an estimated position error of approximately 0.11 inches, two orders of magnitude greater than the design requirement. The results are shown in Figure 54.

Also important to observe is the difference between the acceleration plots in cam drive and servomotor drive modes. It is possible to conclude that the vibration present in the system not only exceeds the maximum in terms of position error but may also result in forces on the system well beyond the design target.

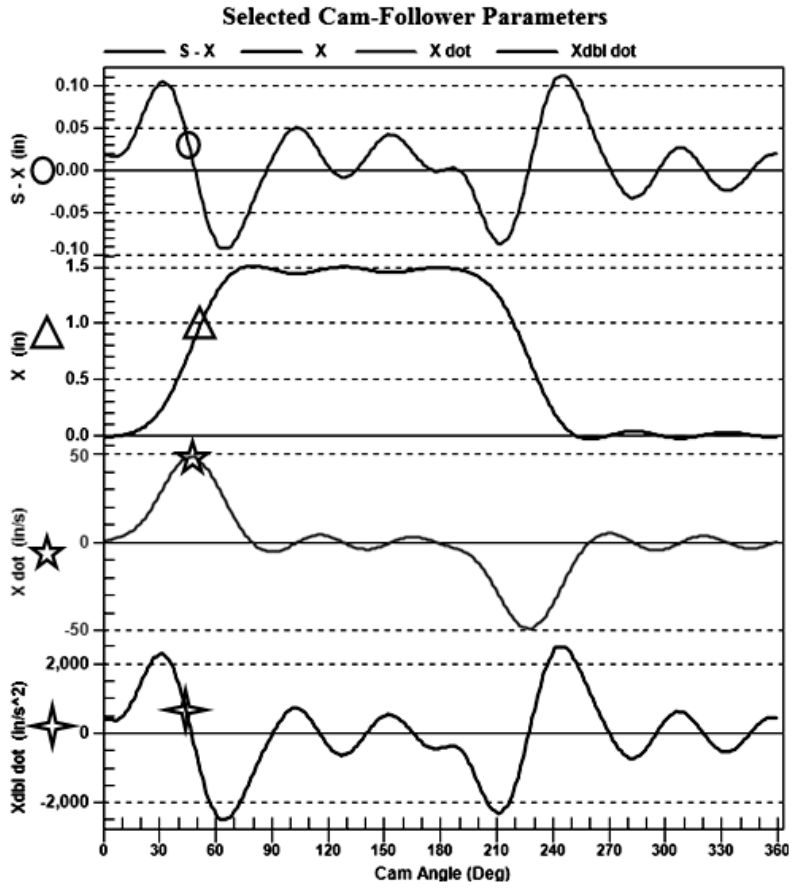

Figure 54: Servo Mode Position Error, Follower Position, Velocity, and Acceleration

A brief sensitivity analysis was done to see of any easy design changes could significantly reduce the estimated position error. The two options developed were to use steel-cord timing belts, which are approximately 3 times stiffer than glass-fiber cord belts (assuming similar cord geometry) and to stiffen the links themselves, primarily the crank as it was the least stiff as an initially aluminum cantilever by a wide margin. These two methods were the only ones available; increasing shaft diameter or belt width would push the inertia of the machine beyond the power limits of the servomotor. Considering the design changes made already with this design to reduce inertia to an acceptable level for the power limitations of the servomotor, these measures were not considered as viable options for increasing system stiffness.

Changing the belt cords to steel and specifying a steel crank link increased the system spring constant to approximately 1530 lb/in. This in turn reduced the estimated position error to approximately 0.4 inches, still far greater than allowable. Also, both of these changes increased the torque demand on the motor which was very close to exceeding the nameplate limitations already. While the steel belt specification was retained, the less significant steel crank specification was scrapped due to the significant increase in inertia. The steel belts alone raised the system spring rate to 1455 lb/in.

Dissection of the stiffness equation showed that the primary factors in the system were the lever ratios presented by the speed-reduction pulleys. These were the greatest contributors to the poor stiffness of the system and due to their necessity in allowing the underpowered servomotor to drive the device they were essentially unchangeable.

The servomotor drive mode of the single-motor CSTM design would not function properly if built as specified. Due to the constraints of the system and its low sensitivity to increasing the stiffness of individual components, the design team concluded that a completely different design was required to meet the task specifications.

8.6.1 Implications of the Servomotor Driven System on Position Error of the Slider

In a servomotor driven system, the control loop is closed at the output, which follows from the very definition of what constitutes a servomotor system. In the system considered, however, the servomotor control loop is closed with the resolver providing feedback on servomotor shaft position only, at the input end of the drive train. This does not necessarily equate to accurate feedback of the output of the system (as the vibration analysis shows);

accurate servomotor positioning (down to 0.1 degrees/revolution, as the servomotor is capable of providing) does not, in a compliant system, provide reliable output positioning.

If the machine *had* been built with its compliant timing belt drive train, it would be possible that from the servomotor's perspective, everything would be fine at the input and miserable at the output, i.e. the servomotor shaft position vis-à-vis the resolver could be entirely as expected while the motion at the output was unacceptable. It is also possible that the resonance in the system would be enough to cause destructive "hunting" as the servomotor attempted to compensate in vain for the oscillations carried back through the drive-train. If the loop was instead closed at the slider (with a linear encoder providing this information) with anything less than a rigid linkage between motor and slider, then such hunting would be inevitable, as lag between the impact of corrective motion made at the servomotor and results at the output would make the system extremely difficult to tune.

9 Conclusion

The process of designing the single-motor CSTM involved design of a crank-slider linkage, creation of a cam profile to drive the linkage, optimization analyses to determine the neutral angle and crank length of the linkage, and geometric constraints to optimize the positioning of the cam relative to the linkage. Incorporating the servomotor required performing a dynamic analysis on the linkage, designing and specifying a two-stage speed reduction, incorporating the reduction components into the dynamic model, and reducing the mass and inertia of the reduction components. Once these had been accomplished, the mechanism was packaged for construction and stress analysis and vibration calculations were performed.

The vibration analysis indicated that the single-motor CSTM design would not perform well enough to be a valid instrument for comparing the two driving modes. The performance gap was such that changes to the design such as part or belt material or even part geometry would not stiffen the system enough to bring it up to specification.

Arguably the most important concluding statement to be made from the single-motor CSTM design process was that using belts for speed reductions, even timing belts, significantly compromises the precision of any machine. In the two-stage speed reduction specified for the single-motor CSTM even with relatively stiff moving components the reduction ratios served to reduce the effective spring rate of the system by the square of the total ratio (in this case 19:1) multiplied by the square of the first-stage ratio (approximately 3:1). These two factors resulted in a system stiffness reduction of 97.5% compared to the direct-drive design which has no speed reduction.

10Recommendations

It is clear that any timing belt speed reduction is unsuitable for use in this, and possibly any, servomotor application due to a lack of system rigidity. Alternatives needed consideration. After further discussion, three categories for further development emerged:

1. A high precision gearbox with the same servomotor
2. Direct mounting of a (bigger) servomotor to the camshaft
3. A different linkage solution to the same problem without a timing belt reduction

Each option would be developed conceptually to a point at which the relative merits could be discussed with clarity.

10.1 Anti-Backlash Gearbox

With any speed reduction via timing belts rejected, one of the heirs apparent would be the use of some sort of geared reduction. The relative rigidity of gears versus the compliance of belts in the previous iteration would be a welcome alleviation to the slop issue. Although the servomotor control loop would still be closed at the input end of the drive train, the accuracy of the output motion would still see a great improvement.

Another problem is introduced instead: backlash. Tolerances inherent to manufacture of gears in the real world preclude each tooth being exactly the same, so there must be some gap (however infinitesimal) between tooth thickness and space width of the gear teeth as they enter and leave mesh. As the torque function changes sign, there would be some amount of hysteresis as the system took up the gaps between gear teeth. With the servomotor loop not closed around the problem, so to speak, the risk of “hunting” would be fairly minimal, but with

the precision of the slider movement being a critical aspect of the application, backlash would necessitate some time-consuming adjustment to incorporate this backlash take-up into the servo program. It would inherently be an empirical process and an unsavory one to a mind accustomed to concrete matters. It follows, then, that the amount of backlash must be minimized, preferably to the point where acceptable accuracy could be attained without changing the servomotor program.

A number of anti-backlash gearboxes are available for princely sums from various manufacturers of drive train components. Given that the servomotor on hand has an IEC standard faceplate and shaft, it would seem most logical to choose a European manufacturer, so that the servomotor could simply be bolted on without the expense and complication of adapter plates and couplings. Further, a speed reduction on the same order as the timing belt train would have produced would be ideal, about 20:1. With that in mind, design options fall into two broad categories: a precision planetary gearbox (with output co-axial to input) or a servomotor worm gearbox (with the output at a right angle to input, and vertically displaced).

It is most useful to consider an actual product as representative of the class being considered. To that end, we shall first consider a high-precision planetary gearbox from Tramec, an Italian manufacturer. Tramec's REP series of planetary precision gearboxes are made to endure, with a case of nitride steel and case-hardened alloy steel gears. This translates to a fair level of durability, with the bearings rated for 20,000 hours, more than enough for the application. A 20:1 reduction gearbox (Tramec part number REP0752C20AU12FLTAE11P04), with a low mass moment of inertia (0.055 lb-in^2) is available from this manufacturer.

Maximum nominal input speed of 2500rpm and maximum transmitted torque of 85 ft-lb would put operation of both the linkage and cam well within the box's capability. With the vast reduction in mass moment of inertia of the drive train (from a series of pulleys and shafts to direct attachment) the servomotor would probably last much longer. The Tramec gearbox promises less than 6 arc-minutes of backlash, and a torsional rigidity of about 8 ft-lb per arc-minute. With a maximum torque at the crank pin provided of close to 100 lb-in, this amount of torsional rigidity would only result in an additional arc-minute of angular compliance.

A German manufacturer, Atlanta Drive Systems Inc, offers a series of worm reducers intended for use with servomotor systems that promise backlash between 1 and 14 arc-minutes in magnitude. The most likely candidate would be 59 01 020, A worm gear reducer with a 19.5:1 ratio and a center distance of 32 mm. This would also be a low-inertia system, with a mass moment of inertia of approximately 0.07 lb-in^2, comparable to the planetary gearbox considered earlier. The efficiency of this unit is worse than the one previously discussed, 81% efficient at 1500 RPM compared to the 93% dynamic efficiency cited by Tramec, as expected with worm gearing. Expected backlash is stated as less than 6 arc-minutes, less than the approximately 14 arc-minutes of angular error introduced by the resolver of the servomotor on hand and much less than the 2 degree error that results from a law of cosines calculation taking into account the 0.11 inch position uncertainty from the servomotor drive mode vibration analysis in Section 7.6.

While the gearboxes considered represent the bulk of the servomotor gearbox market, with comparable degrees of backlash present on most offerings studied, it *is* possible to obtain

higher-precision units. Güdel, a Swiss manufacturer, offers a line of adjustable worm-gear boxes with backlash of 30-70 arc seconds, a large improvement that surely carries a price premium.

To understand the implications of the backlash expected, it might be useful to compare the expected backlash to the accuracy of the resolver: as mentioned previously, the resolver is expected to only be accurate to about 14 arc-minutes. A major difference in importance is that the resolver's accuracy is passed through a 20:1 reduction before having any impact on the slider position. The backlash from the gearbox, however, becomes an unexpected displacement of the wrist pin at the zero crossing of the torque function of up to 0.005 inch with a 3 inch crank, or at the presumably massive expense of the Güdel box, 0.0004 inch to 0.001 inch.

The gearbox would be bolted directly onto the servomotor used in previous design iterations, and mounted via a detachable coupling to the crank shaft. The two-motor solution would be simplest, with the Leeson motor mounted onto a lower table in the machine enclosure and driving the cam shaft via v-belt.

10.2 Motor Re-Selection

The CSTM as designed constituted a low-speed, high inertia application. The torque requirements were modest. There are many servomotors on the market with the power to drive the system at the prescribed speed of 200 rotations per minute.

The high inertia of the system mandated a servomotor with high internal shaft inertia. This may seem counter-intuitive as increasing shaft inertia increases the torque requirement; in servomotor design however, manufacturers recommend a load inertia no more than 10 times the internal inertia of the servomotor. The reason for this is the encoder's/resolver's position at the back end of the servomotor shaft. Loading the shaft excessively creates the potential for

problematic servomotor shaft deflection; shaft deflection from load-end to encoder-end not only reduces the mechanical accuracy of the servomotor but could result in system instability and total failure if the inertia ratio exceeded manufacturer recommendations. In servomotor application design there is a difference between rotating a small mass at high speed and a large mass at low speed even if the power requirements are numerically equal especially if frequent stops are required; large load inertia requires a more robust servomotor shaft to limit deflection from load-end to encoder-end and thus preserve system stability.

A few notable servomotor manufacturers (Siemens and Parker-Hannifin, namely) offer high-inertia (HI) servomotors specifically for high-load-inertia applications. The essential difference between these motors and their normal counterparts is an internal flywheel on the servomotor shaft. Greater internal inertia requires these models to have more robust powering electronics which come at a greater cost than conventional servomotors.

The servomotor chosen for the direct-driven CSTM design is an HI model from Parker (MPJ-1424B), one of the leading servomotor manufacturers in the world. The model selected costs $2338 for the motor only. Other servomotors were researched, such as a rotary stage from Aerotech; these solutions proved to be unnecessarily accurate and thus expensive (Aerotech quoted approximately $9000 for their proposed servomotor solution, motor only) for this application.

Table 9 presents the relevant capabilities of the chosen servomotor compared with the calculated requirements of the CSTM. The load- to internal-inertia ratio is slightly better than 3:1 and well inside the design requirement of 10:1. The rest of the servomotor capabilities

show that it is more than capable of powering the CSTM; they also imply that servomotors are not ideal for such low-speed applications.

	MPJ-1424B	CSTM	Safety Factor / Ratio
Inertia (lbm-in^2)	26.941	76.299	0.353
Cont. Torque (lb-in.)	171.8	116.30	1.503
Peak Torque (lb-in.)	544.0	164.25	3.312
Rated Speed (rpm)	3145	114.7	27.419

Table 9: Comparison of Servomotor Capabilities

10.3 CSTM Design Changes

The original design for the CSTM included the two drive shafts at different vertical distances from the base plate. In the original design, this was useful; as both shafts were belt-driven, it allowed the transmission shaft to be located such that it was equidistant from both the cam and servomotor shafts and so only one belt was needed to drive the mechanism in either “mode”.

In the direct-drive design, however, it became immediately apparent that having two shafts at different heights from the base mounting plate would require more parts, more machine time, and more complexity than was desired. To eliminate all of this, the entire mechanism was effectively rotated by the appropriate angle (approximately 58 degrees) to locate each shaft at the same vertical position. This configuration is shown in Figure 55.

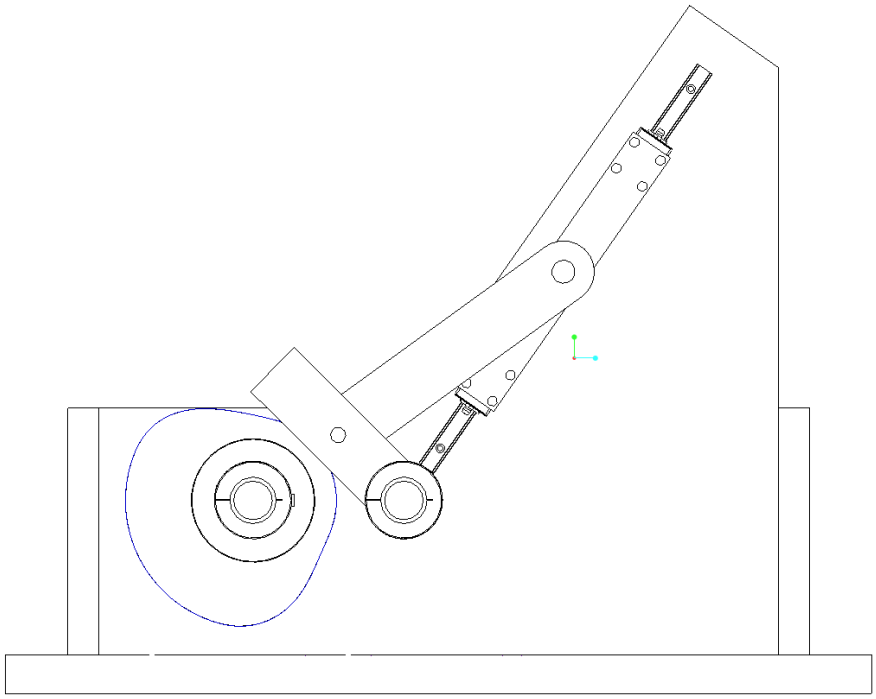

Figure 55: "Rotated" Direct-Drive Cam-Servo Test Machine Linkage

While rotating the machine in this manner will introduce acceleration due to gravity on the slider, this is considered a decent alternative. The acceleration will be identical for both drive configurations, therefore keeping all forces and inertias constant, as this is a design requirement.

Locating the shafts in this position simplified the mounting apparatus as well. A single motor is permanently mounted to one relatively complicated mounting fixture. The fixture is then bolted into one of two positions; one for each “mode”. The base plate of the machine is the vertical position reference for shaft alignment; the axial position reference is the face of the linkage side support; finally, two dowel inserts in the face of the linkage side support mate with two precision holes in the mating face of the mounting fixture to reference lateral position. The mounting fixture is shown in Figure 56.

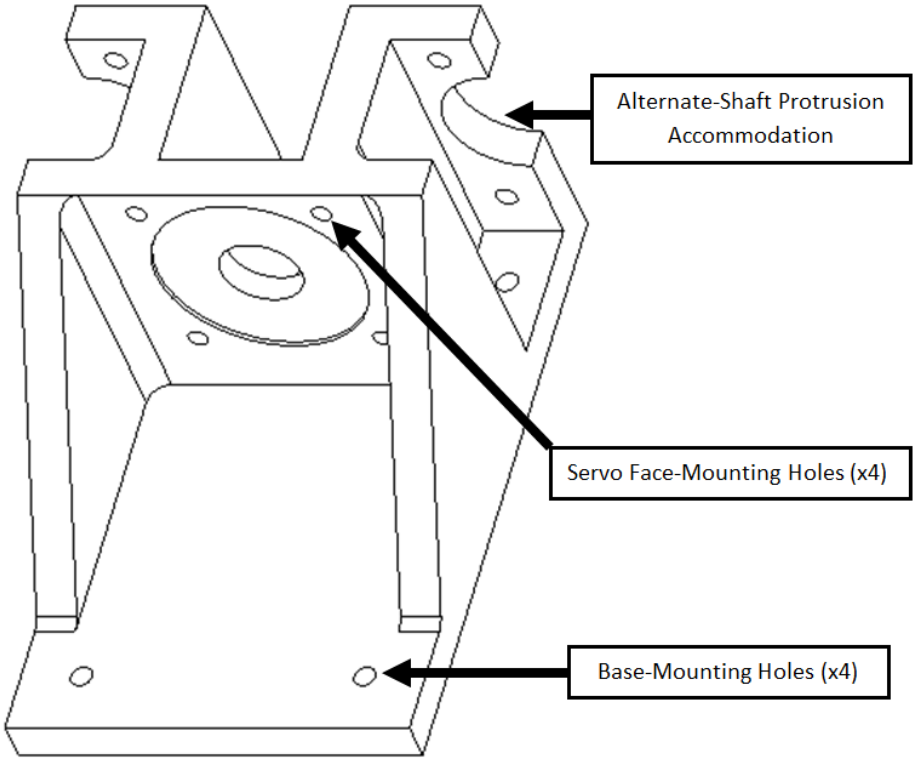

Figure 56: Direct-Drive Cam-Servo Test Machine Servomotor Mounting Fixture Design

Rotating the linkage mechanism had the added benefit of reducing the overall size of the CSTM considerably; the direct drive design utilizes a 28-inch square base plate including outer margins of 2 inches.

10.4 Shaft Coupling and Phase Preservation

The remaining design considerations of the direct-drive servomotor solution were specification of an apparatus to couple the shafts and a means of keeping phase between the servomotor and crank shafts. The need for coupling was obvious; the need for phase consistency stemmed from the servomotor programming, which would use absolute position data for its motion profile and so required the crank to be mounted in the same absolute position in order to not have to generate a new absolute motion profile at every mode switch. A flexible coupling was necessary due to the extreme difficulty of aligning the servo and crank/cam shafts to the degree required by a rigid coupling.

Fortunately a solution was found to satisfy all of these design considerations in the form of a two-piece steel-bellows coupling with a single-position, tapered press-fit attachment design. Manufacturer R+W claims zero backlash and torque transmitting capabilities far beyond the requirements of the CSTM. The two pieces can be ordered together or separately and are available in differing bores; this is useful considering that the Parker servomotor has a 28mm diameter metric shaft and the drive shafts of the CSTM are specified to a 1.25 inch diameter. This particular size can accommodate bores of both sizes without any customization. Also, while Figure 57 shows the general design of the coupling, the multi-position fitting is shown; the single-position fitting is also a standard feature even though it is not shown. The total cost of the coupling pieces (one bellows half, two clamp-only halves) was quoted to be $353.98.

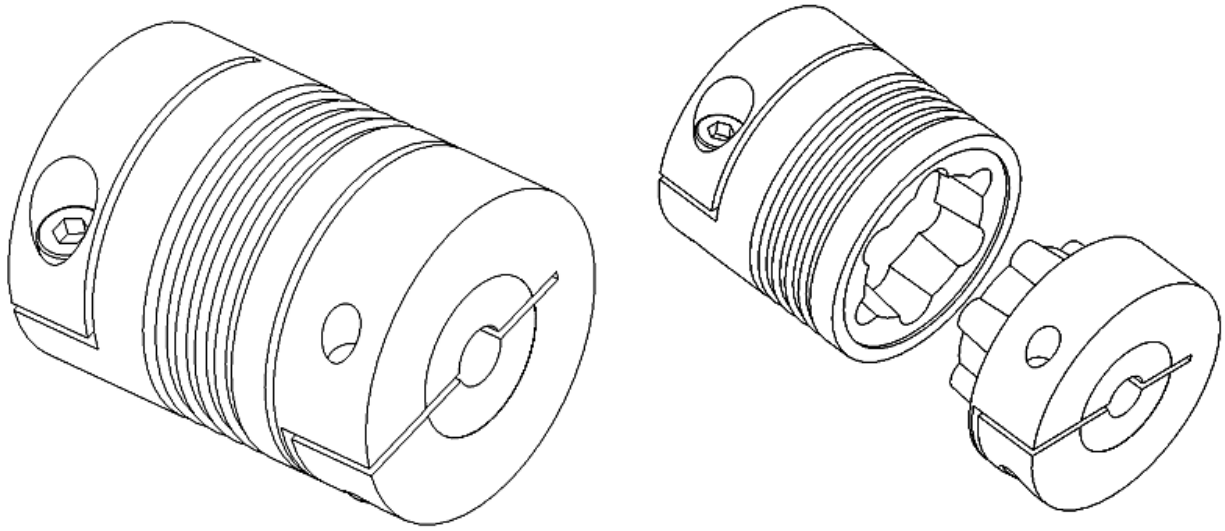

Figure 57: R+W Flexible Two-Piece Coupling

This coupler requires axial pre-tensioning in order to function properly and keep the two halves from separating. The maximum axial preload displacement for the selected model is 1.5mm which results in an axial preload force of approximately 15lbs. This preload can be "programmed" by clamping the halves of the coupler to their respective shafts with the proper

displacement accounted for; mounting the servomotor mounting fixture then automatically preloads the coupling.

10.5 Additional Considerations

The other requirements of the servomotor will be discussed here as well. The servomotor itself costs approximately $2300. The driver/controller module for the motor costs $4211. The cables alone cost $300. That brings the total purchased-materials cost up to about $7200 for the direct-drive servomotor solution. Without including manufacturing costs, the cost of such a system is high.

10.6 Vibration Analysis

The theoretical accuracy of the system was calculated to be very high. The servomotor selected is mechanically accurate to 18 arc-seconds (18/3600ths of one degree) which translated to an uncertainty at the slider of approximately 2.00×10^{-4} inches. This position error is very insignificant compared to the position error contributed by vibration.

The spring rate of the system in servomotor driven operation was approximately 23210 lb/inch. The components included in the spring model (calculations discussed in Section 7 and Appendix E) are shown in Figure 58.

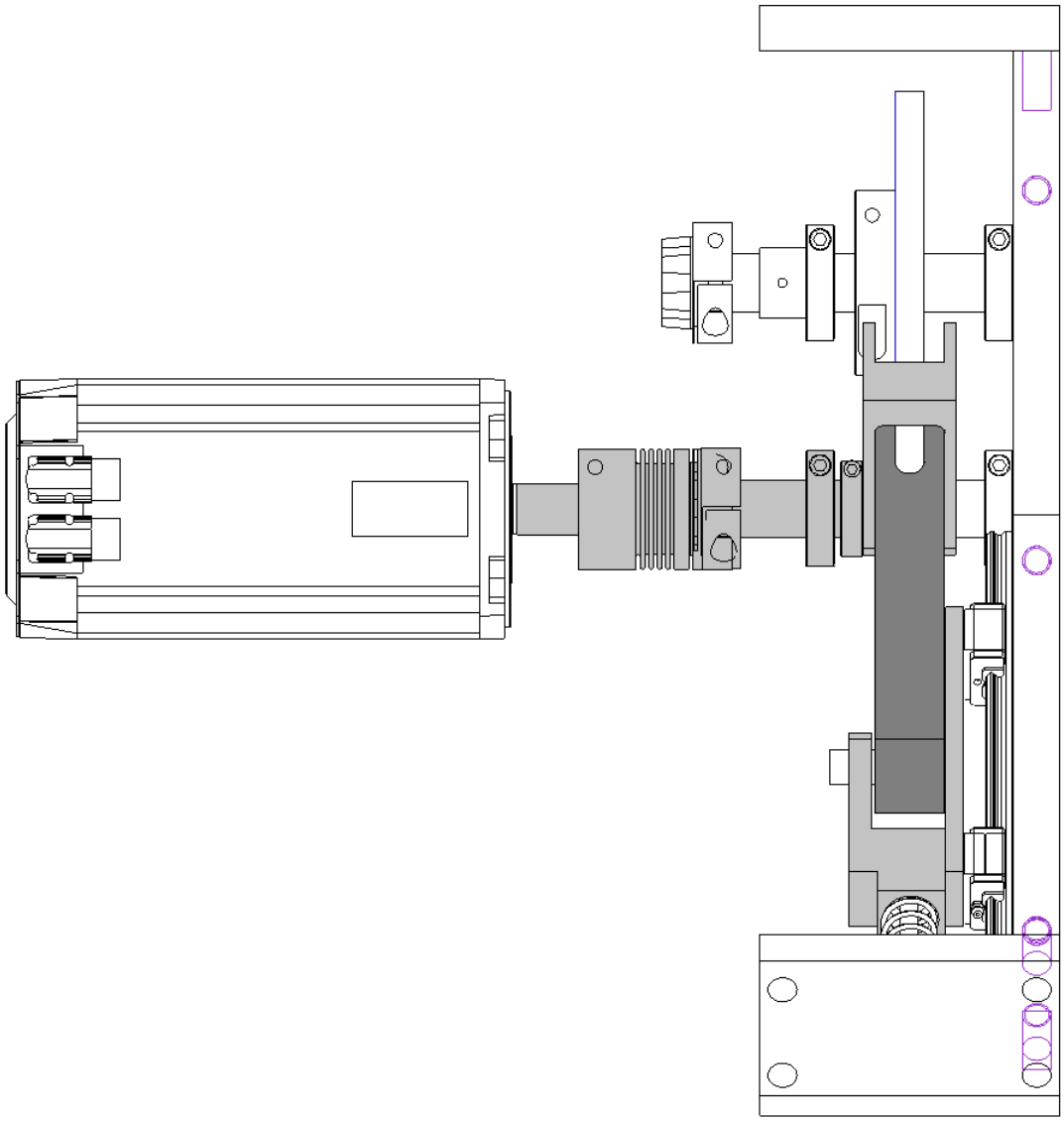

Figure 58: Direct-Drive Cam-Servo Test Machine Assembly, Top View

(Supports hidden, spring components grayed)

The results of the vibration analysis are shown in Figure 59. The Direct-Drive Cam-Servo Test Machine design shows acceptable position error (±0.0022 inches) under the given parameters. It is important to note, however, that the cam driven mode position error simulation exhibits less than a quarter of that of the servomotor driven mode. The flexible coupling is the component that contributes the most to stiffness loss; if necessary, position error could be reduced somewhat by using a more torsionally rigid coupling (R+W offers larger

coupling models that are stiffer but have significantly higher inertias. Such a change may require a more powerful servomotor model).

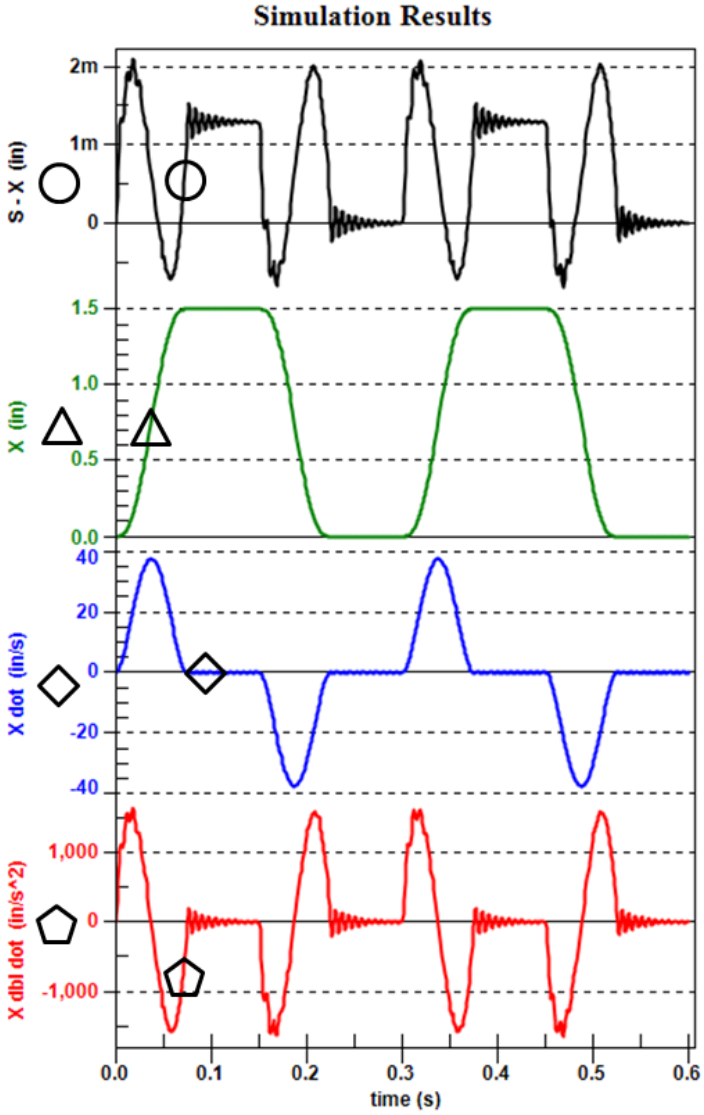

Figure 59: Vibration Analysis of Direct-Drive Cam-Servo Test Machine in Servomotor Driven Mode

10.7 Re-Design Overview

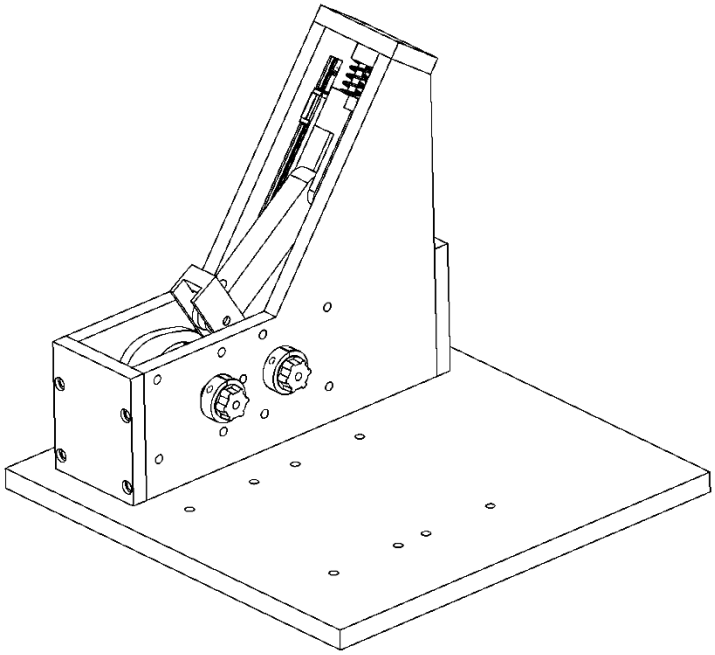

Figure 60: Direct-Drive Cam-Servo Test Machine, No Motor

(Note: Two male halves of coupling, one on each shaft)

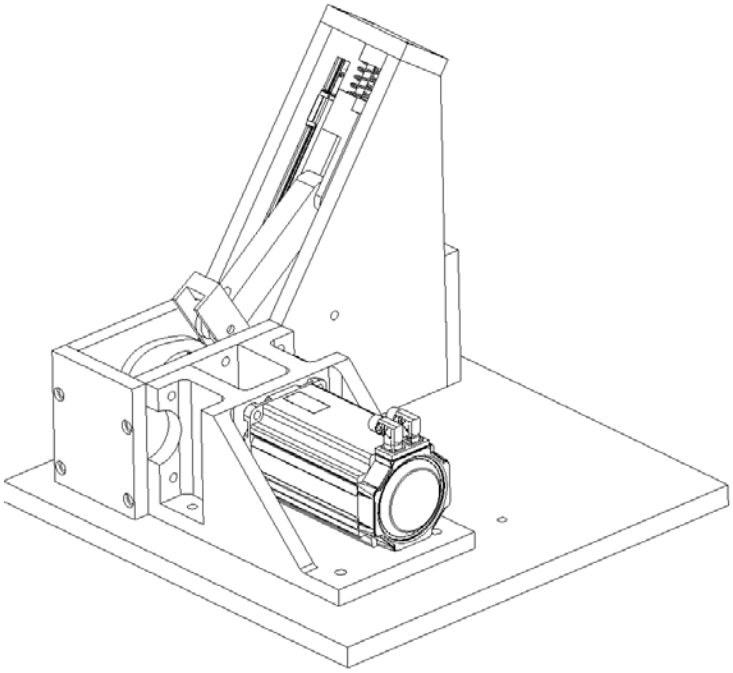

Figure 61: Direct-Drive Cam-Servo Test Machine, Cam Mode

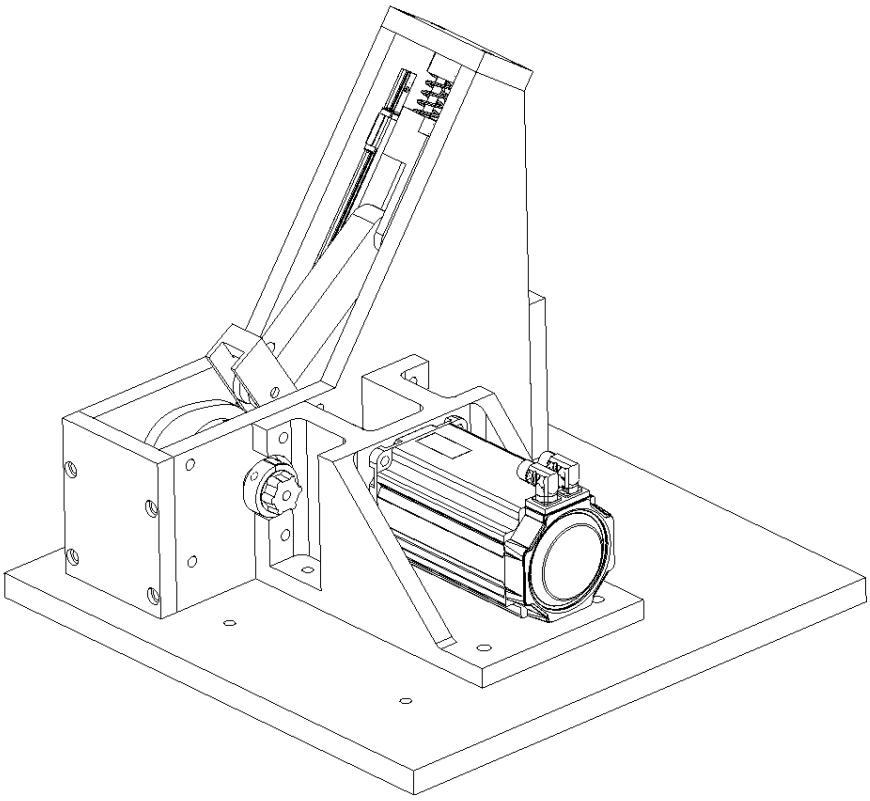

Figure 62: Direct-Drive Cam-Servo Test Machine, Servo Mode

Figure 60, Figure 61, and Figure 62 present the design in its fully constructed state. The mode is switched by unfastening the 8 bolts that fix the mounting fixture to the base and linkage box and physically moving the motor fixture to align with the appropriate shaft, ensuring that the alignment dowels are ready to mesh correctly, pressing the face of the mounting fixture to the face of the linkage box, and fastening the fixture in place.

The Direct-Drive Cam-Servo Test Machine design fulfills the task specifications for this project. It is favored over the anti-backlash gearbox solution because those gearboxes still exhibit backlash and as such will be less mechanically accurate. Considering the proximity of the position error of the zero-backlash Direct-Drive CSTM design to the allowable limit, an anti-backlash gearbox would have to be extremely low-backlash and, as such, very expensive unless further measures were taken to stiffen the coupling and linkage.

There are measures by which the system could be stiffened that were not fully explored in this report. A large coupling of similar design could be used to increase torsional rigidity on the crank shaft. The crank and cam shaft diameters could be increased; however any significant increase to the crank shaft would require that a portion of the shaft be turned down to accommodate the travel of the cam profile. In the Direct-Drive CSTM there existed approximately 0.15 inches of clearance between the outermost diameter of the cam and the 1.25inch-diameter crank shaft; altering the distance between the cam and crank shafts would break the geometric relations between the cam and linkage (discussed in Section 3). One possible option was to reduce the prime radius and thus the overall size of the cam. This is a viable option down to a prime radius of 2.75inches (all CSTM cam designs have a prime radius of 3.197 inches) which is the minimum allowable for the supplied cam blank and a 1-inch roller follower. However decreasing the prime radius increases pressure angle on the roller follower. Due to the compromising nature of these changes and the Direct-Drive CSTM design's acceptable calculated performance, none of them were implemented in the final design.

11 References

Ashford, N. A., & Foundation, F. (1976). *Crisis in the workplace: Occupational disease and injury : a report to the Ford Foundation.* Cambridge: MIT Press.

Baumeister, T., Theodore, A. M., & Avallone, E. A. (2007). *Marks' Standard Handbook For Mechanical Engineers.* New York: McGraw-Hill.

Centers for Disease Control and Prevention. (2008, October 22). *National Health Statistics Reports*. Retrieved from Centers for Disease Control and Prevention: http://www.cdc.gov/nchs/data/nhsr/nhsr010.pdf

Dul, J., & Weerdmeester, B. A. (1993). *Ergonomics for Beginners: A Quick Reference Guide.* London: Taylor & Francis.

Eckhardt, H. D. (1998). *Kinematic Design of Machines and Mechanisms .* New York: McGraw-Hill.

Machinetoolhelp.com LLC. (2010). *Top ten stepper motor & DC motor advantages and disadvantages | DC stepper motor benefits and drawbacks*. Retrieved from CNC Machine Tool Help | Learn CNC | CNC Programming | Learn cnc | CNC Training information and CNC articles: http://www.machinetoolhelp.com/Automation/systemdesign/stepper_dcservo.html

Marmaras, N., Poulakakis, G., & Papakostopoulos, V. (1999). Ergonomic Design in Ancient Greece. *Applied Ergonomics , Volume 30* (Issue 4), 361-368.

Norton, R. L. (2009). *Cam Design and Manufacturing Handbook* (2nd Edition ed.). New York: Industrial Press.

Norton, R. L. (2008). *Design of Machinery: An Introduction to the Synthesis and Analysis of Mechanisms and Machines* (4th Edition ed.). Boston: McGraw-Hill Higher Education.

Norton, R. L. (2011). *Machine Design: An Integrated Approach* (4th Edition ed.). Boston: Prentice Hall.

Penton Media, Inc. & Machine Design magazine. (2010). *Servo Motors - Basics of Servo Motor Design & Engineering*. Retrieved from Electric Motors & DC Motors: http://www.electricmotors.machinedesign.com/guiEdits/Content/bdeee4a/bdeee4a_1.aspx

U.S. Department of Labor. (n.d.). Retrieved from Occupational Safety and Health Administration: http://www.osha.gov/

12 Bibliography

[1] Design of Machinery, 5th ed. R. L. Norton, pg.784
McGraw-Hill, New York, 2011

[2] Design of Machinery, 5th ed. R. L. Norton, pg.783
McGraw-Hill, New York, 2011

[3] Design of Machinery, 5th ed. R. L. Norton, pg.789
McGraw-Hill, New York, 2011

[4] Design of Machinery, 5th ed. R. L. Norton, pg.797
McGraw-Hill, New York, 2011

[5] Design of Machinery, 5th ed. R. L. Norton, pg.801
McGraw-Hill, New York, 2011

[6] Cam Design and Manufacturing Handbook, 2nd ed. R. L. Norton, pg.6
Industrial Press, Inc, New York, 2009

[7] Cam Design and Manufacturing Handbook, 2nd ed. R. L. Norton, pg.3
Industrial Press, Inc, New York, 2009

[8] Design of Machinery, 5th ed. R. L. Norton, pg.802
McGraw-Hill, New York, 2011

[9] Cam Design and Manufacturing Handbook, 2nd ed. R. L. Norton, pg.251
Industrial Press, Inc, New York, 2009

[10] Design of Machinery, 5th ed. R. L. Norton, pg.140
McGraw-Hill, New York, 2011

[11] Design of Machinery, 5th ed. R. L. Norton, pg.402
McGraw-Hill, New York, 2011

[12] Design of Machinery, 5th ed. R. L. Norton, pg.660
McGraw-Hill, New York, 2011

[13] Catalog, McMaster-Carr Inc, p 1036
Robbinsville, NJ

[14] Catalog, McMaster-Carr Inc, p 1015
Robbinsville, NJ

[15] Design of Machinery, 5th ed. R. L. Norton, pg.491
McGraw-Hill, New York, 2011

[16] "Racehorse | PowerGrip GT 2 Belt Drives," Drive Design Manual
The Gates Rubber Company, Retrieved from Web 1/2/2011

[17] Catalog, McMaster-Carr Inc, p 1022
Robbinsville, NJ

[18] Design of Machinery, 5th ed. R. L. Norton, pg. 663
McGraw-Hill, New York, 2011

[19] Machine Design: An Integrated Approach, 4th ed. R.L. Norton, pg.73
McGraw-Hill, New York, 2010

[20] "Encoder vs. Resolver-Based Servo Systems," Technical Guide
ORMEC Systems Corp. Retrieved from Web 1/2/2011

[21] Design of Machinery, 5th ed. R. L. Norton, pg.491
McGraw-Hill, New York, 2011

13 Appendix A: Vector Loop Analysis for Fourbar Linkage with zero offset

13.1 Position Analysis

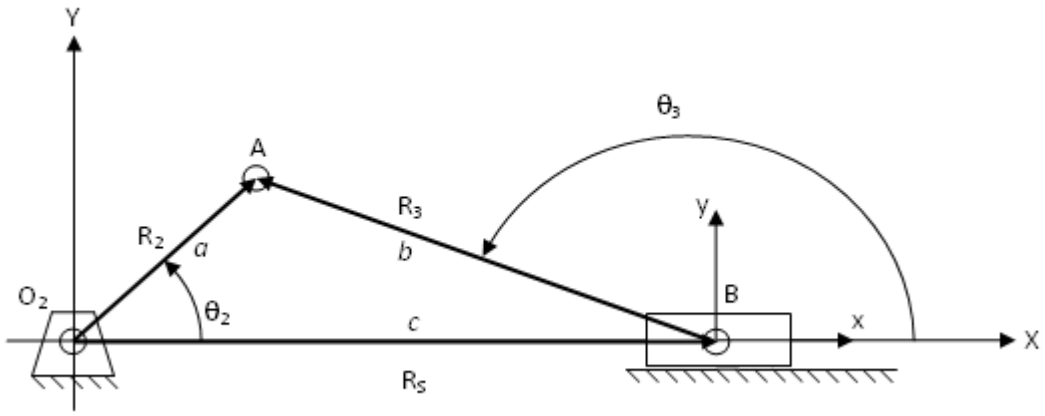

Figure 63: Position Vector Loop for slider-crank fourbar with zero offset

For the linkage shown in Figure 63 the vector loop is as follows:

$$R_2 - R_3 - R_S = 0$$

Using the vector magnitudes (link lengths) and corresponding angles the vector loop becomes:

$$ae^{j\theta_2} - be^{j\theta_3} - ce^{j\theta_1} = 0$$

Applying Euler equivalents:

$$a(\cos\theta_2 + j\sin\theta_2) - b(\cos\theta_3 + j\sin\theta_3) - c(\cos\theta_1 + j\sin\theta_1) = 0$$

Separating the real and imaginary components:

The real, or X component:

$$a\cos\theta_2 - b\cos\theta_3 - c\cos\theta_1 = 0$$

But $\theta_1 = 0$, therefore:

$$a\cos\theta_2 - b\cos\theta_3 - c = 0$$

The imaginary, or Y components:

$$aj\sin\theta_2 - jb\sin\theta_3 - c\sin\theta_S = 0$$

But$\theta_S = 0$, therefore:

$$a\sin\theta_2 - b\sin\theta_3 = 0$$

Taking the final X and Y components and solving for *c* and θ_3:

$$c = a\cos\theta_2 - b\cos\theta_3$$

$$\theta_3 = \sin^{-1}\left(\frac{a\sin\theta_2}{b}\right)$$

Therefore *c,* or the distance along the X axis of the slider is a function of the link lengths *a* and *b* and angles $\theta_2$and θ_3, all of which are known.

$$c = f(a, b, \theta_2, \theta_3)$$

$\theta_3$is a function of link lengths *a* and *b* and angles θ_2.

$$\theta_3 = f(a, b, \theta_2)$$

13.2 Velocity Analysis

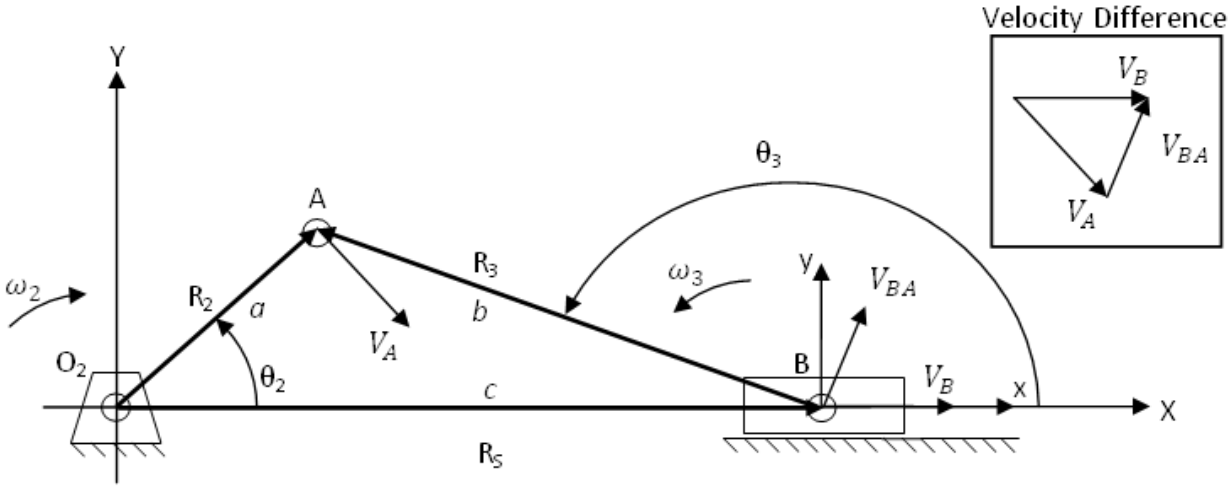

Figure 64: Velocity Vector Loop for slider-crank fourbar with zero offset

Using the vector loop equation from the position analysis (repeated here):

$$R_2 - R_3 - R_S = 0$$

$$ae^{j\theta_2} - be^{j\theta_3} - ce^{j\theta_S} = 0$$

Differentiating with respect to time will result in the following velocity equations:

$$ja\omega_2 e^{j\theta_2} - jb\omega_3 e^{j\theta_3} - \dot{c} = 0$$

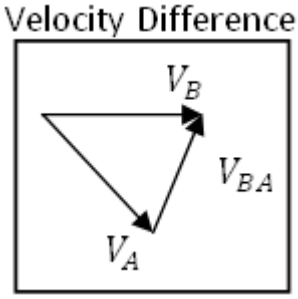

Figure 65: Resulting Velocity Difference from Vector Loop

Using the velocity loop triangle, the following relationship is found:

$$V_A + V_{BA} - V_B = 0$$

$$V_B = V_A + V_{BA}$$

Applying Euler equivalents:

$$ja\omega_2(\cos\theta_2 + j\sin\theta_2) - jb\omega_3(\cos\theta_3 + j\sin\theta_3) - \dot{c} = 0$$

$$a\omega_2(-\sin\theta_2 + jcos\theta_2) - b\omega_3(-\sin\theta_3 + jcos\theta_3) - \dot{c} = 0$$

Separating the real and imaginary components:

The real, or X component:

$$-a\omega_2\sin\theta_2 + b\omega_3\sin\theta_3 - \dot{c} = 0$$

The imaginary, or Y components:

$$a\omega_2\cos\theta_2 - b\omega_3\cos\theta_3 = 0$$

Taking the final X and Y components and solving for $\dot{c}$ and ω_3:

$$\omega_3 = \frac{a\cos\theta_2}{b\cos\theta_3}\omega_2$$

$$\dot{c} = -a\omega_2\sin\theta_2 + b\omega_3\sin\theta_3$$

Therefore $\dot{c}$, or the velocity of the slider along the X axis is a function of the link lengths *a* and *b* and angles θ_2, θ_3, and the angular velocities ω_2, ω_3; all of which are known.

$$\dot{c} = f(a, b, \theta_2, \theta_3, \omega_2, \omega_3)$$

ω_3 is a function of link lengths *a* and *b*, angles θ_2, $\theta_3$and angular velocities ω_2.

$$\omega_3 = f(a, b, \theta_2, \theta_3, \omega_2)$$

13.3 Acceleration Analysis

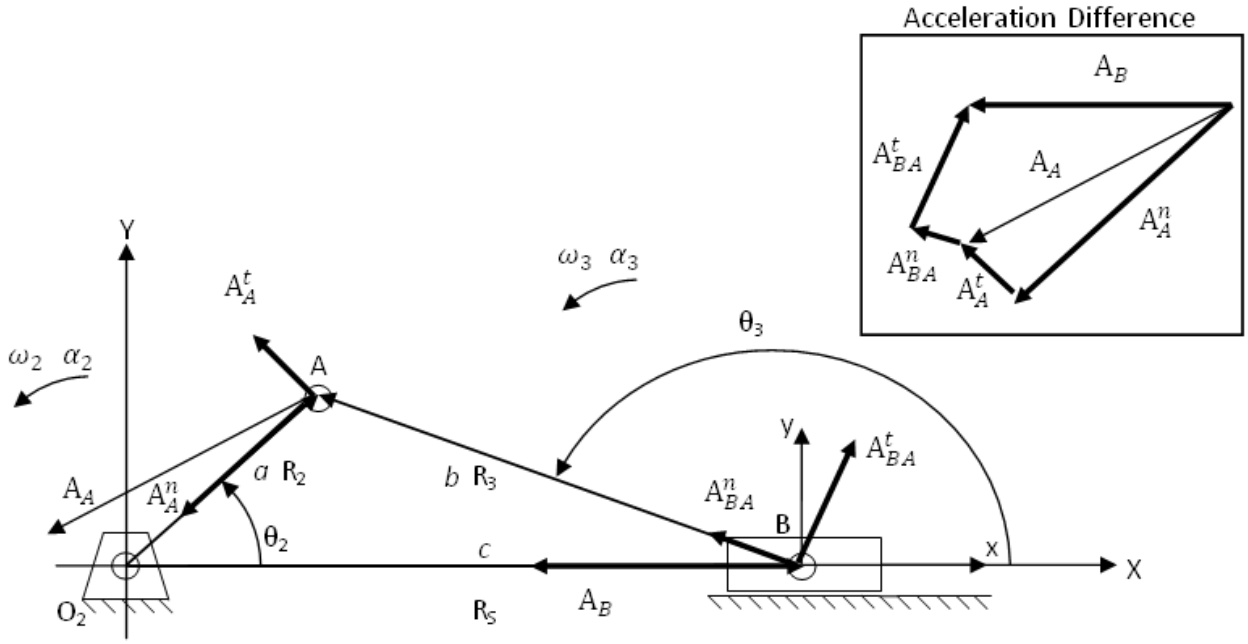

Figure 66: Acceleration Vector Loop for slider-crank fourbar with zero offset

Using the vector loop equation from the position analysis (repeated here):

$$R_2 - R_3 - R_S = 0$$

$$ae^{j\theta_2} - be^{j\theta_3} - ce^{j\theta_S} = 0$$

Differentiating with respect to time will result in the following velocity equations:

$$ja\omega_2 e^{j\theta_2} - jb\omega_3 e^{j\theta_3} - \dot{c} = 0$$

$$\left(ja\alpha_2 e^{j\theta_2} + j^2 a\omega_2^2 e^{j\theta_2}\right) - \left(jb\alpha_3 e^{j\theta_3} + j^2 b\omega_3^2 e^{j\theta_3}\right) - \ddot{c} = 0$$

$$\left(a\alpha_2 j e^{j\theta_2} - a\omega_2^2 e^{j\theta_2}\right) - \left(b\alpha_3 e^{j\theta_3} - b\omega_3^2 e^{j\theta_3}\right) - \ddot{c} = 0$$

Applying Euler equivalents:

$$a\alpha_2(-\sin\theta_2 + j\cos\theta_2) - a\omega_2^2(\cos\theta_2 + j\sin\theta_2) - b\alpha_3(-\sin\theta_3 + j\cos\theta_3) + b\omega_3^2(\cos\theta_3 + j\sin\theta_3) - \ddot{c} = 0$$

Separating the real and imaginary components:

The real, or X component:

$$-a\alpha_2\sin\theta_2 - a\omega_2^2\cos\theta_2 + b\alpha_3\sin\theta_3 + b\omega_3^2\cos\theta_3 - \ddot{c} = 0$$

The imaginary, or Y components:

$$a\alpha_2\cos\theta_2 - a\omega_2^2\sin\theta_2 + b\alpha_3\cos\theta_3 + b\omega_3^2\sin\theta_3 = 0$$

Taking the final X and Y components and solving for $\ddot{c}$ and α_3:

$$\alpha_3 = \frac{a\alpha_2\cos\theta_2 - a\omega_2^2\sin\theta_2 + b\omega_3^2\sin\theta_3}{b\alpha_3\cos\theta_3}$$

$$\ddot{c} = -a\alpha_2\sin\theta_2 - a\omega_2^2\cos\theta_2 + b\alpha_3\sin\theta_3 + b\omega_3^2\cos\theta_3$$

Therefore $\ddot{c}$, or the acceleration of the slider along the X axis is a function of the link lengths *a* and *b*, angles θ_2, θ_3, the angular velocities ω_2, ω_3, and angular acceleration α_2, and α_3; all of which are known.

$$\ddot{c} = f(a, b, \theta_2, \theta_3, \omega_2, \omega_3, \alpha_2, \alpha_3)$$

$\alpha_3$is a function of link lengths *a* and *b*, angles θ_2, θ_3 angular velocities ω_2, ω_3, and angular acceleration α_2.

$$\alpha_3 = f(a, b, \theta_2, \theta_3, \omega_2, \omega_3, \alpha_2)$$

14 Appendix B: Preliminary Designs

14.1 Lead Screw

While the initial brainstorming sessions focused on traditional linkage and direct-mount servo solutions, radical departures from such were considered. One admittedly off-the-wall suggestion concerned the use of a lead screw to transform rotary output from the servo to linear motion of a sliding slider. Combinations of several of these on gantries are the kinematic chain for many kinds of automated machinery, including high-speed pick and place assembly cells in electronics manufacture. To adapt the concept for a cam/servo comparison, a simpler version was needed, consisting of a single lead screw moving a platform.

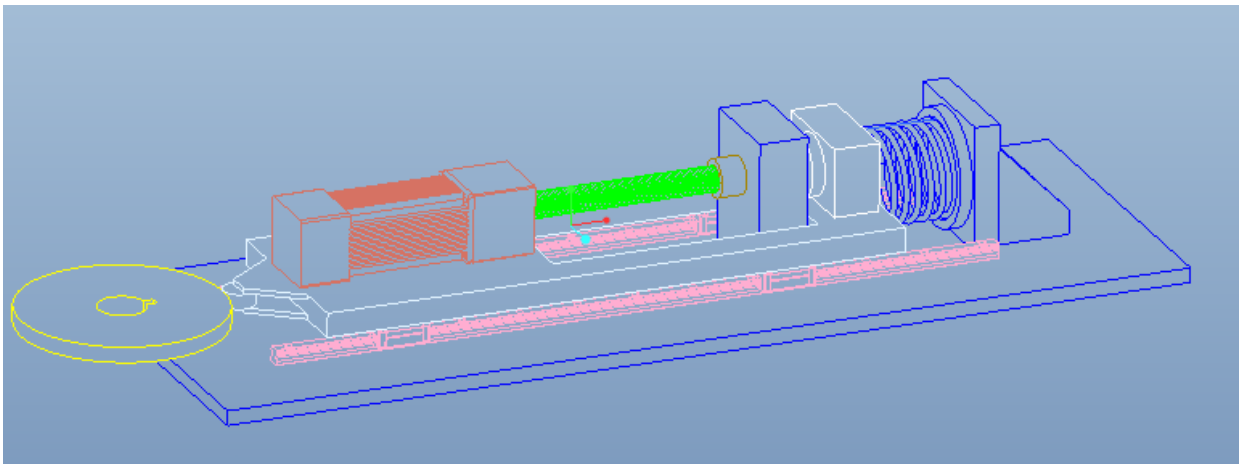

Figure 67: Lead Screw System Diagram

The linear guides (pink) provide one degree of freedom to a slider (white) while supporting the load. The base plate (deep blue) carries both a load spring assembly and a post where a nut (brown) is mounted. The servo and gearbox (red) are connected to the lead screw (green) with a coupling. As the motor turns the lead screw, the nut, which has a protrusion locked into the lead screw's groove, causes the slider to move relative to the table. The other

end of the screw is supported in an end block, which also white. In the configuration shown above, when the cam (yellow) is turning, the servo and lead screw are back-driven. It may prove necessary to provide either a disconnect-able nut or a clutch instead of the coupling if either turning the lead screw by exerting co-axial force or back-driving the servo (respectively) require too much torque from the motor driving the cam.

The fatal flaw of this prospective design is that the cycle speed specified (200 cycles per minute) is not readily achievable with a lead screw mechanism as shown, chiefly due to the fact that without some sort of reduction, the servomotor on hand would not be able to supply enough torque.

14.2 Rack and Pinion Solution

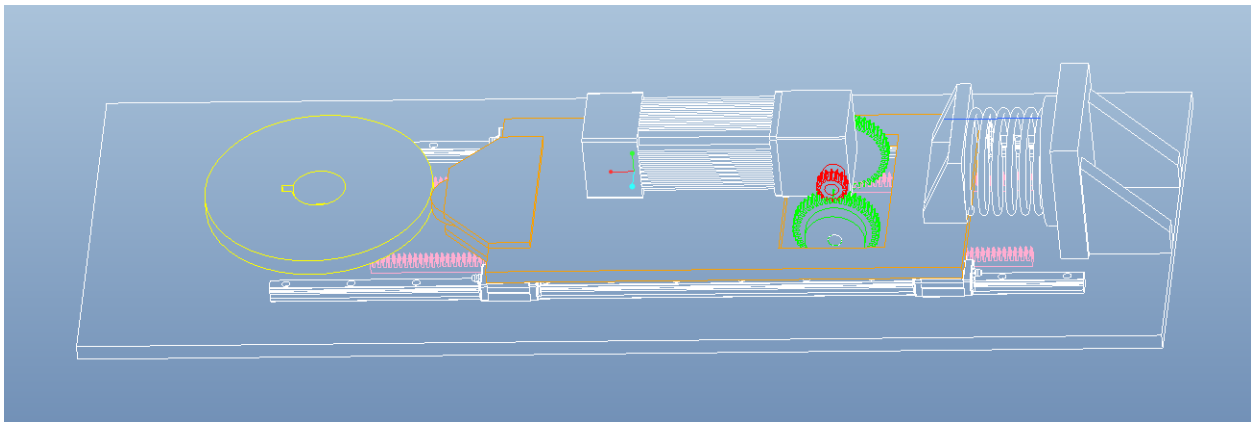

Figure 68: Rack and Pinion System Diagram

A similar design involves the substitution of gearing for a lead screw. This substitution was made in an effort to avoid the difficulty of disconnecting the servo drive train in this configuration, obviating the need for a clutch or disconnect-able nut. In this case, displacement of the motor upward (as drawn above) would pull the pinion (red) out of mesh with the other spur gears (green). When the servo is engaged, the pinion drives the spurs, which drive against the racks (pink). It was originally intended to use an anti-backlash helical rack, but no suitable

one could be found readily. Some degree of backlash take-up could be achieved by setting the green gears on the shaft (not shown) slightly twisted relative to each other. Backlash from the pinion/spur connection would remain, however. The underlying tradeoff is mechanical simplicity versus accuracy.

Either of these designs would require a total re-creation of the CAD files with more realistic assumptions and more calculation to ensure viability. For example, the servomotor and gearboxes would need to be mounted very rigidly to the slider, a need unaddressed in the designs above. Further, gearboxes for each would need to be specified and calculations would need to be performed to verify their suitability. In the case of the rack and pinion design, questions of tooth geometry remain. For the purposes of mocking up the design, 16 pitch 14.2-degree gears were chosen. With a bearing face of half an inch and steel construction, it would seem a safe bet that they would suffice. It might prove necessary, however, to change the pitch or the contact angles if loads turned out to be more intense. A very useful step, given the opportunity, would be revising these models into ones capable of dynamic analysis.

15 Appendix C: Geometry Selection

Selecting a particular geometry for the linkage and cam combination presented a sophisticated design problem. Of the many adjustable parameters, some subset must be free, determining every other parameter. On top of that, any given configuration of free variable inputs entered into DYNACAM would then produce a set of outputs, which then had to be checked against several constraints (such as motor torque, pin forces, and resultant pressure angles). How then, to search for the free variables?

As always, the first step was a diagram of the system, with the basic assumption of co-linearity between the crank pivot's connection to ground and the travel of the slider. This will simplify the math and packaging greatly. Some of the potential variables are color-coded below, for ease of discussion. Conspicuously absent is the precise geometry of the cam, not shown here but discussed later.

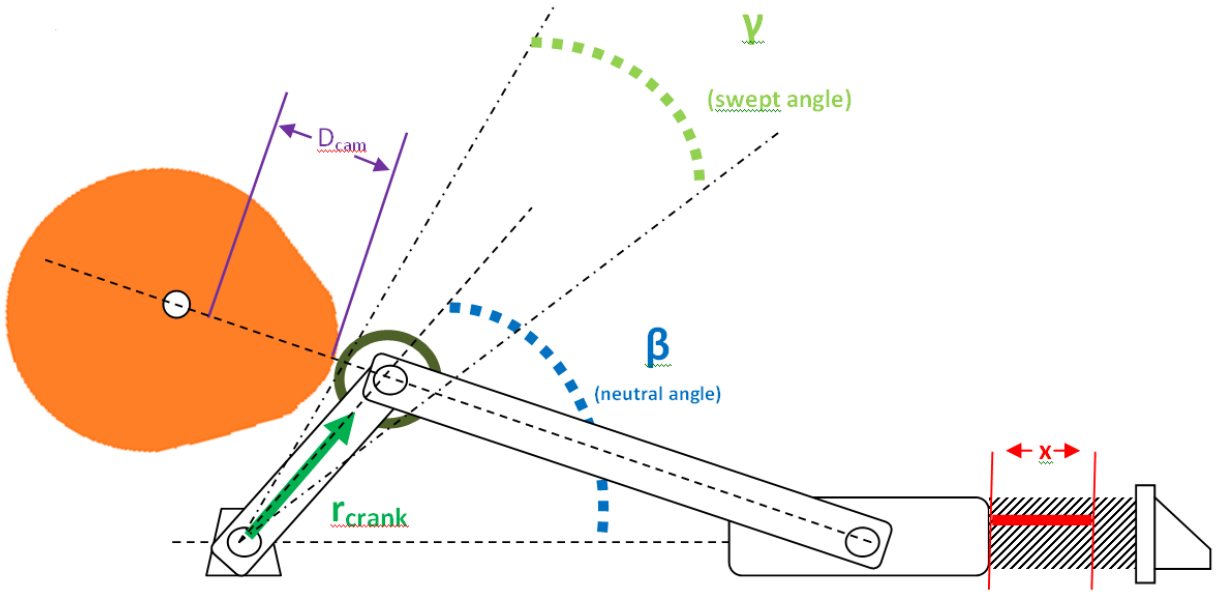

Figure 69: System Parameters

The 3:1 crank ratio (chosen as standard in mechanical design) simplifies description of the linkage geometry, especially in conjunction with the known travel. The **absolute magnitude of the crank**, then, is a natural choice as a free variable. If a **crank length** is chosen, the connecting rod length is then known. It is clear from the diagram that for a given **crank length** and **neutral angle**, everything else pertaining to the linkage geometry can be determined. Below is an expression of x in terms of r_{crank}, β, and γ. This was derived from position analysis based on the fact that (β-γ/2) is the end point of the stroke and that (β+γ/2) is its beginning. From a vector loop equation, their relationship was determined.

Given

$$x = \left(r_{crank}\cdot\cos\left(\beta - \frac{\gamma_1}{2}\right) - r_{coupler}\cdot\cos\left(\operatorname{asin}\left(r_{crank}\cdot\frac{\sin\left(\beta - \frac{\gamma_1}{2}\right)}{r_{coupler}}\right)\right)\right) - \left(r_{crank}\cdot\cos\left(\beta + \frac{\gamma_1}{2}\right) - r_{coupler}\cdot\cos\left(\operatorname{asin}\left(r_{crank}\cdot\frac{\sin\left(\beta + \frac{\gamma_1}{2}\right)}{r_{coupler}}\right)\right)\right)$$

While the previously discussed variables determine the linkage geometry, there is another degree of freedom introduced by the cam. It was convenient to think of it first in terms of the follower travel. D_{cam} shown above is the length of travel of the follower's surface, the difference between the cam radiuses at its farthest and closest points. From basic trigonometry, we can state that:

$$D_{cam} := 2 \cdot r_{crank} \cdot \sin\left(\frac{\gamma_1}{2}\right)$$

It is dependent on the crank and gamma angles for its value. We also know that the prime radius can be expressed in terms of the diameter of the cam blank (to ease machining), the follower radius, and that travel, as follows:

$$R_p := R_f + 4.125 - D_{cam}$$

Since we know that the cam travel is stated above in terms of the two other variables, we are left with a choice of follower radius alone as a free variable. Ergo, all possible geometries of cam and linkage can be expressed as some value of the three free variables, R_f, β and γ.

Constraints on each free variable were immediately apparent. The crank was the first to be confined. The minimum crank radius was deemed to be 0.75in, as anything shorter would be very difficult to package properly. Constraints on the crank upper bounds (without recourse to DYNACAM output such as torque requirement) stemmed from overall size. The machine had to be kept to a reasonable scale; the machine was to be four feet long at absolute most, a tabletop size. If the crank and connecting rod were laid flat, they would be on the same line as the slide travel, which also could not extend outside the 48in envelope.

With the 3:1 connecting rod-crank ratio, then:

crank + connecting rod + travel = 48in
$r_{crank} + 3r_{crank} + 1.5in = 48in$
$r_{crankMAX} = 11.625in$

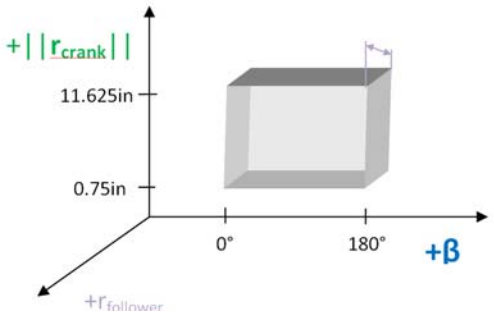

Figure 69: Raw Solution Space

The crank radius was then constrained to the interval 0.75in – 11.625in, inclusive. If an exhaustive search of the solutions were to be computed, points separated by an interval of less than an inch would probably be necessary, requiring at least 10 iterations per line in the solution space.

The neutral angle could be anywhere between 0° and 180°, exclusively, as either one exactly would result in the mechanism delivering crushing blows to the crank at the end of the stroke, and probably over-swinging into an inverted position. If an exhaustive search of the area was necessary, the points would probably be separated by at least 15°, necessitating 24 iterations per line in the solution space.

In the absence of any concavities on the cam's surface which might not be fully accessible with an excessively large cam, it seems relatively unimportant except for convenience of packaging. Since the follower contacts the cam in on only an infinitesimal area, various follower radii behave very similarly except for their mass. Therefore, an arbitrary follower radius (except for helping determine the machine geometry) is acceptable, as many follower diameters are available.

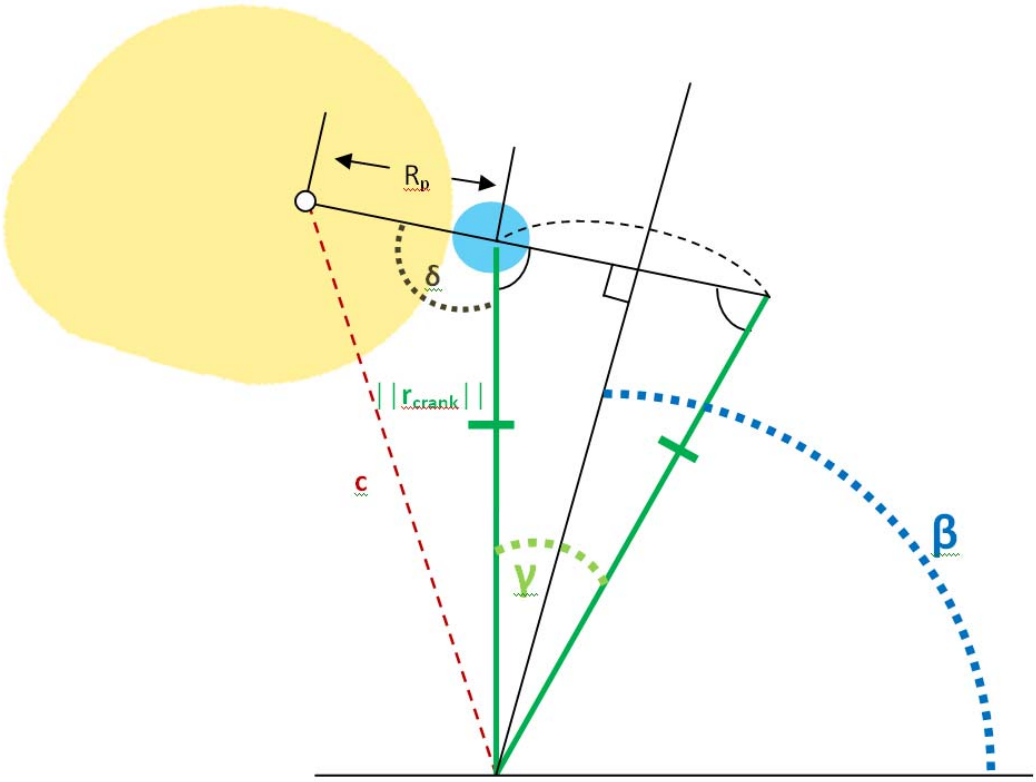

Figure 71: The Perpendicularity Constraint

Two considerations prompted a further geometric constraint (removing the remaining degree of freedom incurred from cam placement). First, ease of comparison of servo and cam dynamics would require that the cam motion provide its force with a pressure angle as close to 0° as possible because the servo would be providing tangential force to the crank-connecting rod pivot from its torque. If the cam were not providing force at close to 0° pressure angle, down and side forces would play a larger role in the motion of the slider, which would not correspond well to servo actuation. Second, a symmetrical spread of pressure angles (with the greatest in magnitude at the ends of the stroke) would provide the best dynamic balancing of the mechanism and the most effective transfer of power.

Given then, that the pressure angle should be 90° at the middle of the stroke, the centerline shown above, separated by the angle β from the ground plane is the where the follower is at the center point of the stroke. From the geometry of this arrangement, the following descriptive equation emerges:

$$\boldsymbol{c} = SQRT(\boldsymbol{r_p}^2+\boldsymbol{r_{crank}}^2-2*R_p*\boldsymbol{r_{crank}}*cos(\varphi))$$

Within the rectangular prism defined by the limitations on the three free variables (the raw design space), all possible solutions fitting those requirements resided. Exhaustive searching of this space was deemed to be prohibitively time-consuming. With reasonable intervals, the number of required combinations would be:

Possible values within prism (θ $||r_{crank}||$ * $r_{follower}$)*
*24 * 10 * 5 = 1200 permutations*

The number of calculations could be reduced by figuring out boundaries within that would enclose a more suitable solution solid (defined as the region within the design space that yields solutions that do not yield unacceptable results with regard to the design requirements). A given requirement, say torque, corresponds to a section of the prism that is out of bounds (labeled “prohibited” below). Without calculation, any shape for the prohibited region is possible. To derive the function in three variables defining it, one would have to do extensive work with the system, for example defining the torque region as some function of crank length. Furthermore, torque is not the only output from DYNACAM constraining the design space, and the boundary of the requirement is not the only time it matters. To wit, any point within the design space has many outputs which must be weighed against the others.

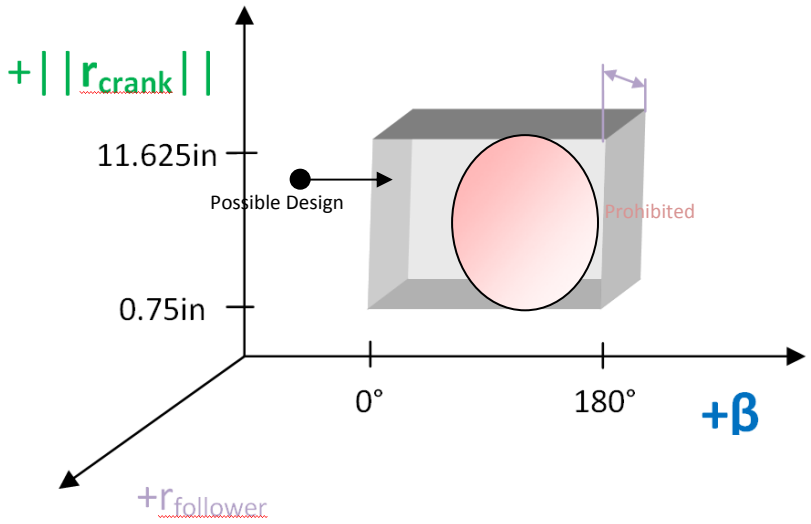

Figure 72: Design Space

The approach to the problem was iterative: pick a known Possible Design and iterate onward within the rectangular prism, recording the data, until boundaries were hit. With enough iteration, the prohibited space surfaces would be determined. With enough points on each surface, an approximate fitting function could be derived (using the three-dimensional equivalent of spline curves, parabolas and so on). Each requirement would eliminate some of the space, eventually paring it down to the solution solid, a complicated 3-dimensional shape that would cover every possible design within the bounds.

What then of finding the BEST solution, rather than one that is just acceptable? If all of the iterated points could be color-coded by one requirement per graph, a four dimensional representation of the designs in terms of each constraint would be at hand, and a qualitative understanding could be attained. If the requirements could be weighted and combined in an index, an absolute measure of a design's suitability could be derived and the graphs could be combined into one, with absolute optimization becoming possible. The index of suitability

might not be well-behaved, mathematically, and could be very complicated. More so, it is a formidable mental challenge to work with a four-dimensional shape.

Given that the amount of time to prepare a design was fast diminishing, and that any acceptable solution would be the same for both the cam and servo modes (if the follower and crank-connecting rod joint was one and the same), a more empirical and subjective process was undertaken. General relationships between the variables could be determined, with a concurrent attempt to find effective compromises.

The first of the three variables whose impact was assessed was crank length $||r||$. One would expect that as the length of the crank decreases, required torque would decrease as the moment arm of the reaction force was reduced. Indeed, this is the case. As seen below, increasing the crank length worsens required torques as expected, with a decreasing effect on the amount of acceleration required at the crank. There is clearly a minimum at $||r||$= 3in that represents a useful compromise in the various characteristics.

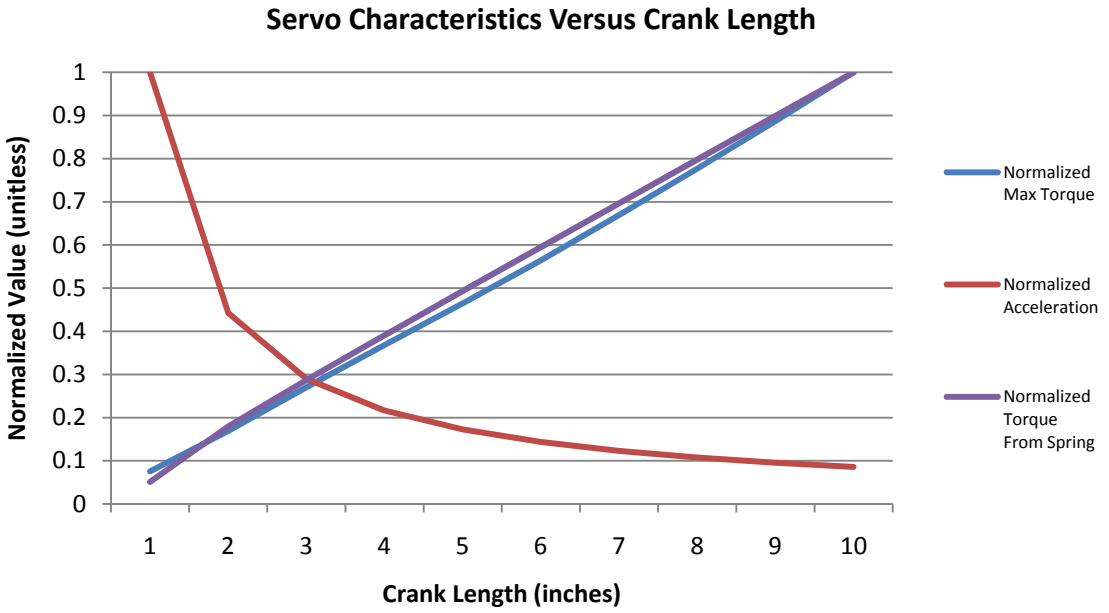

Figure 73

The final system configuration would then be determined by the choice of prime radius and beta angle relative to this ideal value. Since the available cam blank presented an opportunity and an obligation to maximize prime radius to obtain satisfactory pressure angles (with the choice of a suitable follower radius as well), it was only beta angle that remained interesting.

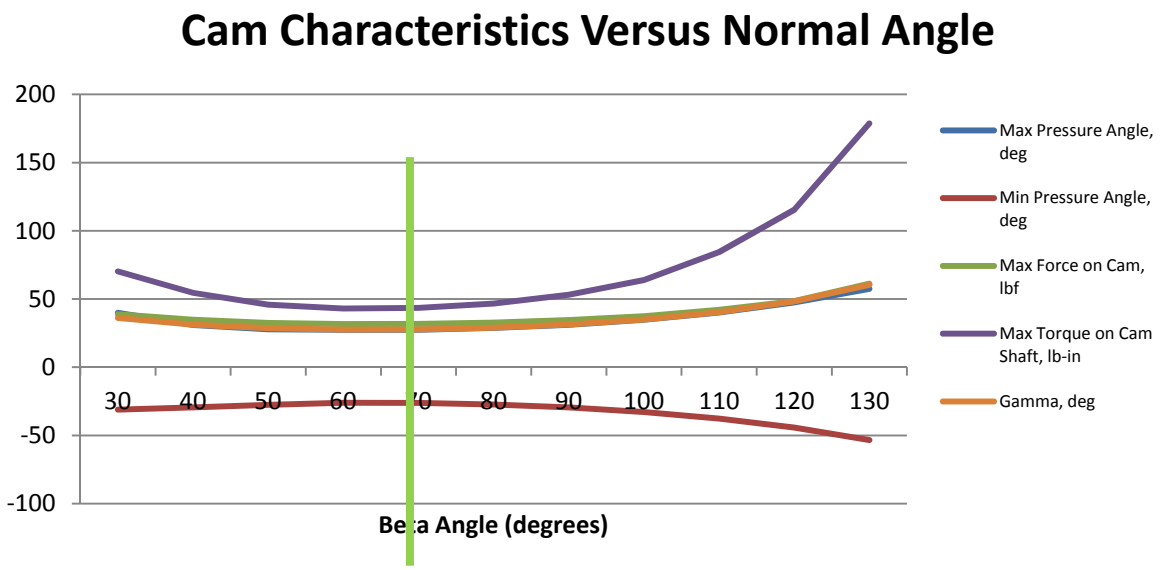

Figure 74

Considering the effect of beta on the Cam dynamic characteristics, it is clear that minimum torques and pressure angles occur near 60-70 degrees, which is desirable. Also of note is the steep incline in torque requirements as beta is pushed upward. As beta is increased beyond the minimum, pressure angles worsen at an increasing pace.

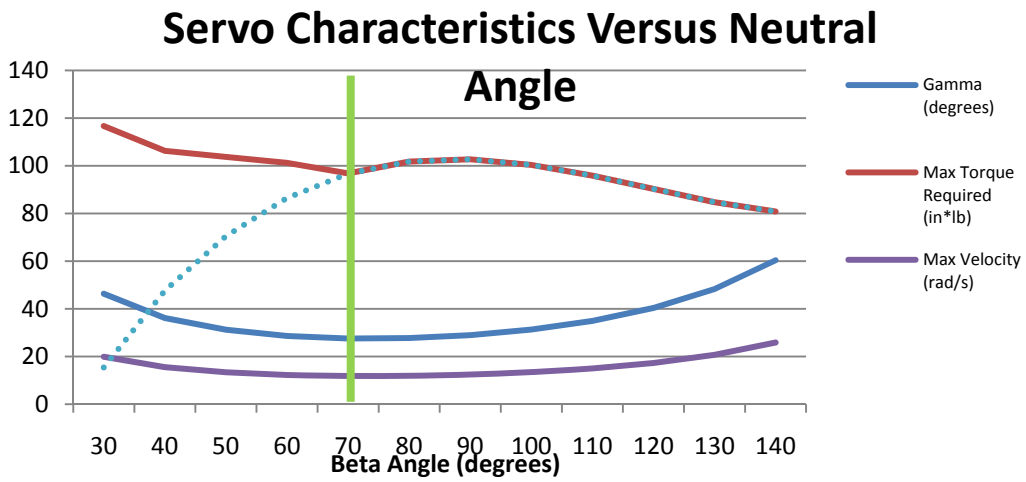

Figure 75

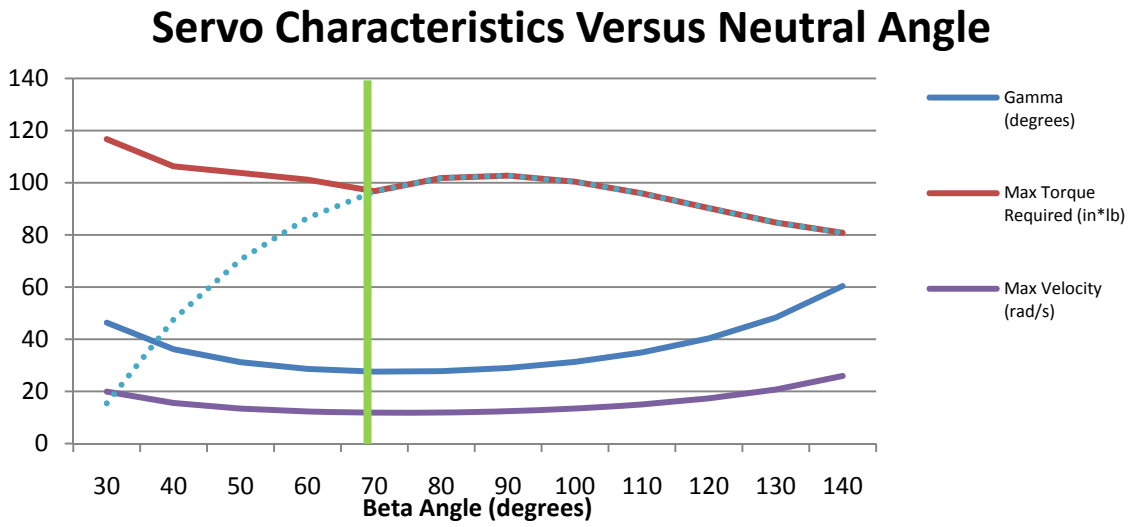

Figure 76

The most striking characteristic of the graph above is the overwhelming dominance of spring torque in the max torque curve above certain threshold value for beta. If beta is increased to reduce servo-side torque (by up to 17% from local minimum on left), dynamics calculations above clearly show that this is disastrous for torque required at the cam (increasing more than 400%). In conclusion, a beta angle of near 70 degrees and a crank length of three inches were agreed upon, along with a maximized prime radius.

16 Appendix D: Linkages

Linkages are a series of links connected in a kinematic chain which can create a controlled output from an input. Some of the most basic linkages are created when four links are connected at their nodes with full joints, called a fourbar linkage. The joints which connect the linkages can be classified into two grouped; Full and Half joints. Full joints are defined as joints that allow only one degree of freedom and half joints have two degrees of freedom. The Degree of Freedom is defined as "the number of inputs that need to be provided in order to create a predictable output; the number of independent coordinates required to define its position" (37). The Degree of Freedom of a mechanism can be found using the following Kutzbach Equation:

$$M = 3(L - 1) - 2J_1 - J_2$$

Where:

M = degree of freedom or mobility

L = number of links

J_1 = number of 1 DOF (full) joints

J_2 = number of 2 DOF (half) joints

The most basic type of fourbar linkage is one which consists or a crank, connecting rod, and rocker arm. In this case the fourth link is the ground plane which connects the crank to the rocker. Figure 77 shows a screenshot from Program LINKAGES of a basic fourbar mechanism.

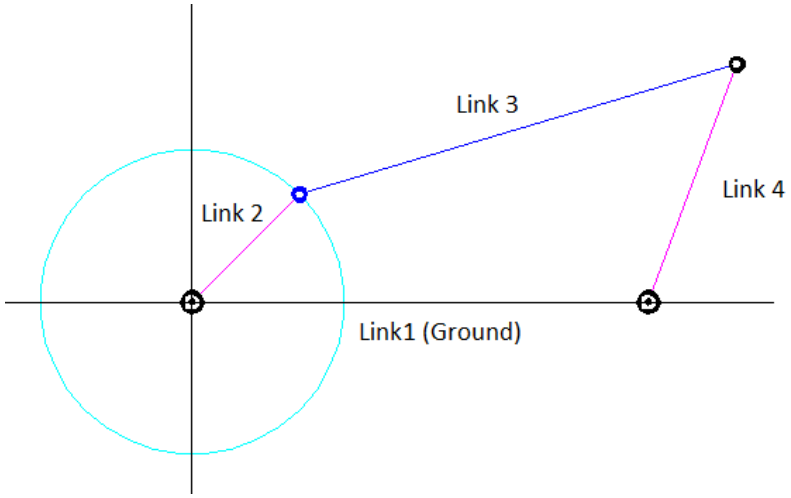

Figure 77: Basic Fourbar Linkage

If the rocker arm, link 4, of this chain is removed and replaced with a slider the resulting linkage is called a Crank-Slider. In this chain there is a crank, and connecting rod, the ground plane, and an effective link 4, which extends downward through the ground plane to infinity. To conceptually understand this re-examine the basic fourbar mechanism shown in Figure 77 imagine the rocker arm to be of infinite length, this would cause the pin between the connecting rod and crank to approximate a straight line motion. Figure 78 shows the resulting coupler curve of the original mechanism in Figure 77.

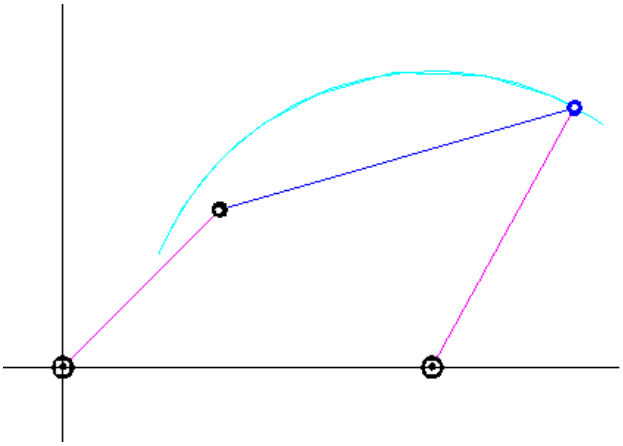

Figure 78: Coupler Curve 1

Figure 79 shows what happens to the same coupler curve as the rocker arm starts to approach infinity. Notice that the resulting coupler curve is much flatter and closer to a straight line.

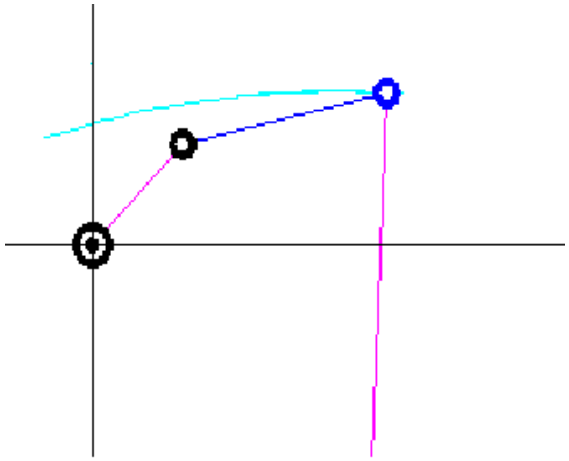

Figure 79: Coupler Curve 2

Now take this pin, place it on a sliding slider, eliminate the rocker arm, and now there is a Crank-Slider configuration. Figure 80 shows a crank slider mechanism from program LINKAGES.

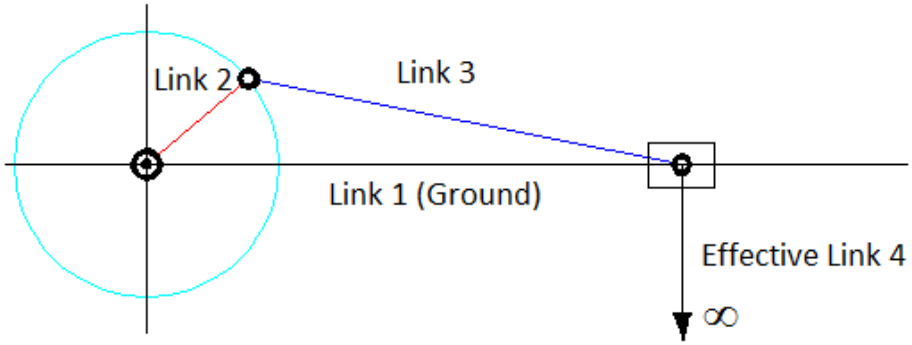

Figure 80: Fourbar Slider

Using the Kutzbach Equation on this Crank-Slider linkage results in 1 DOF

$$M = 3(L - 1) - 2J_1 - J_2$$

$$M := 3(4 - 1) - 2(4) - 0$$

$$M = 1$$

One degree of freedom means that with an input provided at the crank, there will be one output at the slider. When the crank rotates about pin 1, 2 the slider will move back and forth along the x axis. This Crank-Slider shown can be driven by a motor placed at pin 1, 2. This will cause the crank to rotate, push the connecting rod, and move the slider. This can be achieved by something as simple as a DC motor, or as complicated as a servomotor. An alternative way of driving the mechanism would be through placing a Cam at pin 2, 3.

16.1 Cams

A cam-follower system is another way of generating an output from an input. These cam follower systems are very popular in modern machinery. The valves on cars are driven by a radial cam and linear follower, dials and knobs on dishwasher and appliances of the like are also driven by cams. Cams can take many forms ranging from radial cams to axial. These cams are defined by the motion of the follower in relation to the cam. The types of followers can also differ greatly. There are flat-faced followers such as in most internal combustion engines valve trains, mushroom followers, and roller follower. The means in which the follower is kept in contact with the cam can also differ. Some followers are kept in place by the design of the cam its self such as cams with tracks. These are called form-closed systems. Another means of keeping a follower in contact with the cam is by the use of external forces. This can be accomplished by a spring in many cases. This is called a force closed system. Again, this is the system that exists in IC engines. The motion of the follower in respect with the cam can also

change. Some systems have linear motion, where others have oscillating followers. A linear motion is where the motion of the follower is radial to the cam and always inline. An oscillating follower moves in a radial direction, but there is an offset between the centerline of the cam and the line of motion of the follower.

16.2 Combining Cams and Motor Driven Linkages

In the linkage shown in Figure 80 is a basic slider linkage driven by a motor, this can be alternatively driven by a cam. If the motor is disengaged and a cam placed at pin 2, 3 the cam can drive the connecting rod to move the slider. The cam will be a radial plate cam, with a force closed roller follower. The pin 2, 3 will act as the roller, and the load spring attached to the slider will provide the force needed to keep the roller in contact with the cam. Due to the configuration of the linkage, the crank will cause the roller to oscillate with reference to the cam. Knowing the parameters of the linkage, a cam was developed using the program DYNACAM and LINKAGE. This process of developing the linkage geometry and cam geometry was iterative. Every change to the linkage requires a change of the cam and vice versa. The process was done multiple times until a linkage cam mechanism was created which balanced forces throughout the machine.

Given certain criteria that the machine must complete gave the basis for the creation. It was given that the cam would spin at 200RPM, and must drive the slider a total displacement of 1.5 inches.

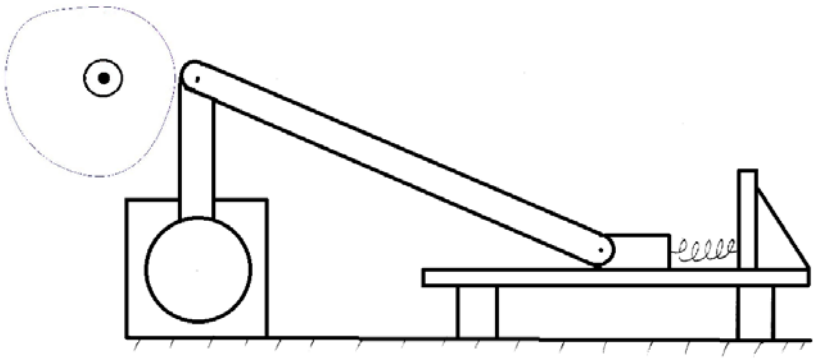

Figure 80 - Design Sketch

Figure 80 shows the preliminary sketch for this mechanism. The servomotor, located at the far left, connected to the crank, is attached to the crank shaft of the fourbar slider mechanism. The servo will be able to rock the crank back and forth creating linear motion at the slider on the linear guides. The servo will be attached to the crank with a clutch mechanism so that it can be disengaged when the servo input is not needed. The cam, located in the top left, will be driven by a belt which will be attached to a DC motor located below the ground link (table). The Cam will be on an axel which can slide along the z axis to disengage from the system when not needed. There will also be a locking mechanism for the spring to disengage the load when the device is not in use and when the drive systems must be changed.

Due to the geometry of the fourbar slider, the joint created by the crank and the connecting rod will be used for the follower mechanism of the cam. The load spring will provide the force needed to keep the follower pressed against the cam. This force-closed cam follower will also oscillate when driven. This requires further design of the cam. The rocker arm may be extended in future designs as to allow the follower to approximate straight line motion which will lessen how much it oscillates, and provide better pressure angles with reference to the cam face.

The cam profile used in this design is based on the Double Dwell Radial Cam for an oscillating cam follower provided in the program DYNACAM. For the more specific application of a cam in this system DYNACAM was used to configure a custom cam. The cam is split into 4 regions; Rise, Dwell, Fall, Dwell. The values of displacement at the first region for the displacement, velocity and acceleration must be zero. From here the cam will create a displacement and enter into the first dwell. Here the displacement must be 30 degrees, the velocity and acceleration zero. The beginning of the third section, the fall, will have the same inputs as the beginning of the dwell. The starting parameters for the final dwell will have the same inputs as the start of the rise section. This results in a 345 polynomial for the rise and a 345 order polynomial for the fall.

17 Appendix E: MathCAD Calculations

17.1 Linkage Analysis

Cam Position vs. Crankshaft Calculations

Independent values are crank length (r), neutral angle (β), follower roller radius (Rf), coupler length (rcoupler), and slider total displacement (Dslider). Coupler length was determined from accepted crank/coupler ratio. Slider displacement was specified in project task specifications.

Neutral angle and crank length were determined from iterative analyses of the dynamics and kinematics of the cam and linkage (Appendix D). A follower roller radius of 0.5 inches was chosen as a standard part.

$r := 3 \quad \beta := 71.564deg \quad R_f := .5 \quad r_{coupler} := 3r \quad D_{slider} := 1.5 \quad \gamma_1 := 2deg$

Units in inches unless otherwise noted

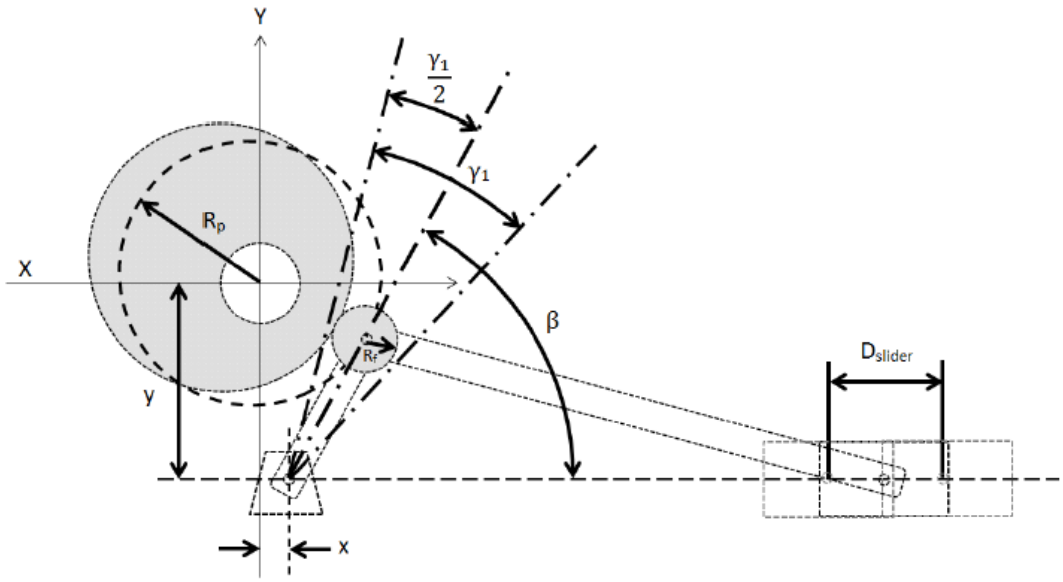

This equation expresses Dslider in terms of crank angle. Through this equation we solve for γ.

Given

$$D_{slider} = \left(r\cdot\cos\left(\beta-\frac{\gamma_1}{2}\right)-r_{coupler}\cdot\cos\left(\operatorname{asin}\left(-r\cdot\frac{\sin\left(\beta-\frac{\gamma_1}{2}\right)}{r_{coupler}}\right)+\pi\right)\right)\ldots$$
$$+-\left(r\cdot\cos\left(\beta+\frac{\gamma_1}{2}\right)-r_{coupler}\cdot\cos\left(\operatorname{asin}\left(-r\cdot\frac{\sin\left(\beta+\frac{\gamma_1}{2}\right)}{r_{coupler}}\right)+\pi\right)\right)$$

$\gamma_1 := \text{Find}(\gamma_1)$

$D_{cam} := 2\cdot r\cdot\sin\left(\frac{\gamma_1}{2}\right)$ This is the chord length of the arc at the crank pin made by the oscillating roller follower. It is used to determine the difference between the maximum and minimum diameter of the cam profile: the total displacement of the cam profile.

$D_{cam} = 1.428$ <-- If this is greater than 2.125", the profile won't fit the blank.

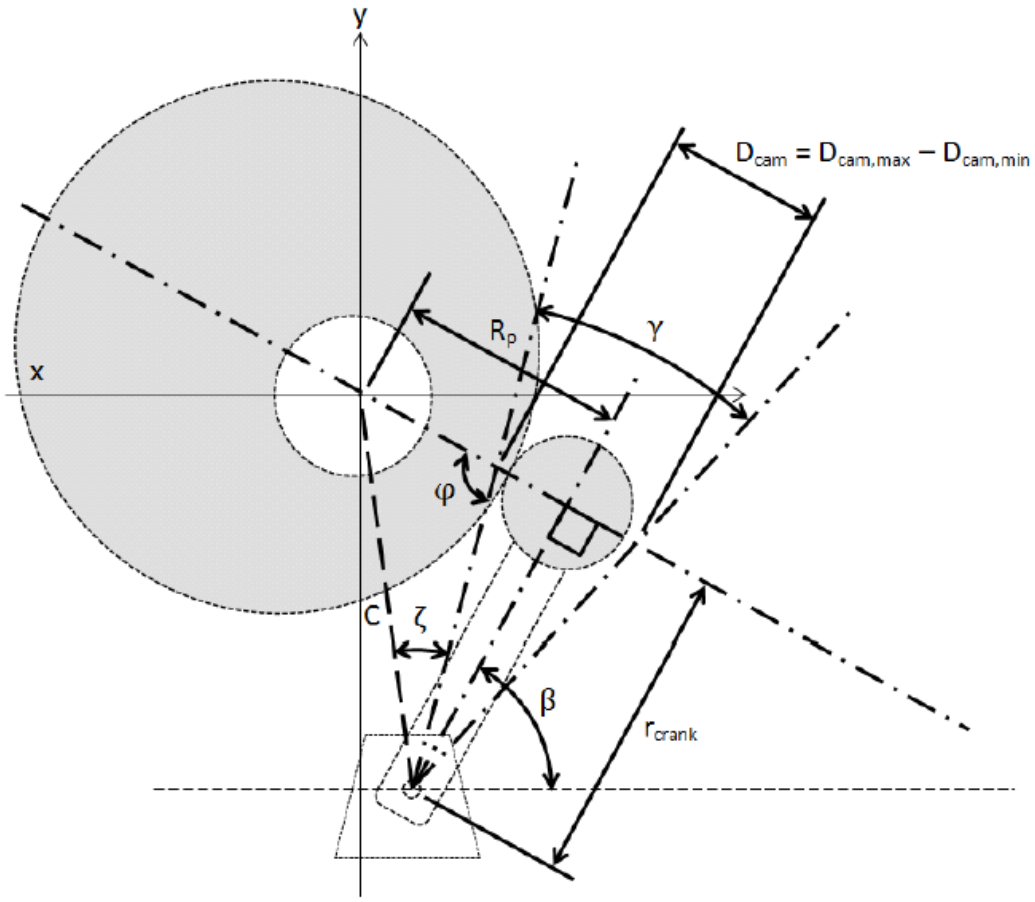

$\phi := 90 \cdot deg + \frac{\gamma_1}{2}$ Geometric relation; see above figure.

$R_p := R_f + 4.125 - D_{cam}$ This equation forces the prime radius to be as large as the cam blank permitted. The cam blank had a radius of 4.125" and thus was set as the maximum radius of the cam profile.

$c := \sqrt{R_p^{\,2} + r^2 - 2R_p \cdot r \cdot \cos(\phi)}$ Geometric relation using law of cosines to find the distance between the cam and crank shafts. See figure above.

$\zeta := \operatorname{asin}\left(R_p \cdot \frac{\sin(\phi)}{c}\right)$

$x := c \cdot \cos\left(180deg - \beta - \frac{\gamma_1}{2} - \zeta\right)$

$y := -c \cdot \sin\left(180deg - \beta - \frac{\gamma_1}{2} - \zeta\right)$

These equations express the distance c in terms of x and y coordinates holding the cam shaft axis as the origin. This is the coordinate system that DYNACAM uses on its profile design page.

DynaCam Variable Inputs

$x = 2.789$ $y = -4.001$ $R_p = 3.197$ $\gamma_1 = 27.527 \cdot deg$

The result of the above calculations were the rest of the independent variables needed to fully define the cam profile parameters and its position relative to the linkage.

17.2 Servomotor Analysis

$blob := 12slug$

Replicating the Cam means servo dosplacement will have a 3-4-5 polynomial angular position function with the following form (with respect to time):

$$s := C_0 + C_1 \cdot t + C_2 \cdot t^2 + C_3 \cdot t^3 + C_4 \cdot t^4 + C_5 \cdot t^5$$

Deriving:

$$v := C_1 + 2C_2 \cdot t + 3C_3 \cdot t^2 + 4C_4 \cdot t^3 + 5C_5 \cdot t^4$$

$$a := 2C_2 + 6C_3 \cdot t + 12C_4 \cdot t^2 + 20C_5 \cdot t^3$$

Boundary Conditions: Rise

On the cam, each segment takes place in 90 degree increments. This means, at a rotational speed of 200rpm, that the time for each segment is given by:

Given Variables:

$t_0 := 0 \quad t_1 := 0.075$

$\beta_1 := 71.565deg \quad r := 3in$

$\gamma_1 := 27.527deg \quad r_c := 3r$

"Guess" Variables (MathCAD syntax)

$C_0 := 4 \; C_1 := 5 \; C_2 := 6 \; C_3 := 1 \quad C_4 := 2 \quad C_5 := 3$

Given

$$\beta_1 - \frac{\gamma_1}{2} = C_0 + C_1 \cdot t_1 + C_2 \cdot t_1^2 + C_3 \cdot t_1^3 + C_4 \cdot t_1^4 + C_5 \cdot t_1^5 \qquad \beta_1 + \frac{\gamma_1}{2} = C_0 + C_1 \cdot t_0 + C_2 \cdot t_0^2 + C_3 \cdot t_0^3 + C_4 \cdot t_0^4 + C_5 \cdot t_0^5$$

$$0 = C_1 + 2C_2 \cdot t_1 + 3C_3 \cdot t_1^2 + 4C_4 \cdot t_1^3 + 5C_5 \cdot t_1^4 \qquad 0 = C_1 + 2C_2 \cdot t_0 + 3C_3 \cdot t_0^2 + 4C_4 \cdot t_0^3 + 5C_5 \cdot t_0^4$$

$$0 = 2C_2 + 6C_3 \cdot t_1 + 12C_4 \cdot t_1^2 + 20C_5 \cdot t_1^3 \qquad 0 = 2C_2 + 6C_3 \cdot t_0 + 12C_4 \cdot t_0^2 + 20C_5 \cdot t_0^3$$

$$\begin{pmatrix} C_0 \\ C_1 \\ C_2 \\ C_3 \\ C_4 \\ C_5 \end{pmatrix} := \text{Find}(C_0, C_1, C_2, C_3, C_4, C_5) = \begin{pmatrix} 1.489 \\ 0 \\ 0 \\ -1.139 \times 10^4 \\ 2.278 \times 10^5 \\ -1.215 \times 10^6 \end{pmatrix}$$

Crank "Rise" kinematic equations

$$\theta_R(t) := rad \cdot \left(C_0 + C_1 \cdot t + C_2 \cdot t^2 + C_3 \cdot t^3 + C_4 \cdot t^4 + C_5 \cdot t^5 \right)$$

$$\omega_R(t) := \frac{rad}{s} \cdot \left(C_1 + 2C_2 \cdot t + 3C_3 \cdot t^2 + 4C_4 \cdot t^3 + 5C_5 \cdot t^4 \right)$$

$$\alpha_R(t) := \frac{rad}{s^2} \cdot \left(2C_2 + 6C_3 \cdot t + 12C_4 \cdot t^2 + 20C_5 \cdot t^3 \right)$$

Coupler "Rise" kinematic equations

$$\theta_{3R}(t) := \operatorname{asin}\left[\frac{\left[-(r)\cdot\sin\left(\theta_R(t)\right)\right]}{(r_c)}\right] + \pi$$

$$\omega_{3R}(t) := \frac{\omega_R(t)\cdot(r)\cdot\cos\left(\theta_R(t)\right)}{(r_c)\cdot\cos\left(\theta_{3R}(t)\right)}$$

Slider Velocity for Rise

$$v_T(t) := -(r)\cdot\omega_R(t)\cdot\sin\left(\theta_R(t)\right) + (r_c)\cdot\omega_{3R}(t)\cdot\sin\left(\theta_{3R}(t)\right)$$

Polynomial equation for "Fall"

Time variables:

$t_2 := 2t_1$

$t_3 := 3.t_1$

"Guess" variables

$$\begin{pmatrix} C_{0d} \\ C_{1d} \\ C_{2d} \\ C_{3d} \\ C_{4d} \\ C_{5d} \end{pmatrix} := \begin{pmatrix} 1 \\ 2 \\ 3 \\ 4 \\ 5 \\ 6 \end{pmatrix}$$

Given

$$\beta_1 - \frac{\gamma_1}{2} = C_{0d} + C_{1d}\cdot t_2 + C_{2d}\cdot t_2^{\,2} + C_{3d}\cdot t_2^{\,3} + C_{4d}\cdot t_2^{\,4} + C_{5d}\cdot t_2^{\,5}$$

$$0 = C_{1d} + 2C_{2d}\cdot t_2 + 3C_{3d}\cdot t_2^{\,2} + 4C_{4d}\cdot t_2^{\,3} + 5C_{5d}\cdot t_2^{\,4}$$

$$0 = 2C_{2d} + 6C_{3d}\cdot t_2 + 12C_{4d}\cdot t_2^{\,2} + 20C_{5d}\cdot t_2^{\,3}$$

$$\beta_1 + \frac{\gamma_1}{2} = C_{0d} + C_{1d}\cdot t_3 + C_{2d}\cdot t_3^{\,2} + C_{3d}\cdot t_3^{\,3} + C_{4d}\cdot t_3^{\,4} + C_{5d}\cdot t_3^{\,5}$$

$$0 = C_{1d} + 2C_{2d}\cdot t_3 + 3C_{3d}\cdot t_3^{\,2} + 4C_{4d}\cdot t_3^{\,3} + 5C_{5d}\cdot t_3^{\,4}$$

$$0 = 2C_{2d} + 6C_{3d}\cdot t_3 + 12C_{4d}\cdot t_3^{\,2} + 20C_{5d}\cdot t_3^{\,3}$$

$$\begin{pmatrix} C_{0d} \\ C_{1d} \\ C_{2d} \\ C_{3d} \\ C_{4d} \\ C_{5d} \end{pmatrix} := \operatorname{Find}(C_{0d}, C_{1d}, C_{2d}, C_{3d}, C_{4d}, C_{5d}) = \begin{pmatrix} -244.975 \\ 6.918\times 10^{3} \\ -7.687\times 10^{4} \\ 4.214\times 10^{5} \\ -1.139\times 10^{6} \\ 1.215\times 10^{6} \end{pmatrix}$$

Crank kinematic equations for "Fall" segment

$$\theta_f(t) := \text{rad}\cdot\left(C_{0d} + C_{1d}\cdot t + C_{2d}\cdot t^2 + C_{3d}\cdot t^3 + C_{4d}\cdot t^4 + C_{5d}\cdot t^5\right)$$

$$\omega_f(t) := \frac{\text{rad}}{\text{s}}\cdot\left(C_{1d} + 2C_{2d}\cdot t + 3C_{3d}\cdot t^2 + 4C_{4d}\cdot t^3 + 5C_{5d}\cdot t^4\right)$$

$$\alpha_f(t) := \frac{\text{rad}}{\text{s}^2}\cdot\left(2C_{2d} + 6C_{3d}\cdot t + 12C_{4d}\cdot t^2 + 20C_{5d}\cdot t^3\right)$$

Conditional equations tie together the Rise and Fall segments of the polynomial motion function

Crank kinematics for one full continuous cycle

$$\theta_t(t) := \text{if}\left(0 \le t \le t_1, \theta_R(t), \text{if}\left(t_1 < t < 2t_1, \beta_1 - \frac{\gamma_1}{2}, \text{if}\left(2t_1 \le t \le 3t_1, \theta_f(t), \text{if}\left(3t_1 < t \le 4t_1, \beta_1 + \frac{\gamma_1}{2}, 0\right)\right)\right)\right)$$

$$\omega_t(t) := \text{if}\left(0 \le t \le t_1, \omega_R(t), \text{if}\left(t_1 < t < 2t_1, 0, \text{if}\left(2t_1 \le t \le 3t_1, \omega_f(t), \text{if}\left(3t_1 < t \le 4t_1, 0, 0\right)\right)\right)\right)$$

$$\alpha_t(t) := \text{if}\left(0 \le t \le t_1, \alpha_R(t), \text{if}\left(t_1 < t < 2t_1, 0, \text{if}\left(2t_1 \le t \le 3t_1, \alpha_f(t), \text{if}\left(3t_1 < t \le 4t_1, 0, 0\right)\right)\right)\right)$$

Coupler kinematics for one full continuous cycle

$$\theta_{3t}(t) := \text{asin}\left[\frac{\left[-(r)\cdot\sin\left(\theta_t(t)\right)\right]}{\left(r_c\right)}\right] + \pi$$

$$\omega_{3t}(t) := \frac{\omega_t(t)\cdot(r)\cdot\cos\left(\theta_t(t)\right)}{\left(r_c\right)\cdot\cos\left(\theta_{3t}(t)\right)}$$

$$\alpha_{3t}(t) := \frac{r\cdot\alpha_t(t)\cdot\cos\left(\theta_t(t)\right) - r\cdot\omega_t(t)^2\cdot\sin\left(\theta_t(t)\right) + r_c\cdot\omega_{3t}(t)^2\cdot\sin\left(\theta_{3t}(t)\right)}{r_c\cdot\cos\left(\theta_{3t}(t)\right)}$$

Slider kinematics for one full continuous cycle

$$D(t) := r\cdot\cos\left(\theta_t(t)\right) - r_c\cdot\cos\left(\theta_{3t}(t)\right)$$

$$v_{Tt}(t) := -(r)\cdot\omega_t(t)\cdot\sin\left(\theta_t(t)\right) + \left(r_c\right)\cdot\omega_{3t}(t)\cdot\sin\left(\theta_{3t}(t)\right)$$

$$a_T(t) := -r\cdot\alpha_t(t)\cdot\sin\left(\theta_t(t)\right) - r\cdot\omega_t(t)^2\cos\left(\theta_t(t)\right) + r_c\cdot\alpha_{3t}(t)\sin\left(\theta_{3t}(t)\right) + r_c\cdot\omega_{3t}(t)^2\cdot\cos\left(\theta_{3t}(t)\right)$$

Kinetostatic Spring Torque calculation:

$k := 20\frac{\text{lbf}}{\text{in}}$ Spring rate $\qquad k_0 := 20\text{lbf}$ Preload

$$T_s(t) := \left[k\cdot(D(t) - D(0)) + k_0\right]\cdot D(t)\cdot\tan\left(180\text{deg} - \theta_{3t}(t)\right)$$

Component Mass Properties

Pro/E Mass moment data for final shaft and link revisions

Crank shaft with mass-reduced, 7-inch pitch diameter pulley, large pulley bushing, and all shaft collars

$$I_{crnkshft} := 1.617 \cdot 10^{1}\,lbm \cdot in^{2}$$

Crank mass moment about crankshaft axis

$$I_{crank} := 1.1754436 \cdot 10^{1}\,lbm \cdot in^{2}$$

Coupler mass and mass moment about slider link

$$m_{coupler} := 2.7062494\,lbm$$

$$I_{coupler} := 6.815 \cdot 10^{1}\,lbm \cdot in^{2}$$

Link 4 (slider) mass

$$m_{slider} := 3.144\,lbm$$

Transmission Shaft mass moment (3.82-inch pitch diameter pulley and 1.192-inch diameter pulley included

$$I_{trans} := 3.7340833 \cdot 10^{-1} \cdot lbm \cdot in^{2}$$

Servo (small) pulley mass moment

$$I_{srvpull} := 8.1863874 \cdot 10^{-3}\,lbm \cdot in^{2}$$

Servo shaft (nameplate) mass moment

$$I_{srvshft} := 0.000273\,lbm \cdot in^{2}$$

Total servomotor shaft inertia

$$I_{servo} := I_{srvshft} + I_{srvpull} = 8.459 \times 10^{-3} \cdot lbm \cdot in^{2}$$

Equivalent mass moment of linkage at crankshaft

$$I_{linkage}(t) := \frac{\left[\left(I_{cmkshft} + I_{crank}\right)\omega_t(t)^2 + I_{coupler} \cdot \omega_{3t}(t)^2 + \left(m_{coupler} + m_{slider}\right)v_{Tt}(t)^2\right]}{\omega_t(t)^2}$$

Final equivalent mass moment about servo shaft

$$I_{system}(t) := \frac{\left(I_{servo}\right) \cdot \left[\left(\frac{3.820 \cdot 7.162}{1.194^2}\right) \cdot \omega_t(t)\right]^2 + I_{trans} \cdot \left(\frac{7.162}{1.194} \cdot \omega_t(t)\right)^2 + \left(I_{linkage}(t) - \frac{T_s(t)}{\alpha_t(t)}\right) \cdot \left(\omega_t(t)\right)^2}{\left[\left(\frac{3.820 \cdot 7.162}{1.194^2}\right)\omega_t(t)\right]^2}$$

$$T_c(t) := I_{linkage}(t) \cdot \alpha_t(t) - T_s(t)$$

$$T_{crankshaft}(t) := \text{if}\left(t = 0, T_c(.001), \text{if}\left(0 < t \le 0.074775, T_c(t), \text{if}\left(0.074775 < t < 0.15005, T_c(0.074775), \text{if}\left(0.15005 \le t \le 0.224\right.\right.\right.\right.$$

Torque required at the crank shaft (Single-Motor CSTM)

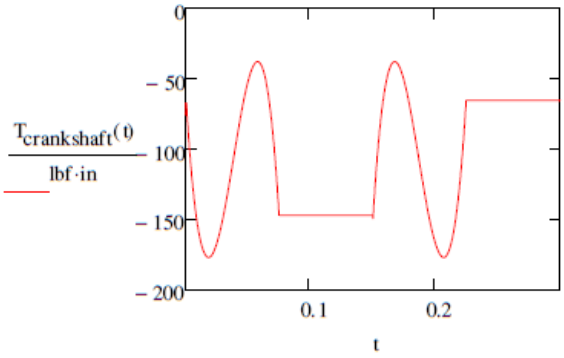

Max = -177in-lb

Min = -38in-lb

RMS = -116in-lb

$$T_{serv}(t) := I_{system}(t) \cdot \left(\frac{3.820 \cdot 7.162}{1.194^2} \cdot \alpha_t(t)\right)$$

$$T_{servo}(t) := \text{if}\left(t = 0, T_{serv}(.001), \text{if}\left(0 < t \le 0.074775, T_{serv}(t), \text{if}\left(0.074775 < t < 0.15005, T_{serv}(0.074775), \text{if}\left(0.15005 \le t \le 0.\right.\right.\right.\right.$$

Torque required at the servo shaft (Single-Motor CSTM)

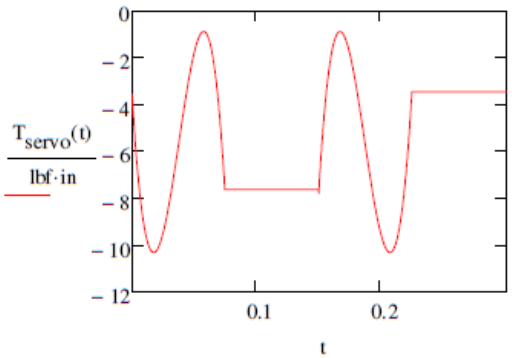

Max = -10.3in-lb

Min = -0.9in-lb

RMS = -6.22in-lb

Kollmorgen Servomotor Specifications:

Continuous Torque: 6.98 in-lb

Peak Torque: 21.1 in-lb

The torque requirements even after a 19:1 speed reduction are very close to the nameplate limitations of the Kollmorgen servomotor. An external motor-cooling apparatus recommended for motor longevity.

Single Motor CSTM Mass Lump for Vibration Model (Servo Mode)

$$m_{eq\_sliderSM}(t) := \frac{I_{servo}\left[\left(\frac{3.820 \cdot 7.162}{1.194^2}\right)\cdot \omega_t(t)\right]^2 + I_{trans}\left(\frac{7.162}{1.194}\cdot \omega_t(t)\right)^2 + I_{linkage}(t)\cdot\left(\omega_t(t)\right)^2}{v_{Tt}(t)^2}$$

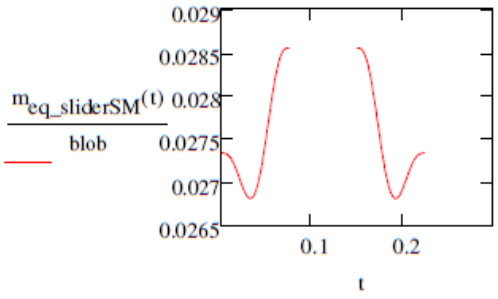

Approximate static value = 0.028 blobs $\quad 0.028\text{blob} = 4.904\,\text{kg}$

Single Motor CSTM Mass lump for vibration model (Cam Mode)

$$I_{large\_pulley} := 1.197\,\text{lbm}\cdot\text{in}^2$$

$$I_{linkageCM}(t) := \frac{\left[\left(I_{crnkshft} + I_{crank} - I_{large\_pulley}\right)\omega_t(t)^2 + I_{coupler}\cdot\omega_{3t}(t)^2 + \left(m_{coupler} + m_{slider}\right)v_{Tt}(t)^2\right]}{\omega_t(t)^2}$$

We remove the large pulley from the crank shaft in cam mode. The cam mass is ignored because it is outside the parameters of the DYNACAM model; i.e. the return spring doesn't can tangibly on the mass or inertia of the cam.

$$m_{eq\_sliderCM}(t) := \frac{I_{linkage}(t)\cdot\omega_t(t)^2}{v_{Tt}(t)^2}$$

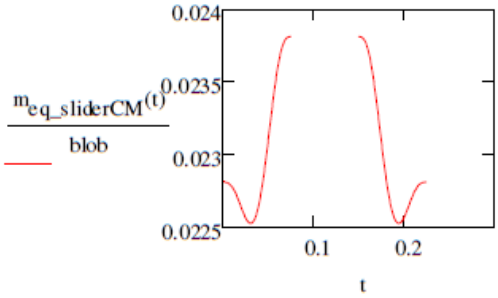

Approximate static value = 0.0235 blobs $\quad 0.0235\text{blob} = 4.115\,\text{kg}$

Direct-Drive CSTM Torque Requirement Calculation

$I_{DDcrankshft} := 5.496 lbm \cdot in^2$ This is the mass moment inertia of the crank shaft with all collars and the R+W BK-60 steel bellows coupling

$I_{MPJ\_1424B} := 7.882 \cdot 10^{-3} kg \cdot m^2$ This is the internal inertia of the Parker MPJ-1424B servomotor selected to drive the Direct-Drive CSTM design.

$$I_{linkageDD}(t) := \frac{\left[\left(I_{DDcrankshft} + I_{crank} + I_{MPJ\_1424B}\right)\omega_t(t)^2 + I_{coupler} \cdot \omega_{3t}(t)^2 + \left(m_{coupler} + m_{slider}\right)v_{Tt}(t)^2\right]}{\omega_t(t)^2}$$

$T_{DD}(t) := I_{linkageDD}(t) \cdot \alpha_t(t) - T_s(t)$

$T_{crankshaftDD}(t) := \text{if}\left(t = 0, T_{DD}(.001), \text{if}\left(0 < t \le 0.074775, T_{DD}(t), \text{if}\left(0.074775 < t < 0.15005, T_{DD}(0.074775), \text{if}\left(0.15005\right.\right.\right.\right.$

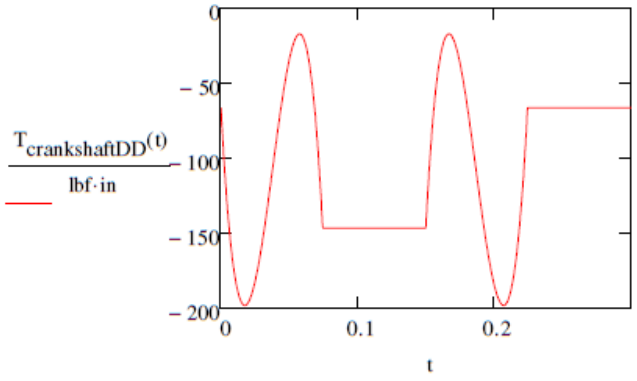

Max = -197.8 in-lb @ 62 rpm

Min = -17.3 in-lb

RMS = -119.3 in-lb

Parker MPJ-1424B Motor Specifications:

Continuous Torque: 171.8 in-lb

Peak Torque: 544.0 in-lb

Torque at "rated speed": 134.2 in-lb @ 3105 rpm

This motor can run the linkage no sweat, especially considering the very low speeds required directly at the crank. Also the servo's internal inertia results in a load to internal inertia ratio better than 4:1. (Max is ~10:1, ideal is ~1:1 as specified by Aerotech (servomotor manufacturer) sales associate.

Direct-Drive CSTM Mass Lump at Slider for Vibration Model (Servo Mode only; the cam mode mass model is the same as it is in the Single Motor CSTM design and has been calculated above).

$$m_{eq\_sliderDD}(t) := \frac{\left[\left(I_{DDcrankshft} + I_{crank} + I_{MPJ\_1424B}\right)\omega_t(t)^2 + I_{coupler}\cdot\omega_{3t}(t)^2 + \left(m_{coupler} + m_{slider}\right)v_{Tt}(t)^2\right]}{v_{Tt}(t)^2}$$

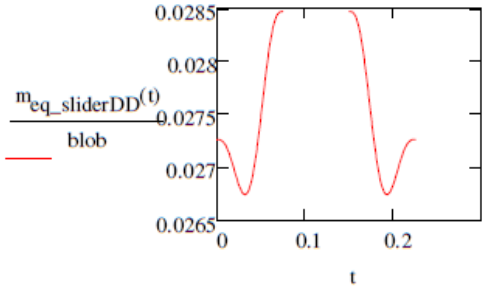

Approximate static value: 0.028 blobs $0.028\,blob = 4.904\,kg$

$$m_{eq\_sliderDD\_CM}(t) := m_{eq\_sliderCM}(t)$$

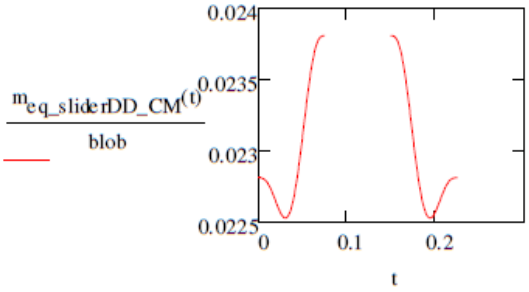

Approximate static value: 0.0235 blobs $0.0235\,blob = 4.115\,kg$

17.3 Stress Analysis

Given:

$L := 8.5in$ Shaft Length

$D := 1.5in$ Shaft Diameter

$r := \frac{D}{2}$ Shaft Raduis

$Area := \pi \cdot r^2 = 1.767 \cdot in^2$

$Finish := "Plain"$ Surface Roughness

$rpm := 200$

$E := 29700ksi = 2.97 \times 10^7 psi$ Young's Mod

$\nu := .29$ Poisson's Ratio

$G := 11600ksi = 1.16 \times 10^7 psi$ Shear Mod (Rigitity)

$S_{ut} := 97900psi$ Tensile Strength Ultimate

$S_y := 58700psi$ Tensile Strength Yield

$S_{us} := .8 \cdot S_{ut}$

$S_{ys} := .577 S_y$

$kpsi := 1000psi$

$\gamma := .284 \frac{lb}{in^3}$

Basic Calculations:

$Area := \frac{\pi \cdot D^2}{4} = 0.012 ft^2$

$Volume := \pi \cdot r^2 \cdot L = 15.021 \cdot in^3$

$mass := Volume \cdot \gamma = 4.266 lb$

$Weight := m \cdot g = 105.558 \frac{ft^2}{s^2}$

$\omega := rpm \cdot \frac{2\pi}{60sec} = 20.944 \frac{1}{s}$ Angular Velocity of Shaft

Second Moments of Interia with respect to each axis

$I := \frac{\pi \cdot D^4}{64} = 0.249 \cdot in^4$

$J := \frac{\pi \cdot D^4}{32}$

$k := \sqrt{\frac{I}{m}} = 1.911 \times 10^{-3} ft^{1.5}$

Finding Corrected Endurance Limit:

$S_{uts} := 97.9 \quad kpsi$

shape := "round"

surface := "machined"

load := "torsion"

$T_{temp} := 26$

$R := .9999$

$A_{95} := \pi\left[\frac{D^2 - (.95D)^2}{4}\right]$

$d_{equiv} := \sqrt{\frac{A_{95}}{.0766}}$

$S_{e'} := \begin{cases} (.5 \cdot S_{uts}) & \text{if } S_{uts} < 1400 \cdot 10^6 \\ (700 \cdot 10^6) & \text{otherwise} \end{cases} = 48.95$

$C_{size} := .869\,(d_{equiv})^{-.097} \cdot ft^{.097} = 1.063$

$C_{load} := \begin{cases} 1 & \text{if load = "bending"} \\ 1 & \text{if load = "torsion"} \\ .7 & \text{if load = "axial"} \end{cases} \quad C_{load} = 1$

$A := \begin{cases} 1.34 & \text{if surface = "ground"} \\ 2.7 & \text{if surface = "machined"} \\ 2.7 & \text{if surface = "cold\_rolled"} \\ 14.4 & \text{if surface = "hot\_rolled"} \\ 39.9 & \text{if surface = "forged"} \end{cases} = 2.7$

$b := \begin{cases} -.085 & \text{if surface = "ground"} \\ -.265 & \text{if surface = "machined"} \\ -.265 & \text{if surface = "cold\_rolled"} \\ -.718 & \text{if surface = "hot\_rolled"} \\ -.995 & \text{if surface = "forged"} \end{cases} = -0.265$

$C_{surf} := A \cdot (S_{uts})^b = 0.801$

$C_{reliab} := \begin{cases} 1.000 & \text{if } R = .5 \\ .897 & \text{if } R = .9 \\ .814 & \text{if } R = .99 \\ .753 & \text{if } R = .999 \\ .702 & \text{if } R = .9999 \\ .659 & \text{if } R = .99999 \end{cases} = 0.702$

$C_{temp} := \begin{cases} 1 & \text{if } T_{temp} \le 840 \\ \left[1 - .0058 \cdot (T_{temp} - 450)\right] & \text{otherwise} \end{cases} = 1$

$S_e := C_{load} \cdot C_{surf} \cdot C_{temp} \cdot C_{size} \cdot C_{reliab} \cdot S_{e'} = 29.277 \quad kpsi$

$S_m := \begin{cases} (.75 \cdot S_{ut}) & \text{if load = "axial"} \\ (.9 \cdot S_{ut}) & \text{otherwise} \end{cases}$

$S_{eu} := S_e \cdot kpsi$ Adding Units to Se Calculation

$z := -3 \qquad b := \frac{1}{z} \cdot \log\left(\frac{S_m}{S_{eu}}\right) = -0.16 \qquad a := \frac{S_m}{(10^3)^b} = 2.652 \times 10^5\ psi$

$S_f(N) := \begin{cases} a \cdot N^b & \text{if } N < 10^6 \\ S_{eu} & \text{otherwise} \end{cases}$

Pulley and Belt Diagram

Some belt and pulley system diagrams and formulas are cited and derived from "Shigley's Mechanical Engineering Design".

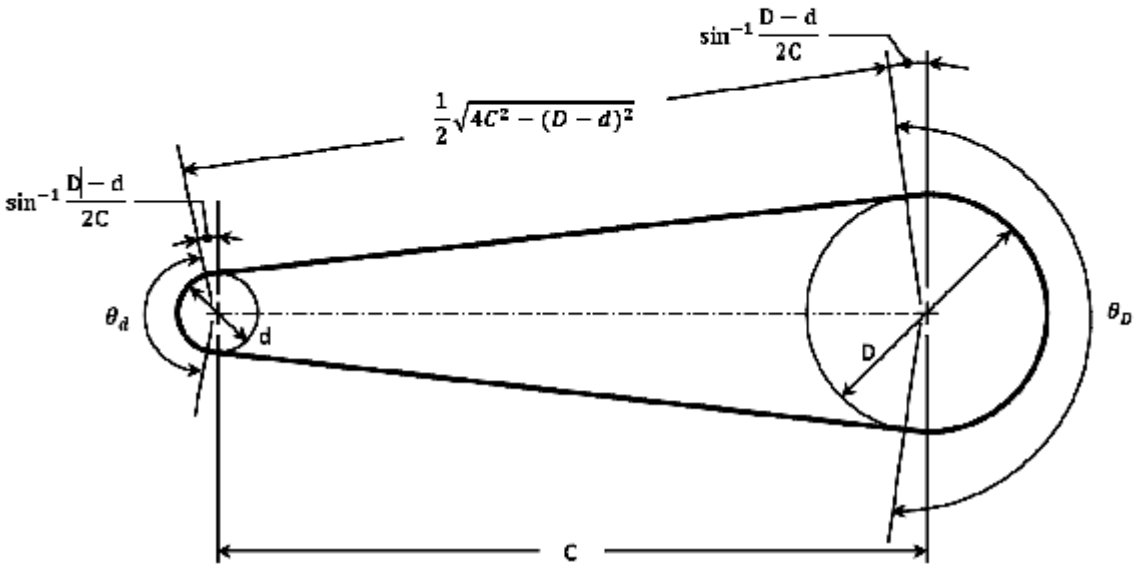

Defines the distance between the pulleys and thier angles of wrap (Shigley 881)

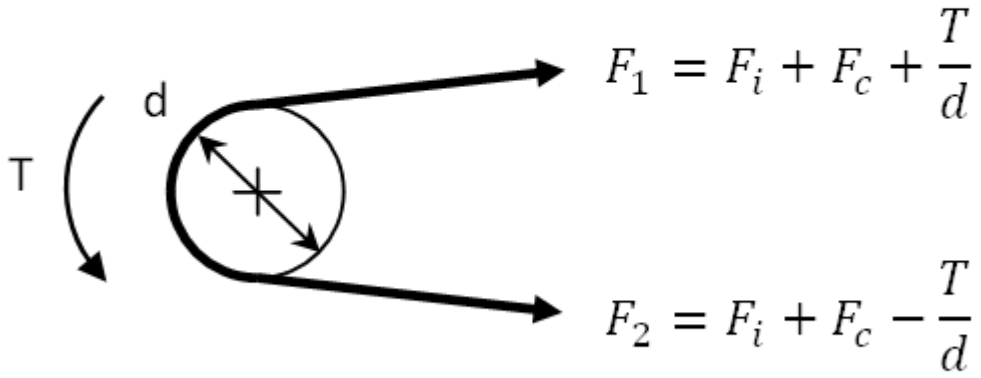

Defnes the formulas for finding the tension in the belt on both sides based on the applied Torque. (Shigley 885)

Belt System Properties and Geometry:

$Dpulley_1 := 1.194in$

$Dpulley_2 := 7.162in$

Diameter of Pulleys

$L_{belt} := 30in$ Length of Belt

$w := .5in$ width

$t := .062in$ thickness

$\gamma_{belt} := .045 \frac{lbf}{in^3}$ Weight Density

$\omega eight := 12 \gamma_{belt} \cdot w \cdot t$

$F_f := .8$ Coefficient of Friction

$n := \frac{200}{sec}$ Rotational Speed

$V := \frac{\pi \cdot Dpulley_1 \cdot n}{12} = 312.588 \cdot \frac{ft}{min}$ Belt Speed

$k := 4 \cdot L_{belt} - 6.28 \cdot (Dpulley_2 + Dpulley_1)$

$c2c := \frac{\left[k + \sqrt{k^2 - 32 (Dpulley_2 - Dpulley_1)^2}\right]}{16} = 7.875 \cdot in$ Center to Center distance of the pulleys

$k := 4 \cdot L_{belt} - 6.28 \cdot (Dpulley_2 + Dpulley_1)$

$\varphi := \operatorname{asin}\left[\frac{(Dpulley_2 - Dpulley_1)}{2 \cdot c2c}\right] = 22.266 \cdot deg$

$L_p := 2 \cdot c2c \cdot \cos(\varphi) + \frac{\pi (Dpulley_2 + Dpulley_1)}{2} + \frac{\pi \cdot \varphi \cdot (Dpulley_2 - Dpulley_1)}{180} = 27.742 \cdot in$

$\theta_d := \pi - 2 \operatorname{asin}\left(\frac{Dpulley_2 - Dpulley_1}{2c2c}\right) = 135.468 \cdot deg$ Angle of Wrap for small pulley

$\phi := \theta_d$

$\theta_D := \pi + 2 \operatorname{asin}\left(\frac{Dpulley_2 - Dpulley_1}{2c2c}\right) = 224.532 \cdot deg$ Angle of Wrap for large pulley

$$F_c := \frac{weight}{g}\left(\frac{V}{60}\right)^2 = 4.707 \times 10^{-5}\,lbf$$

Hoop tension due to centrifugal force

$$T := 70lbf \cdot in$$

Torque needed to drive CamShaft. Value taken from DYNACAM

$$F_i := \frac{T}{Dpulley_1} \cdot \frac{\left[e^{(F_f \cdot \phi)} + 1\right]}{\left[e^{(F_f \cdot \phi)} - 1\right]} = 79.456\,lbf$$

Initial Tension in Belt

$$F_1 := F_i + F_c + \frac{T}{Dpulley_1} = 138.082\,lbf$$

Driving side tension

$$F_2 := F_i + F_c - \frac{T}{Dpulley_1} = 20.829\,lbf$$

Slack side tension

$$Tension_1 := F_1$$

Establishing variables for loading analysis

$$Tension_2 := F_2$$

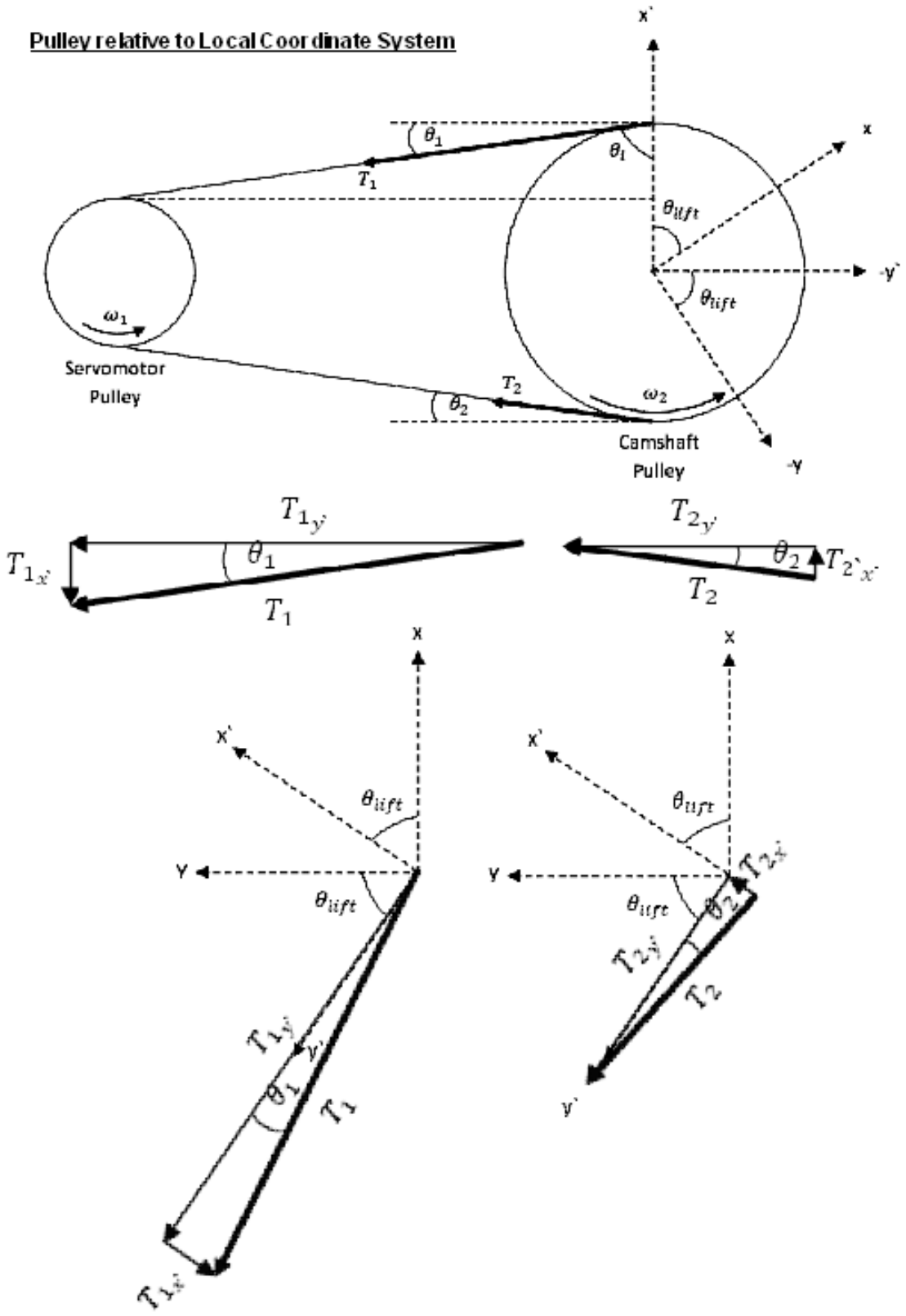
Pulley relative to Local Coordinate System
x`
x
-y`
-Y
θ_1
T_1
θ_{lift}
ω_1
Servomotor
Pulley
T_2
θ_2
ω_2
Camshaft
Pulley
$T_{1y`}$
$T_{1x`}$
$T_{2y`}$
$T_{2`x`}$
X
Y
y`

Pulley relative to Global Coordinate System

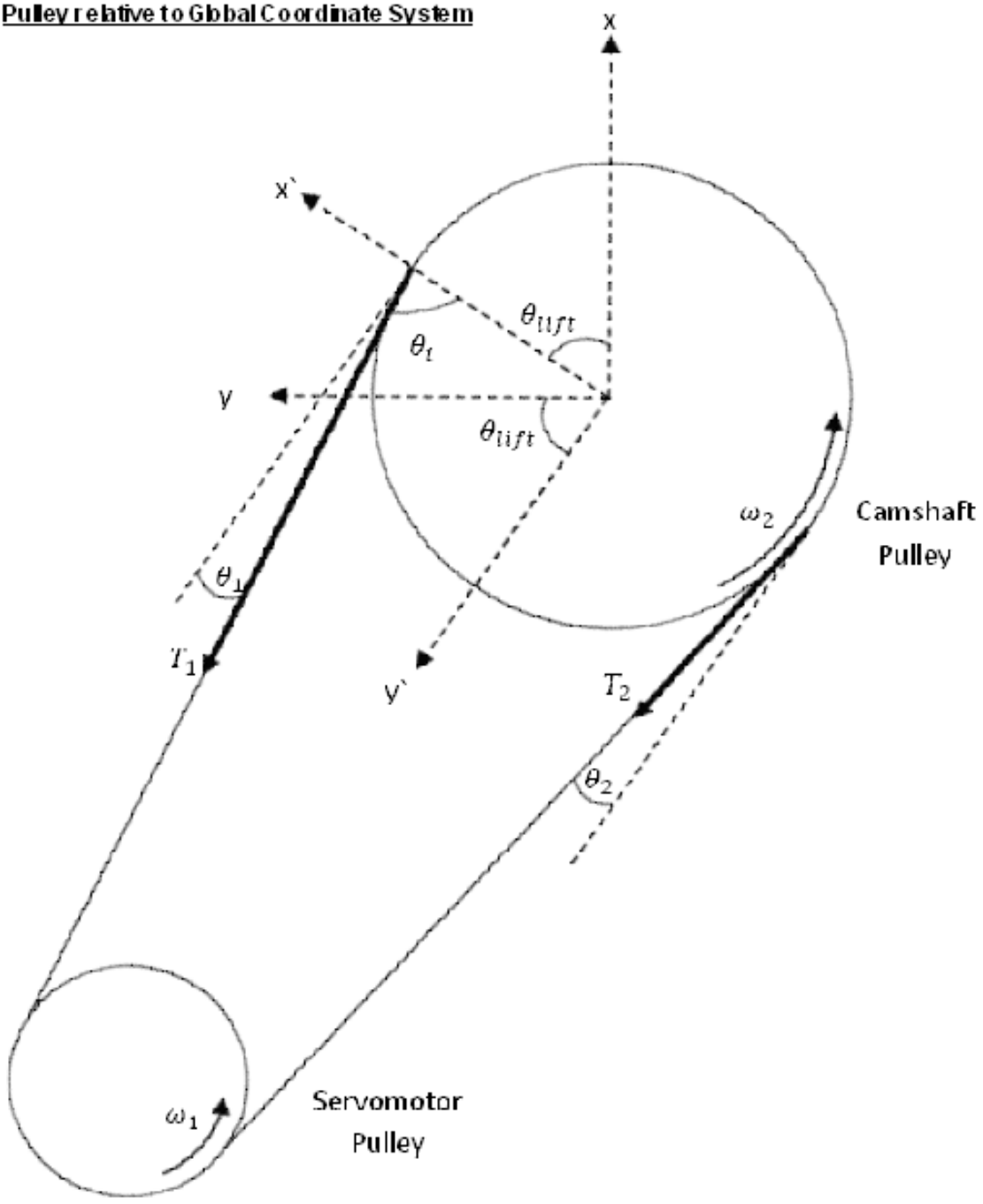

$$\theta_0 := \operatorname{atan}\left(\frac{c2c}{\frac{Dpulley_2}{2} - \frac{Dpulley_1}{2}}\right) = 69.248 \cdot deg \qquad \theta_{lift} := \operatorname{asin}\left(\frac{6.5}{7.875}\right) = 55.629 \cdot deg$$

$$\theta_1 := 90deg - \theta_0 = 20.752 \cdot deg$$

$$\theta_2 := \theta_1$$

$$Tension_{1x} := \sin(\theta_{lift} + \theta_1) \cdot Tension_1 = 134.2\,lbf \qquad Tension_{2x} := \sin(\theta_{lift} - \theta_1) \cdot Tension_2 = 11.91\,lbf$$

$$Tension_{1y} := \cos(\theta_{lift} + \theta_1) \cdot Tension_1 = 32.514\,lbf \qquad Tension_{2y} := \cos(\theta_{lift} - \theta_1) \cdot Tension_2 = 17.088\,lbf$$

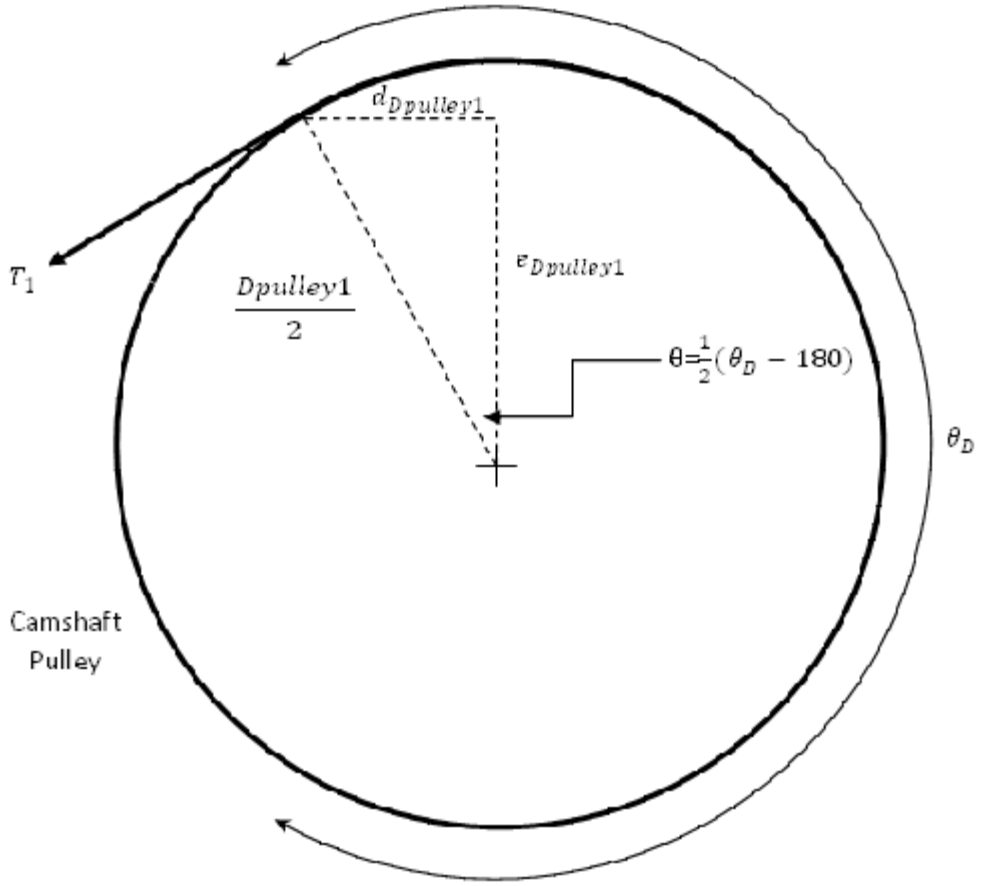

To find the torque applied by the tension couple, their respective perpendicular distances must be found.

$$d_{Dpulley2} := \cos\left[\frac{1}{2}(\theta_D - 180deg)\right] \cdot \frac{Dpulley_2}{2} = 3.314 \cdot in$$

$$e_{Dpulley2} := \sin\left[\frac{1}{2}(\theta_D - 180deg)\right] \cdot \frac{Dpulley_2}{2} = 1.357 \cdot in$$

Torque from Tensions in component form:

$T_{Tension1x} := Tension_{1x} \cdot d_{Dpulley2} = 444.735 \cdot lbf \cdot in$

$T_{Tension1y} := Tension_{1y} \cdot e_{Dpulley2} = 44.117 \cdot lbf \cdot in$

$T_{Tension2x} := Tension_{2x} \cdot d_{Dpulley2} = 39.471 \cdot lbf \cdot in$

$T_{Tension2y} := Tension_{2y} \cdot e_{Dpulley2} = 23.187 \cdot lbf \cdot in$

$T_{Ax} := -T_{Tension1x} + T_{Tension2x}$

$T_{Ay} := -T_{Tension1y} + T_{Tension2y}$

$T_{total} := \sqrt{T_{Ax}^2 + T_{Ay}^2} = 405.804 \cdot lbf \cdot in$

$F_{cam} := 56.038 lbf \qquad \theta_{cam} := \operatorname{atan}\left(\frac{.904}{3.173}\right) = 15.902 \cdot deg$

The magnitude of the cam force is found from DYNACAM. Its position is also given. From here it is divided up into its global X and Y components

$F_{camx} := \sin(\theta_{cam}) \cdot (F_{cam}) = 15.354 lbf$

$F_{camy} := \cos(\theta_{cam}) \cdot (F_{cam}) = 53.893 lbf$

$T_{camx} := F_{camx} \cdot .904in = 13.88 \cdot lbf \cdot in$

$T_{camy} := F_{camy} \cdot 3.173in = 171.004 \cdot lbf \cdot in$

Camshaft x-y-z Axis

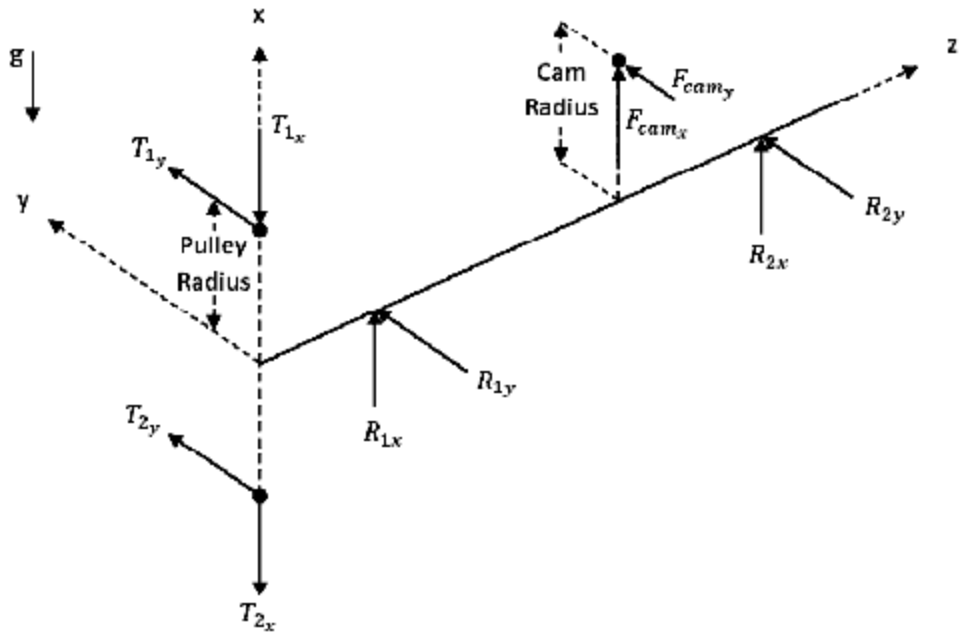

Loading with Singularity Functions:

Camshaft x-z Axis

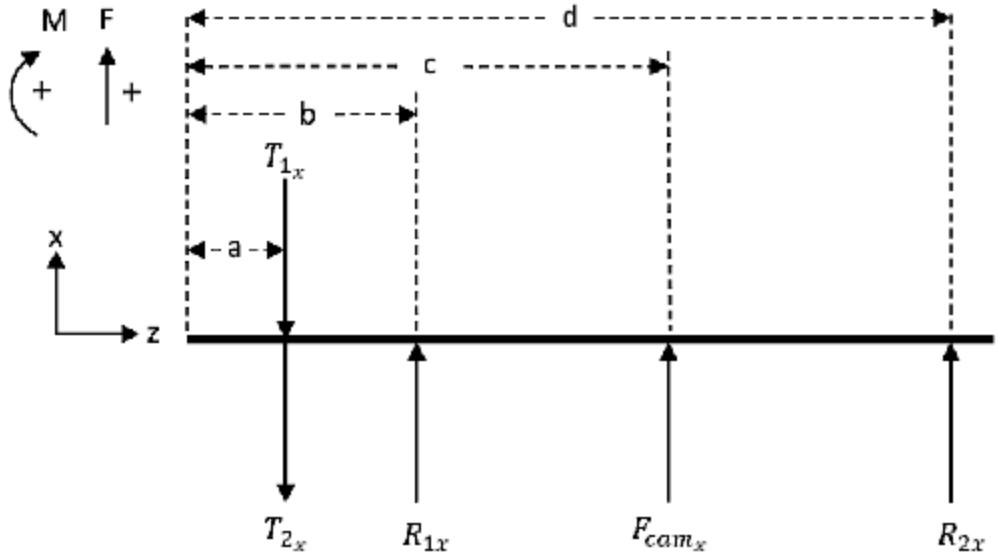

Distances along the z direction of the shaft

$a := 1in$ $c := 5.25in$

$b := 2.5in$ $d := 8in$

$S(x,z) := if(x \geq z, 1, 0)$

$x := 0in, .001in .. 8.5in$

Loading Conditions X-Z Plane:

$R_{1x} := 15lbf$

$R_{2x} := 15lbf$ Guesses to satisfy Mathcad

Given

$0 = -Tension_{1x} - Tension_{2x} + R_{1x} + F_{camx} + R_{2x}$

$0 = -R_{1x}(b - a) - F_{camx}(c - a) - R_{2x}(d - a)$

$Find(R_{1x}, R_{2x}) = \begin{pmatrix} 178.281 \\ -47.526 \end{pmatrix} lbf$

$R_{1x} := 178.281 \cdot lbf$ $R_{2x} := -47.526 \cdot lbf$

$$q_x(x) := -Tension_{1x}\cdot S(x,a)\cdot(x-a)^{-1} - Tension_{2x}\cdot S(x,a)\cdot(x-a)^{-1} \ldots$$
$$q_x(x) := -Tension_{1x}\cdot S(x,a)\cdot(x-a)^{-1} - Tension_{2x}\cdot S(x,a)\cdot(x-a)^{-1} \ldots$$
$$+R_{1x}\cdot S(x,b)\cdot(x-b)^{-1} + F_{camx}\cdot S(x,c)\,(x-c)^{-1} \ldots$$
$$+R_{2x}\cdot S(x,d)\,(x-d)^{-1}$$

$$V_x(x) := -Tension_{1x}\cdot S(x,a)\cdot(x-a)^{0} - Tension_{2x}\cdot S(x,a)\cdot(x-a)^{0} \ldots$$
$$+R_{1x}\cdot S(x,b)\cdot(x-b)^{0} + F_{camx}\cdot S(x,c)\,(x-c)^{0} \ldots$$
$$+R_{2x}\cdot S(x,d)\,(x-d)^{0}$$

$$M_x(x) := -Tension_{1x}\cdot S(x,a)\cdot(x-a)^{1} - Tension_{2x}\cdot S(x,a)\cdot(x-a)^{1} \ldots$$
$$+R_{1x}\cdot S(x,b)\cdot(x-b)^{1} + F_{camx}\cdot S(x,c)\,(x-c)^{1} \ldots$$
$$+R_{2x}\cdot S(x,d)\,(x-d)^{1}$$

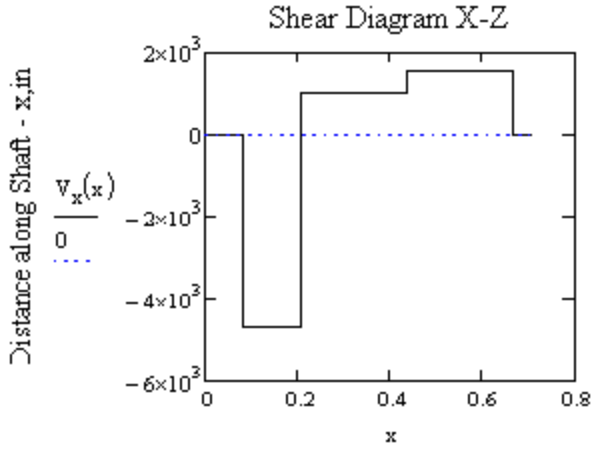

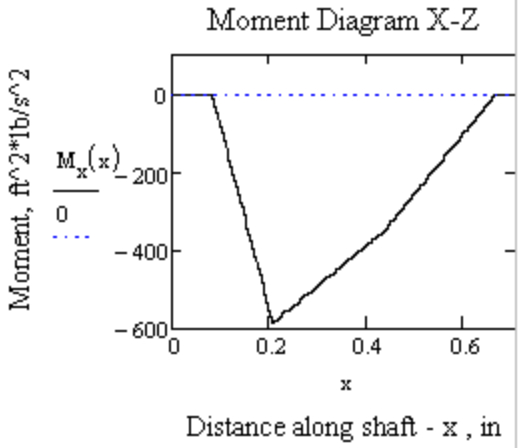

Camshaft y-z Axis

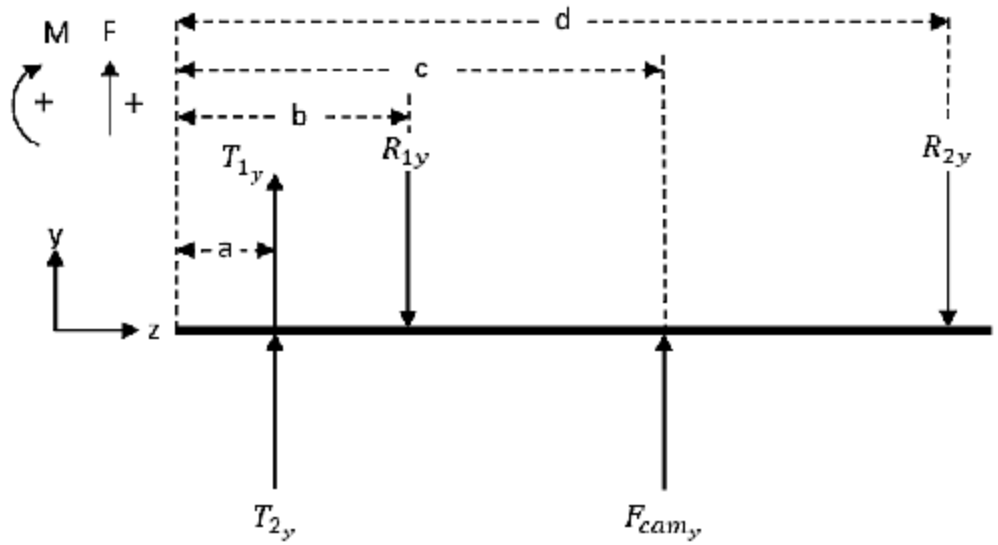

Loading Conditions Y-Z Plane:

$R_{1y} := 15lbf$

Guesses to satisfy Mathcad

$R_{2y} := 15lbf$

Given

$0 = Tension_{1y} + Tension_{2y} - R_{1y} + F_{camy} - R_{2y}$

$0 = -R_{1y}\cdot(b - a) + F_{camy}\cdot(c - a) - R_{2y}\cdot(d - a)$

$Find(R_{1y}, R_{2y}) = \begin{pmatrix} 90.076 \\ 13.419 \end{pmatrix} lbf \qquad R_{1y} := 90.076\cdot lbf \qquad R_{2y} := 13.419\cdot lbf$

$q_y(x) := Tension_{1y}\cdot S(x,a)\cdot(x - a)^{-1} + Tension_{2y}\cdot S(x,a)\cdot(x - a)^{-1} \ldots$
$+ -R_{1y}\cdot S(x,b)\cdot(x - b)^{-1} + F_{camy}\cdot S(x,c)\,(x - c)^{-1} \ldots$
$+ -R_{2y}\cdot S(x,d)\,(x - d)^{-1}$

$V_y(x) := Tension_{1y}\cdot S(x,a)\cdot(x - a)^{0} + Tension_{2y}\cdot S(x,a)\cdot(x - a)^{0} \ldots$
$+ -R_{1y}\cdot S(x,b)\cdot(x - b)^{0} + F_{camy}\cdot S(x,c)\,(x - c)^{0} \ldots$
$+ -R_{2y}\cdot S(x,d)\,(x - d)^{0}$

$M_y(x) := Tension_{1y}\cdot S(x,a)\cdot(x - a)^{1} + Tension_{2y}\cdot S(x,a)\cdot(x - a)^{1} \ldots$
$+ -R_{1y}\cdot S(x,b)\cdot(x - b)^{1} + F_{camy}\cdot S(x,c)\,(x - c)^{1} \ldots$
$+ -R_{2y}\cdot S(x,d)\,(x - d)^{1}$

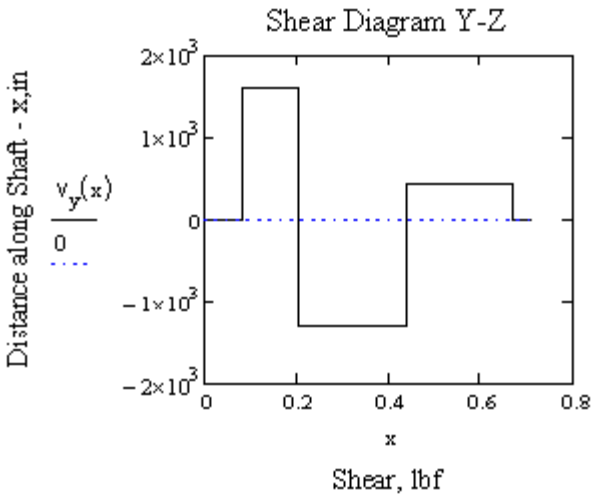
Shear Diagram Y-Z
Distance along Shaft - x,in
$v_y(x)$
0
2×10^3
1×10^3
0
-1×10^3
-2×10^3
0
0.2
0.4
0.6
0.8
x
Shear, lbf

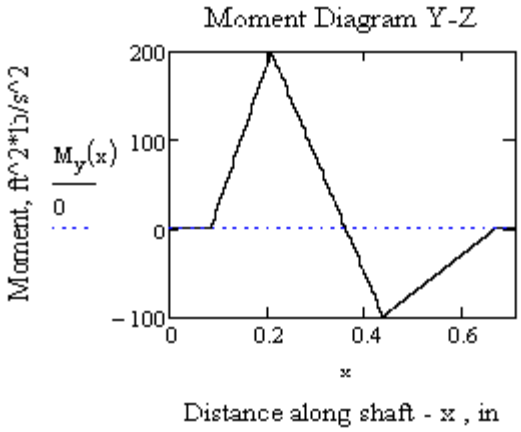
Moment Diagram Y-Z
Moment, ft^2*lb/s^2
$M_y(x)$
0
200
100
0
−100
0
0.2
0.4
0.6
x
Distance along shaft - x , in

$$M(x) := \sqrt{M_x(x)^2 + M_y(x)^2}$$

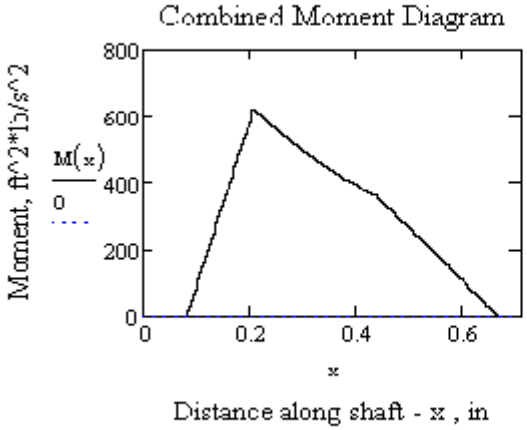

At Point b along the z axis of the shaft

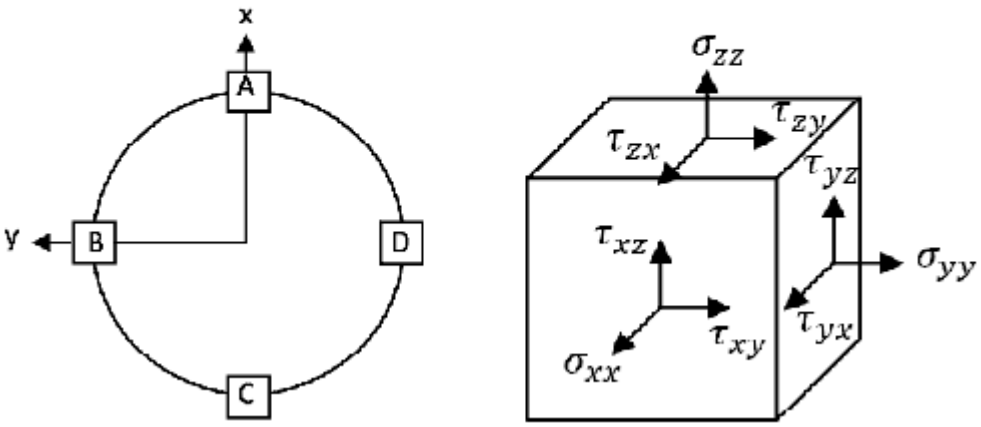

Alternating Stresses:

Point A:

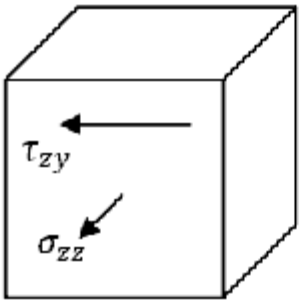

Point B:

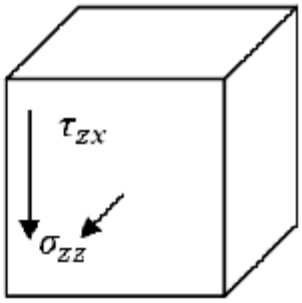

Point C:

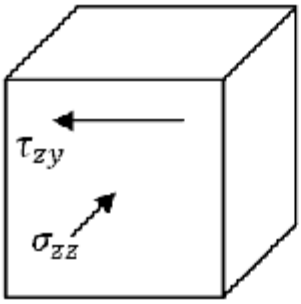

Point D:

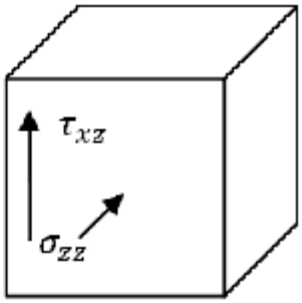

Mean Stresses:

Point A:

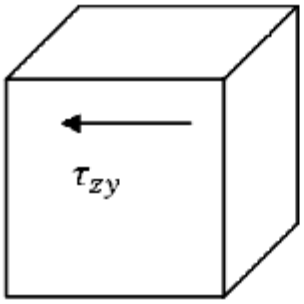

Point B:

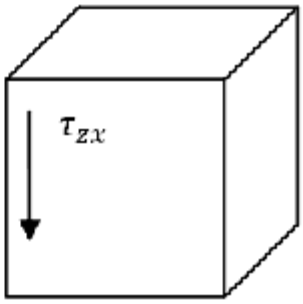

Point C:

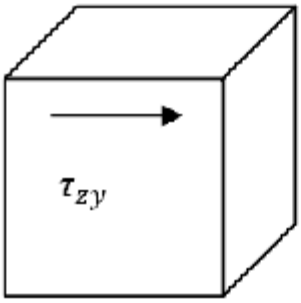

Point D:

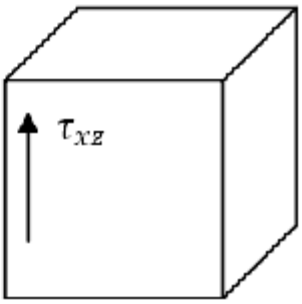

General Von Mises Equation

$$\sigma'_{\cdot} = \sqrt{\sigma_{\cdots}^{2} + \sigma_{\cdots}^{2} - \sigma_{\cdots}\cdot\sigma_{\cdots} + 3\tau_{\cdots}^{2}}$$

$$\sigma'_{a} = \sqrt{\sigma_{xa}^{2} + \sigma_{ya}^{2} - \sigma_{xa}\cdot\sigma_{ya} + 3\tau_{xya}^{2}}$$

$$\sigma'_{m} = \sqrt{\sigma_{xm}^{2} + \sigma_{ym}^{2} - \sigma_{xm}\cdot\sigma_{ym} + 3\tau_{xym}^{2}}$$

Determining Critical Points

Point (A)

Alternating:

$$\tau_{xzaa} := \frac{4\cdot V_{y}(b)}{3\,Area} = -30.538\cdot psi$$

$$\sigma_{zzaa} := \frac{M_{x}(b)\cdot r}{I} = -661.453\,psi$$

Mean:

$$\tau_{zyam} := \frac{T_{total}\cdot r}{J} = 612.369\,psi$$

Von Mises

$$\sigma'_{aa} := \sqrt{\sigma_{zzaa}^{2} + 3\tau_{xzaa}^{2}} = 663.564\,psi$$

$$\sigma'_{am} := \sqrt{3\tau_{zyam}^{2}} = 1.061 \times 10^{3}\,psi$$

Point (B)

Alternating:

$$\tau_{xzba} := \frac{4\cdot V_{x}(b)}{3\,Area} = 24.273\cdot psi$$

$$\sigma_{zzba} := \frac{M_{y}(b)\cdot r}{I} = 224.551\,psi$$

Mean:

$$\tau_{zybm} := \frac{T_{total}\cdot r}{J} = 612.369\,psi$$

Von Mises $\sigma'_{ba} := \sqrt{\sigma_{zzba}^2 + 3\tau_{xzba}^2} = 228.453\,psi$

$\sigma'_{bm} := \sqrt{3\tau_{zybm}^2} = 1.061 \times 10^3\,psi$

Point (C)

Alternating:

$\tau_{xzca} := \frac{4 \cdot V_y(b)}{3Area} = -30.538 \cdot psi$

$\sigma_{zzca} := \frac{-M_x(b) \cdot r}{I} = 661.453\,psi$

Mean:

$\tau_{zycm} := \frac{T_{total} \cdot r}{J} = 612.369\,psi$

Von Mises $\sigma'_{ca} := \sqrt{\sigma_{zzca}^2 + 3\tau_{xzca}^2} = 663.564\,psi$

$\sigma'_{cm} := \sqrt{3\tau_{zycm}^2} = 1.061 \times 10^3\,psi$

Point (D)

Alternating:

$\tau_{xzda} := \frac{4 \cdot V_x(b)}{3Area} = 24.273 \cdot psi$

$\sigma_{zzda} := \frac{-M_y(b) \cdot r}{I} = -224.551\,psi$

Von Mises

$$\sigma'_{da} := \sqrt{\sigma_{zzda}^{\ 2} + 3\tau_{xzda}^{\ 2}} = 228.453\,psi$$

$$\sigma'_{dm} := \sqrt{3\tau_{zydm}^{\ 2}} = 1.061 \times 10^{3}\,psi$$

Point C is the most critical, as both shear stresses are in the same direction, creating a larger total shear

$$N_d := \frac{S_y}{\sigma'_{ca}} = 88.462$$

Modified Goodman Diagram:

$$\tau_a := \tau_{zycm}$$

$$\sigma_m := \sqrt{3\cdot(\tau_{zycm})^2}$$

$$\sigma_{ea} := \sigma'_{ca} + \sqrt{\tau_{zycm}^{\ 2} + \left(\frac{\sigma'_{ca}}{2}\right)^2}$$

$$x := \begin{pmatrix} -S_y & \frac{-3}{2}S_{eu} \\ 0 & 0 \\ S_y & S_{ut} \end{pmatrix} \quad y := \begin{pmatrix} 0 & S_{eu} \\ S_y & S_{eu} \\ 0 & 0 \end{pmatrix} \quad xx := \begin{pmatrix} 0 \\ \sigma_m \end{pmatrix} \quad yy := \begin{pmatrix} 0 \\ \sigma_{ea} \end{pmatrix}$$

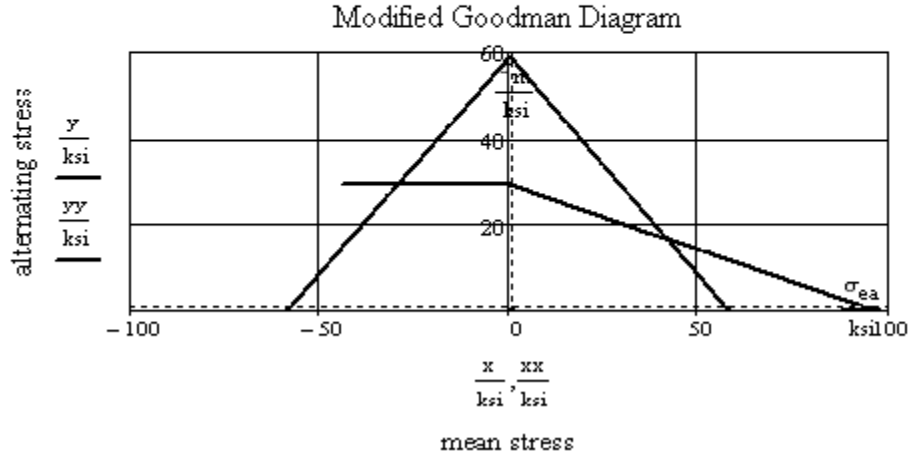

Vibration Analysis (Spring Model): Single-Motor and Direct Drive CSTM

$blob := 12slug$

$G_{st} := 11600ksi$ Shear modulus of steel

$$k_{shaft\_torsion} := \frac{\pi G \cdot d^4}{32L}$$

Crank Shaft torsional stiffness constant:

$$k_{torsion\_crankshaft} := \left[\frac{1}{\left[\frac{\pi G_{st} \cdot (2.122in)^4}{32 \cdot 0.437in}\right]} + \frac{1}{\left[\frac{\pi G_{st} \cdot (1.25in)^4}{32 \cdot 1.1875in}\right]} + \frac{1}{\left[\frac{\pi G_{st} \cdot (2.5in)^4}{32 \cdot .5938in}\right]} + \frac{1}{\left[\frac{\pi G_{st} \cdot (1.25in)^4}{32 \cdot 0.1359in}\right]} + \frac{1}{\left[\frac{\pi G_{st} \cdot (2.06254in)^4}{32 \cdot 0.49in}\right]}\right]^{-1}$$

Transmission Shaft torsional stiffness constant

$$k_{transmission} := \left[\frac{1}{\left[\frac{\pi G_{st} \cdot (1.25in)^4}{32 \cdot 1.115in}\right]} + \frac{1}{\left[\frac{\pi G_{st} \cdot (0.75in)^4}{32 \cdot 1in}\right]} + \frac{1}{\left[\frac{\pi G_{st} \cdot (.88in)^4}{32 \cdot 1in}\right]}\right]^{-1}$$

Servo Shaft torsional stiffness constant

$d_{servo} := 0.432in$ Servo shaft diamter

$L_{servoshft} := 1.289in$ Servo shaft exposed length

$$k_{srvshft} := \frac{\pi G_{st} \cdot (d_{servo})^4}{32 \cdot \left(\frac{L_{servoshft}}{2}\right)}$$

Timing Belts

Cord specific stiffness (stiffness per unit length) = 25.3kN/mm/mm

9 cords in our 1/2inch belts; 9 springs in parallel.

$S_{servtran} := 5.083in$ Straight line length from servo pulley to transmission pulley

$S_{trancrnk} := 7.288in$ Straight line length from transmission pulley to crank pulley

$$k_{srvbelt} := 9 \cdot 25.3 \frac{kN \cdot mm}{mm} \cdot \frac{1}{S_{servtran}} = 1.007 \times 10^4 \cdot \frac{lbf}{in}$$

$$k_{tranbelt} := 9 \cdot 25.3 \frac{kN \cdot mm}{mm} \cdot \frac{1}{S_{trancrnk}} = 7.024 \times 10^3 \cdot \frac{lbf}{in}$$

Glass-fiber cord belt stiffnesses

$$k_{srvbeltST} := 3 \cdot 9 \cdot 25.3 \frac{kN \cdot mm}{mm} \cdot \frac{1}{S_{servtran}} = 3.021 \times 10^4 \cdot \frac{lbf}{in}$$

$$k_{tranbeltST} := 3 \cdot 9 \cdot 25.3 \frac{kN \cdot mm}{mm} \cdot \frac{1}{S_{trancrnk}} = 2.107 \times 10^4 \cdot \frac{lbf}{in}$$

steel-cord belt stiffnesses

Linearizing Torsional Spring Constants

$pd_{small} := 1.194in$ Small pulley pitch diameter

$$k_{Lsrvshft} := \frac{k_{srvshft}}{\left(\frac{pd_{small}}{2}\right)^2} = 1.727 \times 10^5 \cdot \frac{lbf}{in}$$

Servo Shaft spring rate, linearized at end of small pulley

$$k_{servo} := \left(\frac{1}{k_{Lsrvshft}} + \frac{1}{k_{srvbelt}}\right)^{-1} = 9.516 \times 10^3 \cdot \frac{lbf}{in}$$

Servo belt and servo shaft spring rates combined; springs in series

$$k_{Ltransmission} := \frac{k_{transmission}}{\left(\frac{pd_{small}}{2}\right)^2} = 6.046 \times 10^5 \cdot \frac{lbf}{in}$$

Transmission shaft spring rate, linearized at end of small pulley

$$k_{trans} := \left(\frac{1}{k_{Ltransmission}} + \frac{1}{k_{tranbelt}} \right)^{-1} = 6.943 \times 10^{3} \cdot \frac{lbf}{in}$$ Transmission shaft and belt springs combined; springs in series

$$k_{Lcrankshft} := \frac{k_{torsion\_crankshaft}}{(3in)^{2}} = 2.088 \times 10^{5} \frac{lbf}{in}$$ Crank shaft spring rate, linearized at end of crank link

Linkage spring rate:

$E_{Al} := 10000ksi$ Elastic Modulus of aluminum; does not vary significantly from alloy to alloy (www.matweb.com)

$I_{L1} := \frac{1}{12} \cdot .25in \cdot (2in)^{3}$ Second moment area of single leg of crank shaft

$L_1 := 3in$ Crank link length (load-bearing)

Crank, modeled as two parallel cantilevered beams:

$k_{eq} := \frac{3E \cdot I}{L^{3}}$ Equivalent spring for cantilever beam w/ end load

$k_{crank} := 2 \cdot \frac{3 \cdot E_{Al} \cdot I_{L1}}{L_1^{3}} = 3.704 \times 10^{5} \cdot \frac{lbf}{in}$ Crank link spring rate (multiplied by 2 because crank has two "prongs" See CAD model).

Coupler, modeled as two small parallel beams in series with a larger one (see figure in section 6), axial loads only.

$k_{eq} := \frac{E \cdot A}{L}$ k-equiv for rod in compression:

$k_{d1} := 2 \cdot \frac{E_{Al} \cdot (1in \cdot .25in)}{1.75in} = 2.857 \times 10^{6} \cdot \frac{lbf}{in}$ $k_{d2} := \frac{E_{Al} \cdot \left(1in^{2}\right)}{7.25in} = 1.379 \times 10^{6} \cdot \frac{lbf}{in}$

$k_{coupler} := \frac{k_{d1} \cdot k_{d2}}{k_{d1} + k_{d2}} = 9.302 \times 10^{5} \cdot \frac{lbf}{in}$

For slider, modeled in compression only

$L_{slidelegs} := 3.4in \quad A_{slidelegs} := 1.47in \cdot 0.5 \cdot in$ Slider geometry

$L_{slideblock} := 1.6in \quad A_{slideblock} := 2.6in \cdot 1.6in$

$$k_{slider} := \left[\frac{1}{\left(\frac{E_{Al} \cdot A_{slideblock}}{L_{slideblock}} \right)} + \frac{1}{2 \cdot \frac{E_{Al} \cdot A_{slidelegs}}{L_{slidelegs}}} \right]^{-1} = 3.707 \times 10^6 \cdot \frac{lbf}{in}$$ Slider spring rate

Combining linkage spring rates with reflected linear crank shaft spring rate

$$k_{links} := \left(\frac{1}{k_{crank}} + \frac{1}{k_{coupler}} + \frac{1}{k_{slider}} + \frac{1}{k_{Lcrankshft}} \right)^{-1} = 1.132 \times 10^5 \frac{lbf}{in}$$ Complete linkage spring constant including crank shaft

Now every component is included in three equivalent springs.

$$k_{servo} = 9.516 \times 10^3 \cdot \frac{lbf}{in}$$

$$k_{trans} = 6.943 \times 10^3 \cdot \frac{lbf}{in}$$

$$k_{links} = 1.132 \times 10^5 \cdot \frac{lbf}{in}$$

Including pulley pitch radii:

$R_{Crank} := 3in$ Crank length

$R_{P1} := 1.91in$ Medium pulley pitch radius

$R_{P2} := 0.597in$ Small pulley pitch radius

$R_{P3} := 3.81in$ Large pulley pitch radius

Single-Motor CSTM system stiffness combined to single spring (Servo Mode):

$$k_{systemSM} := \left[\frac{1}{k_{servo}} + \frac{1}{\left(\frac{R_{P2}}{R_{P1}}\right)^2 \cdot k_{trans}} + \frac{1}{\left(\frac{R_{P2}}{R_{P1}}\right)^2 \cdot \left(\frac{R_{Crank}}{R_{P3}}\right)^2 k_{links}} \right]^{-1} = 579.66 \frac{lbf}{in}$$

Single-Motor CSTM system single-spring stiffness (cam mode):

$$k_{crank\_compression} := \frac{E_{Al} \cdot (0.25in \cdot 2in)}{3in}$$

$$k_{systemCM} := \left(\frac{1}{k_{coupler}} + \frac{1}{k_{slider}} + \frac{1}{k_{crank\_compression}} \right)^{-1} = 5.142 \times 10^5 \frac{lbf}{in}$$

Direct Drive CSTM system stiffness (servo mode, as cam mode is the same as Single-motor design):

$k_{coupling} := 38 \cdot 10^3 \frac{N \cdot m}{rad}$ Torsion spring rate of R+W coupling (as specified by manufacturer)

$k_{DDservo} := \frac{\pi \cdot G_{st} \cdot (1.10in)^4}{32 \cdot 1.42in}$ Torsion spring rate of the servomotor shaft (only exposed length accounted for)

The rest of the crank shaft is the same as the single-motor design:

$$k_{crankshaftDD} := \left[\frac{1}{k_{DDservo}} + \frac{1}{k_{coupling}} + \frac{1}{\left[\frac{\pi G_{st} \cdot (1.25in)^4}{32 \cdot 1.1875in}\right]} + \frac{1}{\left[\frac{\pi G_{st} \cdot (2.5in)^4}{32 \cdot .5938in}\right]} + \frac{1}{\left[\frac{\pi G_{st} \cdot (1.25in)^4}{32 \cdot 0.1359in}\right]} + \frac{1}{\left[\frac{\pi G_{st} \cdot (2.06254in)^4}{32 \cdot 0.49in}\right]} \right]^{-1}$$

$$k_{systemDD} := \left[\frac{1}{\left[\frac{k_{crankshaftDD}}{(3in)^2}\right]} + \frac{1}{k_{crank}} + \frac{1}{k_{coupler}} + \frac{1}{k_{slider}} \right]^{-1} = 2.321 \times 10^4 \frac{lbf}{in}$$

18 Appendix F: Guidelines for Industrial Design

The Cam-Servo Test Machine must be safe to operate as well as maintain the operator's health. To achieve this, OSHA regulation and guidelines were researched and combined with ergonomics studies to optimize human interaction with the machine.

18.1 OSHA

OSHA is the main federal agency associated with safety and health legislation. It is part of the United States Department of Labor, and was created under the Occupational Safety and Health Act on December 30, 1970 (Nixon administration). OSHA guidelines and regulations are responsible for assuring that every working employee has a safe and healthy working environment. The Cam-Servo Test Machine incorporates OSHA and its ergonomic guidelines to ensure that the mechanism is not only safe to the operator's immediate health, but also to the operators comfort and long term health.

18.2 Ergonomics

A crude version of ergonomics was believed to exist in the 5th century BC, used by the Hellenic civilization in their design of tools. World War II marked a new chapter for ergonomics, as technology was rapidly advancing during the period, especially in weaponry and complex machinery (Poulakakis[3]). Human factor engineering was suddenly in demand. The concept continues to maintain a major influence on industry today.

The Centers for Disease Control and Prevention publish a National Health Statistics Report documenting reference data for children and adults. As of the October 22, 2008 edition, the average US female stands 162.2cm tall and the average male stands 1 tall (Centers for Disease Control and Prevention[3]). Using these two numbers, an average height of 169.25cm for both male and female Americans can be determined.

	short	average	Tall
Standing			
1. Stature	150.5	167.5	185.5
2. Forward grip reach	65.0	74.3	83.5
3. Chest depth	21.0	25.0	28.5
4. Vertical grip reach	179.0	198.3	219.0
5. Eye height	140.5	156.8	174.5
6. Shoulder height	121.5	136.8	153.5
7. Elbow height	93.0	104.8	118.0
8. Knuckle height	66.0	73.8	82.5
Sitting			
11. Sitting height	79.5	88.0	96.5
12. Sitting eye height	68.5	76.5	84.5
13. Sitting elbow height	18.5	24.0	29.5
14. Popliteal height	35.5	42.0	49.0
15. Elbow-grip length	30.4	34.3	38.7
16. Buttock-popliteal length	43.5	48.8	55.0
17. Buttock-knee length	52.0	58.3	64.5

Table 10 - Body Sizes of British Adults

(Dul[1])

The book “Ergonomics for Beginners A Quick Reference Guide”, Chapter 2, Posture and Movement, is a table of body dimensions on (Table 10 above) stating that the average height of a Great Brittan adult is 167.5cm.This table also states, the distance from the ground to the persons elbow is 104.8cm.

Type of task	Work height
Use of eyes: frequent Use of hands/arms: infrequent	10-30 cm below eye height
Use of eyes: frequent Use of hands/arms: frequent	0-15 cm above elbow height
Use of eyes: infrequent Use of hands/arms: frequent	0-30 cm below elbow height

Table 11 - Guidelines for the Height of the Hands and Focal Point

(Dul[2])

The distance from the ground, to the elbow, when standing, is important to mai[illegible] correct ergonomic posture. Table 11 above, from the text, “Ergonomics for Beginners a [illegible] Reference Guide”, states that “the guidelines for the height of the hands and focal point, for

carrying out various tasks while seated or standing should be 0-15cm above the elbow height for frequent use of eyes and hands." By using the ratio:

$$\frac{169.25}{167.5} = \frac{h}{table\ h}$$

The variable *h* is determined as 105.895cm for the average elbow height of an American circa 2008. Taking the average elbow height, a range for the working table height off the ground of the Cam-Servo Machine can be set to 105.895cm (3.474ft) to 120.895cm (3.966ft); 15cm above the height of the elbow.

In addition to determining an ergonomically correct working height, the forces applied to pushing and pulling are equally important when transporting the machine. Body weight should always be used when pushing or pulling the machine. Hand grips should be applied to the machine so that the human can exert a maximum force in a comfortable and ergonomic position for the hands and wrists. The machine should be equipped with two large hard rubber swivel wheels to limit resistance and allow maneuverability.

[1] Ergonomics for Beginners A Quick Reference Guide, J. Dul, B. A. Weerdmeester, pg.11 Taylor & Francis Ltd, London, 1993

[2] Ergonomics for Beginners A Quick Reference Guide, J. Dul, B. A. Weerdmeester, pg.15 Taylor & Francis Ltd, London, 1993

[3] Centers for Disease Control and Prevention. (2008, October 22). *National Health Statistics Reports*. Retrieved from Centers for Disease Control and Prevention: http://www.cdc.gov/nchs/data/nhsr/nhsr010.pdf

[4] Marmaras, N., Poulakakis, G., & Papakostopoulos, V. (1999). Ergonomic Design in Ancient Greece. *Applied Ergonomics , Volume 30* (Issue 4), 361-368.

19 Appendix G: Nylon Pulley Catalog Page

TIMING BELT PULLEYS – NYLON SERIES

New

FOR BELTS 3/8 WIDE

3/8" PITCH (.375" C.P.)

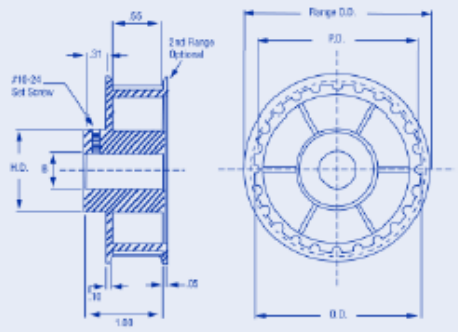

Figure 1

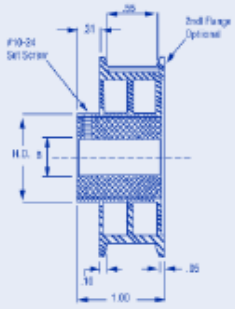

Figure 2

F

MATERIAL: Glass Reinforced Nylon with **Metal Hub.**
See section F index for 3/8 pitch belts.

ORDER BY CATALOG NUMBER

Catalog Number						Flange Code	Number of Teeth	Pitch Diameter P.D.	Outside Diameter O.D. ± .005	Flange Diameter	Hub Diameter H.D.	Type
Bore B 1/4"	Bore B 5/16"	Bore B 3/8"	Bore B 1/2"	Bore B 5/8"	Bore B 3/4"							
FZX-E1-10	FZX-E2-10	FZX-E3-10	FZX-E4-10	–	–	SF / DF	10	1.194	1.164	1.49	.88	Figure 1
FZX-E1-11	FZX-E2-11	FZX-E3-11	FZX-E4-11	–	–	SF / DF	11	1.313	1.283	1.63	.88	
FZX-E1-12	FZX-E2-12	FZX-E3-12	FZX-E4-12	–	–	SF / DF	12	1.432	1.402	1.73	.88	
FZX-E1-13	FZX-E2-13	FZX-E3-13	FZX-E4-13	–	–	SF / DF	13	1.552	1.522	1.79	1.00	
FZX-E1-14	FZX-E2-14	FZX-E3-14	FZX-E4-14	FZX-E5-14	FZX-E6-14	SF / DF	14	1.671	1.641	2.00	1.25	
FZX-E1-15	FZX-E2-15	FZX-E3-15	FZX-E4-15	FZX-E5-15	FZX-E6-15	SF / DF	15	1.790	1.760	2.12	1.25	
FZX-E1-16	FZX-E2-16	FZX-E3-16	FZX-E4-16	FZX-E5-16	FZX-E6-16	SF / DF	16	1.910	1.880	2.22	1.25	
FZX-E1-17	FZX-E2-17	FZX-E3-17	FZX-E4-17	FZX-E5-17	FZX-E6-17	SF / DF	17	2.029	1.999	2.34	1.25	
FZX-E1-18	FZX-E2-18	FZX-E3-18	FZX-E4-18	FZX-E5-18	FZX-E6-18	SF / DF	18	2.149	2.119	2.47	1.25	Figure 2
FZX-E1-19	FZX-E2-19	FZX-E3-19	FZX-E4-19	FZX-E5-19	FZX-E6-19	SF / DF	19	2.268	2.238	2.50	1.25	
FZX-E1-20	FZX-E2-20	FZX-E3-20	FZX-E4-20	FZX-E5-20	FZX-E6-20	SF / DF	20	2.387	2.357	2.74	1.25	
FZX-E1-21	FZX-E2-21	FZX-E3-21	FZX-E4-21	FZX-E5-21	FZX-E6-21	SF / DF	21	2.507	2.477	2.85	1.25	
FZX-E1-22	FZX-E2-22	FZX-E3-22	FZX-E4-22	FZX-E5-22	FZX-E6-22	SF / DF	22	2.626	2.596	2.96	1.25	
FZX-E1-24	FZX-E2-24	FZX-E3-24	FZX-E4-24	FZX-E5-24	FZX-E6-24	SF / DF	24	2.865	2.835	3.15	1.25	
FZX-E1-28	FZX-E2-28	FZX-E3-28	FZX-E4-28	FZX-E5-28	FZX-E6-28	SF / DF	28	3.342	3.312	3.55	1.25	
FZX-E1-30	FZX-E2-30	FZX-E3-30	FZX-E4-30	FZX-E5-30	FZX-E6-30	SF / DF	30	3.581	3.551	3.78	1.25	
FZX-E1-32	FZX-E2-32	FZX-E3-32	FZX-E4-32	FZX-E5-32	FZX-E6-32	SF / DF	32	3.820	3.790	4.05	1.25	

Please add the flange suffix to the catalog number: **SF**-single flange, **DF**-double flange.
Optional #10-24 set screws are supplied.

20 Appendix H: Cam Profile Points

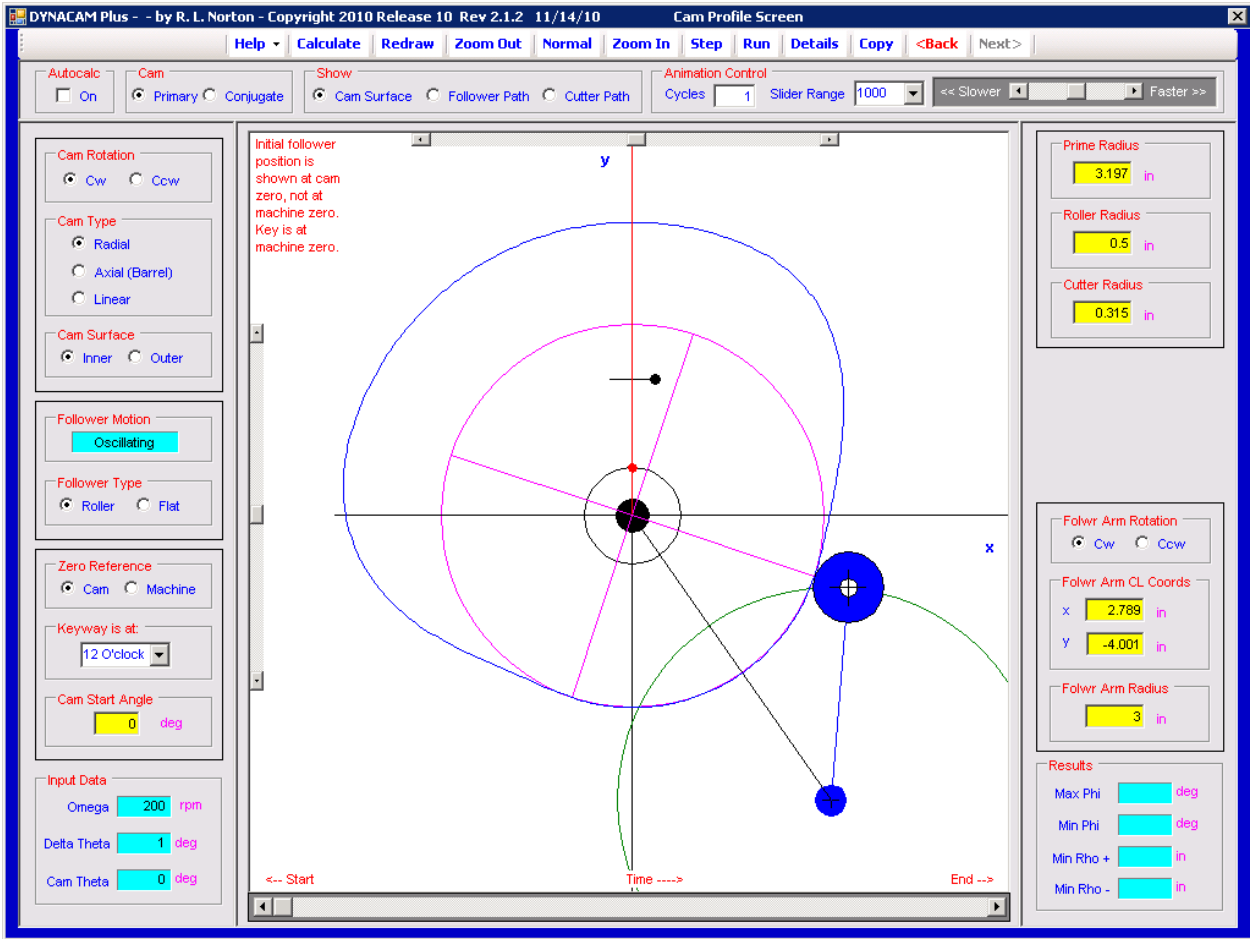

Figure 81: Cam Geometry Showing Coordinate System

X	Y	Z
2.558611	-0.8528284	0.00
2.573276	-0.8075653	0.00
2.587529	-0.7611371	0.00
2.601411	-0.7136152	0.00
2.614967	-0.6650677	0.00
2.628237	-0.6155595	0.00
2.641264	-0.5651506	0.00
2.654085	-0.5138977	0.00
2.666735	-0.4618534	0.00
2.679247	-0.4090652	0.00
2.691646	-0.3555778	0.00
2.703956	-0.3014308	0.00
2.716194	-0.2466591	0.00
2.728371	-0.191295	0.00
2.740494	-0.1353664	0.00
2.752568	-0.07889669	0.00
2.764587	-0.02190649	0.00
2.776545	0.03558649	0.00
2.788429	0.09356732	0.00
2.800224	0.1520233	0.00
2.81191	0.2109444	0.00
2.823463	0.2703202	0.00
2.834855	0.3301425	0.00
2.846057	0.3904025	0.00
2.857036	0.4510921	0.00
2.867756	0.5122022	0.00
2.878179	0.5737215	0.00
2.888266	0.6356401	0.00
2.897974	0.6979427	0.00
2.907261	0.7606162	0.00
2.916081	0.8236424	0.00
2.92439	0.8870013	0.00
2.932139	0.9506708	0.00
2.939283	1.014627	0.00
2.945772	1.078842	0.00
2.95156	1.143286	0.00
2.956596	1.207927	0.00
2.960834	1.272731	0.00
2.964226	1.337661	0.00
2.966723	1.402678	0.00
2.968282	1.46774	0.00
2.968855	1.532805	0.00
2.968399	1.59783	0.00
2.96687	1.662769	0.00
2.964228	1.727574	0.00
2.960433	1.792201	0.00
2.955446	1.856598	0.00
2.949233	1.920721	0.00
2.941758	1.98452	0.00
2.93299	2.047947	0.00
2.922898	2.110955	0.00
2.911456	2.1735	0.00
2.898637	2.235534	0.00
2.884418	2.297014	0.00
2.868777	2.357899	0.00
2.851695	2.418146	0.00
2.833153	2.477717	0.00
2.813134	2.536575	0.00
2.791626	2.594684	0.00
2.768614	2.65201	0.00
2.744087	2.708523	0.00
2.718033	2.764191	0.00
2.690444	2.818987	0.00
2.66131	2.872883	0.00
2.630625	2.925852	0.00
2.598381	2.977871	0.00
2.564575	3.028916	0.00
2.529201	3.078962	0.00
2.492258	3.127987	0.00
2.453743	3.175969	0.00
2.413657	3.222884	0.00
2.372004	3.268711	0.00
2.328787	3.313429	0.00
2.284012	3.357013	0.00
2.237691	3.399446	0.00
2.189835	3.440706	0.00
2.140458	3.480773	0.00
2.089579	3.519631	0.00
2.037219	3.557264	0.00
1.983401	3.593658	0.00
1.928153	3.628804	0.00
1.871501	3.662695	0.00
1.81348	3.69533	0.00
1.754122	3.726711	0.00
1.69346	3.756847	0.00
1.63153	3.785753	0.00
1.568369	3.813451	0.00
1.504012	3.839971	0.00
1.43849	3.865351	0.00
1.37184	3.889641	0.00
1.304089	3.912897	0.00

1.2356	3.935061	0.00
1.166736	3.956025	0.00
1.097516	3.975785	0.00
1.027962	3.994334	0.00
0.9580944	4.011666	0.00
0.8879356	4.027776	0.00
0.8175058	4.042659	0.00
0.7468272	4.056311	0.00
0.6759215	4.068727	0.00
0.6048089	4.079904	0.00
0.5335131	4.089838	0.00
0.4620542	4.098526	0.00
0.3904546	4.105966	0.00
0.3187361	4.112154	0.00
0.2469204	4.117091	0.00
0.1750301	4.120773	0.00
0.1030855	4.1232	0.00
0.03111037	4.124372	0.00
-0.04087467	4.124286	0.00
-0.1128473	4.122945	0.00
-0.1847849	4.120347	0.00
-0.2566674	4.116495	0.00
-0.3284706	4.111389	0.00
-0.4001748	4.10503	0.00
-0.4717562	4.097421	0.00
-0.5431936	4.088563	0.00
-0.6144668	4.07846	0.00
-0.6855517	4.067115	0.00
-0.7564289	4.054531	0.00
-0.8270745	4.040712	0.00
-0.8974682	4.025662	0.00
-0.9675897	4.009387	0.00
-1.037415	3.991889	0.00
-1.106926	3.973175	0.00
-1.176098	3.953252	0.00
-1.244914	3.932124	0.00
-1.313349	3.909798	0.00
-1.381384	3.886282	0.00
-1.448999	3.861582	0.00
-1.516172	3.835705	0.00
-1.582883	3.80866	0.00
-1.649112	3.780454	0.00
-1.714839	3.751098	0.00
-1.780044	3.720598	0.00
-1.844706	3.688966	0.00
-1.908807	3.656209	0.00

-1.972325	3.622339	0.00
-2.035243	3.587366	0.00
-2.097542	3.551299	0.00
-2.159201	3.514152	0.00
-2.220203	3.475933	0.00
-2.280528	3.436656	0.00
-2.340159	3.396331	0.00
-2.399076	3.354973	0.00
-2.457263	3.312593	0.00
-2.514701	3.269202	0.00
-2.571373	3.224817	0.00
-2.627263	3.179449	0.00
-2.682352	3.133113	0.00
-2.736623	3.085823	0.00
-2.790062	3.037591	0.00
-2.84265	2.988436	0.00
-2.894373	2.938369	0.00
-2.945213	2.887408	0.00
-2.995157	2.835567	0.00
-3.044189	2.782863	0.00
-3.092292	2.729311	0.00
-3.139455	2.674927	0.00
-3.18566	2.619729	0.00
-3.230896	2.563732	0.00
-3.275147	2.506955	0.00
-3.3184	2.449414	0.00
-3.360643	2.391126	0.00
-3.401862	2.332111	0.00
-3.442045	2.272385	0.00
-3.481179	2.211967	0.00
-3.519253	2.150875	0.00
-3.556255	2.089128	0.00
-3.592174	2.026745	0.00
-3.626998	1.963744	0.00
-3.660718	1.900145	0.00
-3.693322	1.835968	0.00
-3.724802	1.77123	0.00
-3.755147	1.705954	0.00
-3.784348	1.640157	0.00
-3.812397	1.573862	0.00
-3.839283	1.507087	0.00
-3.865001	1.439852	0.00
-3.889541	1.37218	0.00
-3.912897	1.304088	0.00
-3.934938	1.235924	0.00
-3.955507	1.167972	0.00

-3.974549	1.100173	0.00
-3.992014	1.032476	0.00
-4.007852	0.9648436	0.00
-4.022019	0.897239	0.00
-4.034471	0.8296365	0.00
-4.045167	0.7620209	0.00
-4.054067	0.6943812	0.00
-4.061135	0.6267145	0.00
-4.066337	0.5590252	0.00
-4.06964	0.4913267	0.00
-4.071016	0.4236347	0.00
-4.070438	0.3559768	0.00
-4.067884	0.2883823	0.00
-4.063334	0.2208883	0.00
-4.056775	0.1535384	0.00
-4.048193	0.08637863	0.00
-4.037583	0.01946256	0.00
-4.024941	-0.04715318	0.00
-4.010274	-0.1134094	0.00
-3.993586	-0.1792411	0.00
-3.974893	-0.2445862	0.00
-3.954213	-0.3093732	0.00
-3.931571	-0.3735369	0.00
-3.906997	-0.4370046	0.00
-3.880526	-0.4997087	0.00
-3.852201	-0.5615832	0.00
-3.822065	-0.6225582	0.00
-3.790173	-0.6825698	0.00
-3.756579	-0.7415558	0.00
-3.721344	-0.7994579	0.00
-3.684533	-0.856222	0.00
-3.646215	-0.9117953	0.00
-3.606462	-0.9661331	0.00
-3.565349	-1.019195	0.00
-3.522951	-1.070945	0.00
-3.479348	-1.121354	0.00
-3.43462	-1.1704	0.00
-3.388846	-1.218065	0.00
-3.342109	-1.264338	0.00
-3.294486	-1.309218	0.00
-3.246057	-1.352705	0.00
-3.196899	-1.394809	0.00
-3.147087	-1.435546	0.00
-3.096694	-1.474936	0.00
-3.045788	-1.513008	0.00
-2.994435	-1.549795	0.00

-2.942696	-1.585337	0.00
-2.890631	-1.619675	0.00
-2.838291	-1.65286	0.00
-2.785728	-1.684944	0.00
-2.732983	-1.715982	0.00
-2.680098	-1.746036	0.00
-2.627109	-1.775168	0.00
-2.574046	-1.803442	0.00
-2.520939	-1.830925	0.00
-2.467811	-1.857684	0.00
-2.414682	-1.883788	0.00
-2.361573	-1.909303	0.00
-2.308498	-1.934298	0.00
-2.255474	-1.958835	0.00
-2.202513	-1.982979	0.00
-2.149628	-2.006789	0.00
-2.096834	-2.030322	0.00
-2.044142	-2.053627	0.00
-1.991569	-2.076752	0.00
-1.939126	-2.099738	0.00
-1.886832	-2.122616	0.00
-1.834699	-2.145416	0.00
-1.782749	-2.168154	0.00
-1.730996	-2.190842	0.00
-1.679458	-2.213485	0.00
-1.628154	-2.236078	0.00
-1.577098	-2.258607	0.00
-1.526309	-2.281052	0.00
-1.475803	-2.303383	0.00
-1.425593	-2.325566	0.00
-1.375694	-2.347557	0.00
-1.32612	-2.369307	0.00
-1.276886	-2.390759	0.00
-1.22801	-2.411851	0.00
-1.179506	-2.432518	0.00
-1.131398	-2.452685	0.00
-1.083708	-2.472275	0.00
-1.036466	-2.491207	0.00
-0.9897081	-2.509395	0.00
-0.9434789	-2.526753	0.00
-0.8978316	-2.54319	0.00
-0.8528273	-2.558612	0.00
-0.8080438	-2.573106	0.00
-0.7630141	-2.586816	0.00
-0.717752	-2.599739	0.00
-0.6722713	-2.611869	0.00

-0.6265842	-2.623204	0.00
-0.5807079	-2.63374	0.00
-0.5346547	-2.643474	0.00
-0.4884385	-2.652402	0.00
-0.4420737	-2.660523	0.00
-0.3955726	-2.667833	0.00
-0.3489526	-2.67433	0.00
-0.3022265	-2.680013	0.00
-0.2554078	-2.684879	0.00
-0.2085119	-2.688928	0.00
-0.161552	-2.692157	0.00
-0.1145418	-2.694566	0.00
-0.06749774	-2.696155	0.00
-0.02043338	-2.696923	0.00
0.02663721	-2.696868	0.00
0.07369968	-2.695993	0.00
0.120741	-2.694296	0.00
0.1677445	-2.691778	0.00
0.2146963	-2.688441	0.00
0.2615831	-2.684285	0.00
0.3083904	-2.67931	0.00
0.3551048	-2.67352	0.00
0.40171	-2.666915	0.00
0.4481924	-2.659499	0.00
0.4945387	-2.651272	0.00
0.5407342	-2.642237	0.00
0.5867661	-2.632397	0.00
0.6326184	-2.621756	0.00
0.6782776	-2.610316	0.00
0.7237303	-2.598081	0.00
0.7689638	-2.585054	0.00
0.8139617	-2.57124	0.00
0.8587118	-2.556643	0.00
0.9032006	-2.541267	0.00
0.9474139	-2.525117	0.00
0.9913399	-2.508198	0.00
1.034963	-2.490514	0.00
1.07827	-2.472073	0.00
1.12125	-2.452878	0.00
1.163887	-2.432936	0.00
1.206171	-2.412252	0.00
1.248087	-2.390834	0.00
1.289623	-2.368688	0.00
1.330765	-2.34582	0.00
1.371502	-2.322238	0.00
1.411823	-2.297948	0.00

1.451712	-2.272958	0.00
1.49116	-2.247277	0.00
1.530153	-2.22091	0.00
1.56868	-2.193867	0.00
1.60673	-2.166155	0.00
1.64429	-2.137784	0.00
1.681348	-2.108762	0.00
1.717895	-2.079097	0.00
1.753919	-2.048799	0.00
1.789409	-2.017877	0.00
1.824353	-1.98634	0.00
1.858741	-1.954198	0.00
1.892563	-1.921461	0.00
1.92581	-1.888138	0.00
1.958469	-1.854241	0.00
1.990531	-1.819779	0.00
2.021987	-1.784762	0.00
2.052828	-1.749202	0.00
2.083044	-1.713108	0.00
2.112624	-1.676493	0.00
2.141561	-1.639368	0.00
2.169846	-1.601743	0.00
2.197469	-1.56363	0.00
2.224424	-1.52504	0.00
2.250701	-1.485986	0.00
2.276292	-1.44648	0.00
2.30119	-1.406533	0.00
2.325387	-1.366158	0.00
2.348876	-1.325365	0.00
2.371649	-1.28417	0.00
2.393699	-1.242584	0.00
2.41502	-1.200619	0.00
2.435606	-1.158289	0.00
2.455451	-1.115604	0.00
2.474546	-1.072581	0.00
2.492888	-1.029231	0.00
2.510471	-0.9855675	0.00
2.52729	-0.9416025	0.00
2.543338	-0.8973521	0.00
2.558612	-0.8528284	0.00
2.558611	-0.8528284	0.00

21 Appendix I

The Direct-Drive Cam-Servo Test Machine design as recommended in this report shares with the original Cam-Servo Test Machine Design a crank pin joint that incorporates very little clearance. For example, the clearance of the cut-out on the connecting rod of the roller-follower is only 0.02 inches and the cam blank only clears the crank itself by 0.01 inches on each side. Such a joint demands precise manufacturing and assembly, and as such is less than optimal.

The published design also lacks several features that will prove necessary for the machine to function well if constructed. Two sliding joints do not have the necessary sleeve bearings: crank pin joint and the wrist pin joint. The wrist pin joint in particular is not fully developed. The published design also lacks any allowances for an encoding apparatus that would be necessary to monitor slider position.

Finally, the pin diameters of each joint of the linkage were chosen via first approximation of the expected stress only, with a generous safety factor. Stress analysis of the pins should be undertaken prior to constructing the machine to verify that these choices were reasonable.

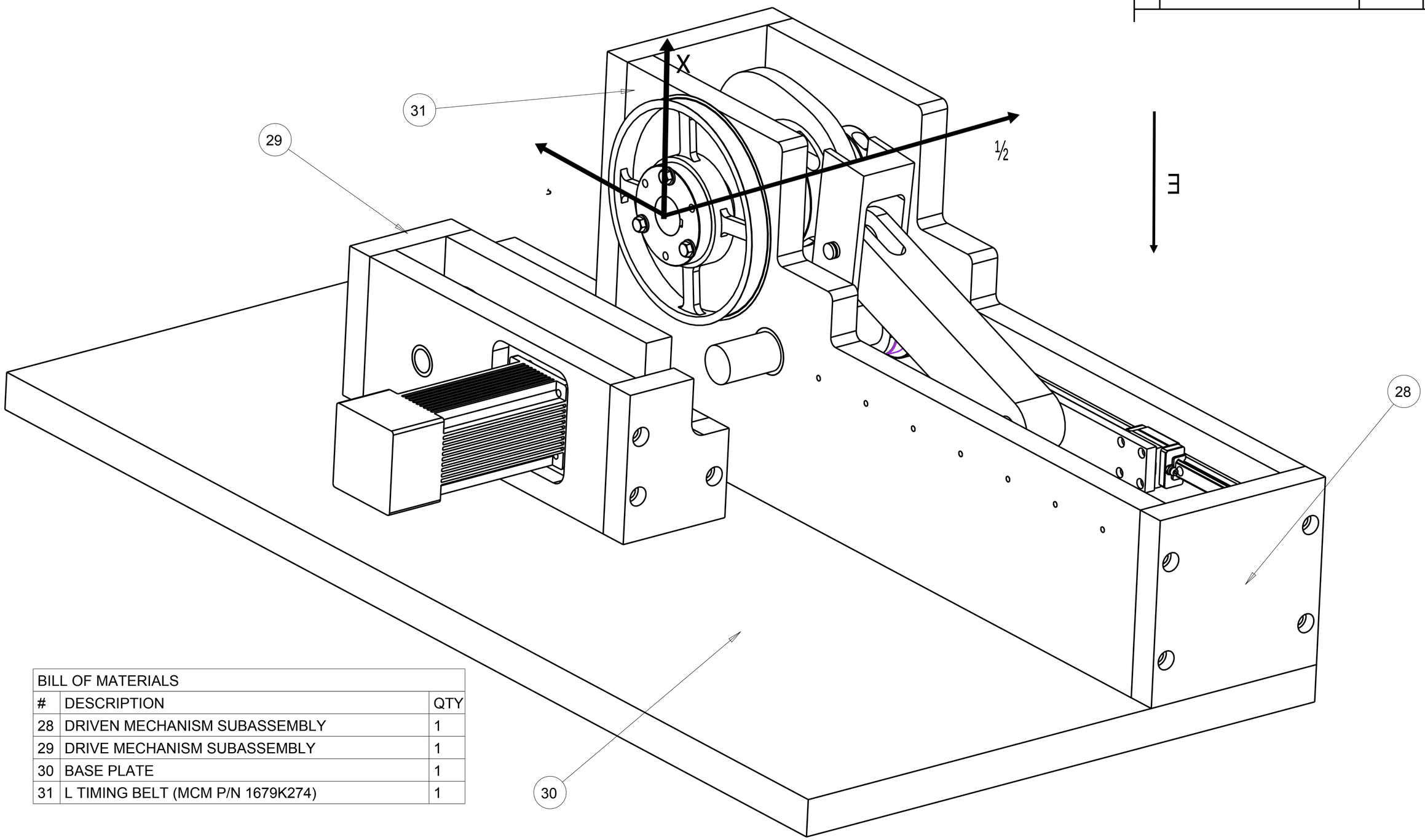

BILL OF MATERIALS		
#	DESCRIPTION	QTY
28	DRIVEN MECHANISM SUBASSEMBLY	1
29	DRIVE MECHANISM SUBASSEMBLY	1
30	BASE PLATE	1
31	L TIMING BELT (MCM P/N 1679K274)	1

WORCESTER POLYTECHNIC INSTITUTE

CAM-SERVO TEST MACHINE, FULL ASSEMBLY
CAM DRIVE CONFIGURATION

C | SCALE 0.45:1 | DRAWING 1-1 | REV A

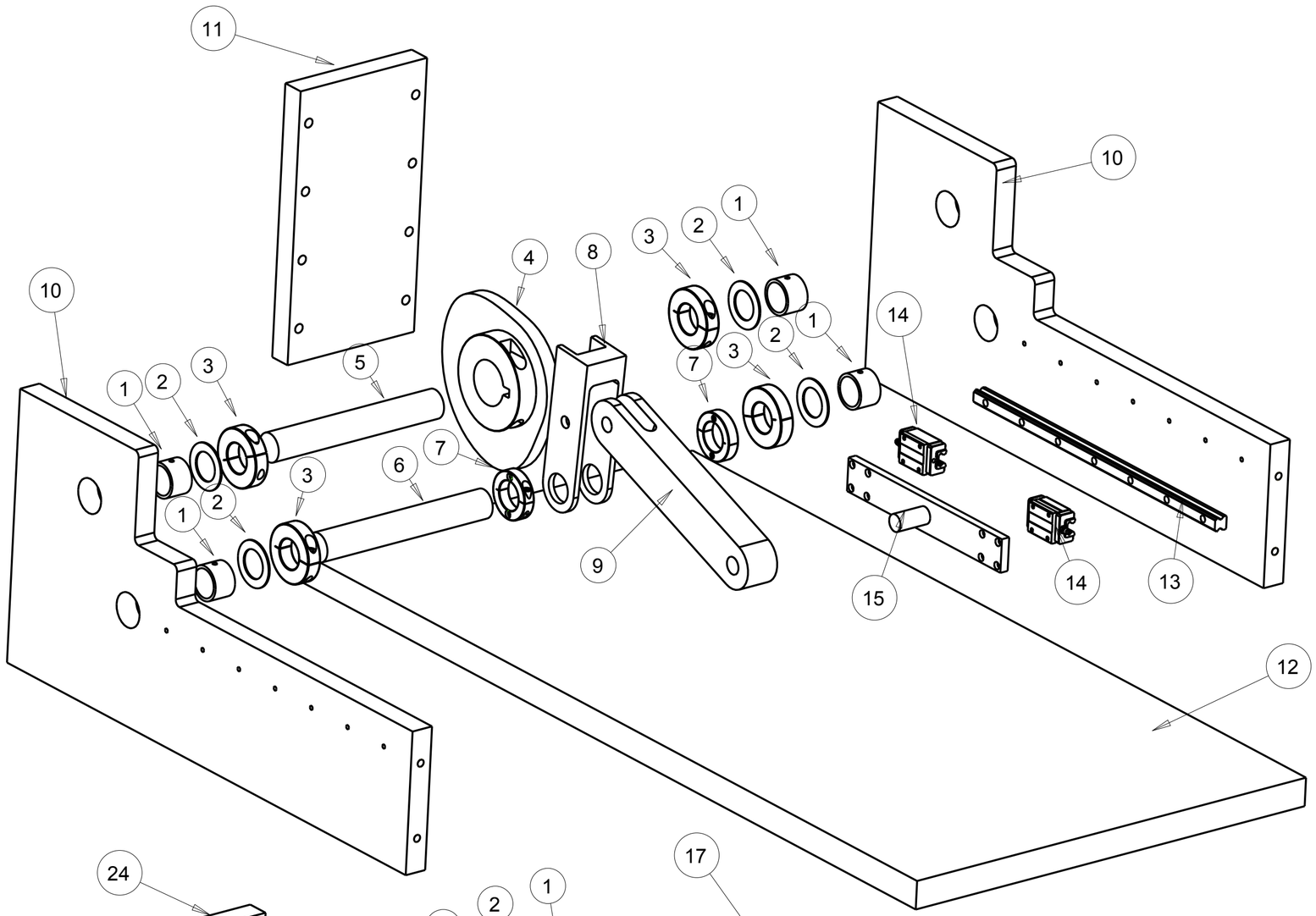

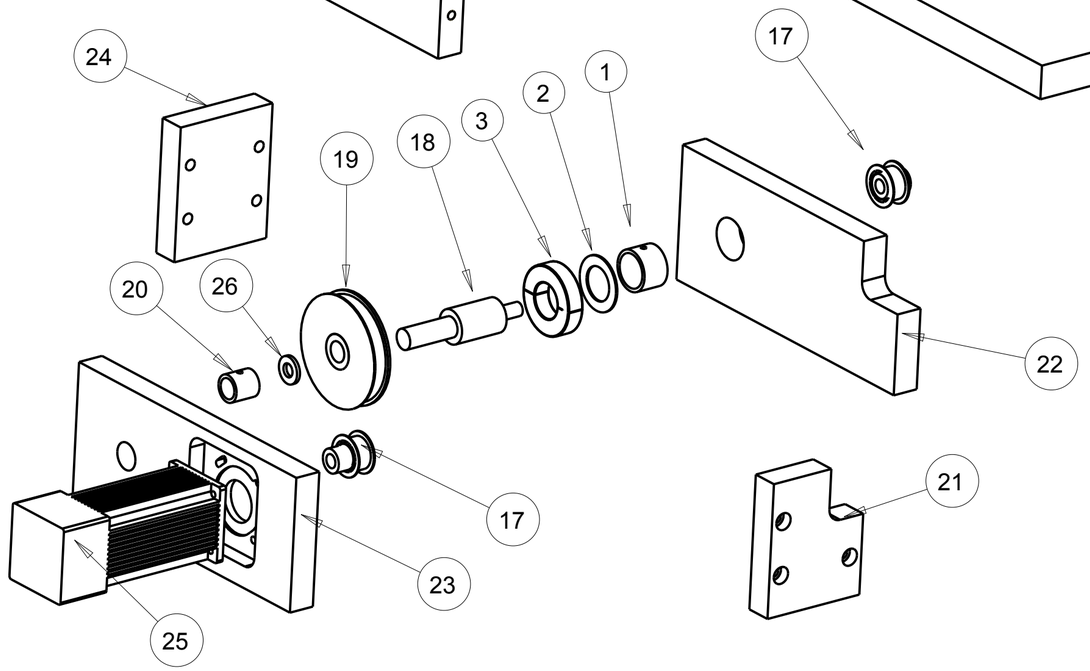

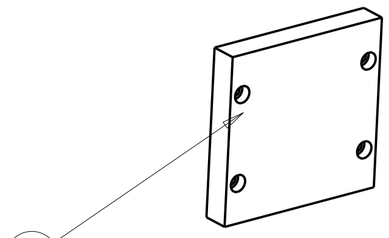

BILL OF MATERIALS	
#	DESCRIPTION
1	SLEEVE BEARING (MCM P/N 7965K54)
2	THRUST BEARING (MCM P/N 3750K28)
3	SHAFT COLLAR (MCM P/N 9951K130)
4	CAM
5	CAM SHAFT
6	CRANK SHAFT
7	CRANK MOUNT SHAFT COLLAR (MCM P/N 9677T400)
8	CRANK
9	CONNECTING ROD
10	CAM SUPPORT PLATE
11	CAM SUPPORT CAM SIDE
12	BASE PLATE
13	LINEAR MOTION RAIL (THK P/N HSR LM)
14	LINEAR MOTION BLOCK (THK P/N HSR15R)
15	SLIDER BLOCK
16	CAM SUPPORT RAIL SIDE
17	1.194 P.D. TIMING BELT PULLEY (NORDEX P/N E4-10DF)
18	TRANSMISSION SHAFT
19	3.820 P.D. TIMING BELT PULLEY (NORDEX P/N E6-32DF)
20	SLEEVE BEARING (MCM P/N 7965K29)
21	SERVOMOTOR CROSS PLATE (SCOOPED)
22	SERVOMOTOR OPPOSING PLATE
23	SERVOMOTOR PLATE
24	SERVOMOTOR CROSS PLATE
25	KOLLMORGEN B-102-A14 SERVOMOTOR
26	THRUST BEARING (MCM P/N 3750K17)

NOTE:
ROLLER FOLLOWER, 7.162 P.D. TIMING BELT PULLEY, AND TIMING BELTS NOT SHOWN INCLUDED IN DETAIL DRAWINGS INSTEAD

	WORCESTER POLYTECHNIC INSTITUTE
	CAM-SERVO TEST MACHINE FULL ASSEMBLY
	C SCALE 0.25:1 DRAWING 1-2 REV A

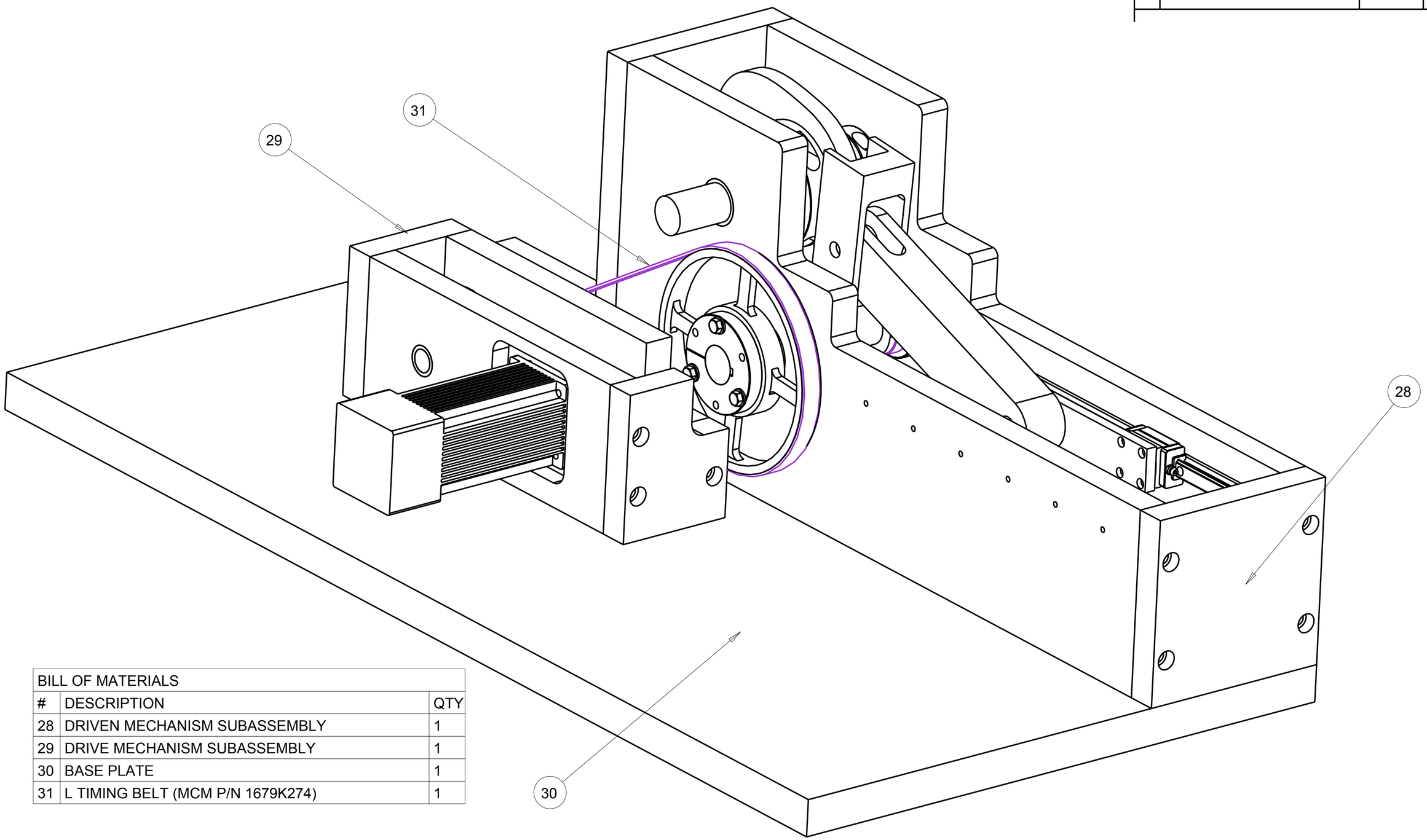

BILL OF MATERIALS		
#	DESCRIPTION	QTY
28	DRIVEN MECHANISM SUBASSEMBLY	1
29	DRIVE MECHANISM SUBASSEMBLY	1
30	BASE PLATE	1
31	L TIMING BELT (MCM P/N 1679K274)	1

WORCESTER POLYTECHNIC INSTITUTE

CAM-SERVO TEST MACHINE, FULL ASSEMBLY
SERVOMOTOR DRIVE CONFIGURATION

C | SCALE 0.45:1 | DRAWING 1-3 | REV A

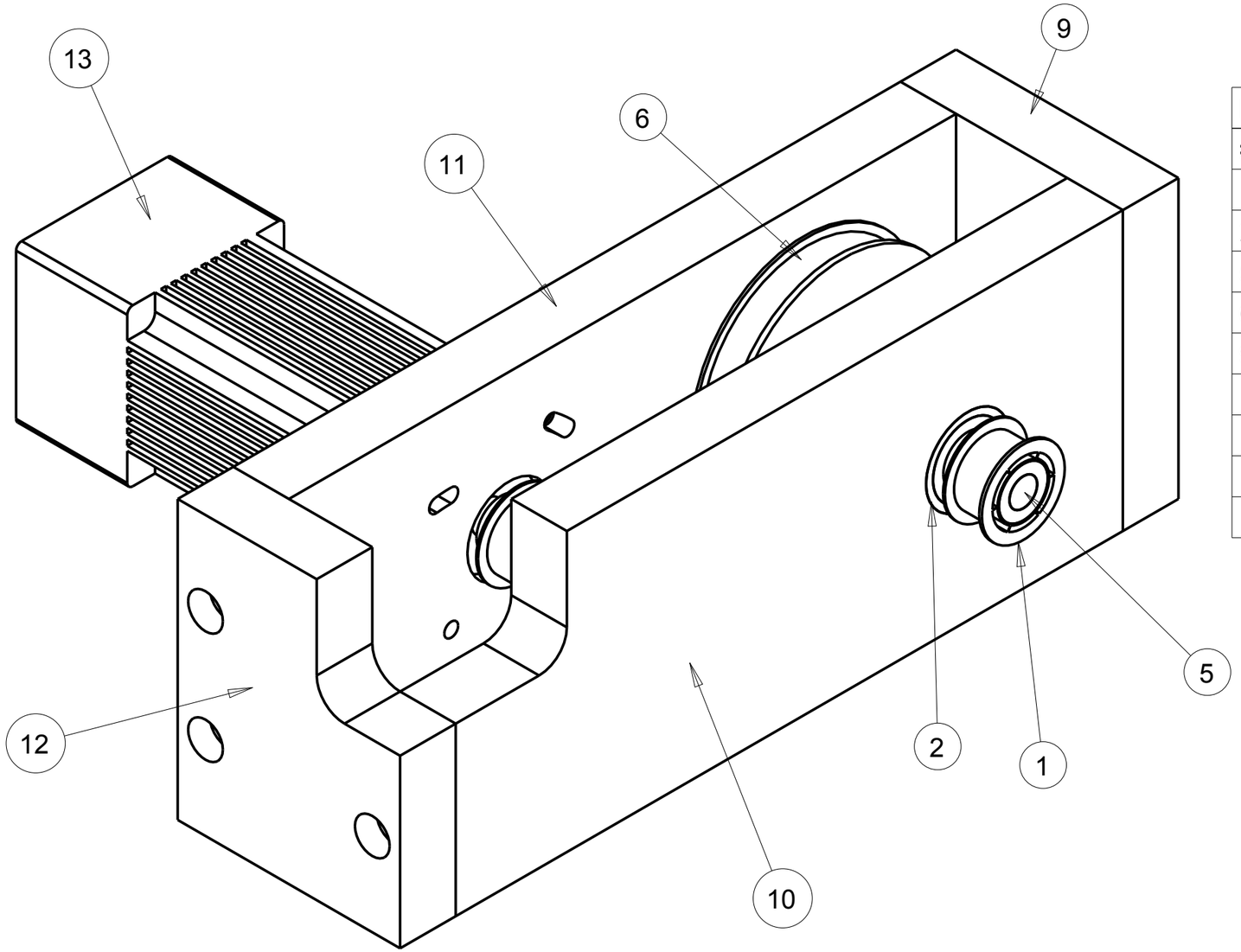

BILL OF MATERIALS		
#	DESCRIPTION	QTY
1	1.194 P.D. TIMING BELT PULLEY (NORDEX P/N E4-10DF)	2
2	SLEEVE BEARING (MCM P/N 7965K54)	1
5	TRANSMISSION SHAFT	1
6	3.820 P.D. TIMING BELT PULLEY (NORDEX P/N E6-32DF)	1
9	SERVOMOTOR CROSS PLATE	1
10	SERVOMOTOR OPPOSING PLATE	1
11	SERVOMOTOR PLATE	1
12	SERVOMOTOR CROSS PLATE (SCOOPED)	1
13	KOLLMORGEN B-102-A14 SERVOMOTOR	1

WORCESTER POLYTECHNIC INSTITUTE

CAM-SERVO TEST MACHINE
DRIVE SUBASSEMBLY

B	SCALE 0.6:1	DRAWING 2-1	REV A

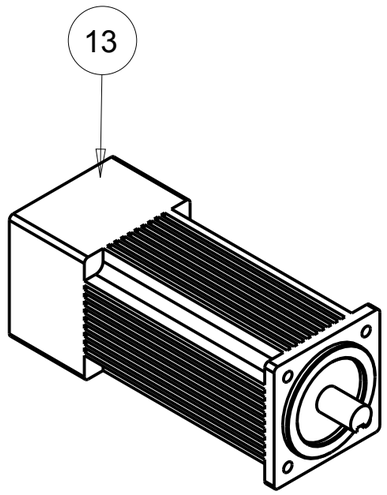

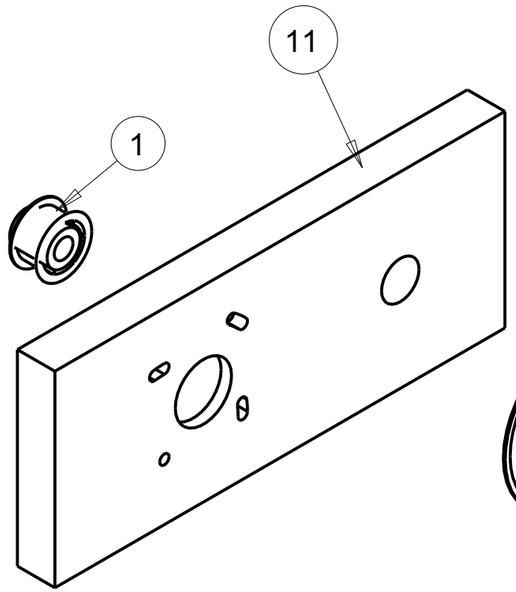

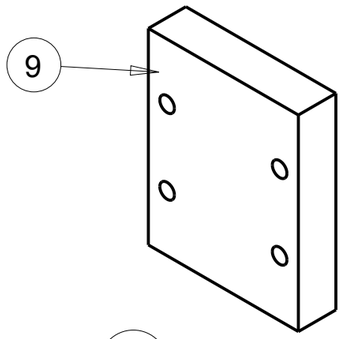

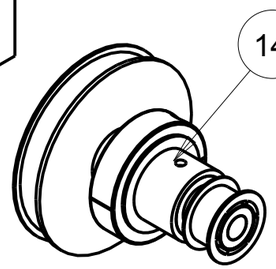

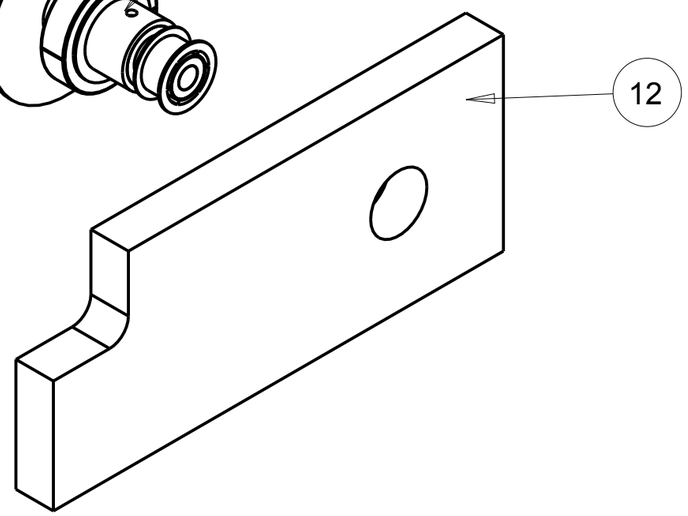

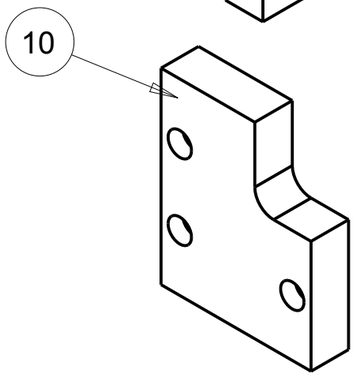

BILL OF MATERIALS		
#	DESCRIPTION	QTY
1	1.194 P.D. TIMING BELT PULLEY (NORDEX P/N E4-10DF)	1
9	SERVOMOTOR CROSS PLATE	1
10	SERVOMOTOR OPPOSING PLATE	1
11	SERVOMOTOR PLATE	1
12	SERVOMOTOR CROSS PLATE (SCOOPED)	1
13	KOLLMORGEN B-102-A14 SERVOMOTOR	1
14	TRANSMISSION SHAFT SUBASSEMBLY	1

NOTE:
187L TIMING BELT (MCM P/N 1679K264)
NOT SHOWN

WORCESTER POLYTECHNIC INSTITUTE

CAM-SERVO TEST MACHINE
DRIVING SUBASSEMBLY

B | SCALE 0.35:1 | DRAWING 2-2 | REV A

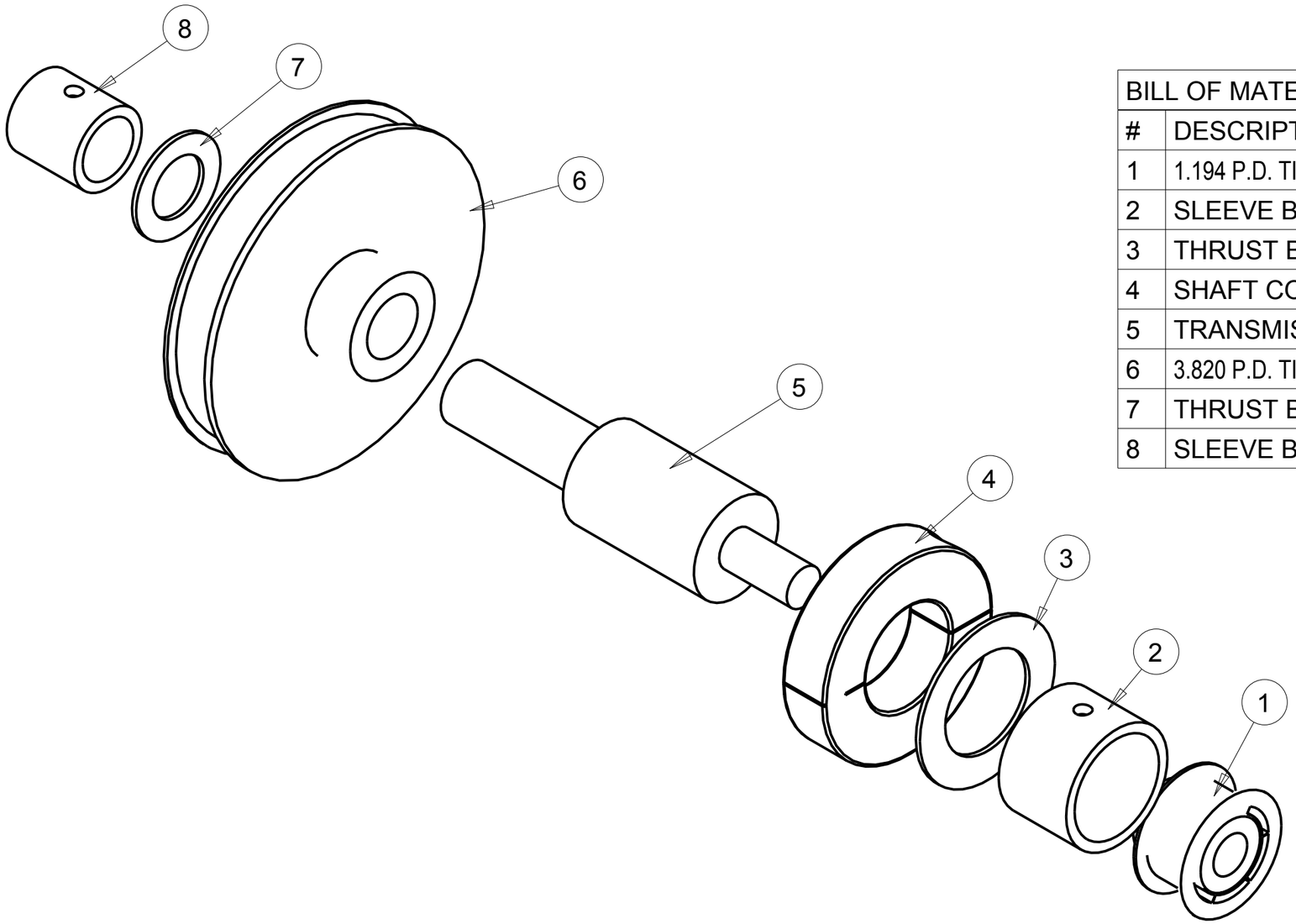

BILL OF MATERIALS		
#	DESCRIPTION	QTY
1	1.194 P.D. TIMING BELT PULLEY (NORDEX P/N E4-10DF)	1
2	SLEEVE BEARING (MCM P/N 7965K54)	1
3	THRUST BEARING (MCM P/N 3750K28)	1
4	SHAFT COLLAR (MCM P/N 9951K130)	1
5	TRANSMISSION SHAFT	1
6	3.820 P.D. TIMING BELT PULLEY (NORDEX P/N E6-32DF)	1
7	THRUST BEARING(MCM P/N 3750K17)	1
8	SLEEVE BEARING (MCM P/N 9765K29)	1

WORCESTER POLYTECHNIC INSTITUTE

CAM-SERVO TEST MACHINE, DRIVE SUBASSEMBLY
TRANSMISSION SHAFT SUBASSEMBLY

B	SCALE 0.75:1	DRAWING 2-3	REV A

BILL OF MATERIALS		
#	DESCRIPTION	QTY
1	1.194 P.D. TIMING BELT PULLEY (NORDEX P/N E4-10DF)	1
2	SLEEVE BEARING (MCM P/N 7965K54)	1
3	THRUST BEARING (MCM P/N 3750K28)	1
4	SHAFT COLLAR (MCM P/N 9951K130)	1
5	TRANSMISSION SHAFT	1
6	3.820 P.D. TIMING BELT PULLEY (NORDEX P/N E6-32DF)	1
7	THRUST BEARING(MCM P/N 3750K17)	1
8	SLEEVE BEARING (MCM P/N 9765K29)	1

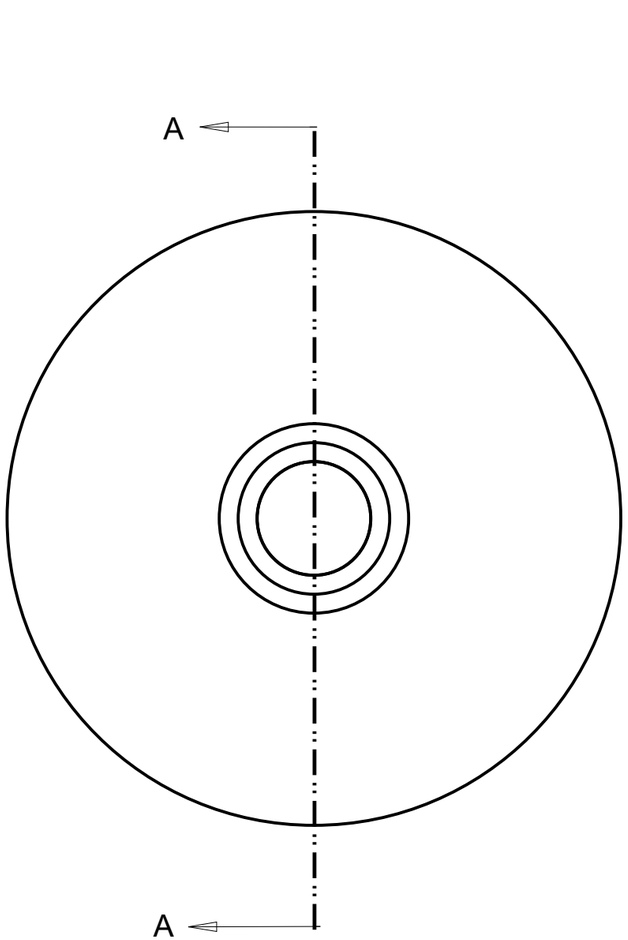

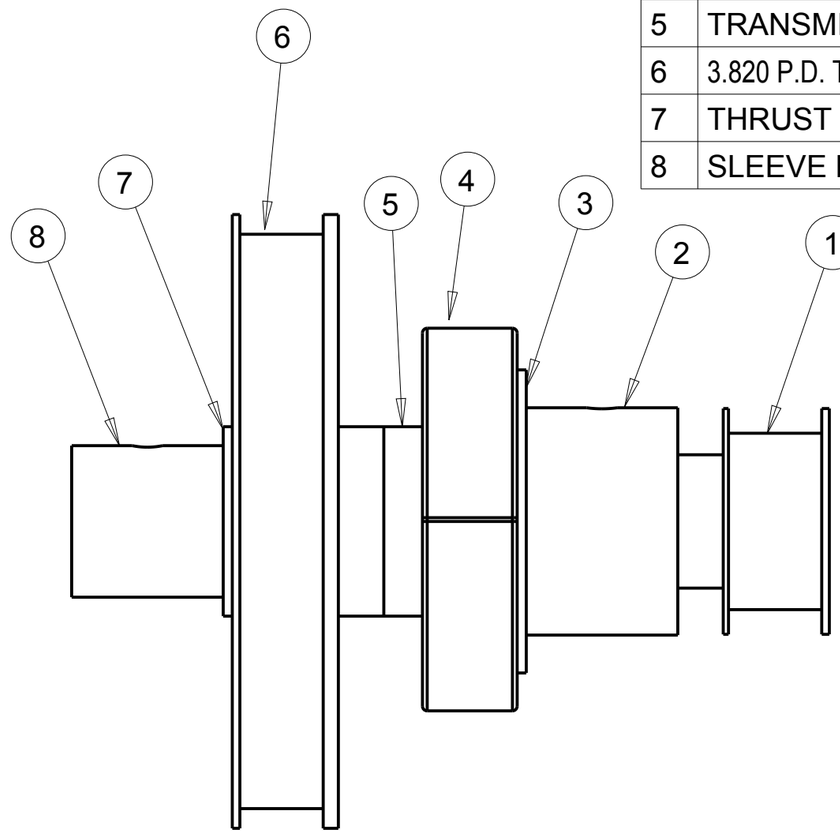

WORCESTER POLYTECHNIC INSTITUTE

CAM-SERVO TEST MACHINE, DRIVE SUBASSEMBLY
TRANSMISSION SHAFT SUBASSEMBLY

B | SCALE 1:1 | DRAWING 2-4 | REV A

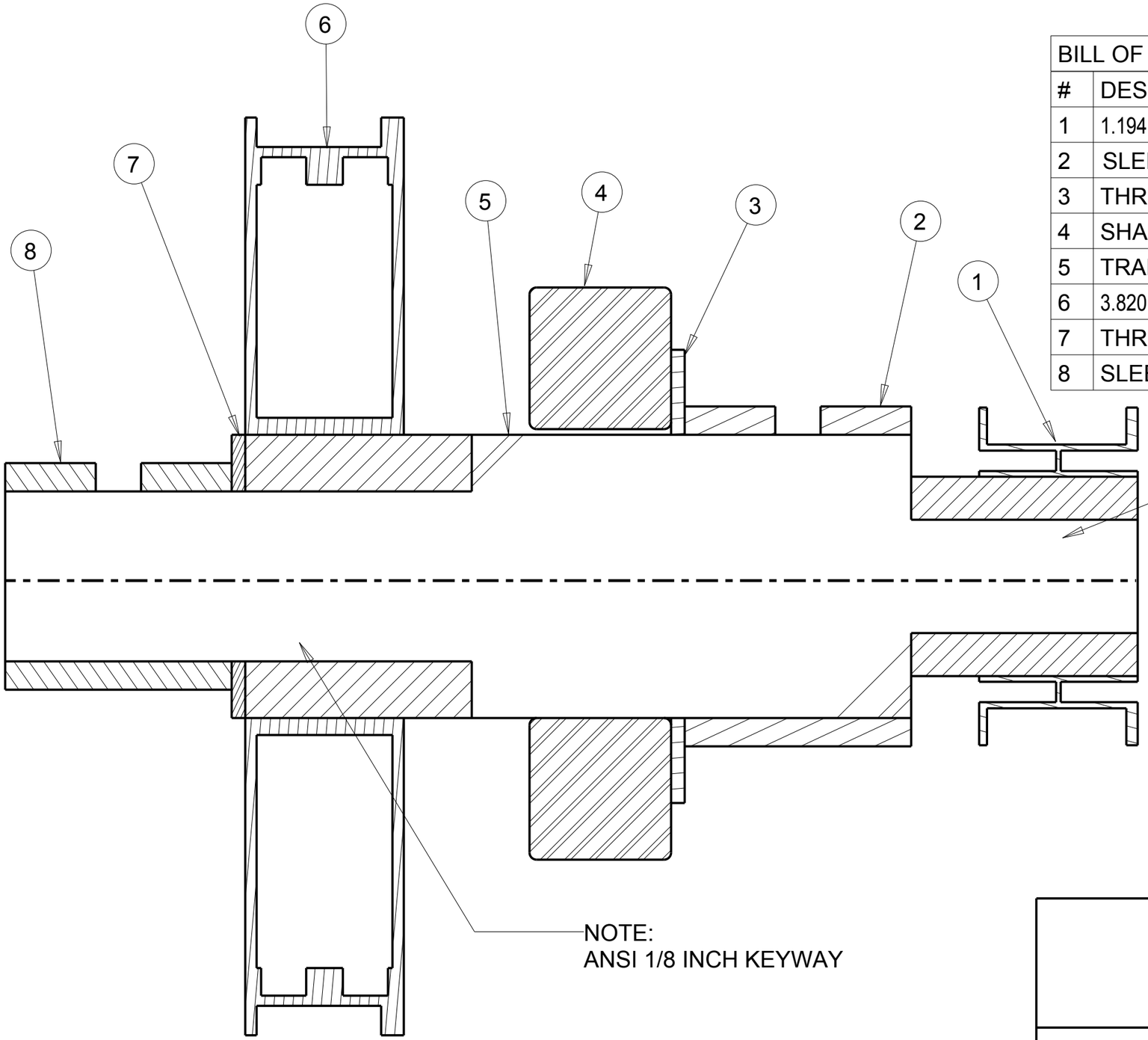

BILL OF MATERIALS		
#	DESCRIPTION	QTY
1	1.194 P.D. TIMING BELT PULLEY (NORDEX P/N E4-10DF)	1
2	SLEEVE BEARING (MCM P/N 7965K54)	1
3	THRUST BEARING (MCM P/N 3750K28)	1
4	SHAFT COLLAR (MCM P/N 9951K130)	1
5	TRANSMISSION SHAFT	1
6	3.820 P.D. TIMING BELT PULLEY (NORDEX P/N E6-32DF)	1
7	THRUST BEARING(MCM P/N 3750K17)	1
8	SLEEVE BEARING (MCM P/N 9765K29)	1

WORCESTER POLYTECHNIC INSTITUTE

CAM-SERVO TEST MACHINE, DRIVE SUBASSEMBLY
TRANSMISSION SHAFT SUBASSEMBLY

B	SCALE 2:1	DRAWING 2-4A	REV A

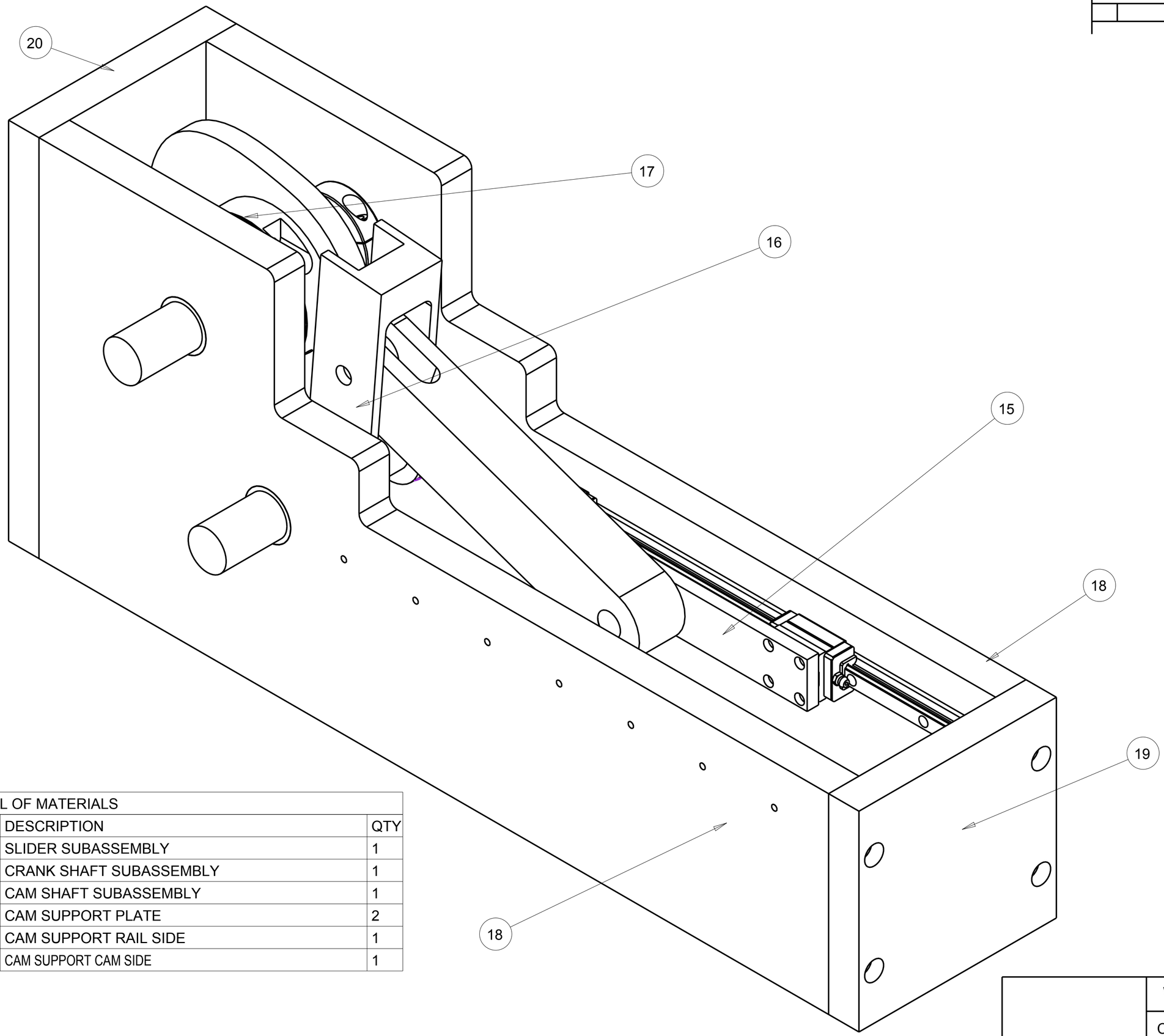

BILL OF MATERIALS		
#	DESCRIPTION	QTY
15	SLIDER SUBASSEMBLY	1
16	CRANK SHAFT SUBASSEMBLY	1
17	CAM SHAFT SUBASSEMBLY	1
18	CAM SUPPORT PLATE	2
19	CAM SUPPORT RAIL SIDE	1
20	CAM SUPPORT CAM SIDE	1

WORCESTER POLYTECHNIC INSTITUTE

CAM-SERVO TEST MACHINE
DRIVEN MECHANISM SUBASSEMBLY

C | SCALE 0.6:1 | DRAWING 3-1 | REV A

BILL OF MATERIALS		
#	DESCRIPTION	QTY
15	SLIDER SUBASSEMBLY	1
16	CRANK SHAFT SUBASSEMBLY	1
17	CAM SHAFT SUBASSEMBLY	1
18	CAM SUPPORT PLATE	2
19	CAM SUPPORT RAIL SIDE	1
20	CAM SUPPORT CAM SIDE	1

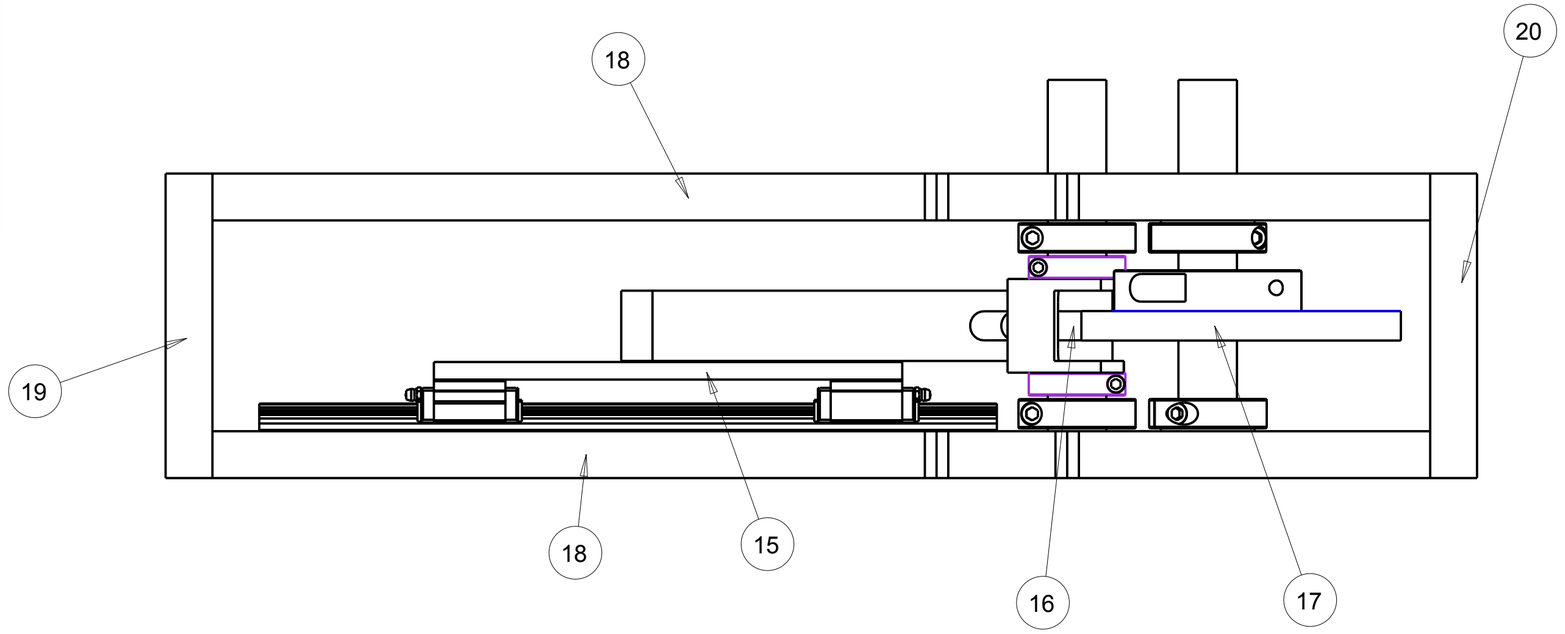

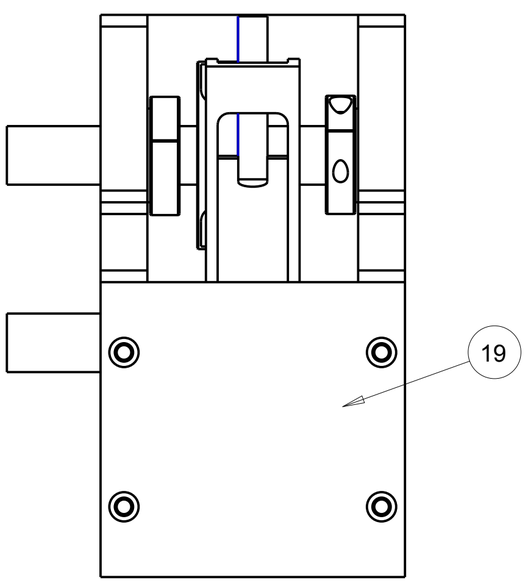

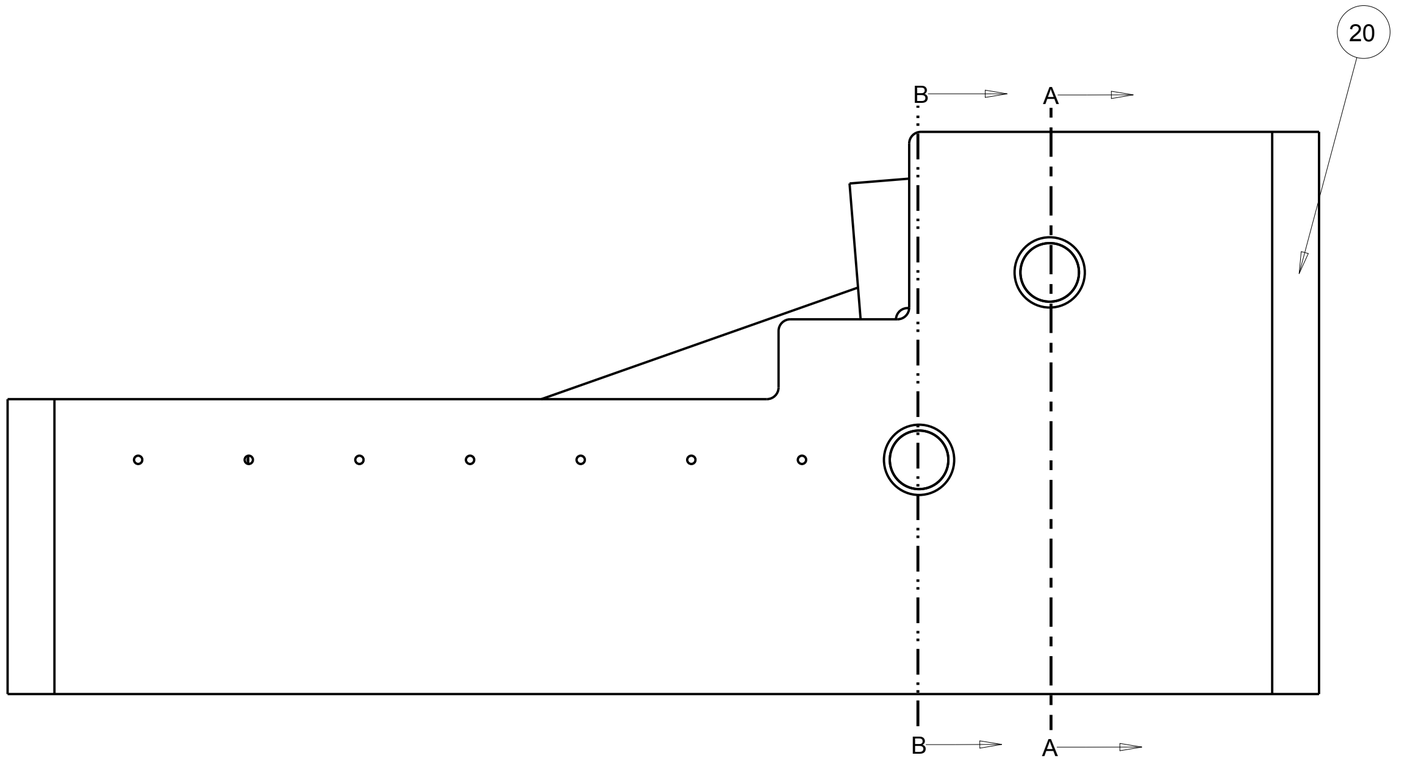

WORCESTER POLYTECHNIC INSTITUTE

CAM-SERVO TEST MACHINE
DRIVEN MECHANISM SUBASSEMBLY

C | SCALE 0.4:1 | DRAWING 3-2 | REV A

DETAIL A

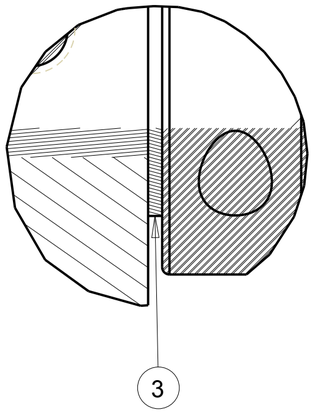

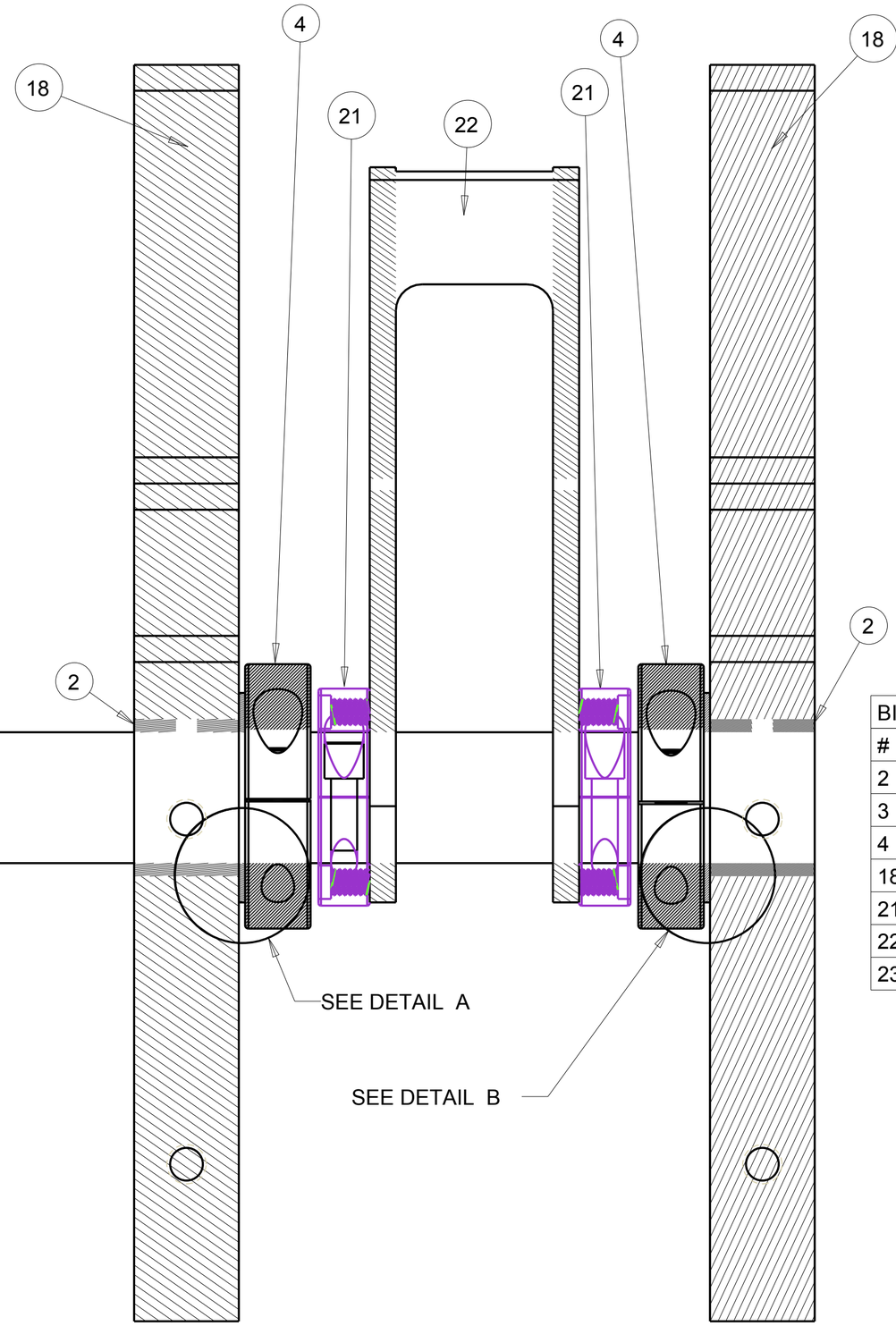

DETAIL B

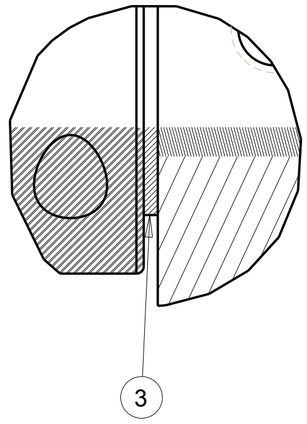

NOTE: CONNECTING ROD, FOLLOWER, AND CRANK PIN ARE NOT SHOWN

BILL OF MATERIALS		
#	DESCRIPTION	QTY
2	SLEEVE BEARING (MCM P/N 7965K54)	2
3	THRUST BEARING (MCM P/N 3750K28)	2
4	SHAFT COLLAR (MCM P/N 9951K130)	2
18	CAM SUPPORT PLATE	2
21	CRANK MOUNT SHAFT COLLAR (MCM P/N 9677T400)	2
22	CRANK	1
23	CRANK SHAFT	1

WORCESTER POLYTECHNIC INSTITUTE

CAM-SERVO TEST MACHINE, DRIVEN SUBASSEMBLY
SECTION VIEW OF CRANKSHAFT SUBASSEMBLY

C | SCALE 1:1 | DRAWING 3-2A | REV A

DETAIL A

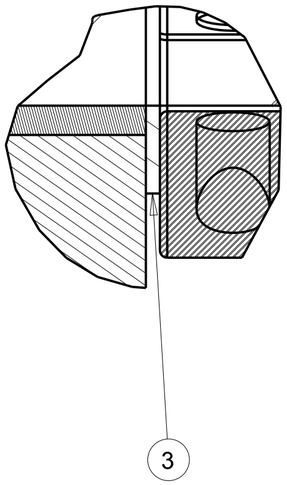

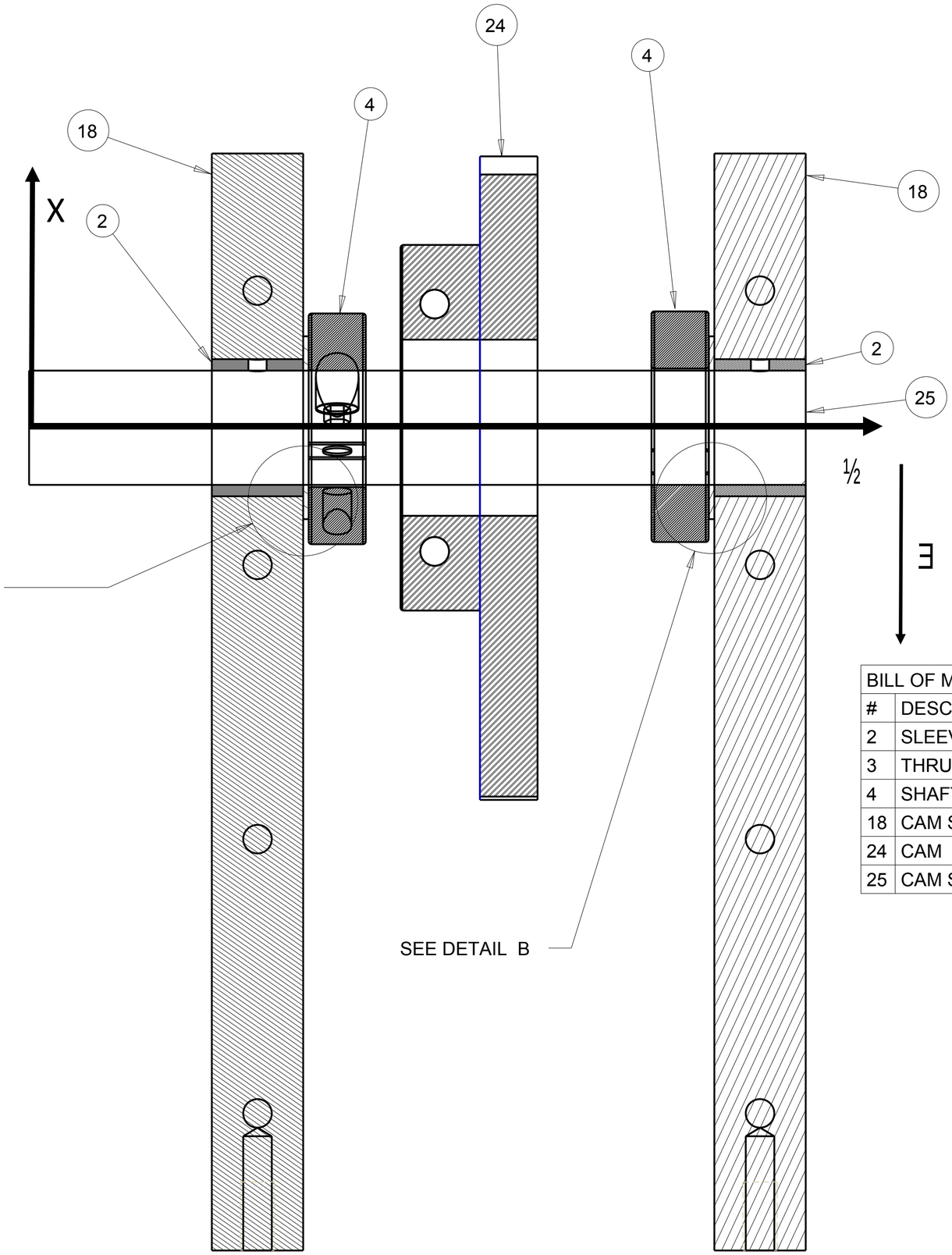

DETAIL B

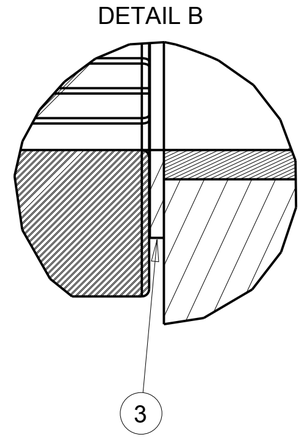

½

E

BILL OF MATERIALS		
#	DESCRIPTION	QTY
2	SLEEVE BEARING (MCM P/N 7965K54)	2
3	THRUST BEARING (MCM P/N 3750K28)	2
4	SHAFT COLLAR (MCM P/N 9951K130)	2
18	CAM SUPPORT PLATE	2
24	CAM	1
25	CAM SHAFT	1

WORCESTER POLYTECHNIC INSTITUTE

CAM-SERVO TEST MACHINE
SECTION VIEW OF CRANK SHAFT SUBASSEMBLY

C | SCALE 1:1 | DRAWING 3-2B | REV A

SHEET 3 OF 3

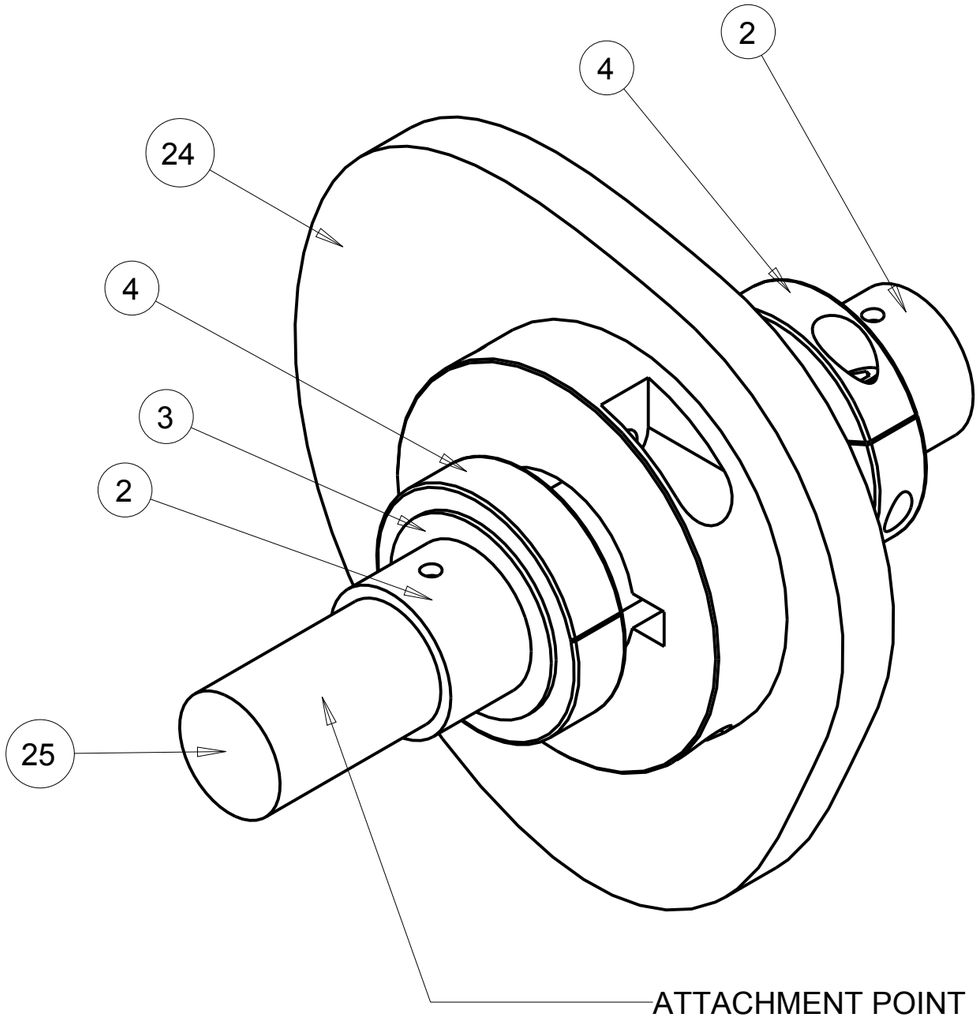

BILL OF MATERIALS		
#	DESCRIPTION	QTY
2	SLEEVE BEARING (MCM P/N 7965K54)	2
3	THRUST BEARING (MCM P/N 3750K28)	2
4	SHAFT COLLAR (MCM P/N 9951K130)	2
24	CAM	1
25	CAM SHAFT	1

WORCESTER POLYTECHNIC INSTITUTE

CAM-SERVO TEST MACHINE, DRIVE SUBASSEMBLY
CAM SHAFT SUBASSEMBLY

B	SCALE 0.75:1	DRAWING 3-3	REV A

NOTE:
ACTUAL ATTACHMENT OF CAM TO
CAM SHAFT NOT DETERMINED
BEFORE ANALYSIS INVALIDATING DESIGN
WAS PERFORMED. IS NOT SHOWN

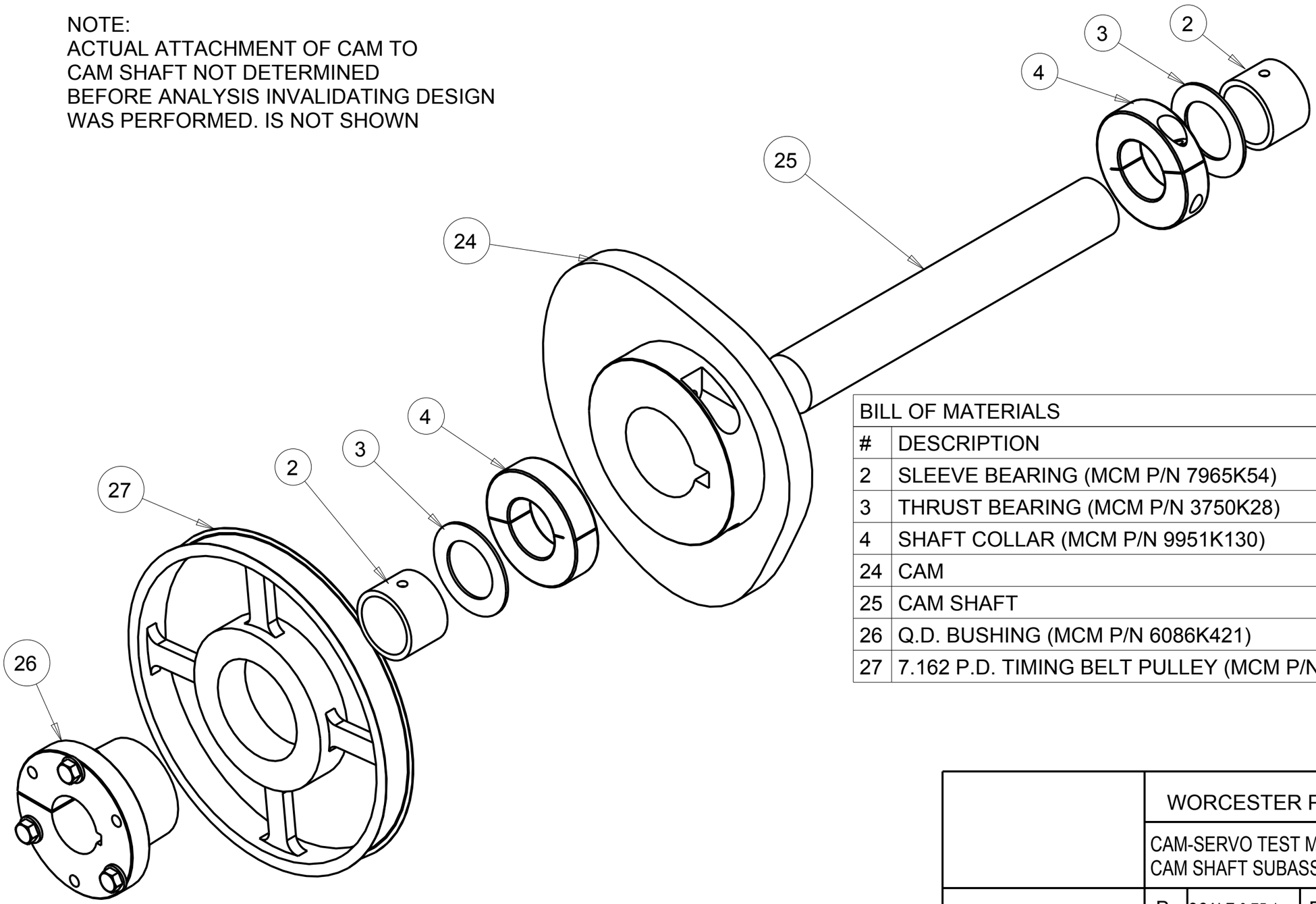

BILL OF MATERIALS

#	DESCRIPTION	QTY
2	SLEEVE BEARING (MCM P/N 7965K54)	2
3	THRUST BEARING (MCM P/N 3750K28)	2
4	SHAFT COLLAR (MCM P/N 9951K130)	2
24	CAM	1
25	CAM SHAFT	1
26	Q.D. BUSHING (MCM P/N 6086K421)	1
27	7.162 P.D. TIMING BELT PULLEY (MCM P/N 6495K222)	1

WORCESTER POLYTECHNIC INSTITUTE

CAM-SERVO TEST MACHINE, DRIVE SUBASSEMBLY
CAM SHAFT SUBASSEMBLY

B	SCALE 0.75:1	DRAWING 3-4	REV A

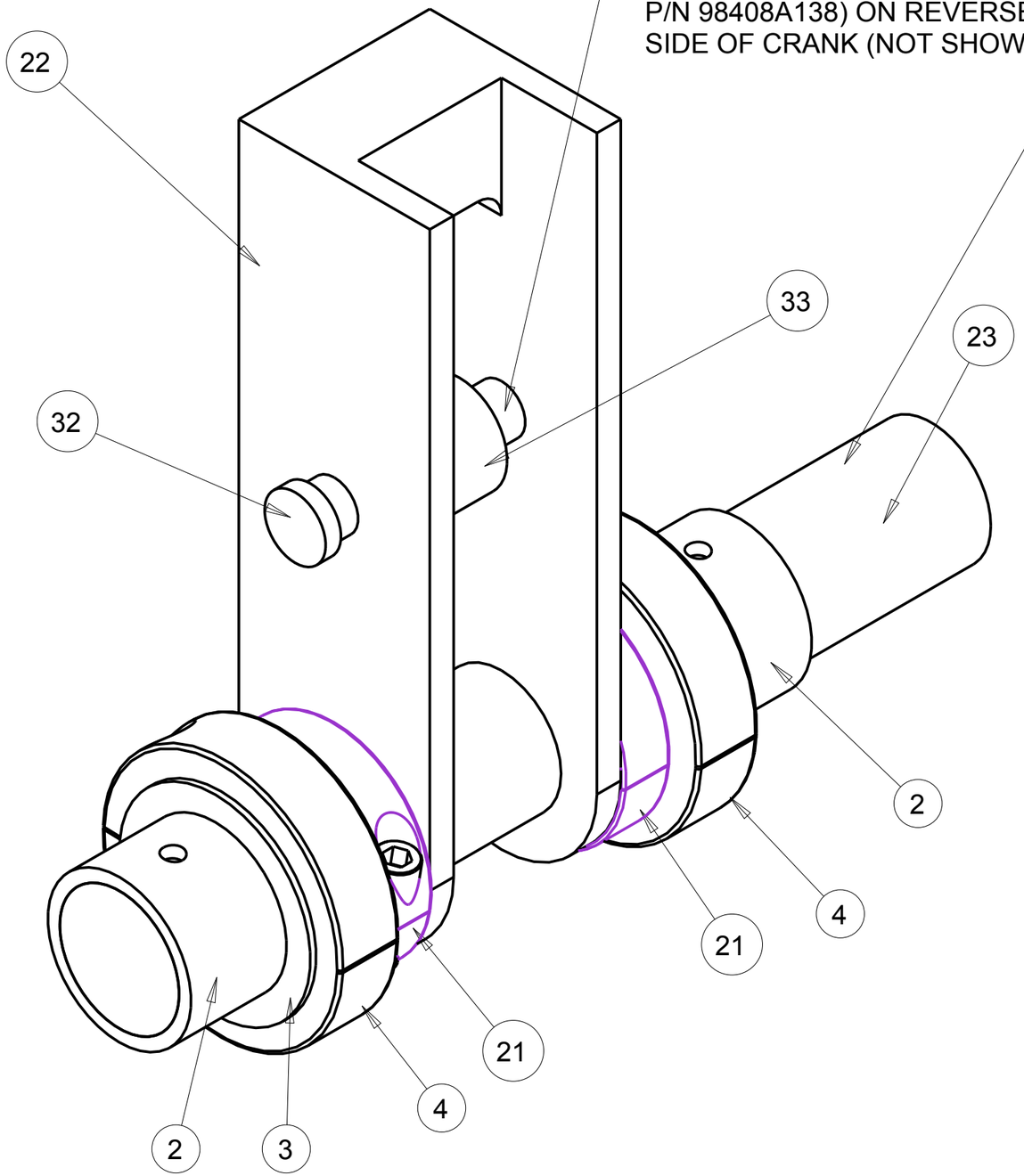

BILL OF MATERIALS		
#	DESCRIPTION	QTY
2	SLEEVE BEARING (MCM P/N 7965K54)	2
3	THRUST BEARING (MCM P/N 3750K28)	2
4	SHAFT COLLAR (MCM P/N 9951K130)	2
21	CRANK MOUNT SHAFT COLLAR (MCM P/N 9677T400)	2
22	CRANK	1
23	CRANK SHAFT	1
32	CLEVIS PIN (MCM P/N 92735A520)	1
33	ROLLER FOLLOWER (MCM P/N 340K21)	1

WORCESTER POLYTECHNIC INSTITUTE

CAM-SERVO TEST MACHINE, DRIVE SUBASSEMBLY
CRANK SHAFT SUBASSEMBLY

B	SCALE 1:1	DRAWING 3-5	REV A

CLEVIS PIN IS RETAINED WITH E-STYLE RETAINING RING (MCM P/N 98408A138) ON REVERSE SIDE OF CRANK (NOT SHOWN)

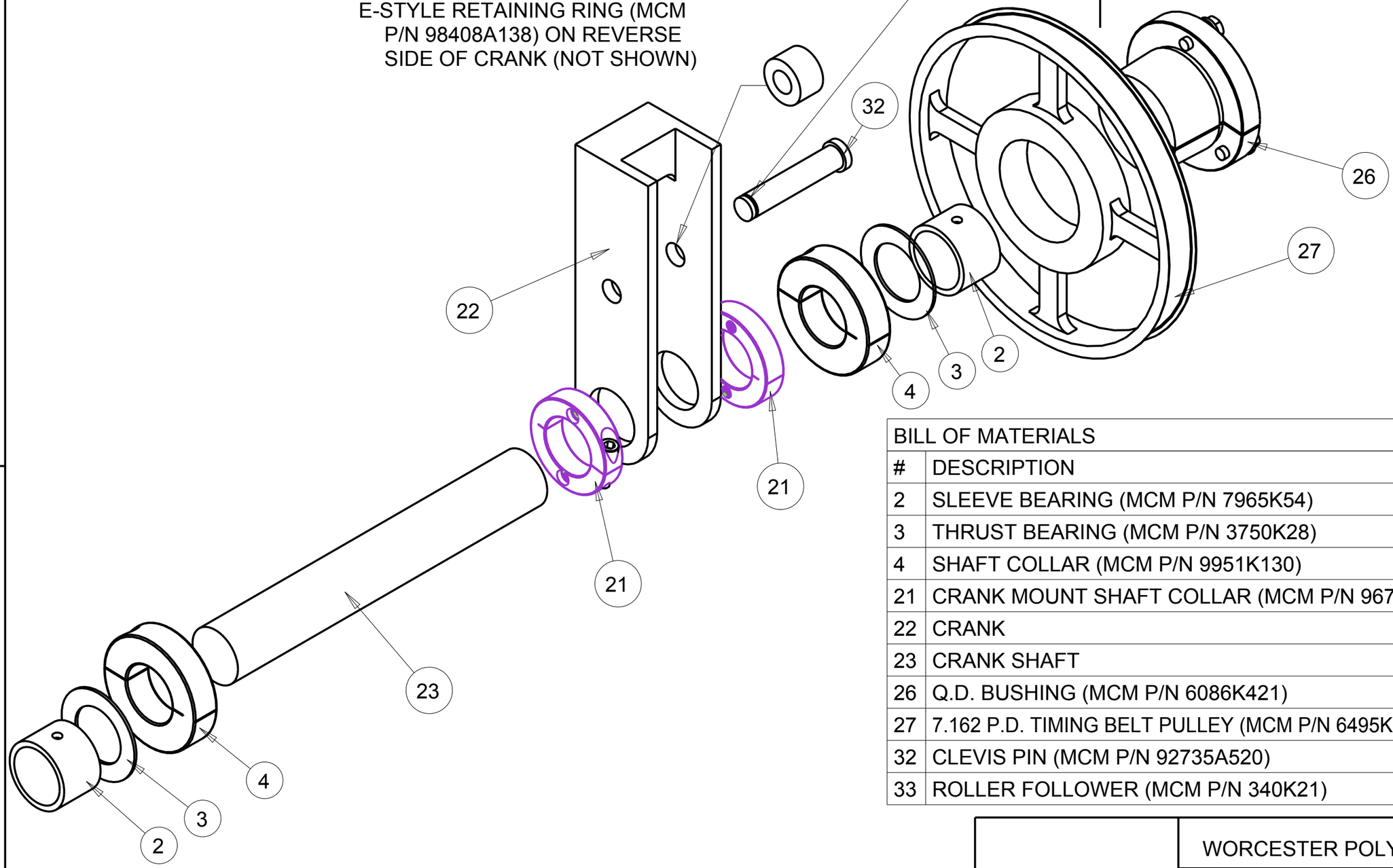

BILL OF MATERIALS		
#	DESCRIPTION	QTY
2	SLEEVE BEARING (MCM P/N 7965K54)	2
3	THRUST BEARING (MCM P/N 3750K28)	2
4	SHAFT COLLAR (MCM P/N 9951K130)	2
21	CRANK MOUNT SHAFT COLLAR (MCM P/N 9677T400)	2
22	CRANK	1
23	CRANK SHAFT	1
26	Q.D. BUSHING (MCM P/N 6086K421)	1
27	7.162 P.D. TIMING BELT PULLEY (MCM P/N 6495K222)	1
32	CLEVIS PIN (MCM P/N 92735A520)	1
33	ROLLER FOLLOWER (MCM P/N 340K21)	1

WORCESTER POLYTECHNIC INSTITUTE

CAM-SERVO TEST MACHINE, DRIVE SUBASSEMBLY
CRANK SHAFT SUBASSEMBLY

B	SCALE 0.5:1	DRAWING 3-6	REV A

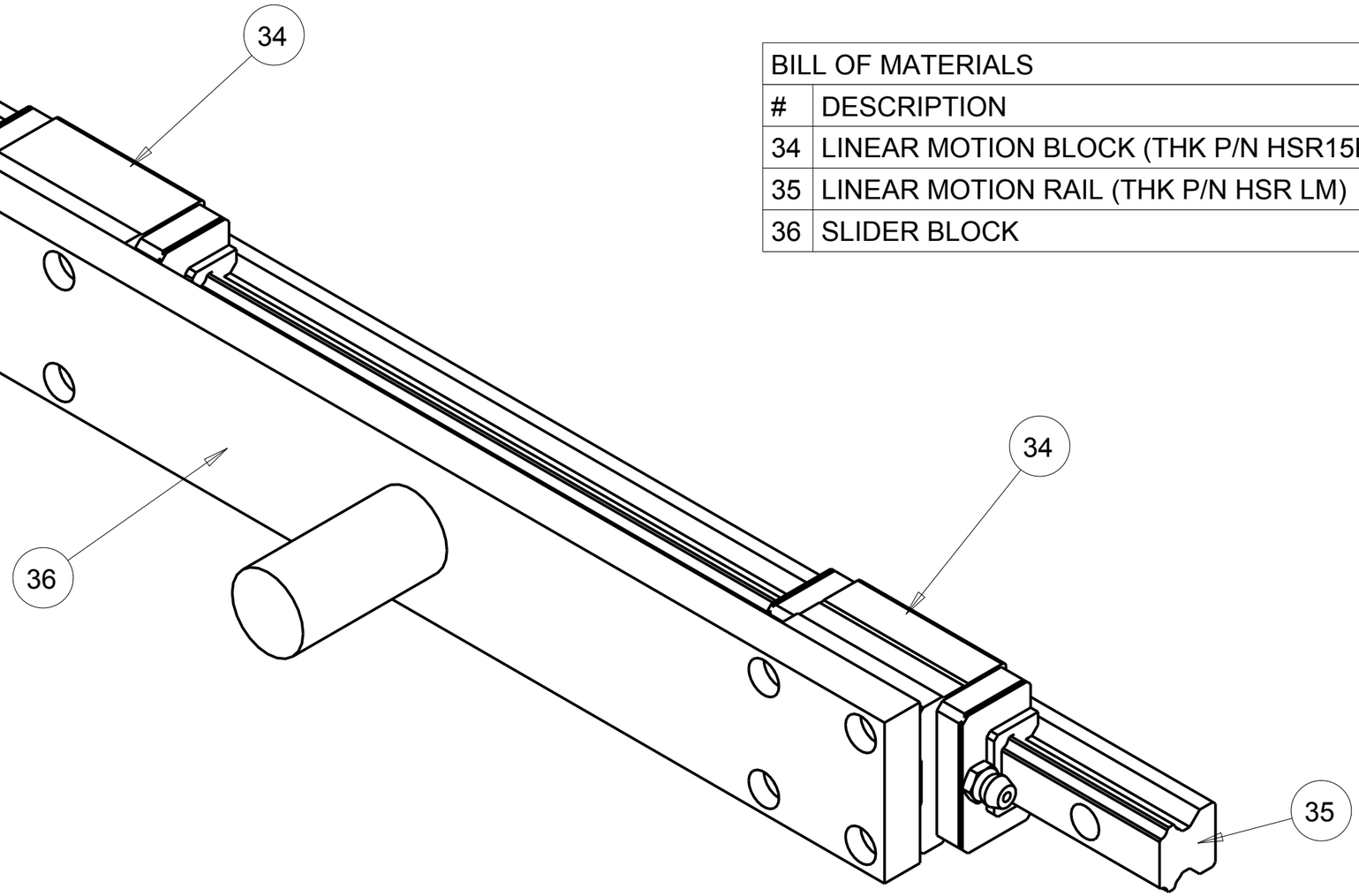

BILL OF MATERIALS		
#	DESCRIPTION	QTY
34	LINEAR MOTION BLOCK (THK P/N HSR15R)	2
35	LINEAR MOTION RAIL (THK P/N HSR LM)	1
36	SLIDER BLOCK	1

WORCESTER POLYTECHNIC INSTITUTE

CAM-SERVO TEST MACHINE, DRIVE SUBASSEMBLY
TRANSMISSION SHAFT SUBASSEMBLY

B	SCALE 1:1	DRAWING 2-4A	REV A

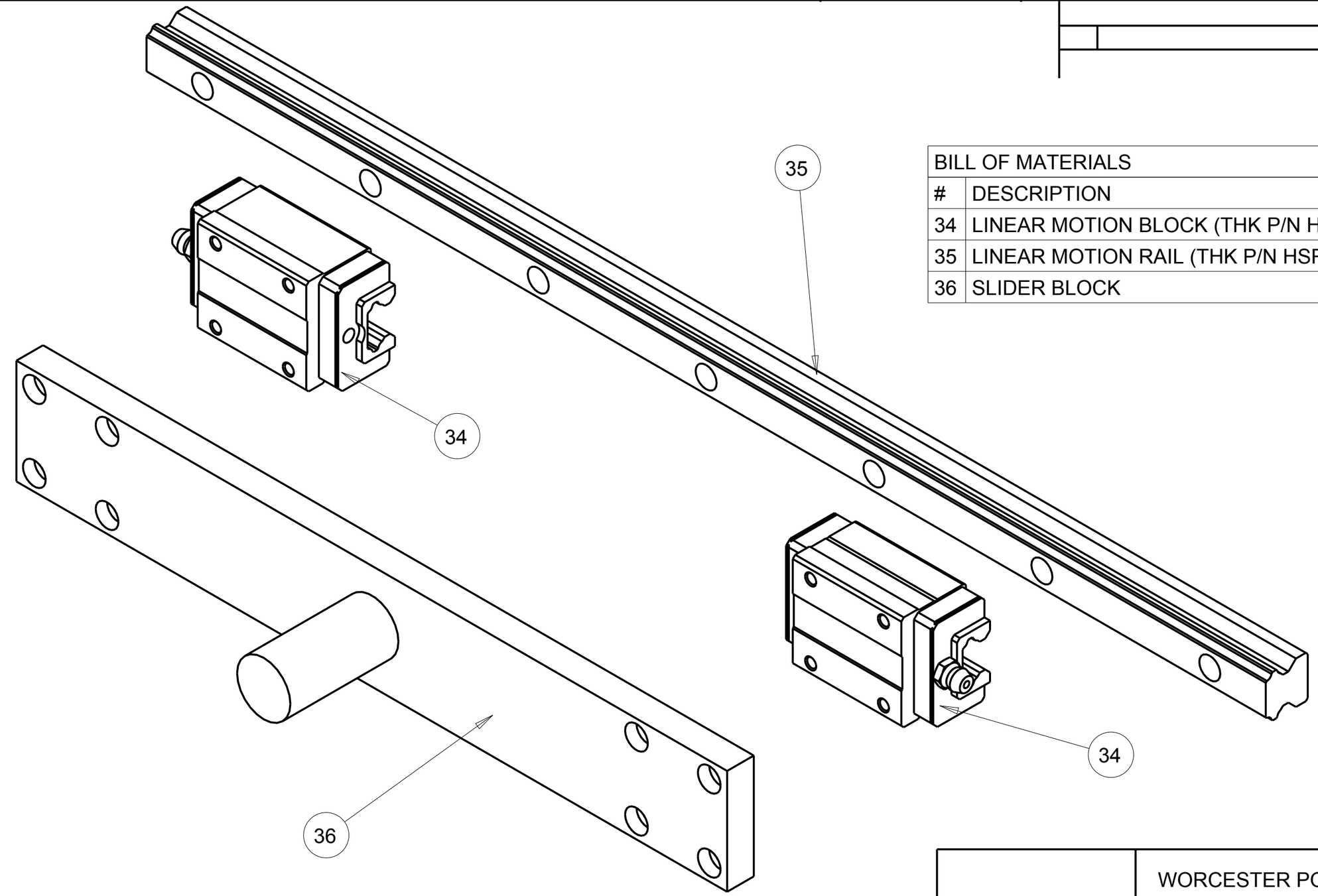

BILL OF MATERIALS		
#	DESCRIPTION	QTY
34	LINEAR MOTION BLOCK (THK P/N HSR15R)	2
35	LINEAR MOTION RAIL (THK P/N HSR LM)	1
36	SLIDER BLOCK	1

WORCESTER POLYTECHNIC INSTITUTE

CAM-SERVO TEST MACHINE, DRIVEN SUBASSEMBLY
SLIDER SUBASSEMBLY

B	SCALE 1:1	DRAWING 4-2	REV A

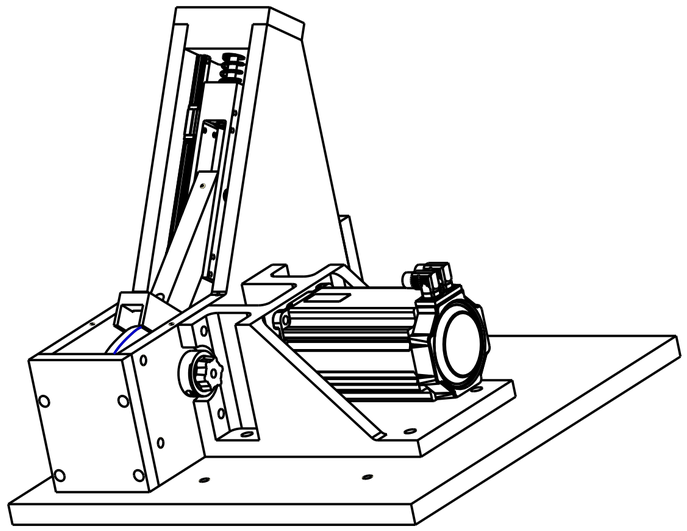

SERVO MODE

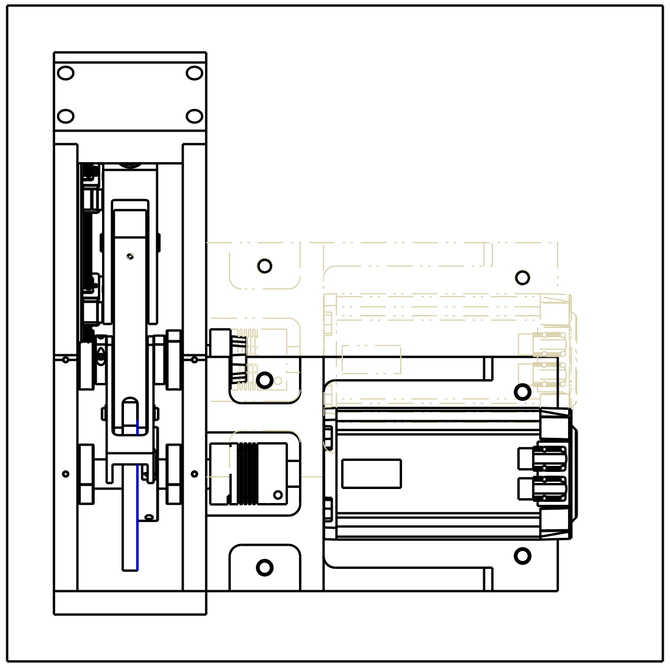

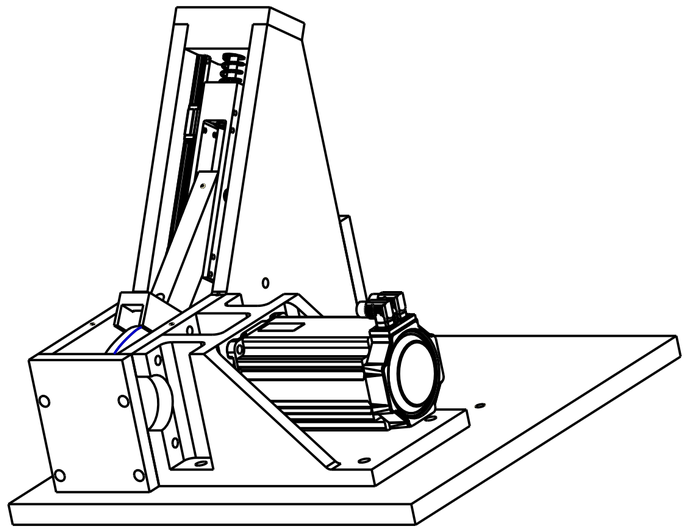

CAM MODE

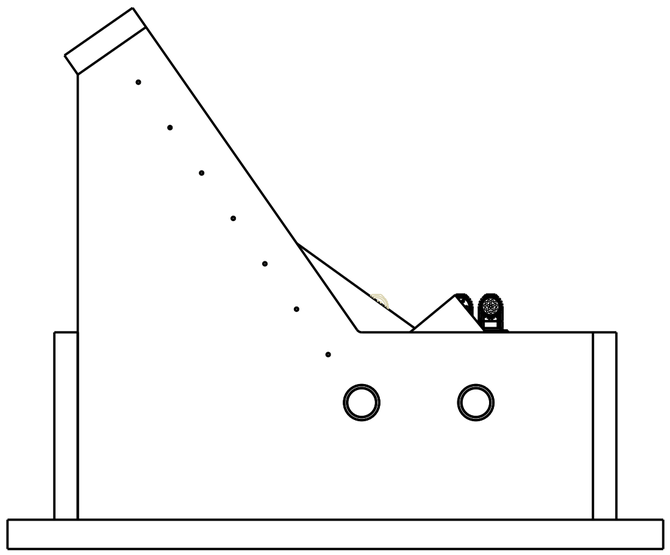

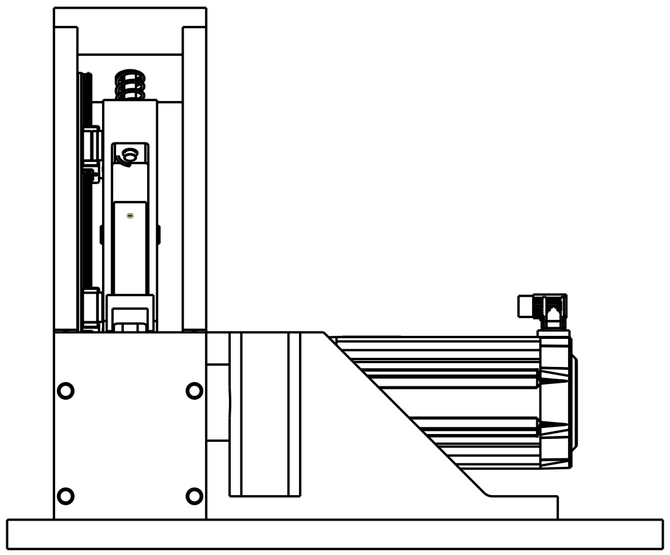

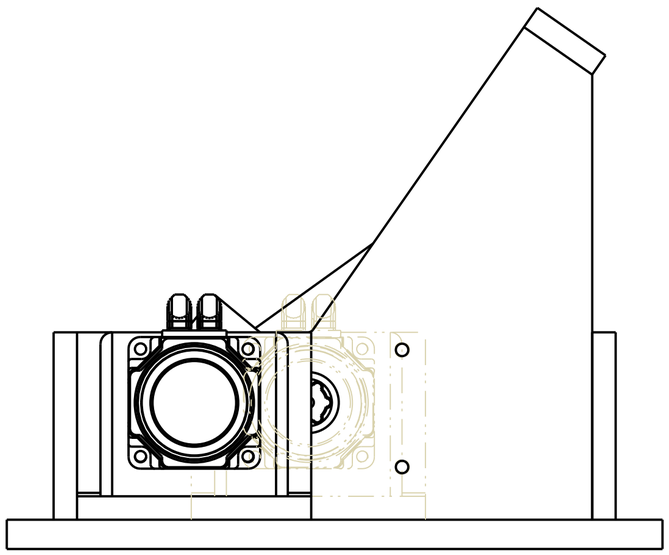

WORCESTER POLYTECHNIC INSTITUTE			
	TITLE: CSTM FULL ASSEMBLY		
	DRAWING: FA-1		
	MODEL: CSTM		
	DRAWN BY: CSTM MQP		
SCALE: 1=5	C	DATE: Jan-12-11	SHEET 1 of 1

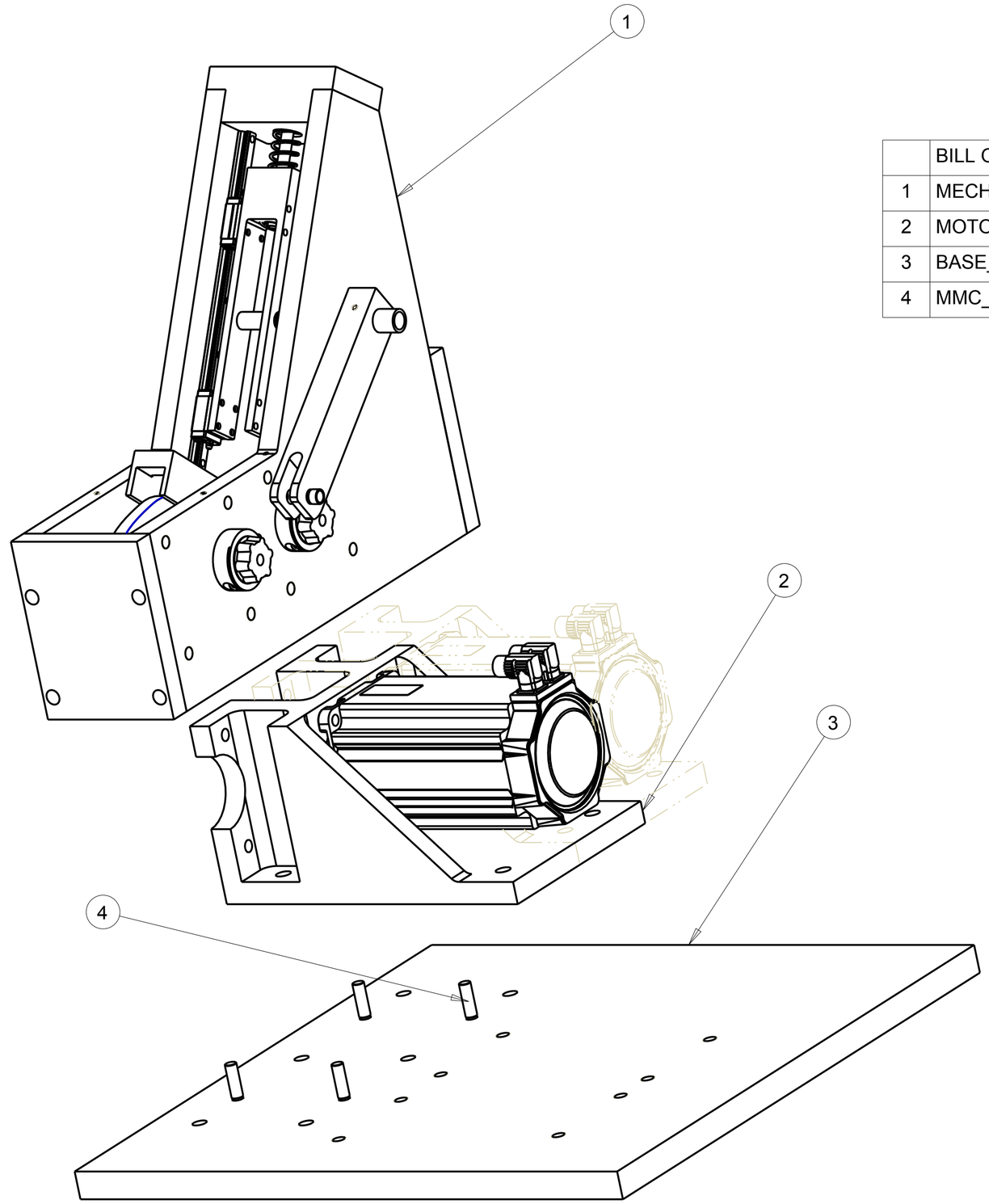

	BILL OF MATERIALS
1	MECHANISM_SIDE
2	MOTOR_SIDE
3	BASE_PLATE
4	MMC_DOWEL_PIN_98381A716

WORCESTER POLYTECHNIC INSTITUTE			
	TITLE: CSTM_EXPLODE		
	DRAWING: FA-2		
	MODEL: CSTM		
	DRAWN BY: CSTM MQP		
SCALE: 1=4	C	DATE: Jan-12-11	SHEET 1 of 1

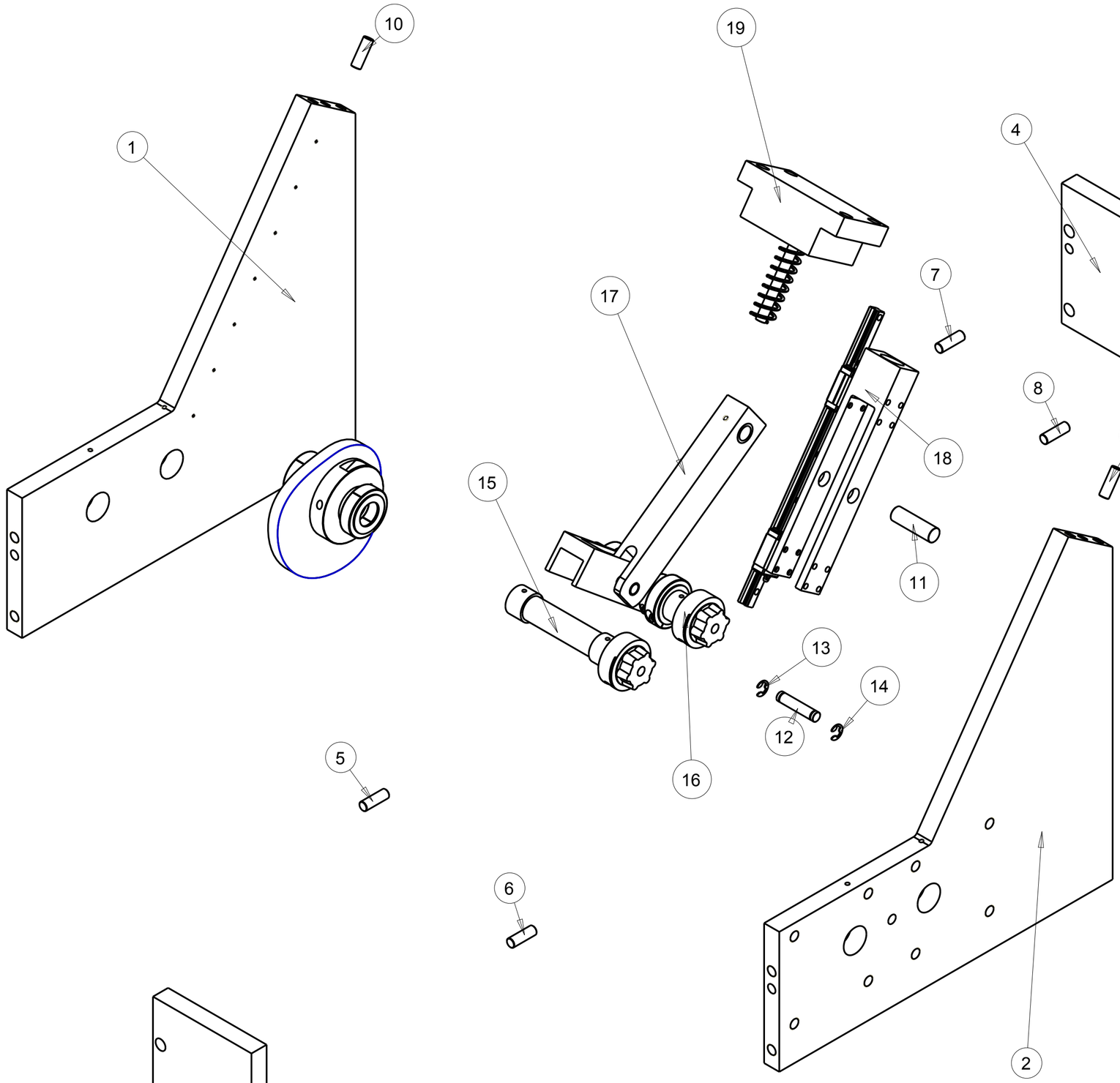

	BILL OF MATERIALS
1	SIDE_SUPPORT_NOMOTOR
2	SIDE_SUPPORT_MOTOR
3	SUPPORT_PLATE
4	SUPPORT_PLATE
5	MMC_DOWEL_PIN_98381A716
6	MMC_DOWEL_PIN_98381A716
7	MMC_DOWEL_PIN_98381A716
8	MMC_DOWEL_PIN_98381A716
9	MMC_DOWEL_PIN_98381A716
10	MMC_DOWEL_PIN_98381A716
11	MMC_PIN_98381A845
12	MMC_PIN_93890A636
13	MMC_RETAINING_RING_98408A138
14	MMC_RETAINING_RING_98408A138
15	CAM_SHAFT_ASSY
16	CRANK_SHAFT_ASSY
17	CON_ROD_ASSY
18	THK_HSR_15R_ASSY
19	SPRING_PLATE_ASSY

WORCESTER POLYTECHNIC INSTITUTE			
	TITLE: MECHANISM SIDE		
	DRAWING: FA-3		
	MODEL: MECHANISM_SIDE		
	DRAWN BY: CSTM MQP		
SCALE: 1=4	C	DATE: Jan-12-11	SHEET 1 of 1

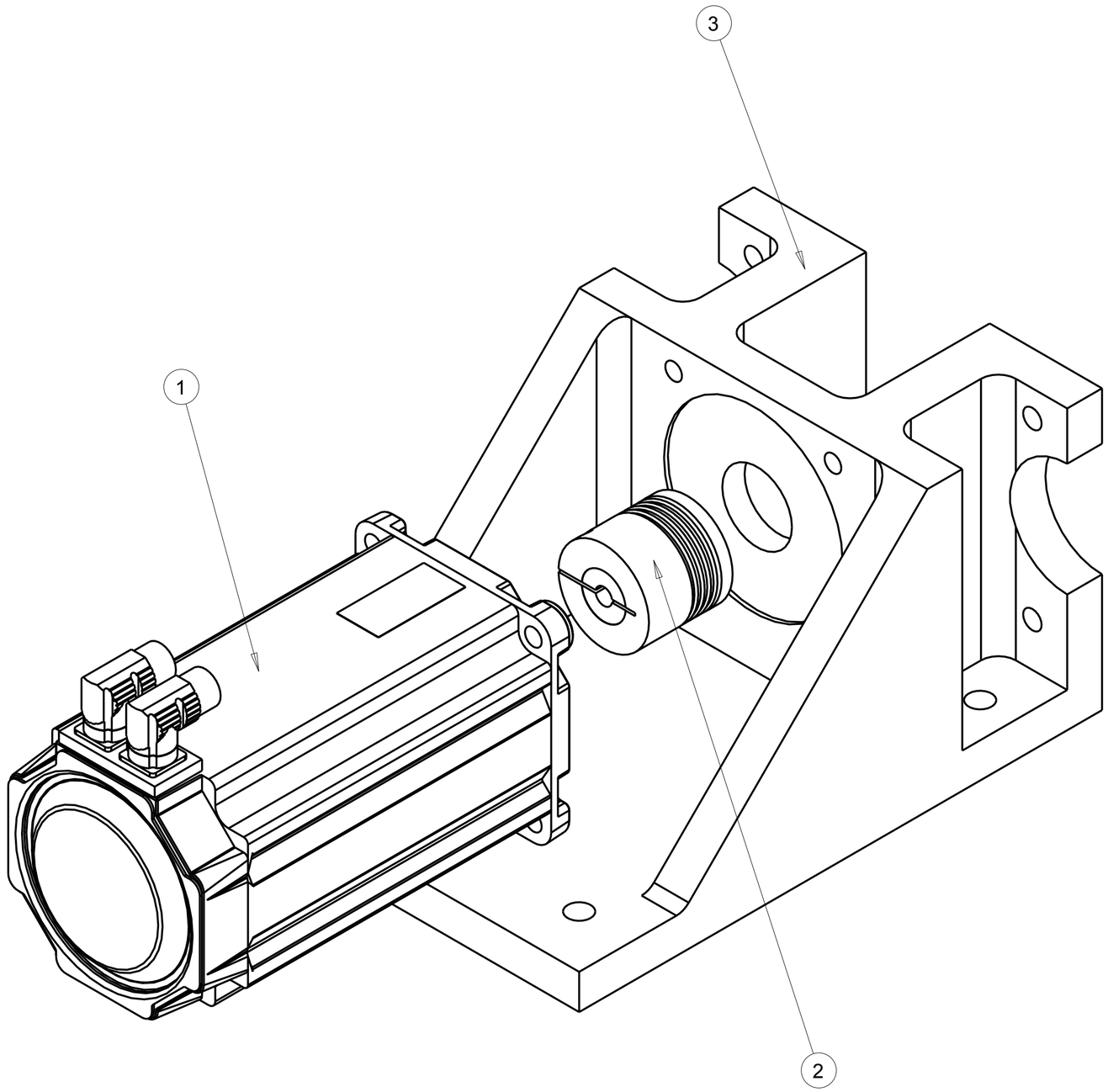

	BILL OF MATERIALS
1	PARKER_SERVOMOTOR_MPJ_1424B
2	RW_AMERICA_BK5-60-85-BALG
3	MOTOR_MOUNT

WORCESTER POLYTECHNIC INSTITUTE			
	TITLE: MOTOR SIDE		
	DRAWING: FA-4		
	MODEL: MOTOR_SIDE		
	DRAWN BY: CSTM MQP		
SCALE: 1=2	C	DATE: Jan-12-11	SHEET 1 of 1

	BILL OF MATERIALS
1	RW_AMERICA_BK5-60-STECK
2	MMC_SLEEVE_BEARING_7965K54
3	MMC_THRUST_BEARING_7447K28
4	MMC_SHAFT_COLLAR_9951K130
5	CAM
6	MMC_SHAFT_COLLAR_9951K130
7	MMC_THRUST_BEARING_7447K28
8	MAIN_SHAFT
9	MMC_SLEEVE_BEARING_7965K54

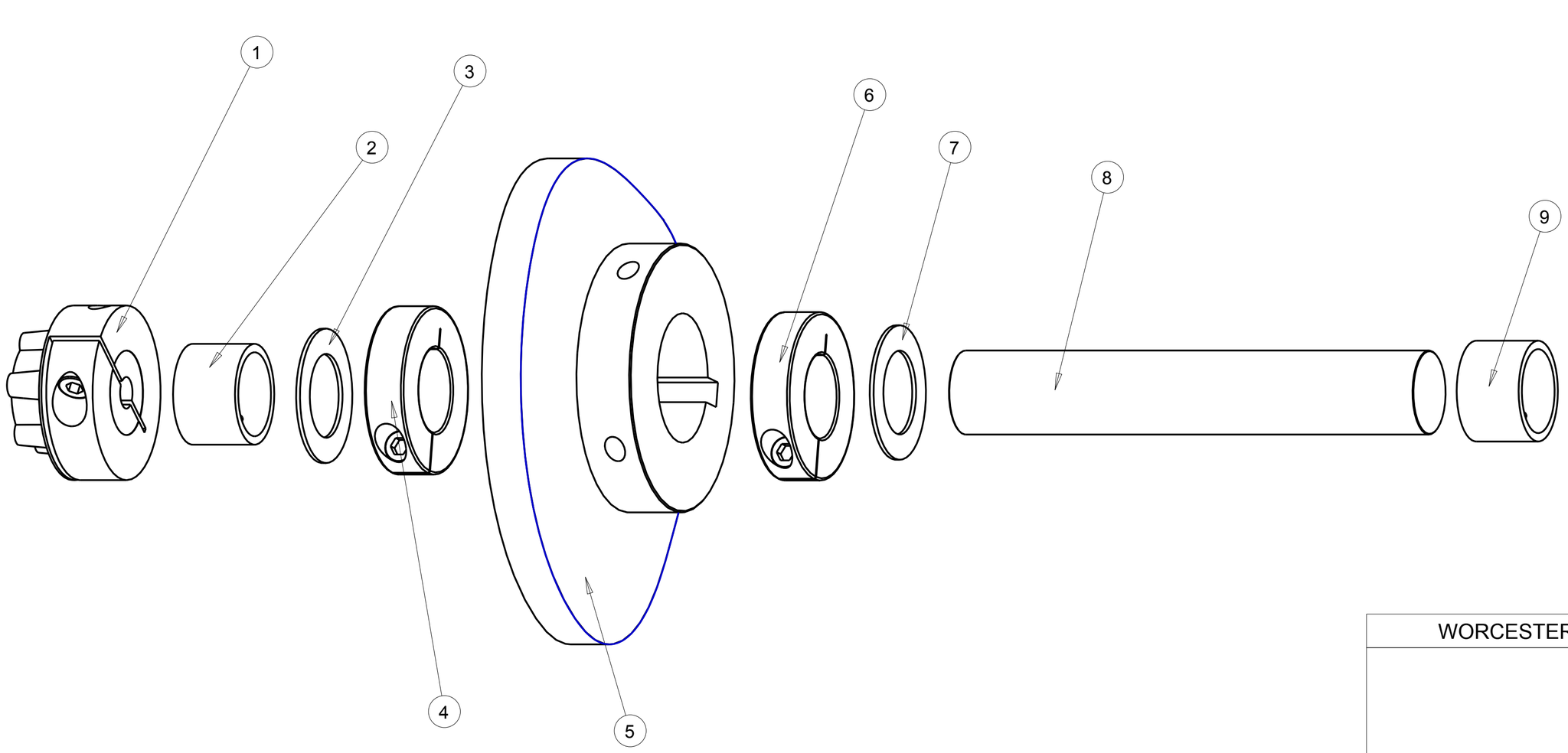

WORCESTER POLYTECHNIC INSTITUTE			
	TITLE: CAM SHAFT ASSY		
	DRAWING: FA-5		
	MODEL: CAM_SHAFT_ASSY		
	DRAWN BY: CSTM MQP		
SCALE: 3=4	C	DATE: Jan-12-11	SHEET 1 of 1

	BILL OF MATERIALS
1	MMC_SLEEVE_BEARING_7965K54
2	MMC_THRUST_BEARING_7447K28
3	MMC_SHAFT_COLLAR_9951K130
4	MMC_SHAFT_COLLAR_9677T400
5	MMC_TRACK_ROLLER_3402K21
6	CRANK
7	MMC_SHAFT_COLLAR_9677T400
8	MAIN_SHAFT
9	MMC_SHAFT_COLLAR_9951K130
10	MMC_THRUST_BEARING_7447K28
11	MMC_SLEEVE_BEARING_7965K54
12	RW_AMERICA_BK5-60-STECK

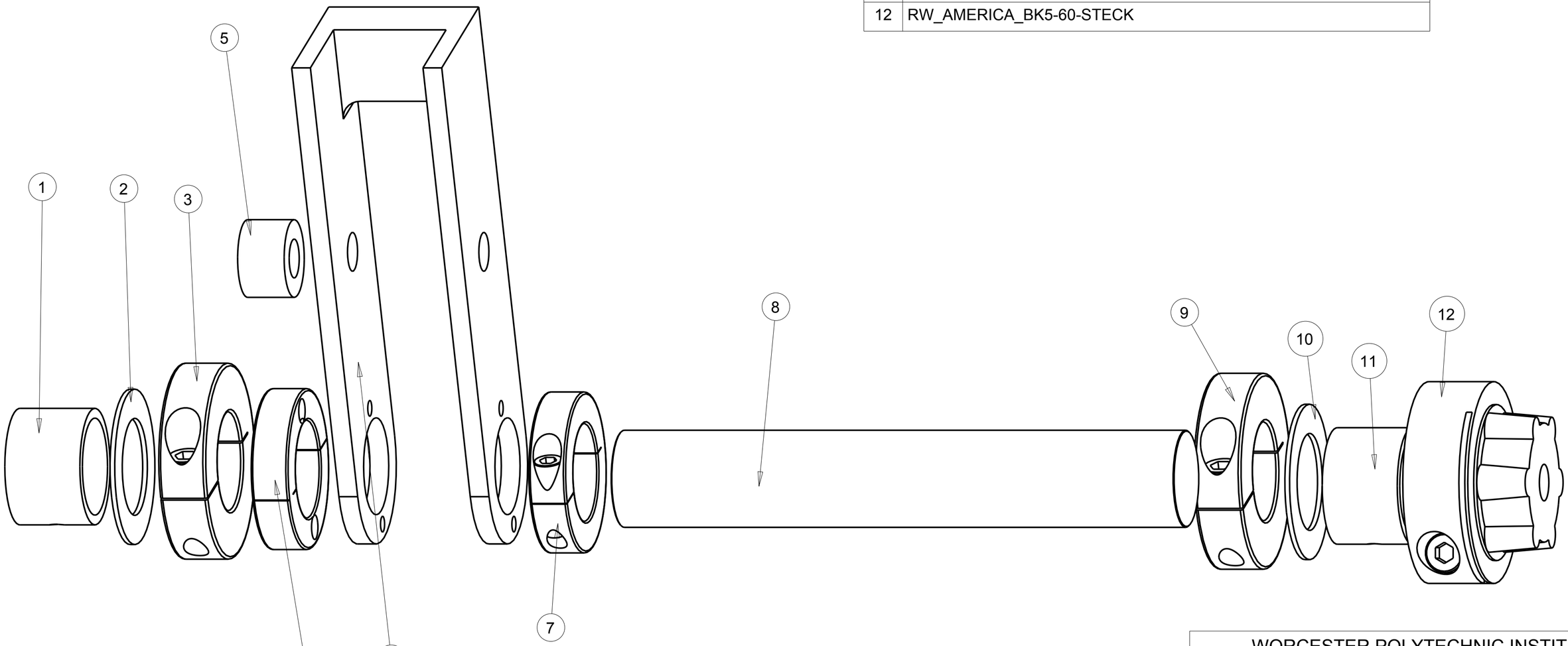

WORCESTER POLYTECHNIC INSTITUTE			
	TITLE: CRANK SHAFT ASSY		
	DRAWING: FA-6		
	MODEL: CRANK_SHAFT_ASSY		
	DRAWN BY: CSTM MQP		
SCALE: 1=1	C	DATE: Jan-12-11	SHEET 1 of 1

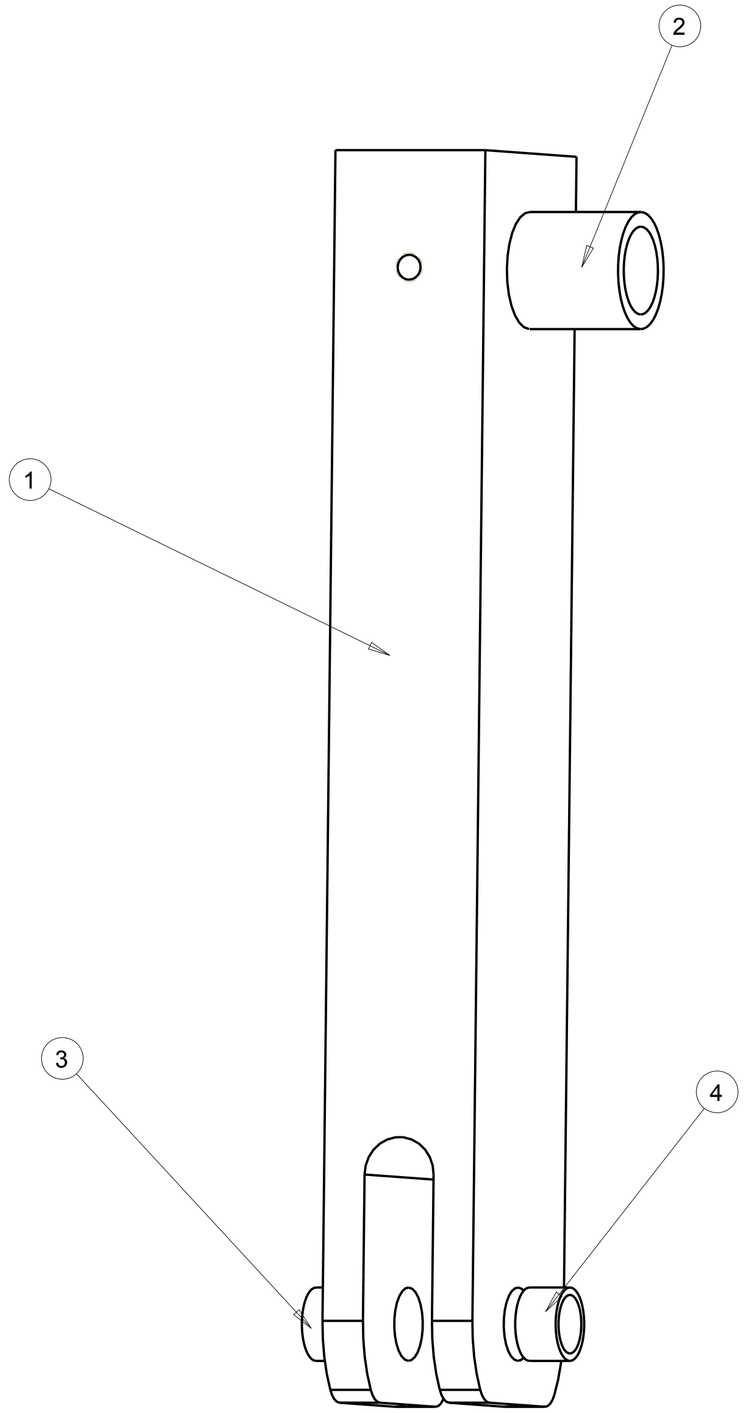

	BILL OF MATERIALS
1	CON_ROD
2	MMC_SLEEVE_BEARING_2924T53
3	MMC_SLEEVE_BEARING_5445K7
4	MMC_SLEEVE_BEARING_5445K7

WORCESTER POLYTECHNIC INSTITUTE			
	TITLE: CON ROD ASSY		
	DRAWING: FA-7		
	MODEL: CON_ROD_ASSY		
	DRAWN BY: CSTM MQP		
SCALE: 1=1	C	DATE: Jan-12-11	SHEET 1 of 1

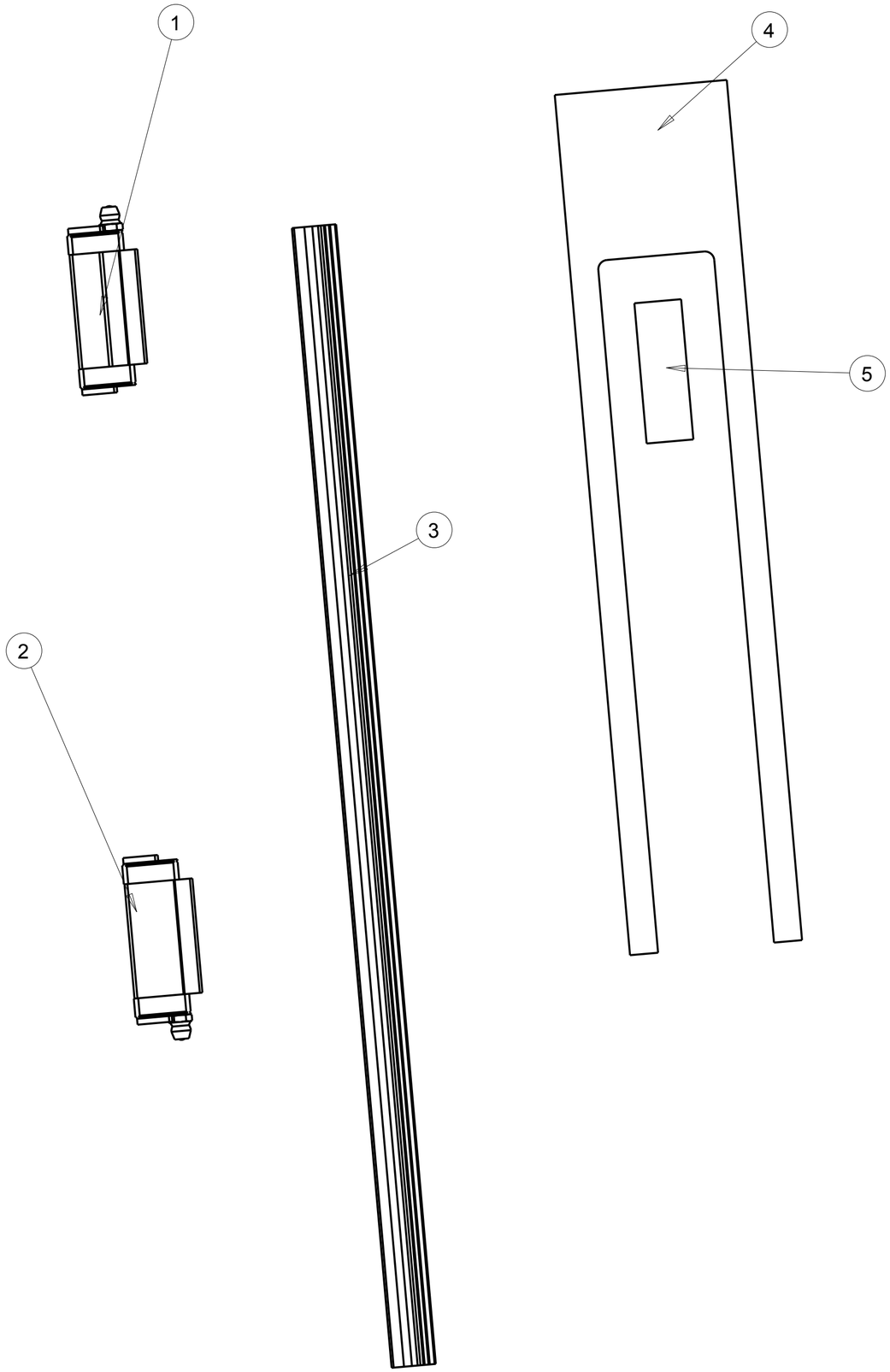

	BILL OF MATERIALS
1	THK_CAR_HSR_15R
2	THK_CAR_HSR_15R
3	THK_RAIL_HSR_15R
4	SPRING_BLOCK
5	MMC_SLEEVE_BEARING_2868T112

NOTE:
SEE MMC_SLEEVE_BEARING_2868T112 PART DRAWING

WORCESTER POLYTECHNIC INSTITUTE			
	THK HSR-15R ASSY		
	DRAWING: FA-8		
	MODEL: THK_HSR_15R_ASSY		
	DRAWN BY: CSTM MQP		
SCALE: 3=4	C	DATE: Jan-12-11	SHEET 1 of 1

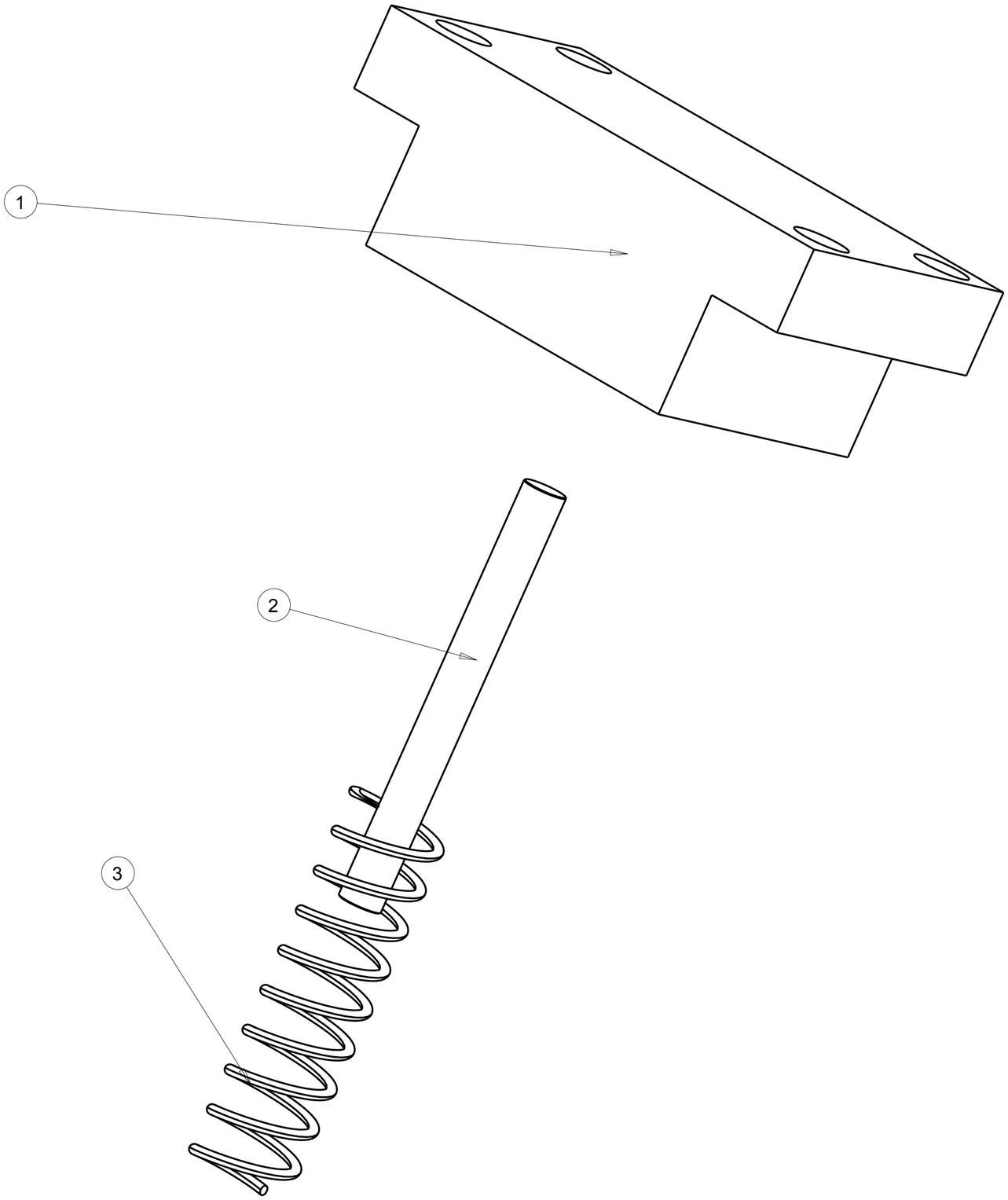

	BILL OF MATERIALS
1	SPRING_PLATE
2	MMC_PIN_98381A734
3	MMC_SPRING_9637K12

WORCESTER POLYTECHNIC INSTITUTE			
	TITLE: SPRING PLATE ASSY		
	DRAWING: FA-9		
	MODEL: SPRING_PLATE_ASSY		
	DRAWN BY: CSTM MQP		
SCALE: 1=1	C	DATE: Jan-12-11	SHEET 1 of 1

BREAK SHARP EDGES AND REMOVE BURRS

QUANTITY: 1

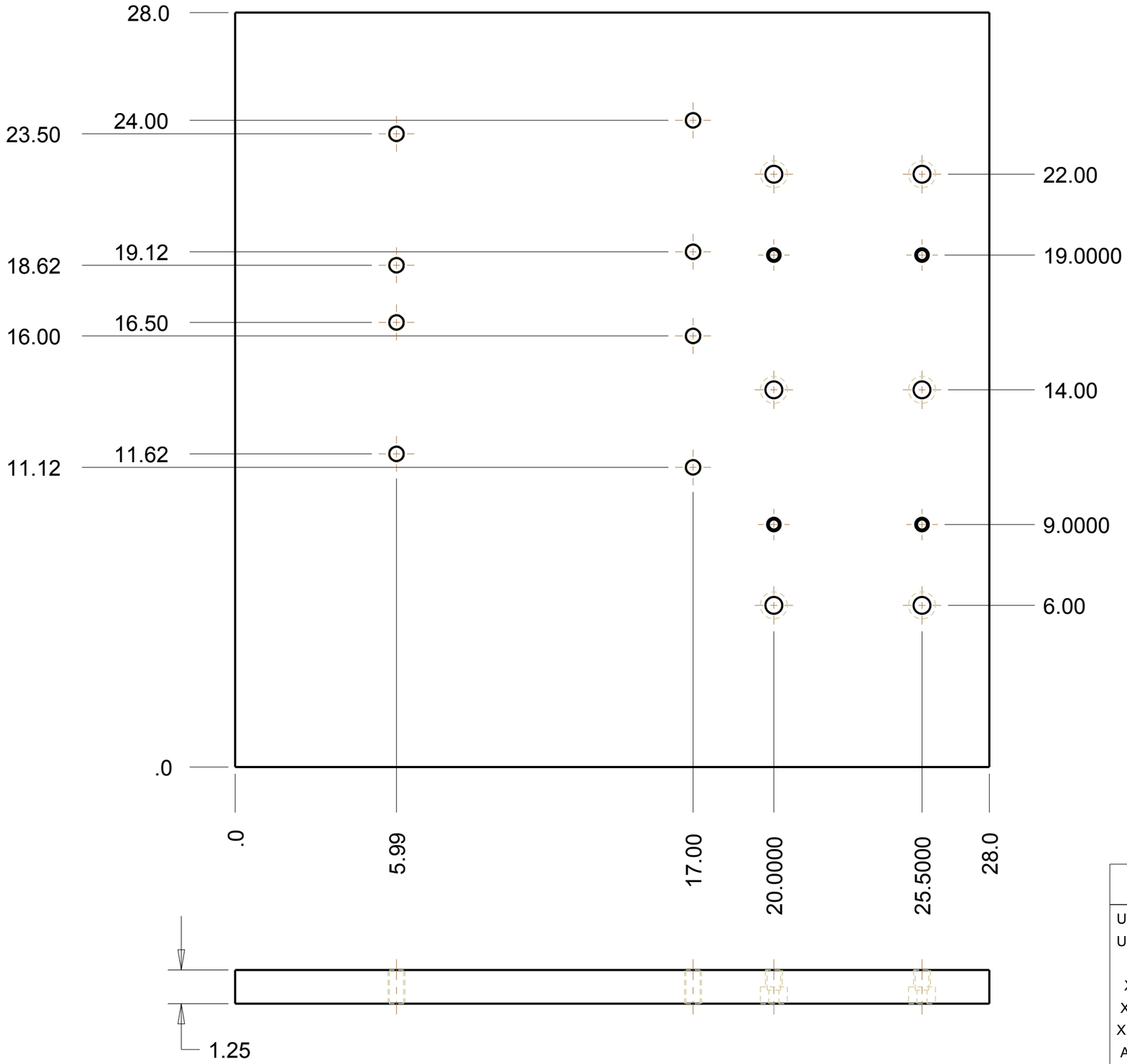

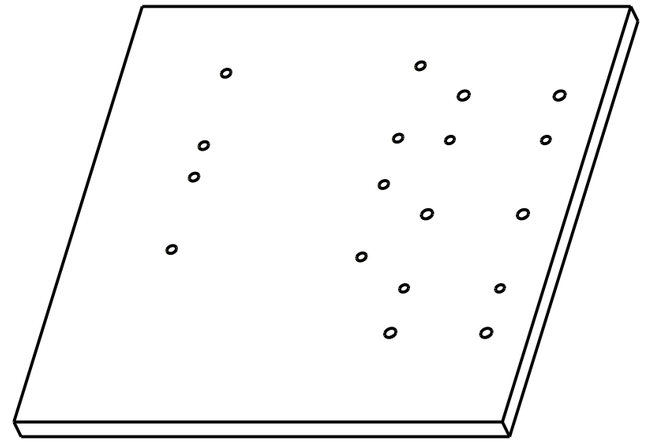

WORCESTER POLYTECHNIC INSTITUTE

UNITS: INCH, DEGREE UNLESS OTHERWISE SPECIFIED, X.X ± 0.1 X.XX ± 0.025 X.XXX ± 0.005 X.XXXX ± 0.0001 ANGLE ± 0.5 °	MATERIAL: ALUMINUM 6061-T6
	DRAWING: F-1
	MODEL: BASE_PLATE
	DRAWN BY: CSTM MQP

SCALE: 1=4	B	DATE: Jan-12-11	SHEET 1 of 2

BREAK SHARP EDGES AND REMOVE BURRS

QUANTITY: 1

TOP

8X 17/32 DRILL (0.531) THRU
5/8-11 UNC - 2B TAP THRU

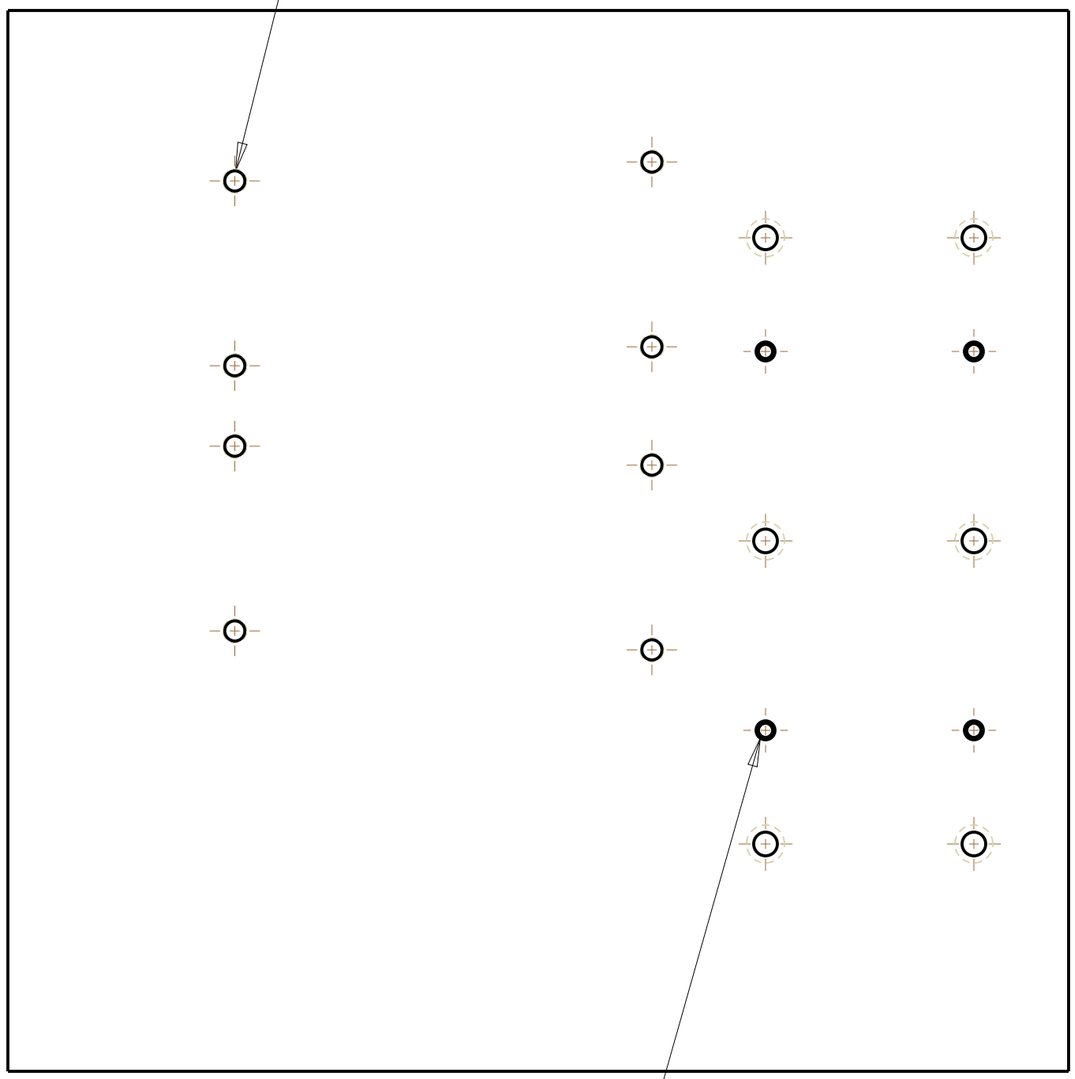

4X 3/8 DRILL (.375) THRU
⌀ 0.4997 REAM ↧ 0.750

BOTTOM

8X 5/8 DRILL (.625) THRU
⌀ 1.0 ↧ 0.625

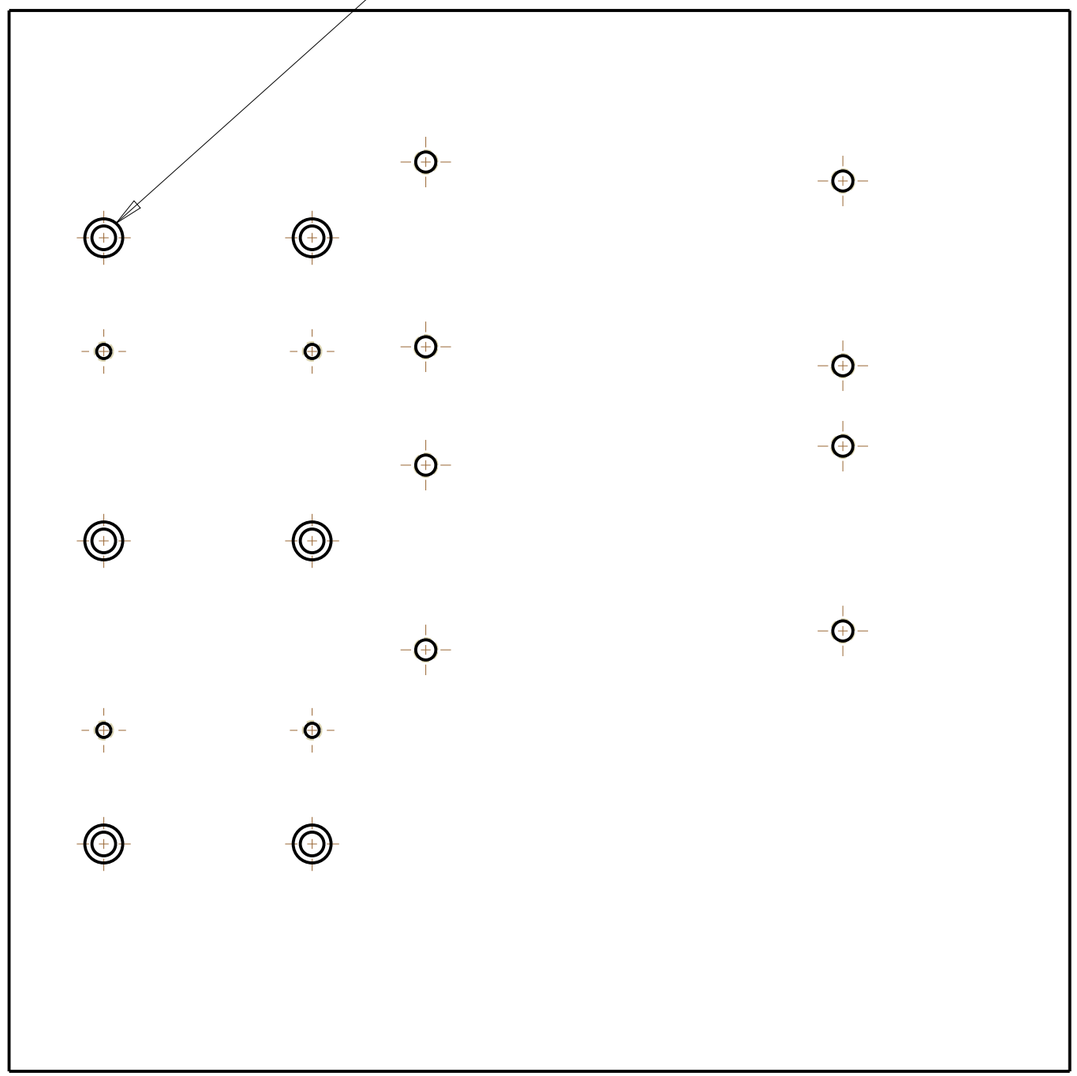

WORCESTER POLYTECHNIC INSTITUTE

UNITS: INCH, DEGREE UNLESS OTHERWISE SPECIFIED, X.X ± 0.1 X.XX ± 0.025 X.XXX ± 0.005 X.XXXX ± 0.0001 ANGLE ± 0.5 °	MATERIAL: ALUMINUM 6061-T6
	DRAWING: F-1
	MODEL: BASE_PLATE
	DRAWN BY: CSTM MQP

SCALE: 1=4	B	DATE: Jan-12-11	SHEET 2 of 2

BREAK SHARP EDGES AND REMOVE BURRS

QUANTITY: 1

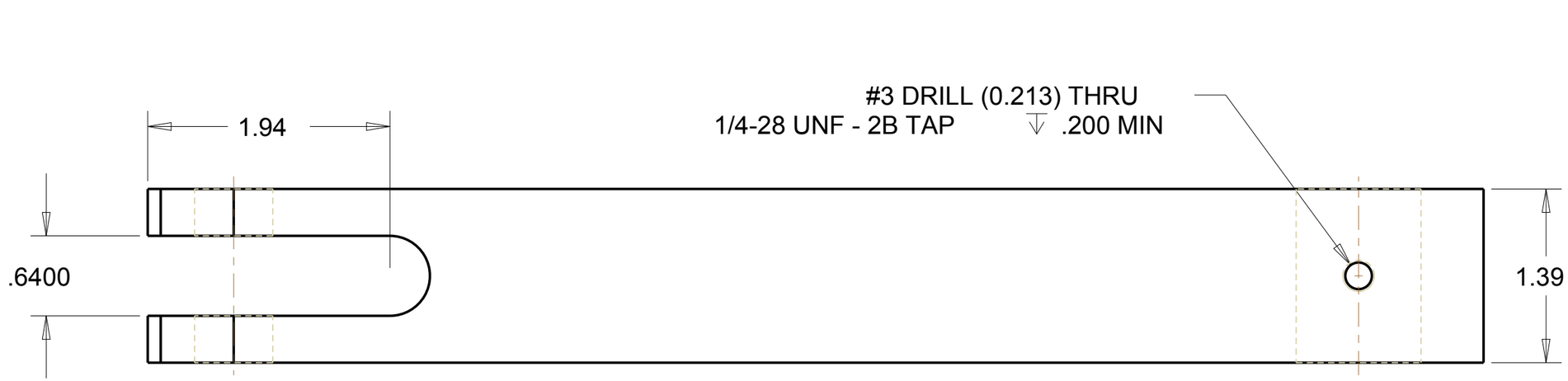

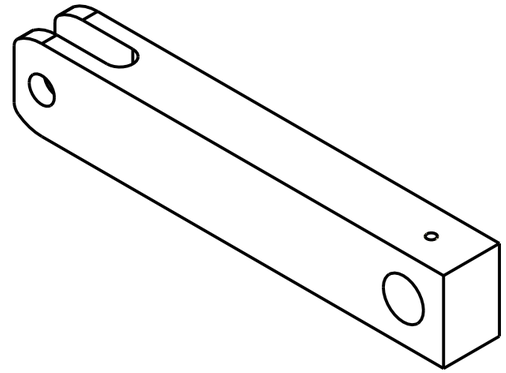

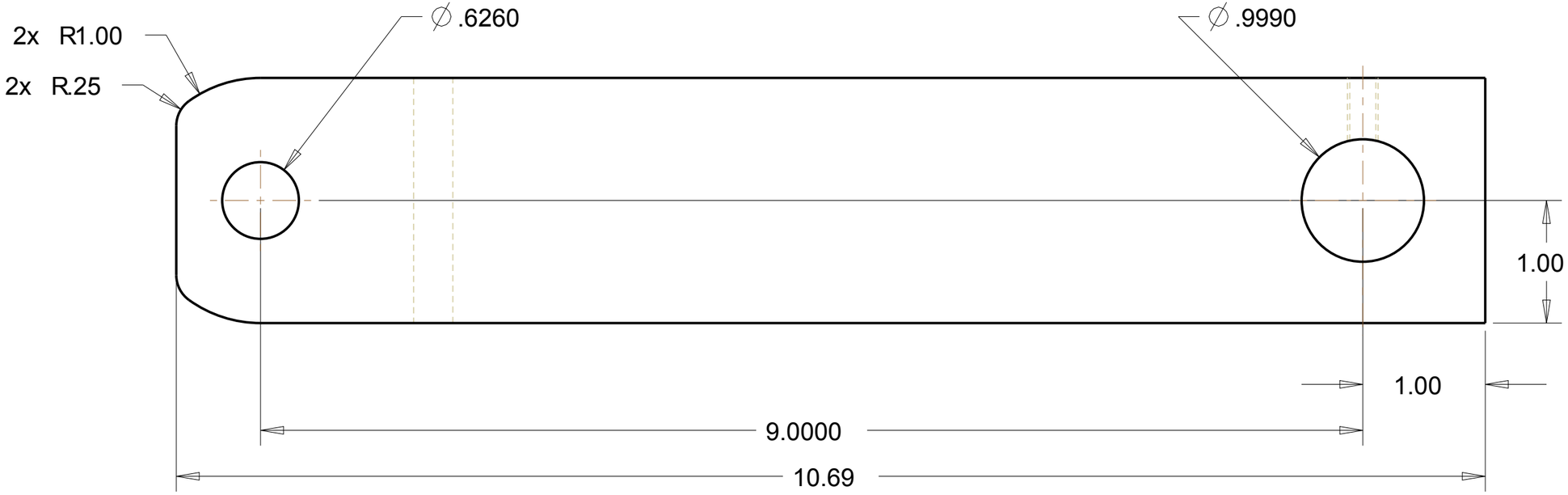

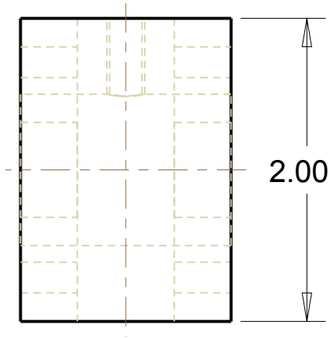

WORCESTER POLYTECHNIC INSTITUTE			
UNITS: INCH, DEGREE UNLESS OTHERWISE SPECIFIED, X.X ± 0.1 X.XX ± 0.025 X.XXX ± 0.005 X.XXXX ± 0.0001 ANGLE ± 0.5 °	MATERIAL: ALUMINUM 6061-T6		
	DRAWING: F-2		
	MODEL: CON_ROD		
	DRAWN BY: CSTM MQP		
SCALE: 1=1	B	DATE: Jan-11-11	SHEET 1 of 1

BREAK SHARP EDGES AND REMOVE BURRS

QUANTITY: 1

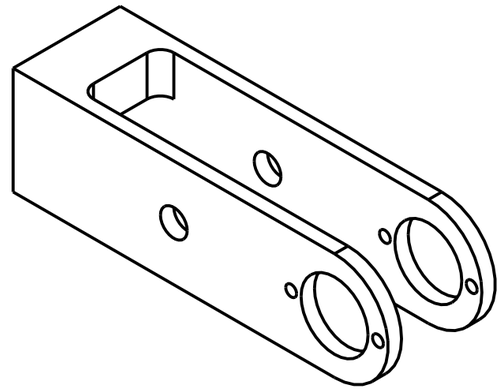

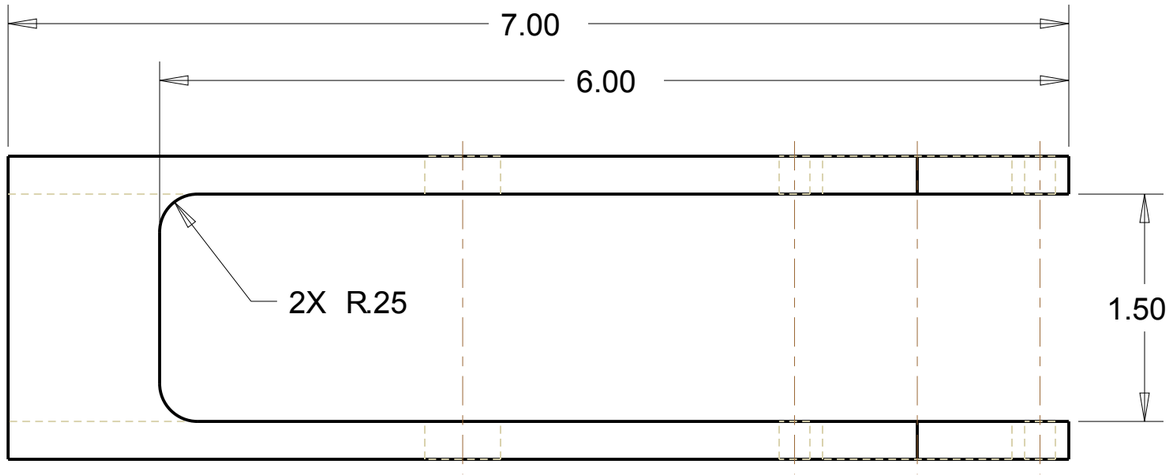

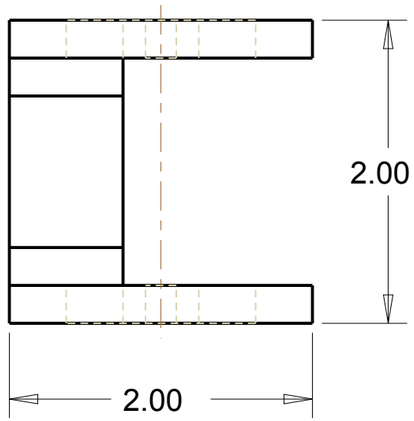

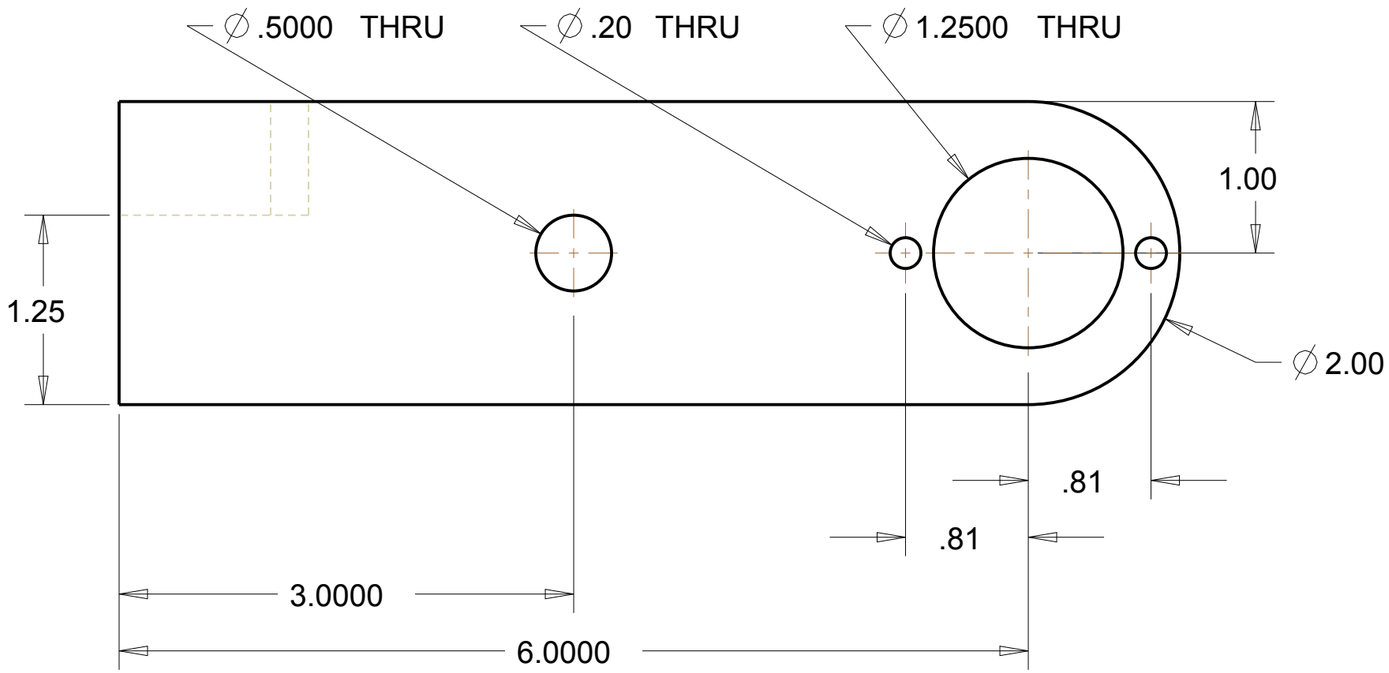

WORCESTER POLYTECHNIC INSTITUTE			
UNITS: INCH, DEGREE UNLESS OTHERWISE SPECIFIED, X.X ± 0.1 X.XX ± 0.025 X.XXX ± 0.005 X.XXXX ± 0.0001 ANGLE ± 0.5 °		MATERIAL: ALUMINUM 6061-T6	
		DRAWING: F-3	
		MODEL: CRANK	
		DRAWN BY: CSTM MQP	
SCALE: 1=1	B	DATE: Jan-12-11	SHEET 1 of 1

QUANTITY: 2

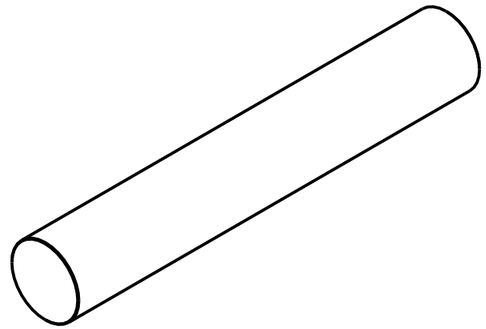

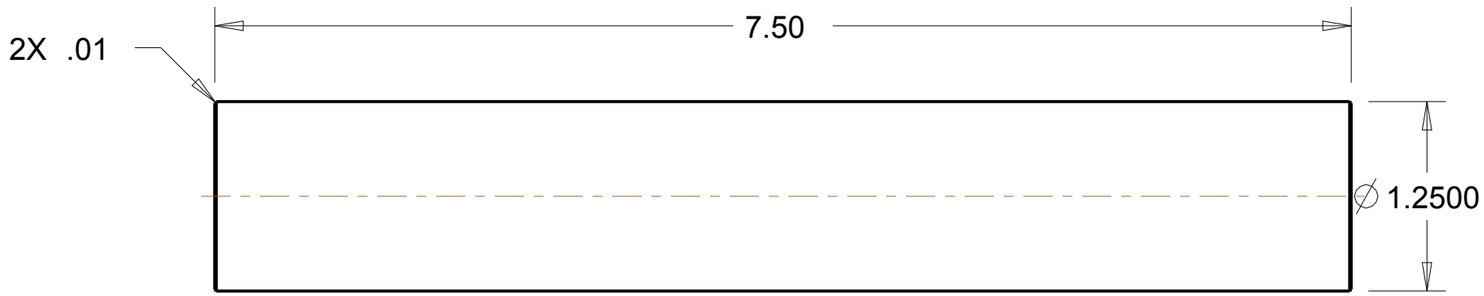

NOTE:
LINE BORE
MMC_SLEEVE_BEARING_7965K54
FOR SHAFT

WORCESTER POLYTECHNIC INSTITUTE			
UNITS: INCH, DEGREE UNLESS OTHERWISE SPECIFIED, X.X ± 0.1 X.XX ± 0.025 X.XXX ± 0.005 X.XXXX ± 0.0001 ANGLE ± 0.5 °	MATERIAL: STEEL		
	DRAWING: F-4		
	MODEL: MAIN_SHAFT		
	DRAWN BY: CSTM MQP		
SCALE: 1=1	B	DATE: Jan-11-11	SHEET 1 of 1

QUANTITY: 1

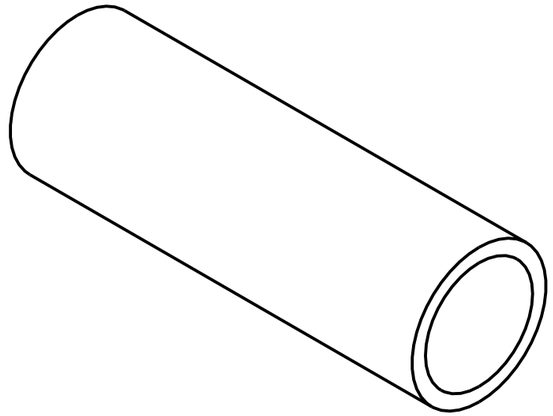

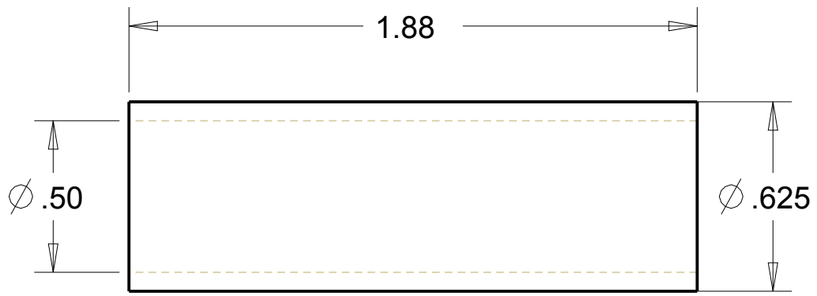

CUT MMC_2868T112 TO DIMENSION LENGTH

WORCESTER POLYTECHNIC INSTITUTE

UNITS: INCH, DEGREE UNLESS OTHERWISE SPECIFIED, X.X ± 0.1 X.XX ± 0.025 X.XXX ± 0.005 X.XXXX ± 0.0001 ANGLE ± 0.5 °	MATERIAL: SAE 863 BRONZE
	DRAWING: F-5
	MODEL: MMC_SLEEVE_BEARING_2868T112
	DRAWN BY: CSTM MQP

SCALE: 2=1	B	DATE: Jan-11-11	SHEET 1 of 1

QUANTITY: 1

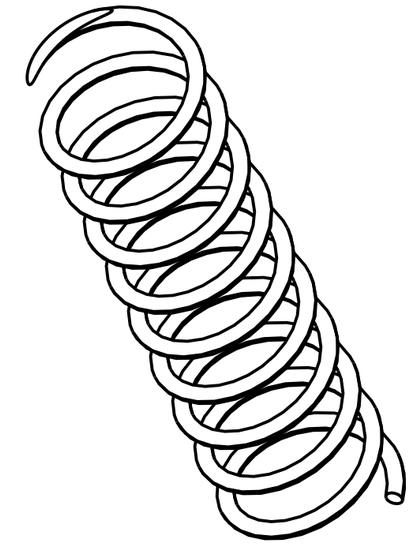

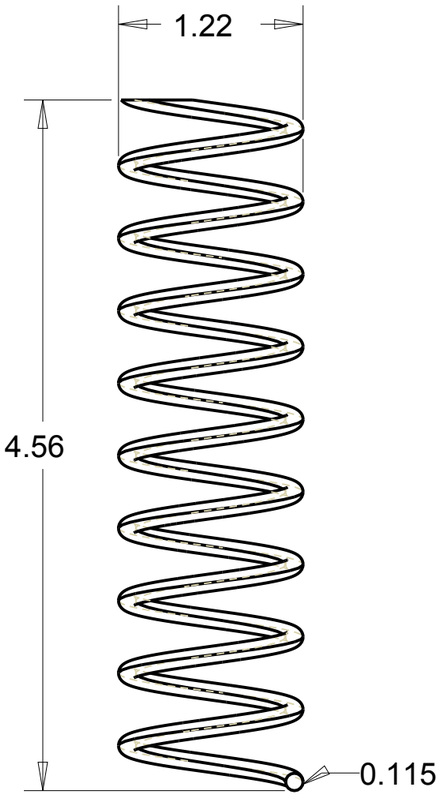

2.09 COILS/INCH

CUT MMC_9637k12 SPRING TO SPECIFIED LENGTH

WORCESTER POLYTECHNIC INSTITUTE			
UNITS: INCH, DEGREE UNLESS OTHERWISE SPECIFIED, X.X ± 0.1 X.XX ± 0.025 X.XXX ± 0.005 X.XXXX ± 0.0001 ANGLE ± 0.5 °		MATERIAL: SPRING STEEL	
		DRAWING: F-6	
		MODEL: MMC_SPRING_9637K12	
		DRAWN BY: CSTM MQP	
SCALE:	B	DATE: Jan-12-11	SHEET 1 of 1

QUANTITY: 1

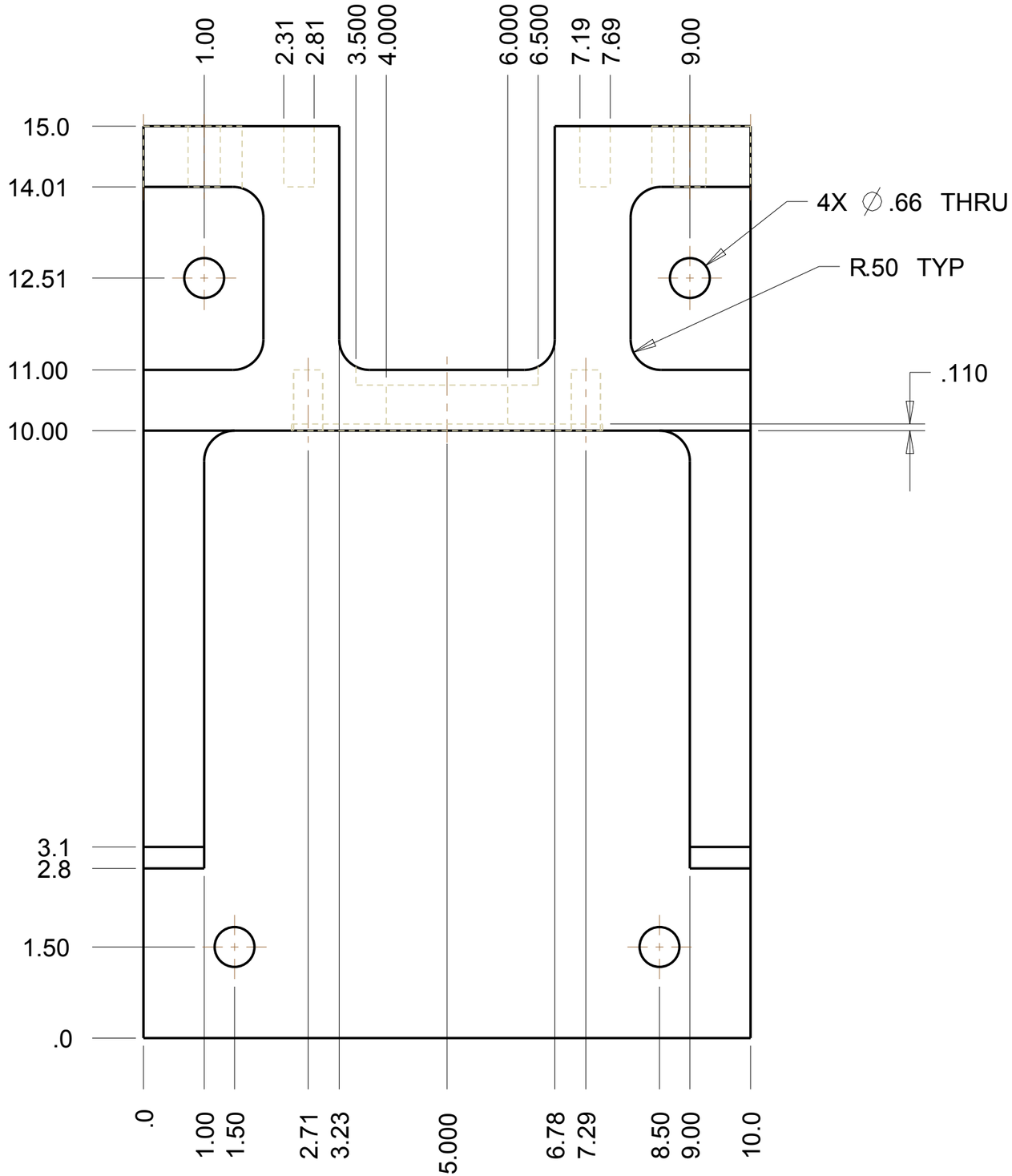

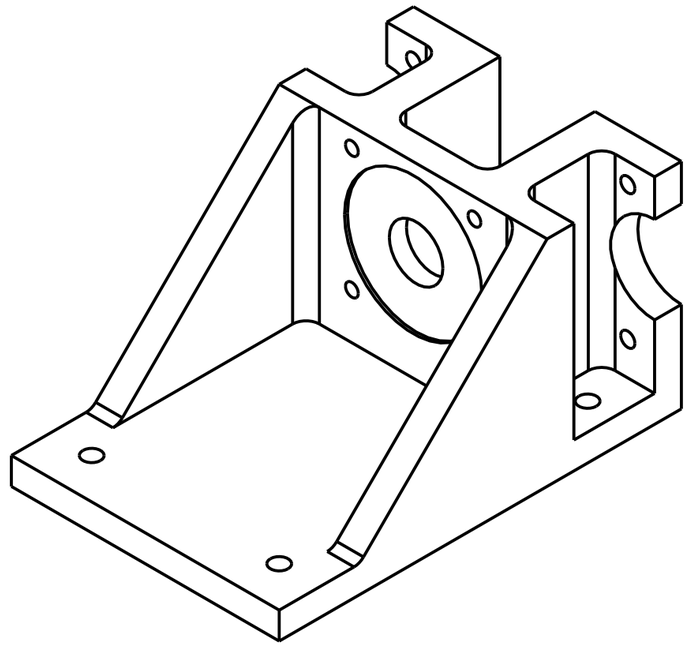

WORCESTER POLYTECHNIC INSTITUTE

UNITS: INCH, DEGREE UNLESS OTHERWISE SPECIFIED, X.X ± 0.1 X.XX ± 0.025 X.XXX ± 0.005 X.XXXX ± 0.0001 ANGLE ± 0.5 °	MATERIAL: ALUMINUM 6061-T6
	DRAWING: F-7
	MODEL: MOTOR_MOUNT
	DRAWN BY: CSTM MQP

SCALE: 1=2	B	DATE: Jan-12-11	SHEET 1 of 2

QUANTITY: 1

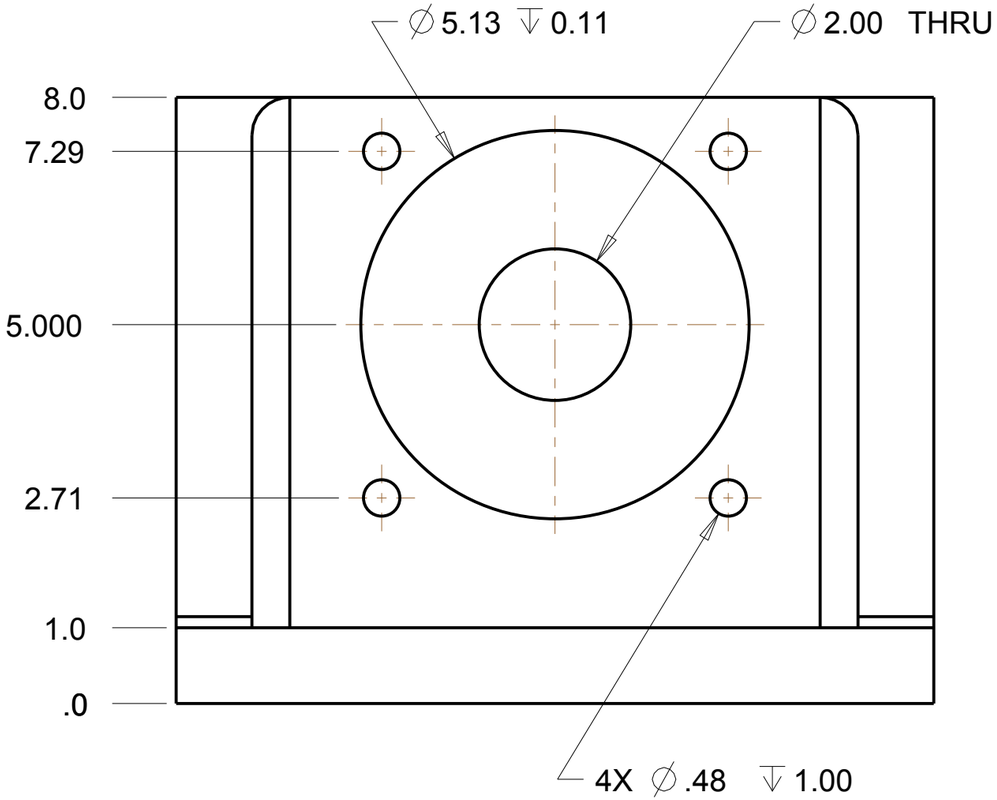

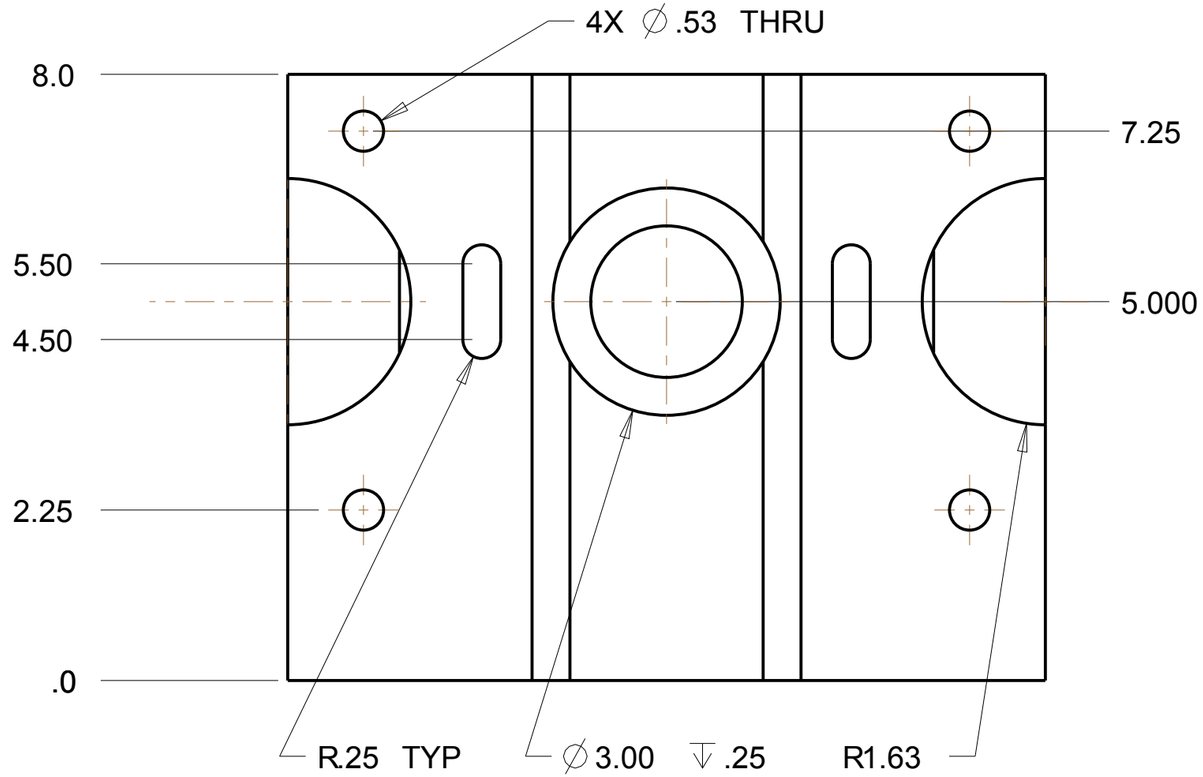

WORCESTER POLYTECHNIC INSTITUTE			
UNITS: INCH, DEGREE UNLESS OTHERWISE SPECIFIED, X.X ± 0.1 X.XX ± 0.025 X.XXX ± 0.005 X.XXXX ± 0.0001 ANGLE ± 0.5 °		MATERIAL: ALUMINUM 6061-T6	
		DRAWING: F-7	
		MODEL: MOTOR_MOUNT	
		DRAWN BY: CSTM MQP	
SCALE: 1=2	B	DATE: Jan-12-11	SHEET 2 of 2

QUANTITY: 1

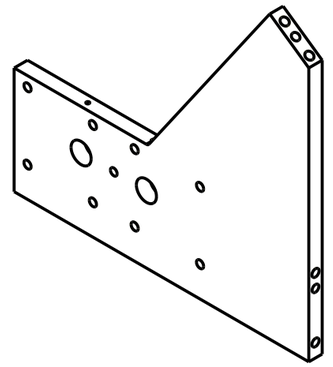

SCALE 0.125

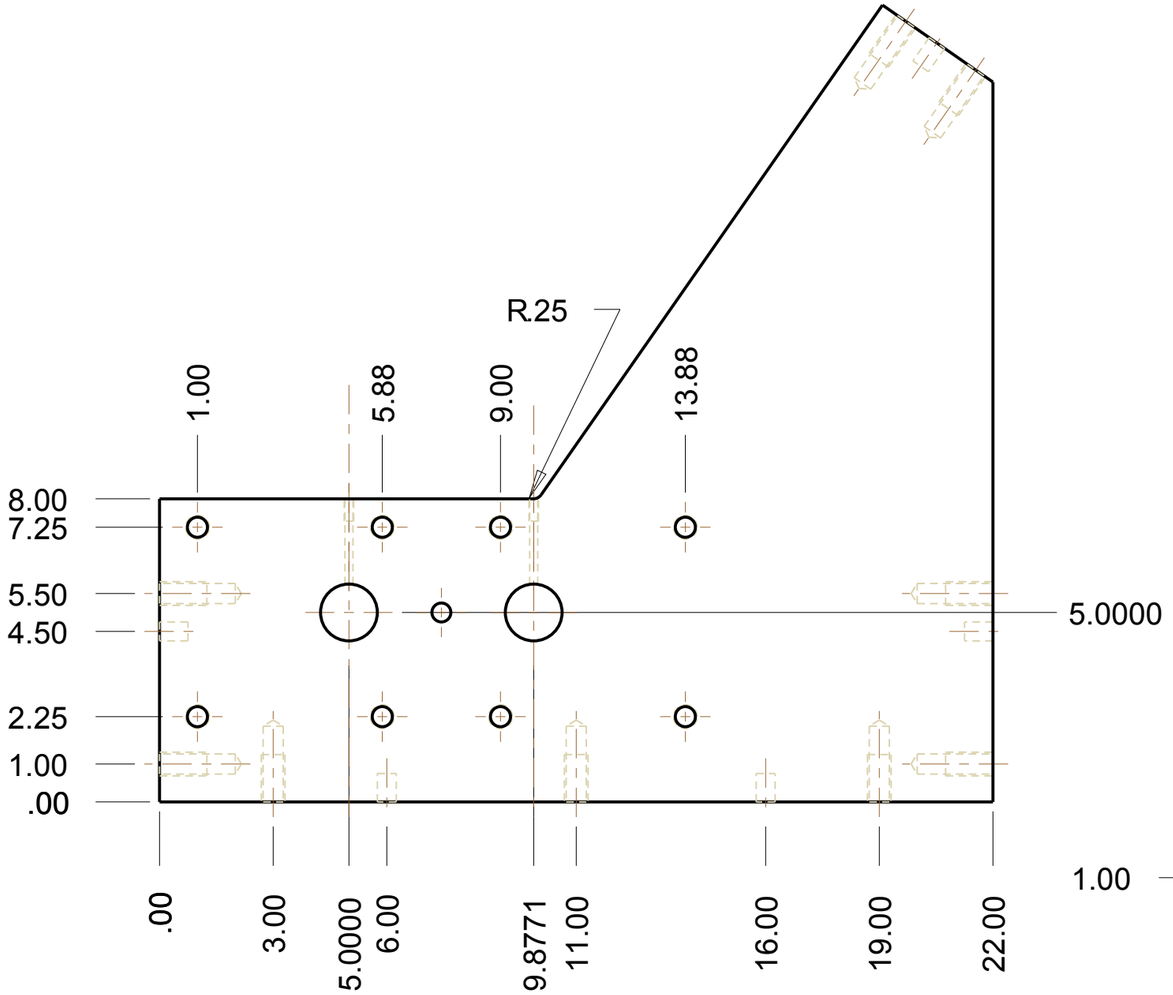

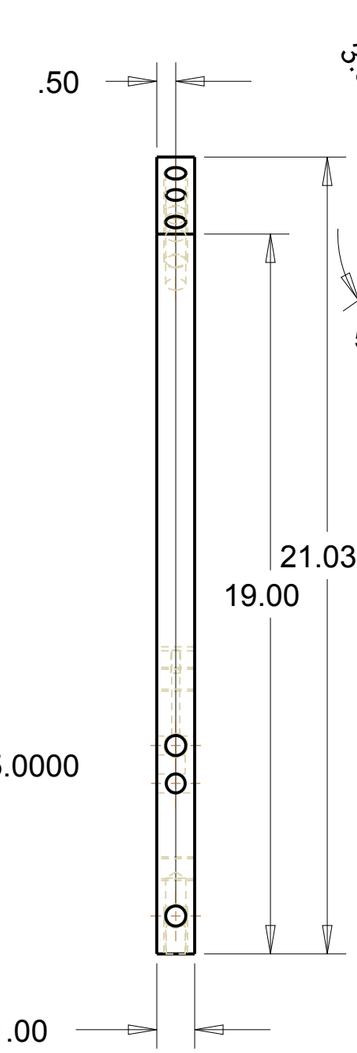

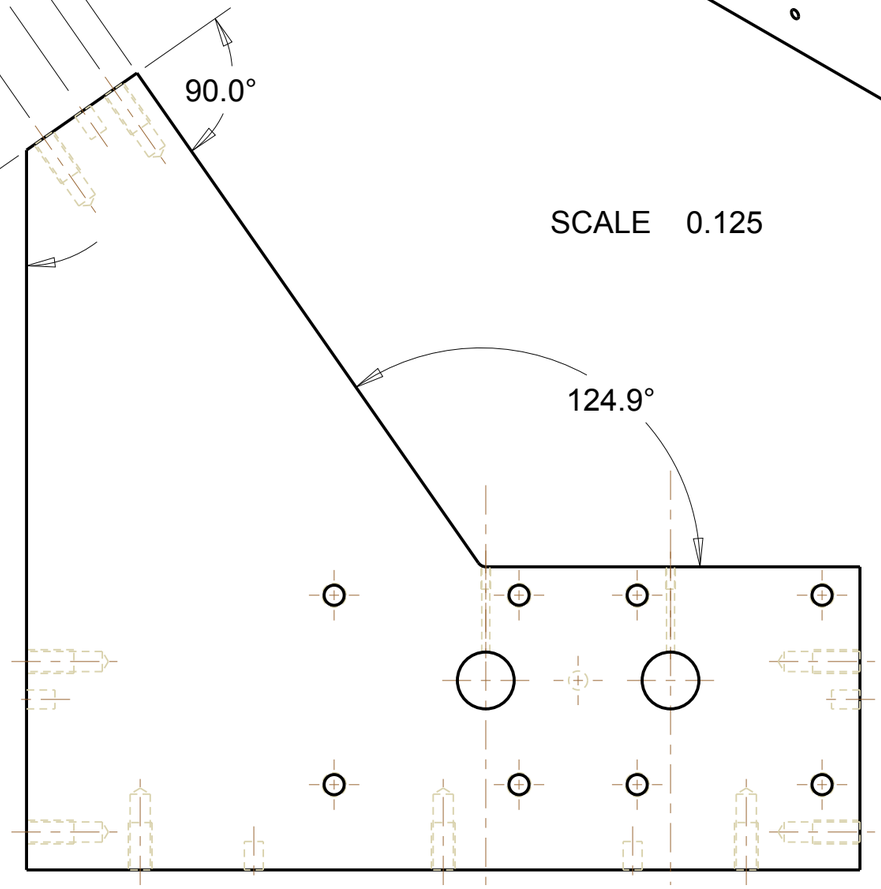

WORCESTER POLYTECHNIC INSTITUTE

UNITS: INCH, DEGREE UNLESS OTHERWISE SPECIFIED, X.X ± 0.1 X.XX ± 0.025 X.XXX ± 0.005 X.XXXX ± 0.0001 ANGLE ± 0.5 °	MATERIAL: ALUMINUM 6061-T6
	DRAWING: F-8
	MODEL: SIDE_SUPPORT_MOTOR
	DRAWN BY: CSTM MQP

SCALE: 1=4	B	DATE: Jan-10-11	SHEET 1 of 2

QUANTITY: 1

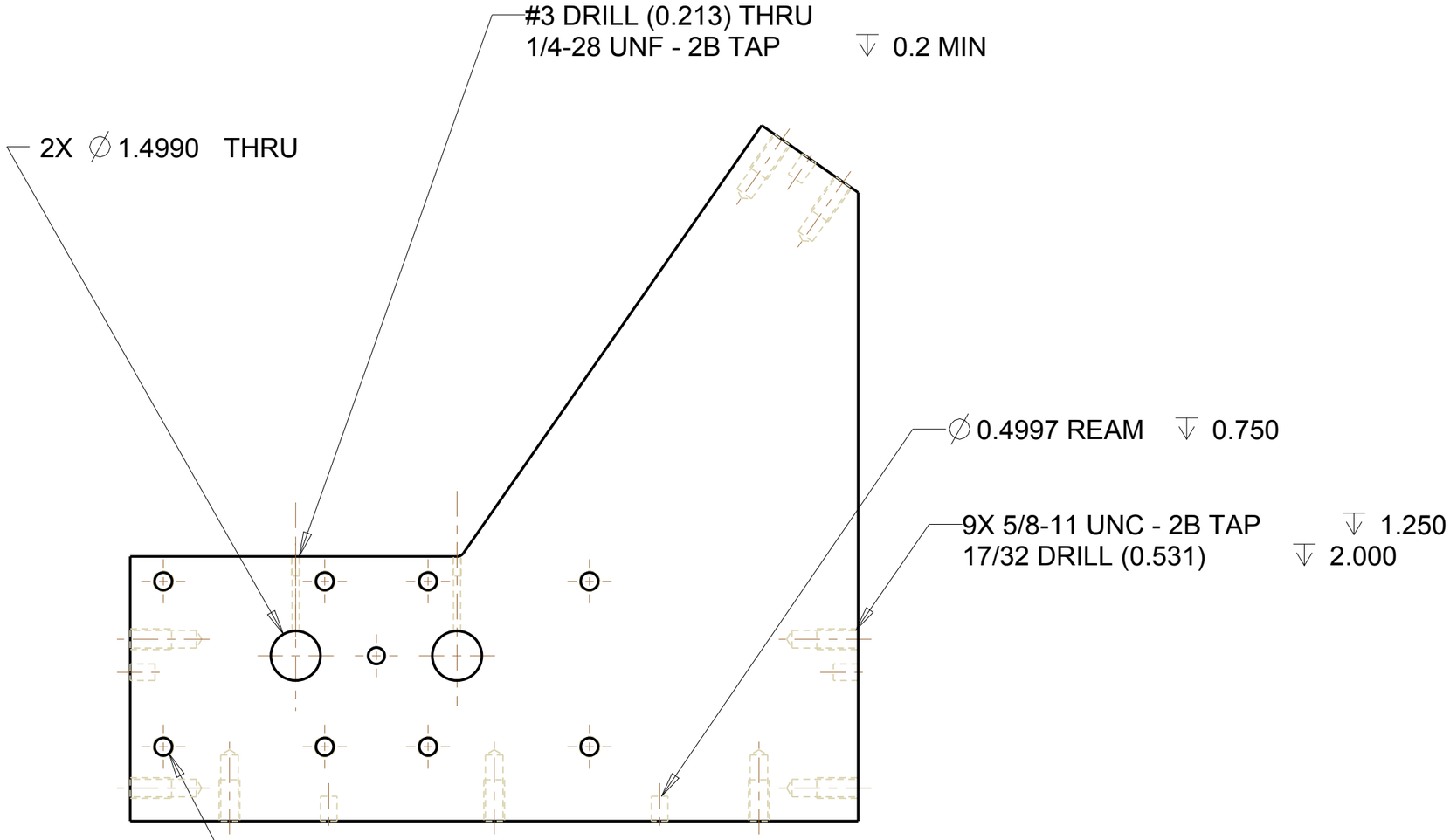

WORCESTER POLYTECHNIC INSTITUTE

UNITS: INCH, DEGREE UNLESS OTHERWISE SPECIFIED, X.X ± 0.1 X.XX ± 0.025 X.XXX ± 0.005 X.XXXX ± 0.0001 ANGLE ± 0.5 °	MATERIAL: ALUMINUM 6061-T6
	DRAWING: F-8
	MODEL: SIDE_SUPPORT_MOTOR
	DRAWN BY: CSTM MQP

SCALE: 1=4	B	DATE: Jan-10-11	SHEET 2 of 2

QUANTITY: 1

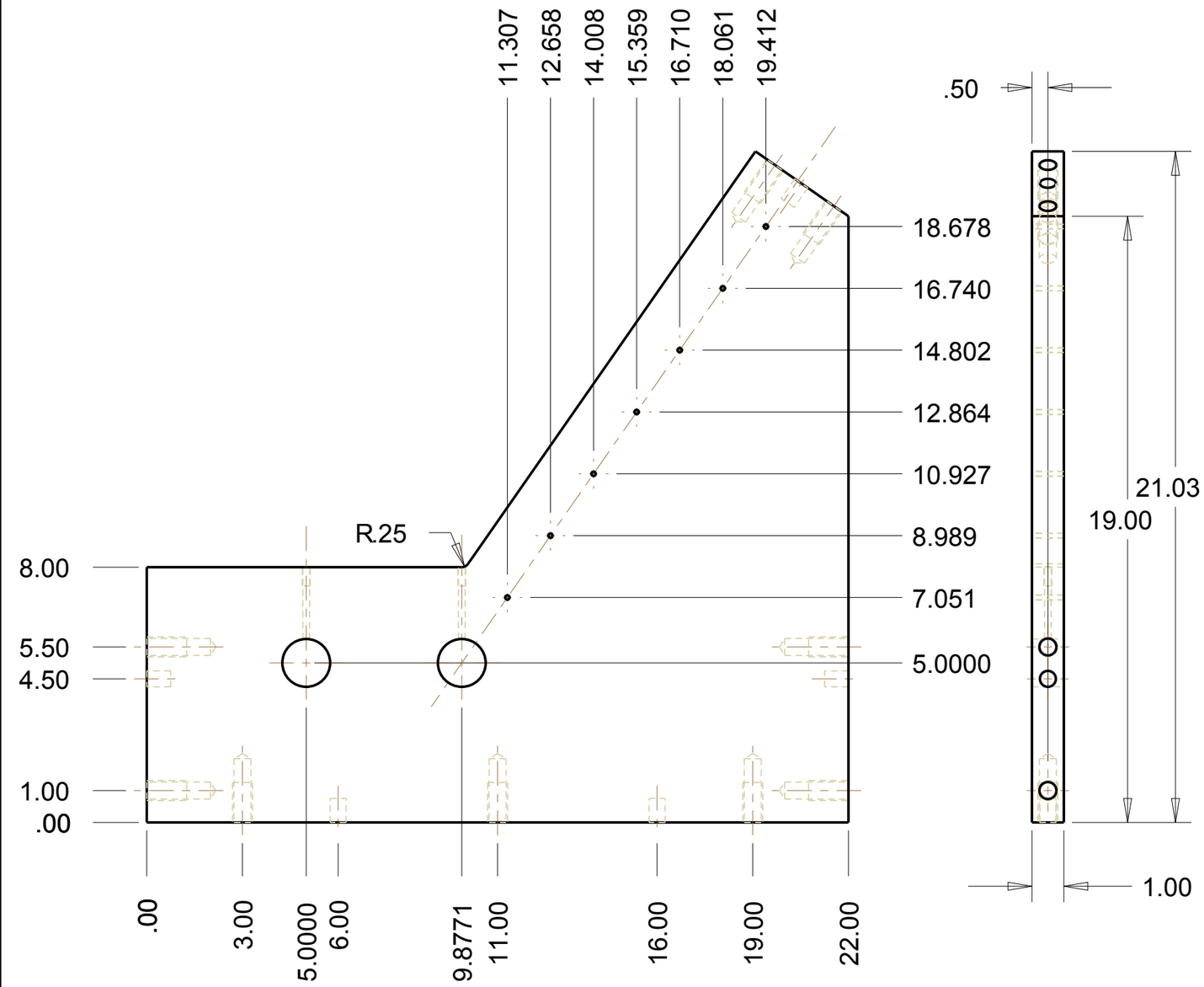

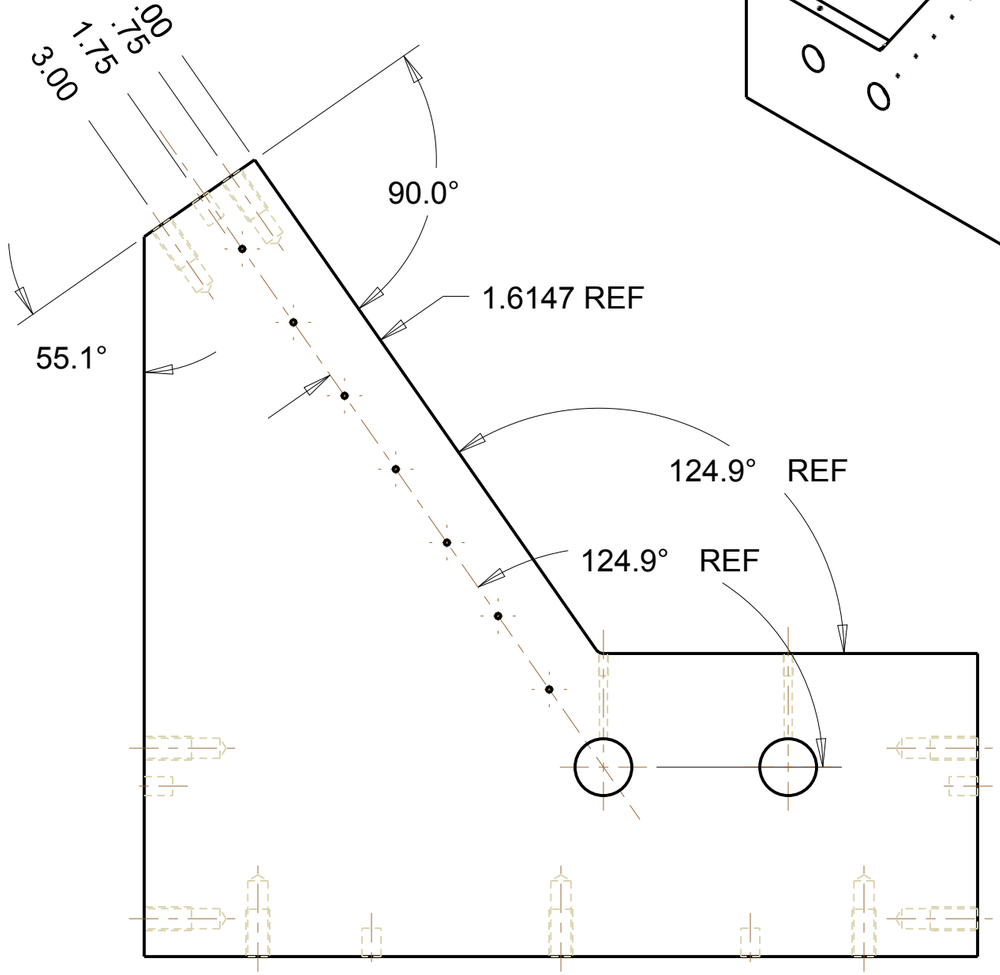

WORCESTER POLYTECHNIC INSTITUTE

UNITS: INCH, DEGREE UNLESS OTHERWISE SPECIFIED, X.X ± 0.1 X.XX ± 0.025 X.XXX ± 0.005 X.XXXX ± 0.0001 ANGLE ± 0.5 °	MATERIAL: ALUMINUM 6061-T6
	DRAWING: F-9
	MODEL: SIDE_SUPPORT_NONMOTO
	DRAWN BY: CSTM MQP

SCALE: 1=4	B	DATE: Jan-10-11	SHEET 1 of 2

QUANTITY: 1

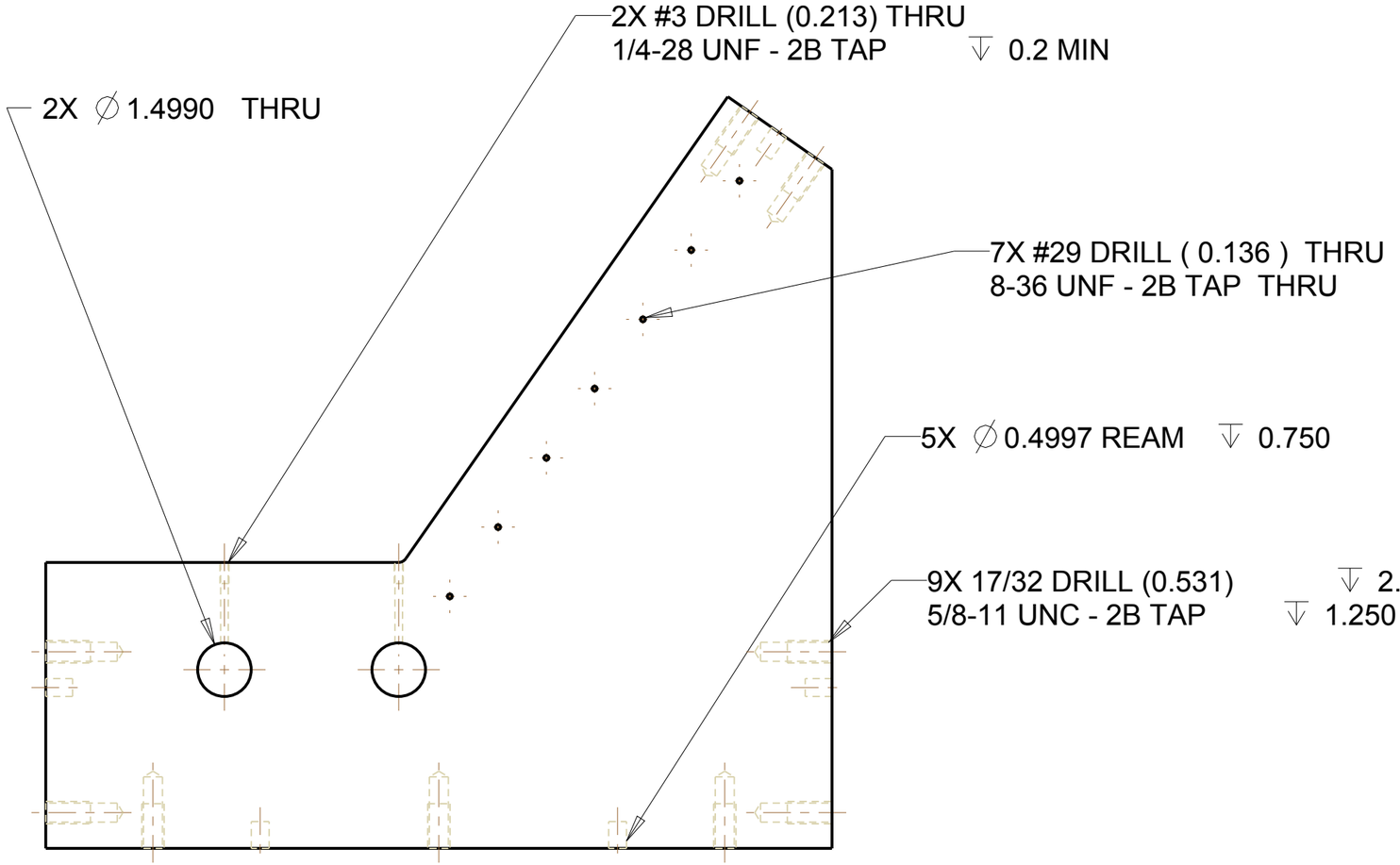

WORCESTER POLYTECHNIC INSTITUTE

UNITS: INCH, DEGREE UNLESS OTHERWISE SPECIFIED, X.X ± 0.1 X.XX ± 0.025 X.XXX ± 0.005 X.XXXX ± 0.0001 ANGLE ± 0.5 °	MATERIAL: ALUMINUM 6061-T6
	DRAWING: F-9
	MODEL: SIDE_SUPPORT_NONMOTO
	DRAWN BY: CSTM MQP

SCALE: 1=4	B	DATE: Jan-10-11	SHEET 2 of 2

QUANTITY: 1

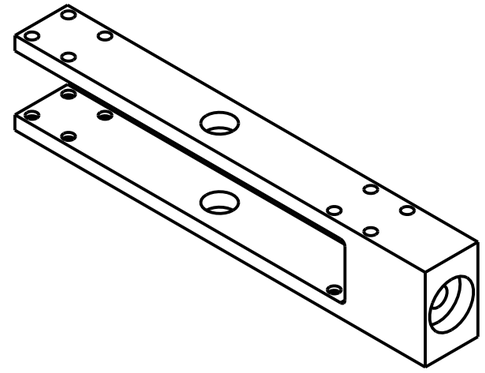

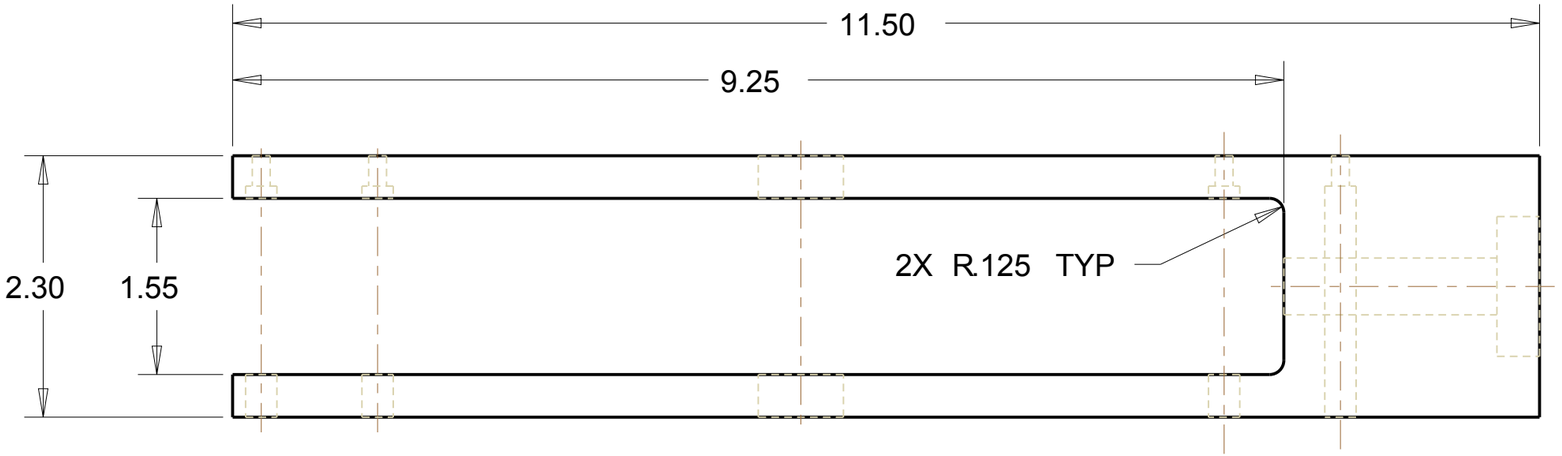

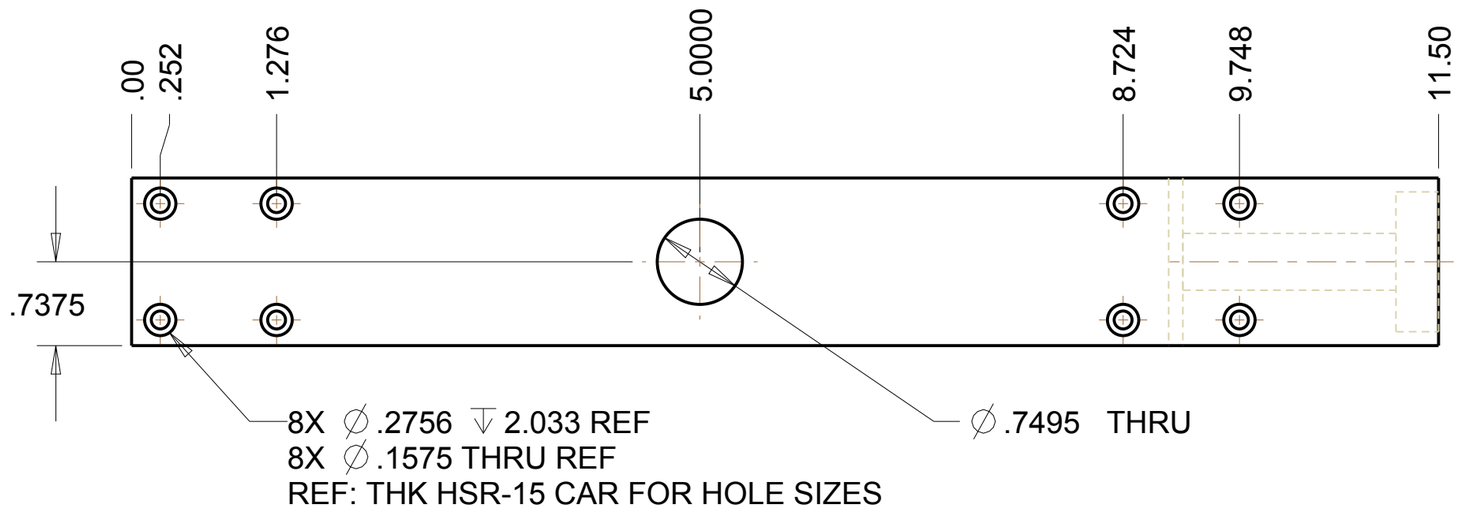

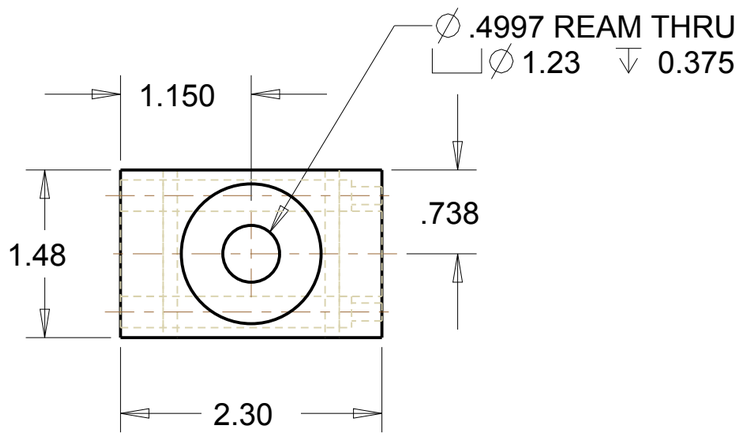

WORCESTER POLYTECHNIC INSTITUTE

UNITS: INCH, DEGREE UNLESS OTHERWISE SPECIFIED, X.X ± 0.1 X.XX ± 0.025 X.XXX ± 0.005 X.XXXX ± 0.0001 ANGLE ± 0.5 °	MATERIAL: ALUMINUM 6061-T6
	DRAWING: F-10
	MODEL: SPRING_BLOCK
	DRAWN BY: CSTM MQP

SCALE: 3=4	B	DATE: Jan-12-11	SHEET 1 of 1

QUANTITY: 1

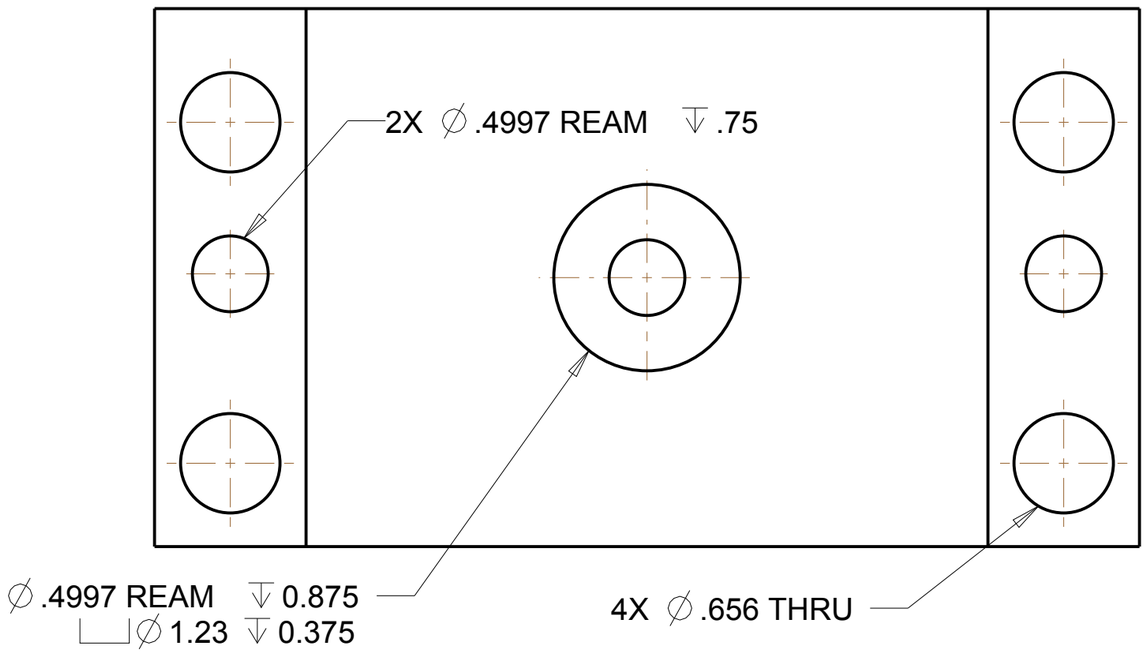

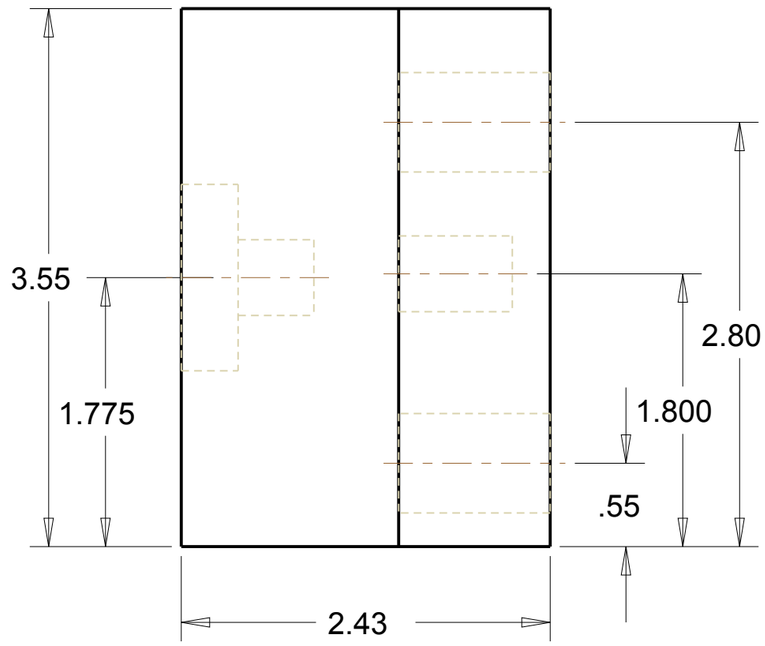

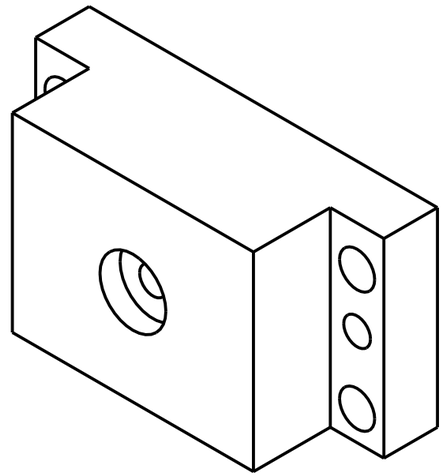

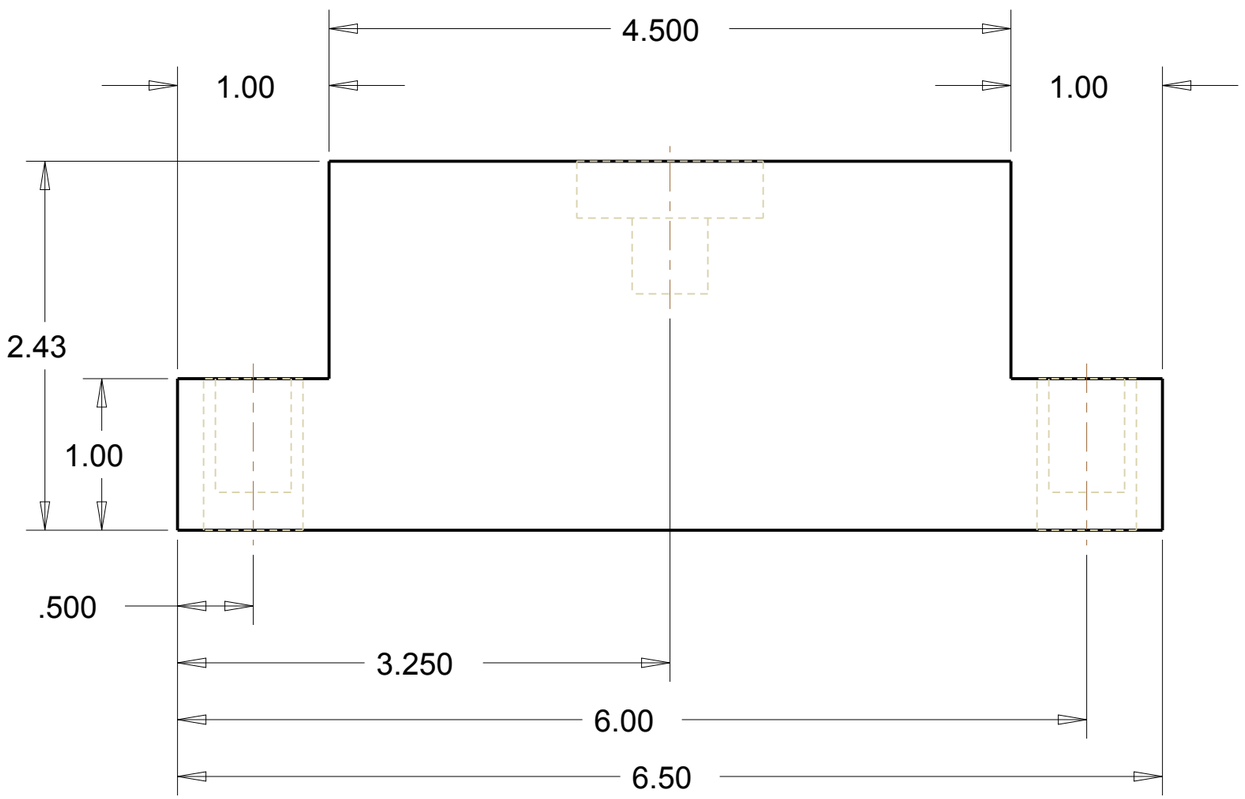

WORCESTER POLYTECHNIC INSTITUTE			
UNITS: INCH, DEGREE UNLESS OTHERWISE SPECIFIED, X.X ± 0.1 X.XX ± 0.025 X.XXX ± 0.005 X.XXXX ± 0.0001 ANGLE ± 0.5 °	MATERIAL: ALUMINUM 6061-T6		
	DRAWING: F-11		
	MODEL: SPRING_PLATE		
	DRAWN BY: CSTM MQP		
SCALE: 1=1	B	DATE: Jan-10-11	SHEET 1 of 1

QUANTITY: 1

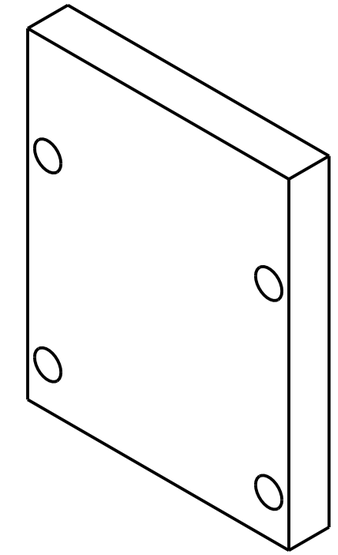

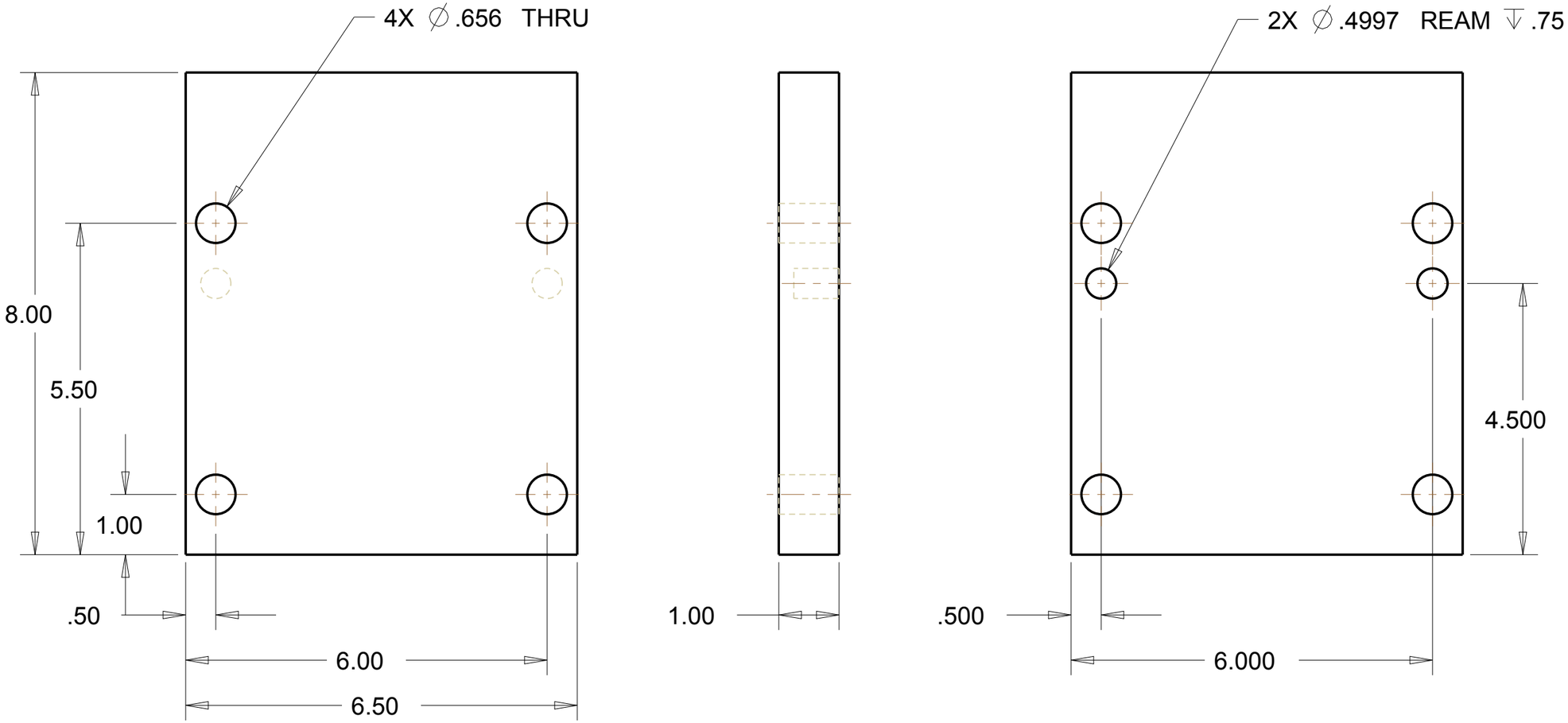

WORCESTER POLYTECHNIC INSTITUTE			
UNITS: INCH, DEGREE UNLESS OTHERWISE SPECIFIED, X.X ± 0.1 X.XX ± 0.025 X.XXX ± 0.005 X.XXXX ± 0.0001 ANGLE ± 0.5 °	MATERIAL: ALUMINUM 6061-T6		
	DRAWING: F-12		
	MODEL: SUPPORT_PLATE		
	DRAWN BY: CSTM MQP		
SCALE: 1=2	B	DATE: Jan-10-11	SHEET 1 of 1

QUANTITY: 1

UNITS IN METRIC
CUT TO SPECIFIED LENTH

WORCESTER POLYTECHNIC INSTITUTE			
UNITS: INCH, DEGREE UNLESS OTHERWISE SPECIFIED, X.X ± 0.1 X.XX ± 0.025 X.XXX ± 0.005 X.XXXX ± 0.0001 ANGLE ± 0.5 °	MATERIAL:		
	DRAWING: F-13		
	MODEL: THK_RAIL_HSR_15R		
	DRAWN BY: CSTM MQP		
SCALE: 3=4	B	DATE: Jan-12-11	SHEET 1 of 1